Centre for Ore Deposit and Exploration Studies

Proterozoic sediment-hosted base metal deposits

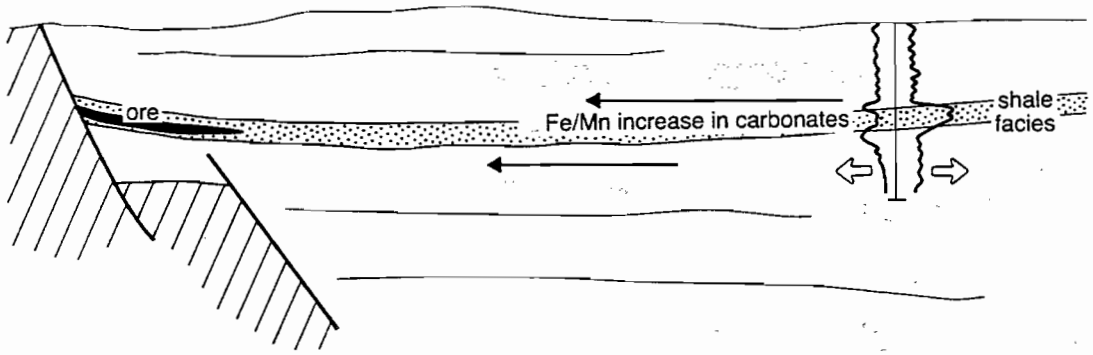

AMIRA/ARC Project P384
Report No.7

UNIVERSITY OF TASMANIA

November 1994

Centre for Ore Deposit and Exploration Studies

Proterozoic sediment-hosted base metal deposits

AMIRA/ARC Project P384
Report No.7

UNIVERSITY OF TASMANIA

November 1994

Contents

Introduction

Project Objectives: P384

1. To determine the primary geological, geochemical and structural controls on the location and timing of base metal deposits in sedimentary basins.

2. To understand the chemical and hydrological evolution of metalliferous brines in selected Proterozoic sedimentary basins of Australia.

3. To develop basin metallogenic models and specific ore deposit models that may be used in the exploration for large-tonnage base-metal ore deposits.

Research framework

This research project involves a multi-disciplinary approach using regional geological, geophysical and structural studies, brine chemical modelling and geochemical and isotopic halo studies to provide a foundation of which to build a network of exploration criteria and ore deposit models for major sediment-hosted base metal deposits.

This report

This report covers work over the past six months (June–November 1994) and is the seventh report for P384. During this period our research has advanced on a number of fronts: in particular the geophysics and structure of the Riversleigh Fold Belt (formerly Lawn Hill Platform) and further refinement of the alteration halo vectors and their relationship to sedimentary facies in the McArthur Basin.

Coordination of the team results outlined in this report into a series of preliminary integrated models on basin architecture and ore deposit halo formation will be presented at the sponsors meeting on November 24–25. A final P384 report which brings together all our research advances will be presented to the sponsors in May 1995.

Ross R. Large
Director, CODES

Executive summaries

REGIONAL GEOPHYSICS — BASIN ARCHITECTURE 5. The Lawn Hill Platform — David Leaman

This report presents an interpretation of regional gravity and magnetic data in the Calvert Hills, Westmoreland, Lawn Hill and Mt Drummond regions, otherwise known as the Lawn Hill Platform, South Nicholson Basin and Murphy Tectonic Ridge with respect to the McArthur Basin and Isa Inlier, has shown that the region has had a continuously active history and that all relationships are consistent with a single basin evolution sequence.

The terms Murphy Teconic Ridge, South Nicholson Basin and Lawn Hill Platform should be discontinued since they are misleading in regional terms and based only on near surface perspectives.

The uplifted block, which has been renamed the Murphy Inlier (McConachie *et al*, 1993), has been active throughout the basin's history since all pre-Tawallah Group rocks appear to thin and onlap it and Tawallah Group rocks are deformed by uplift. Post Tawallah rocks have also been controlled by continued activity and the rocks of the South Nicholson area reflects this.

The region possesses a largely granitic basement overlain by two massive volcanic sequences; the earlier one essentially felsic and the younger predominantly mafic. These gross associations have now been recognised across the entire McArthur Basin west of the Murphy Inlier and are now shown to continue SE beyond the inlier toward Kamarga where thick mafic members of the Haslingden Group are actually exposed. Examination of structural relationships involving these associations suggests that each was controlled by primary basin faulting to yield asymmetric wedges of material but that considerable erosion occurred before and after each sequence. Each association can be defined magnetically and the older, less magnetic or more variable package is much more patchy. The maximum estimated thicknesses within the area studied are much less than have been identified within the McArthur Basin but thickness does increase southward to levels comparable with measured values for the Eastern Creek Volcanics of the Haslingden Group of the Isa region. There is every possibility that this sequence formed a large, continental sheet of flood basalts. Thickness variations are related to primary basin forms or subsequent local uplift and erosion. These volcanic sequences are correlateed with the Leichhardt–Argylla and Haslingden Group packages of the Isa Inlier.

Substantial uplift and erosion has occurred prior to deposition of the South Nicholson Group. The persistent uplift of the Murphy Inlier may be

related to the granitoid balance to north and south. At least three granitic rocks can be defined regionally and geophysically; a more dioritic form north of the inlier and a more granitic form south of it. A lower density phase intrudes both of these batholith complexes and an example penetrates some of the central basin elements at Kamarga.

Regional NW, NE and E–W trend systems are evident in the raw data and explained upon analysis to reflect proportions of the volcanic associations and the balance between cover and basement patterns. Major structures can be traced across the entire region. Particular foci for fracture systems, and substantial variations in cover sequences of all ages, have been recognised near the eastern exposure of the inlier and also a little west of Kamarga.

A major change in basement composition has also been defined. The boundary is oriented NNW and can be traced southward across the region at the longitude of Doomadgee.

Few mineralised sites are known in this region due to thickness and extent of cover sequences. Known mineralisation, of all types, can be associated with the foci recognised as anomalous structural features. The Silver King – Century zone is associated with fundamental basement features and substantial changes in unit thicknesses. The Termite Fault represents a late rejuvenation of a complex primary structure. Many of the defined elements are comparable with those described near HYC in an earlier stage of this study. Other, similar, anomalous zones are rare in this region. Given the substantial cover sequences (Cambrian and younger) this may be important information with considerable ramifications for exploration.

A preliminary structural analysis of the Riversleigh Fold Belt (formerly Lawn Hill Platform) with special reference to structures around the Lady Loretta deposit — Richard A. Keele

Preliminary studies of the Leopard Fault suggests that it was active during the McArthur extension. Minor inversions along this fault represent precursors to the main orogenic event (Mount Isa - D1) in which the sub E-W basinal faults became thrusts. Subsequent upright folding (Mount Isa - D2) has preserved a section through one such a fault. Fault striae analysis in the Lawn Hill Platform gives results that are consistent with the variable effects of the nearby orogen (Mount Isa Orogeny). An early basin-wide pre-orogenic pulse which involved brittle-style wrenching at the end of sag phase sedimentation is probably related to Pb-Zn mineralisation at Lady Loretta. It is followed by thrusts during Isa D1 and shear bands during Isa D2. Partitioning of the regional strain in the Platform suggests that 'indent tectonics' may have been active during the main phase of orogeny.

Modelling the Relationship Between Sedimentary Facies and Alteration Index and Resolution of the "Shale Factor" — Ross R. Large

A study of sediment mixing models for the HYC and Lady Loretta areas has enabled the development of a refined alteration index called AI Mark 3 (AI_3) which utilises Al_2O_3 wt%, in addition to FeO, MnO and MgO wt%. This refined geochemical index vector reduces the "shale-factor" that was prevalent in the Sedex AI, which gave high priority to low carbonate bearing shales, but could not discriminate between barren shales and potentially fertile shale host rocks. Further testing of AI_3 will be required to assess its full potential as a robust exploration vector.

Microprobe analysis of carbonate phases at Lady Loretta — Nathan Duhig

Carbonates from dolomitic and sideritic sediments at Lady Loretta were analysed by microprobe to test the validity of the calculated MnO distributions in the carbonates. A good correlation was obtained between the actual and calculated MnO values. The study also revealed that ankerite, not dolomite, is the dominant carbonate away from the siderite halo. There is varying substitution between Mg & Mn with Fe & Zn (where Zn is available) in the siderites. Further probing and cathode luminescence studies may aid in determining the paragenesis of the carbonate phases and hence the origin of the siderite (and ankerite?) halo.

Petrology and tectonic setting of the Tawallah Group igneous rocks — Jamie Rogers

This paper aims to describe geochemical traits of the Tawallah Group igneous rocks with respect to the tectonic processes that were active during their emplacement. Variations in immobile element compositions allow for geochemical characterisation of the different igneous units and their identification as continental within-plate tholeiites. The latter conclusion enables comparison with tholeiitic basalts and andesites of the Lower Cretaceous Paraná CFB province. Zr/Nb, Y/Nb and REE relationships suggest that the Settlement Creek and Gold Creek Volcanics are derived from a more enriched mantle source (T-type to P-type MORB) than the Seigal Volcanics (T-type MORB). This is interpreted to reflect increased input of relatively enriched deep mantle into sub-continental lithospheric source regions or, alternatively, suggests progressive involvement of a deep mantle source region as the plume system relaxes to depth. In either case, the entire system appears to relax and suggests that rifting in the southern McArthur Basin failed at an early stage.

Depositional attributes of the Barney Creek Formation in DDH BMR McArthur 2 — Stuart Bull

Detailed sedimentological examination and geochemical resampling of DDH BMR McArthur 2 has been carried out to provide a new geochemical data set and to study the effects of sedimentary facies on the alteration index. The sedimentological studies indicate that: (1) The Barney Creek Formation, which comprises the bottom 97 m of the core, was deposited in a quiet (ie. below wave base), anoxic subaqueous environment via hemipelagic suspension deposition interrupted by periodic, small volume mass flows. (2) The upper 25 m of core record gradually shoaling conditions interpreted to represent a gradational contact with the overlying Reward Dolomite. (3) The presence of mass flow beds of peloidal sandstone throughout the Barney Creek Formation, which are similar in composition to sub-tidal peloidal sandstone deposits described from the Reward Dolomite, suggests that the two units are at least partly time equivalent.

With respect to the alteration index, there is no direct relationship to sedimentary facies (which are defined on the basis of dominant depositional mechanism and probably also organic carbon content and are independent of dolomite content), apart from the "shale effect" which has been addressed by creating AI3. There is a crude relationship between AI3 and sulphur content (occurring as pyrite). This results in black (ie. carbonaceous +/pyritic) mudstone-rich samples giving relatively high AI3 values, however, not all samples of this type give high AI3 values. In fact, three of the five samples with high AI3 values which define the AI3 peak in DDH BMR McArthur 2 are from the main facies present which is less carbonaceous and pyritic than the black mudstone facies.

Application of the Alteration Index and MnO_D to the Mount Isa and Hilton zinc-lead-silver deposits — Peter McGoldrick

This report describes an assessment of the applicability of geochemical vectors to mineralisation developed for Lady Loretta and HYC to the giant Mount Isa and Hilton Zn–Pb systems. Several old public domain data sets have been used for this purpose. The data analysis indicates that the 'Sedex Alteration Index' (Large and McGoldrick, 1994), the 'Alteration Index Mk3' (Large, this volume), MnO_D (Large and McGoldrick, 1993) and Tl (McGoldrick, 1986) are all potentially useful vectors to the Mount Isa and Hilton deposits.

The geochemistry of 'barren' late Palaeoproterozoic sediments from the McNamara Group: background values for the 'SEDEX AI', 'AI Mk3' and MnO_D — Peter McGoldrick

This preliminary report presents geochemical data for 43 samples collected from four stratigraphic drill holes through McNamara Group sediments in the Lawn Hill Platform/Riversleigh Fold Belt (McConachie et al., 1993). The geochemical vectors refined by (Large and McGoldrick, 1994) and Large (this volume) are calculated for these samples and the results are used to confirm 'background' values for these indices. This analysis supports intuitive arguments that these samples represent 'typical' compositions for unmineralised fine grained sediments in the McNamara Group.

Conditions of formation for siderite and barite from sedimentary brines: implications for the formation of sediment-hosted base metal deposits — David Cooke

This report presents results of the continuing study into controls on siderite deposition from low-moderate temperature hydrothermal fluids. Some brief comments on siderite deposition from low temperature (50°C) brines are provided prior to a discussion of the relationships between barite, siderite and metalliferous brines. The report concludes with a discussion of preliminary chemical models for sediment-hosted base metal deposits.

REGIONAL GEOPHYSICS — BASIN ARCHITECTURE

5. The Lawn Hill Platform

David Leaman
Centre for Ore Deposit and Exploration Studies

Summary

Interpretation of regional gravity and magnetic data in the Calvert Hills, Westmoreland, Lawn Hill and Mt Drummond regions, otherwise known as the Lawn Hill Platform, South Nicholson Basin and Murphy Tectonic Ridge with respect to the McArthur Basin and Isa Inlier, has shown that the region has had a continuously active history and that all relationships are consistent with a single basin evolution sequence. The region straddles the accepted boundary between rocks of the McArthur Basin and the Isa Inlier although this work would suggest that this is an artificial division in terms of suites which can be recognised to north and south of the Murphy zone. Previous terminology should be dropped in favour of a single basin term while noting that it contains some regions which have been repeatedly, perhaps continuously, uplifted.

The terms Murphy Teconic Ridge, South Nicholson Basin and Lawn Hill Platform should be discontinued since they are misleading in regional terms and based only on near surface perspectives.

The uplifted block, which has been renamed the Murphy Inlier (McConachie *et al*, 1993), has been active throughout the basin's history since all pre-Tawallah Group rocks appear to thin and onlap it and Tawallah Group rocks are deformed by uplift. Post Tawallah rocks have also been controlled by continued activity and the rocks of the South Nicholson area reflects this.

The region possesses a largely granitic basement overlain by two massive volcanic sequences; the earlier one essentially felsic and the younger predominantly mafic. These gross associations have now been recognised across the entire McArthur Basin west of the Murphy Inlier and are now shown to continue SE beyond the inlier toward Kamarga where thick mafic members of the Haslingden Group are actually exposed. Examination of structural relationships involving these associations suggests that each was controlled by primary basin faulting to yield asymmetric wedges of material but that considerable erosion occurred before and after each sequence. Each association can be defined magnetically and the older, less magnetic or more variable package is much more patchy. This may be a primary pattern or it may reflect extended widespread erosion and uplift. The overlying mafics-dominated association is more consistent in thickness — especially north of the Murphy Inlier — but it, too, is variable. The maximum estimated thicknesses within the area studied are much less than have been identified within the McArthur Basin but thickness does increase southward to levels comparable with measured values for the Eastern Creek Volcanics of the Haslingden Group of the Isa region. There is every possibility that this sequence formed a large,

continental sheet of flood basalts. Thickness variations are related to primary basin forms or subsequent local uplift and erosion.

These volcanic sequences have been tentatively linked to the Leichhardt–Argylla and Haslingden Group packages of the Isa Inlier in previous reports and this study unit would appear to confirm this correlation.

Substantial uplift and erosion has occurred prior to deposition of the South Nicholson Group. Granitoids may be related to some of these changes. Some structures appear to be directly related to diapiric forms. The persistent uplift of the Murphy Inlier may be related to the granitoid balance to north and south. At least three granitic rocks can be defined regionally and geophysically; a more dioritic form north of the inlier and a more granitic form south of it. A lower density phase intrudes both of these batholith complexes and an example penetrates some of the central basin elements at Kamarga. This interpretation provides a revised and more detailed view of the Inlier than given in earlier reports.

Regional NW, NE and E–W trend systems are evident in the raw data and explained upon analysis to reflect proportions of the volcanic associations and the balance between cover and basement patterns. Major structures can be traced across the entire region. The frequency of some trends does vary north and south of the Murphy Inlier but some can be extended across it. Such structures change in scale north of the inlier suggesting diffused rejuvenations. Sub E–W structures are dominant in the region south of the inlier. It appears that the Termite Creek Fault may be translated into the Calvert Fault. Particular foci for fracture systems, and substantial variations in cover sequences of all ages, have been recognised near the eastern exposure of the inlier and also a little west of Kamarga.

A major change in basement composition has also been defined. The boundary is oriented NNW and can be traced southward across the region at the longitude of Doomadgee.

Few mineralised sites are known in this region due to thickness and extent of cover sequences. Known mineralisation, of all types, can be associated with the foci recognised as anomalous structural features. The Silver King – Century zone is associated with fundamental basement features and substantial changes in unit thicknesses. The Termite Fault represents a late rejuvenation of a complex primary structure. Many of the defined elements are comparable with those described near HYC in an earlier stage of this study. Other, similar, anomalous zones are rare in this region. Given the substantial cover sequences (Cambrian and younger) this may be important information with considerable ramifications for exploration.

The interpretation can be integrated with regional seismic reflection profiles undertaken for petroleum exploration east of the inlier. The integration shows that the volcanic sequences possess much seismic character and that a major unconformity does exist between the felsic and mafic units.

Introduction

This report outlines analysis of gravity and magnetic data within the Calvert Hills, Westmoreland, Mt Drummond and Lawn Hill 1:250 000 map sheets in the eastern McArthur Basin and northern Isa Basin. I fully support the thrust toward redefinition of terms suggested by McConachie *et al* (1993). The area has been described as the Lawn Hill Platform (Plumb & Derrick, 1975).

Previous work reported for adjacent parts of the basin include:

1. The Batten Trough region (Leaman, 1992)
2. The Wallhallow region (Leaman, 1993a)
3. The Wearyan Shelf and Murphy Inlier (Leaman, 1993d)
4. The Bauhinia Shelf (Leaman, 1993f)

The basic methodology for this analysis has been outlined by Leaman (1992) and clarified in Leaman (1993b, c). Some further information related to the theory and interaction of magnetic responses in basins is included as an appendix to this report (Leaman, 1994).

The principal objectives of the interpretation have been to define general relationships within the basin and provide information which may constrain concepts of structural evolution, fluid motion and mineralisation. Achievement of these goals requires a coherent assessment of the entire basin. The present work completes the fourth stage of this process.

Geology

The geology of the region is shown in Figure 1 to be dominated by the relatively recent cover sequences. There is negligible exposure of any rocks older than the Nicholson or Tawallah Groups and the oldest rocks are exposed along the Murphy Inlier. Much of the cover is Cambrian or post Jurassic in age.

Drilling and seismic survey activity within the region has been limited and only the seismic data east of the inlier offers any substantive supporting or independent control information.

Extracts of the seismic data are shown in Figures 4 to 6 (from McConachie et al., 1993).

Any regional geophysical interpretation in such conditions is essentially blind and must be tied either to better known conditions or be rigorously undertaken to limit possible ambiguities. In this case control is provided by the inlier, the limited seismic coverage and the domal structures and improved exposure in the region near, and south of, Kamarga.

Geophysical data

Only regional gravity and magnetic data have been reviewed. These are illustrated in Figures 2 and 3 (AGSO compilations). Every indication offered by such data is important in view of the limited control offered by surface geological mapping.

Regional magnetic data (Figure 2) pick out some large regional features and some strings of local, shallow elements. There are some marked sub E–W and NW–SE trends but there is no correlation with any aspect of established local geology other than limited responses near minor exposures of high level volcanics within the Tawallah Group within the Calvert Hills sheet. The figure illustrates the variable quality of the data available and this will inevitably limit detailed appraisals south of the inlier. Long wavelength character suitable for regional and basin studies is adequately represented.

The gravity data are very different (Figure 3). E–W elements are not obvious away from the Murphy Inlier and few other trends can be consistently or regionally observed. The gravity field is dominated by large negative features and some N–S ridges between them. A secondary negative element can be directly related to the granite core at Kamarga and there can be little doubt that these large negative anomalies are related to batholiths.

Rock properties

Since there are no significant exposures of any units which may be present between ultimate basement and Upper Tawallah Group, and certainly no property determinations, some properties and characteristics have been assumed. The values used have been based on implications from previous work and reasonable ranges for presumed lithologies.

Previous work has shown that many of the basement granitoids are relatively non magnetic, especially when contrasted with overlying felsic assemblages or mafic volcanics and intrusives. The present work has shown, however, that one of the granitoids does possess recognisable properties. Basement sedimentary assemblages, as exposed near the Murphy Inlier, are also non magnetic in these terms. There is no significant or continuous magnetic basement and no gross simplifying assumptions can be made about basement. It has been presumed to be essentially non magnetic.

Previous response analysis for surveys across the Scrutton Ranges and the Murphy Inlier has indicated that the felsic Scrutton and Cliffdale

Volcanics are significantly magnetised and although the properties are variable, values in excess of 0.001–0.002 cgs (~0.015 SI) are likely as a bulk estimate. It is possible that the variations disguise internal divisions within these units (especially the Cliffdale Volcanics) and more work is necessary. This interpretation indicates that there are two distinct families of properties and responses within the Cliffdale Volcanics near the inlier and this is consistent with petrological characteristics. Two suites are likely. The overall response of the lower member is slightly reversed suggesting that remanence may be a crucial factor. Any such distinction may prove of considerable value in ultimate correlations.

Similar assessments of the mafic volcanic members of the Tawallah Group, coupled with some direct susceptibility measurements (Keele, pers. comm.) show that properties are variable but at least of the same order. Some of these units have clearly been altered and the properties confirm this. Units such as the Peters Creek Volcanics are more magnetic and values in excess of 0.003 cgs (~0.03 SI) are likely.

Thick mafic volcanic sequences common in the Isa Inlier possess bulk contrasts with associated sedimentary successions of at least 0.005 (0.004–0.008) cgs (~0.07 SI). This interpretation uses a basic value of 0.005 cgs for deeper, and thicker, mafic accumulations.

Some members of the Tawallah and McArthur Groups are very slightly magnetised but the effect is insignificant in local and regional terms and at least two orders of magnitude less than observed results for both felsic and mafic rocks in the region. Slightly magnetised granites are also much more magnetic than any sedimentary or altered rock mass.

Cover rocks are essentially non magnetic. No local young flows or intrusives are known to be present within them.

Rock densities are not easily defined given the limited exposures in the basin and the paucity of sampling. Basement rocks may be considered to possess densities in excess of 2.74 t/cu m but their actual properties tend to be largely irrelevant due to the large volumes of associated granitoids. Direct inspection of contrast anomalies indicates that the granitoids have densities of the order of 2.62–2.64 t/cu m. Limits can be placed on this estimate. Densities of such rocks are unlikely to be less than 2.60 in any event and gradient assessments suggest that densities in excess of 2.68 are not realistic. The implied contrast with intruded sedimentary basement is about 0.12 t/cu m but detailed work for this study area has shown that two granite families are represented; with bulk contrasts of about –0.06 and –0.12 t/cu m. These inferences suggest that the basement contains large volumes of material with average densities of either 2.64 or 2.76 t/cu m. Leaman (1993d) indicated that at least part of the basement(?) may have densities of the order of 2.85 t/cu m and be non magnetic. This is confirmed by the present study. Very few sedimentary or igneous lithologies can be suggested for such material but a number of metamorphic possibilities exist.

Previous interpretations have included large thicknesses of volcanic rocks and there can be no doubt of the existence of such accumulations given the magnetic evidence (Leaman, 1993b). But, given the scale implied and the likely densities, some limits are imposed by the total gravity field responses. By comparing effects in those regions where cover is either present or absent, or there are clear structural variations, it is possible to imply that the nominal felsic and mafic associations cannot be denser than 2.79 or 2.85 t/cu m respectively as bulk estimates. This implies that each package includes a moderate proportion of intercalated sediment. The density estimates obtained in this way are credible for the associations implied even if the values cannot be directly verified.

Sedimentary rocks of the Tawallah and McArthur Groups can be judged on their contrast with other materials, especially where closely sampled data constrain the anomalies, to have densities of about 2.71–2.75 t/cu m and 2.74 has been taken as a typical density. The materials of the South Nicholson Group appear to be of lower density, perhaps 2.60–2.64 t/cu m.These results

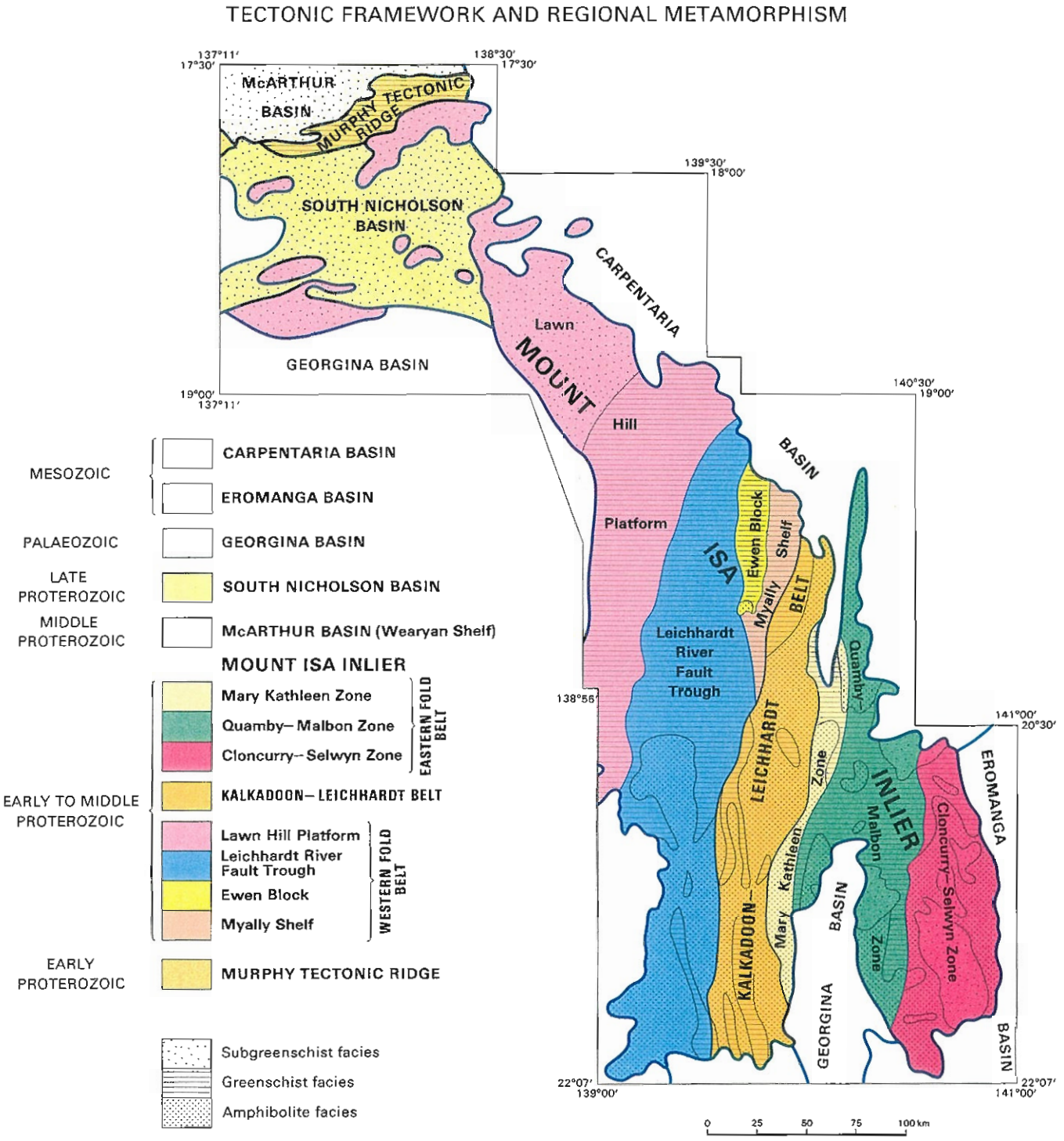

Figure 1—AGSO geological basemap of the Murphy Inlier — "Lawn Hill Platform" region.

back F1

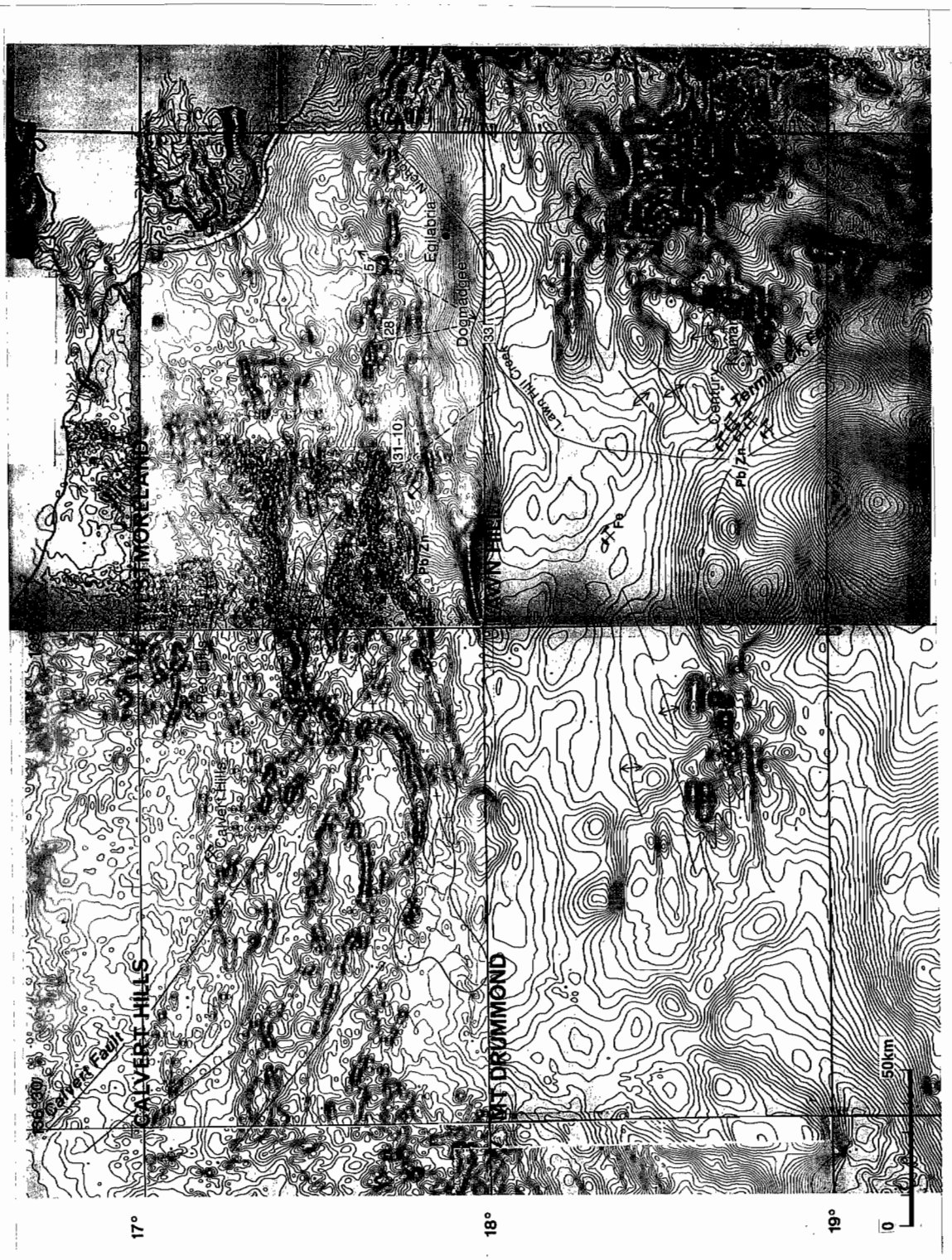

Figure 2—Regional magnetic data compilation Murphy Inlier — Lawn Hill region (AGSO data).

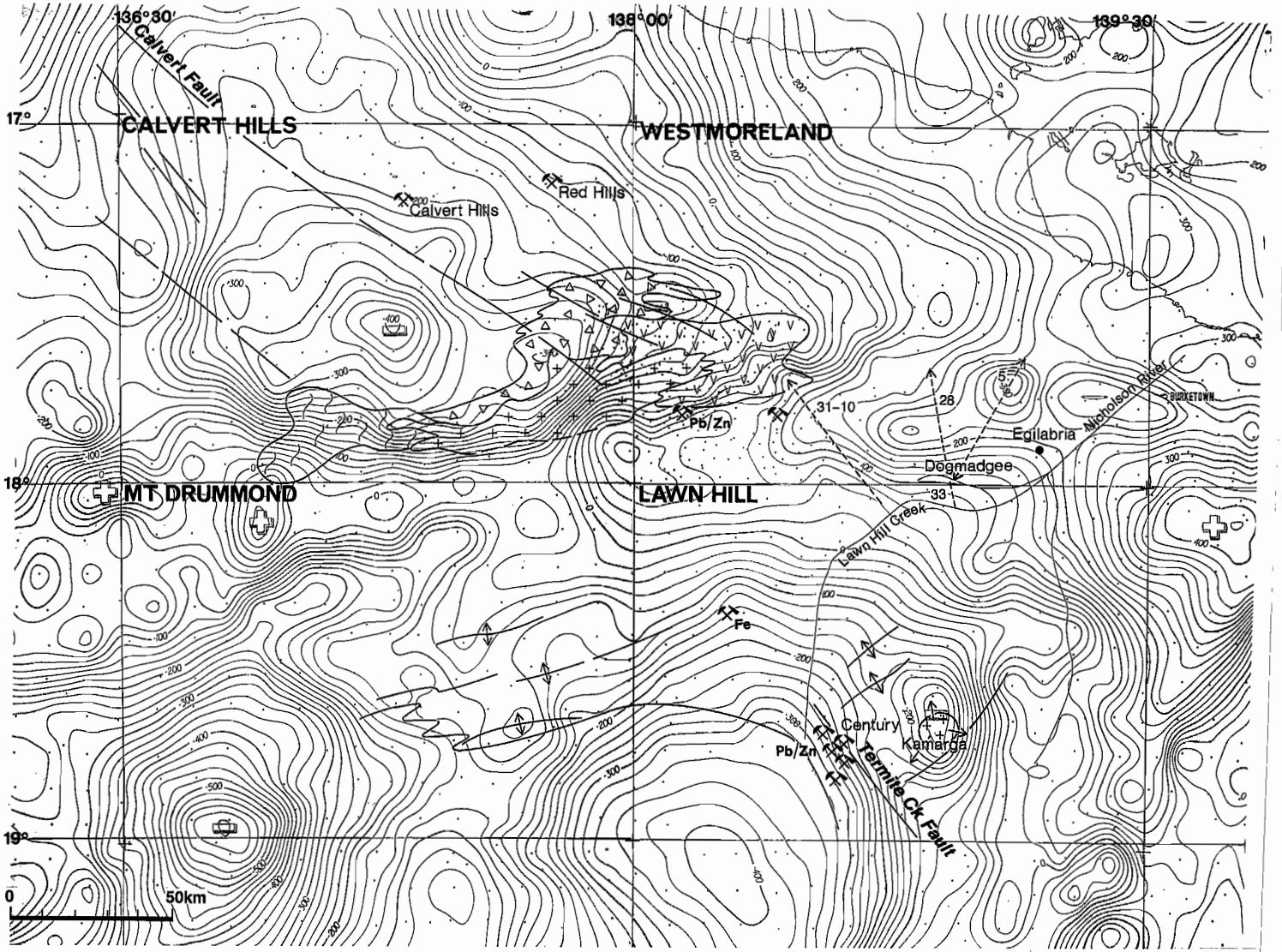

Figure 3—Regional gravity data compilation Murphy Inlier — Lawn Hill region (AGSO data)

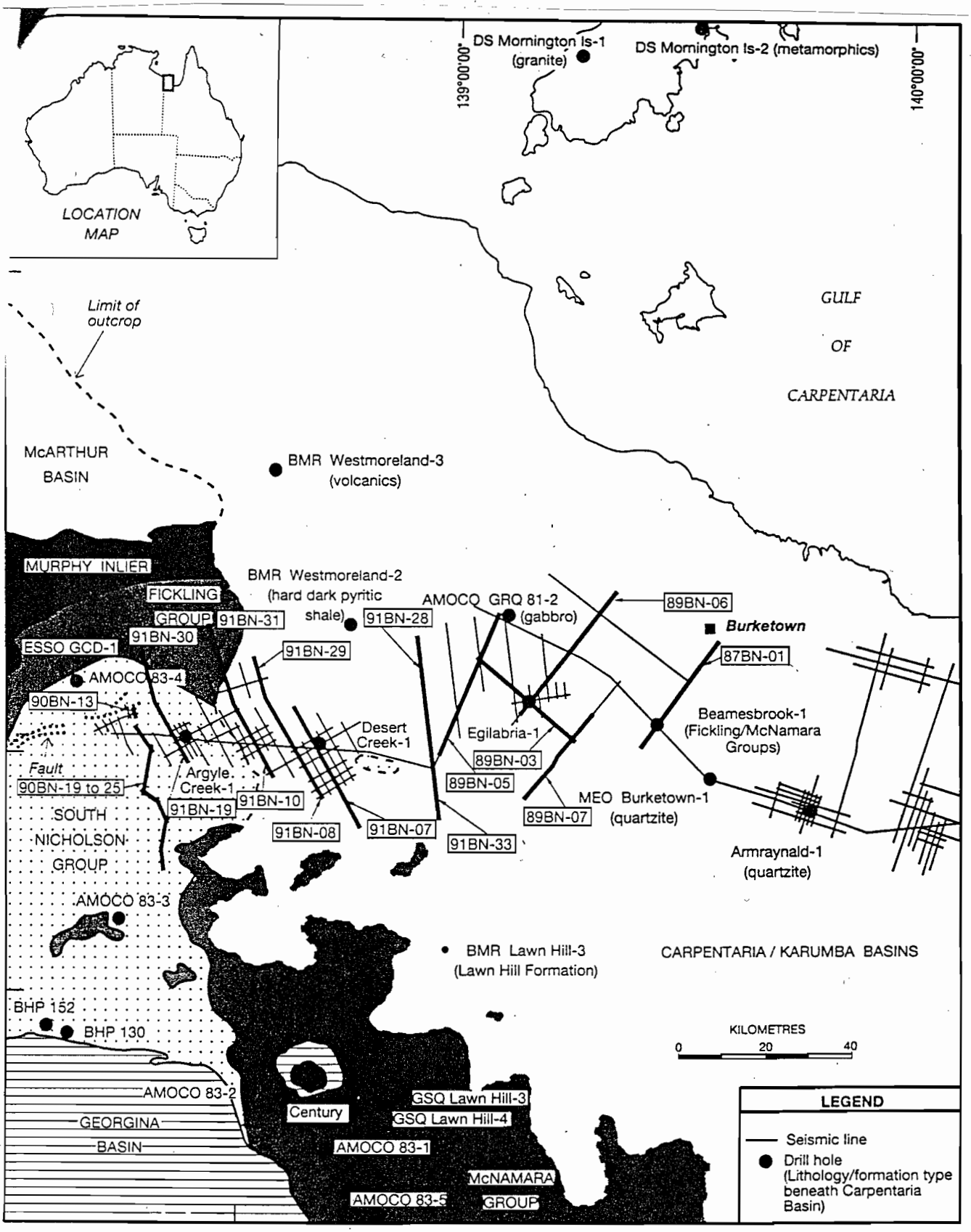

Figure 4—Location of AMOCO seismic lines, Lawn Hill.

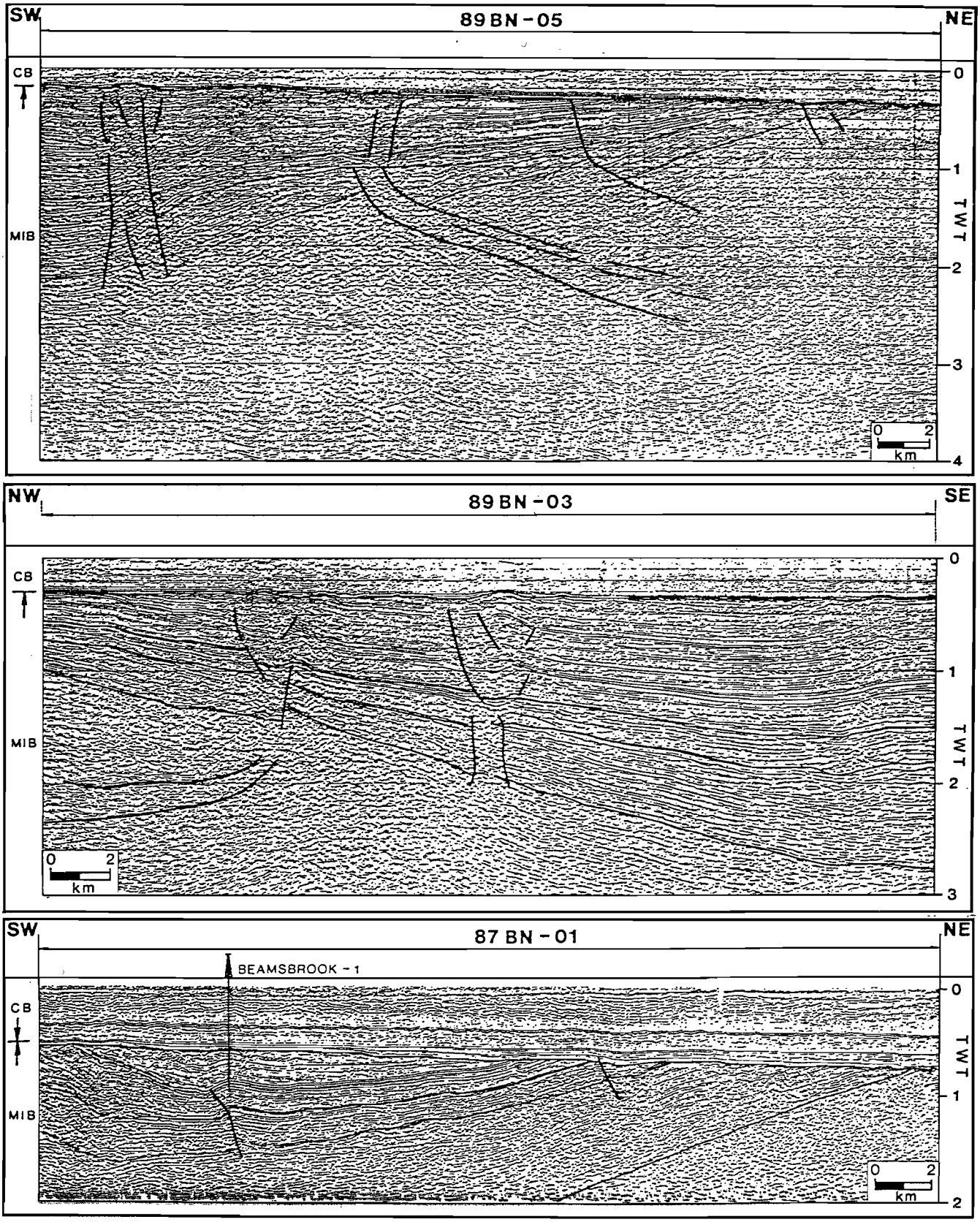

Figure 5—Seismic profiles for lines 1, 3, 5 Lawn Hill. Amoco data.

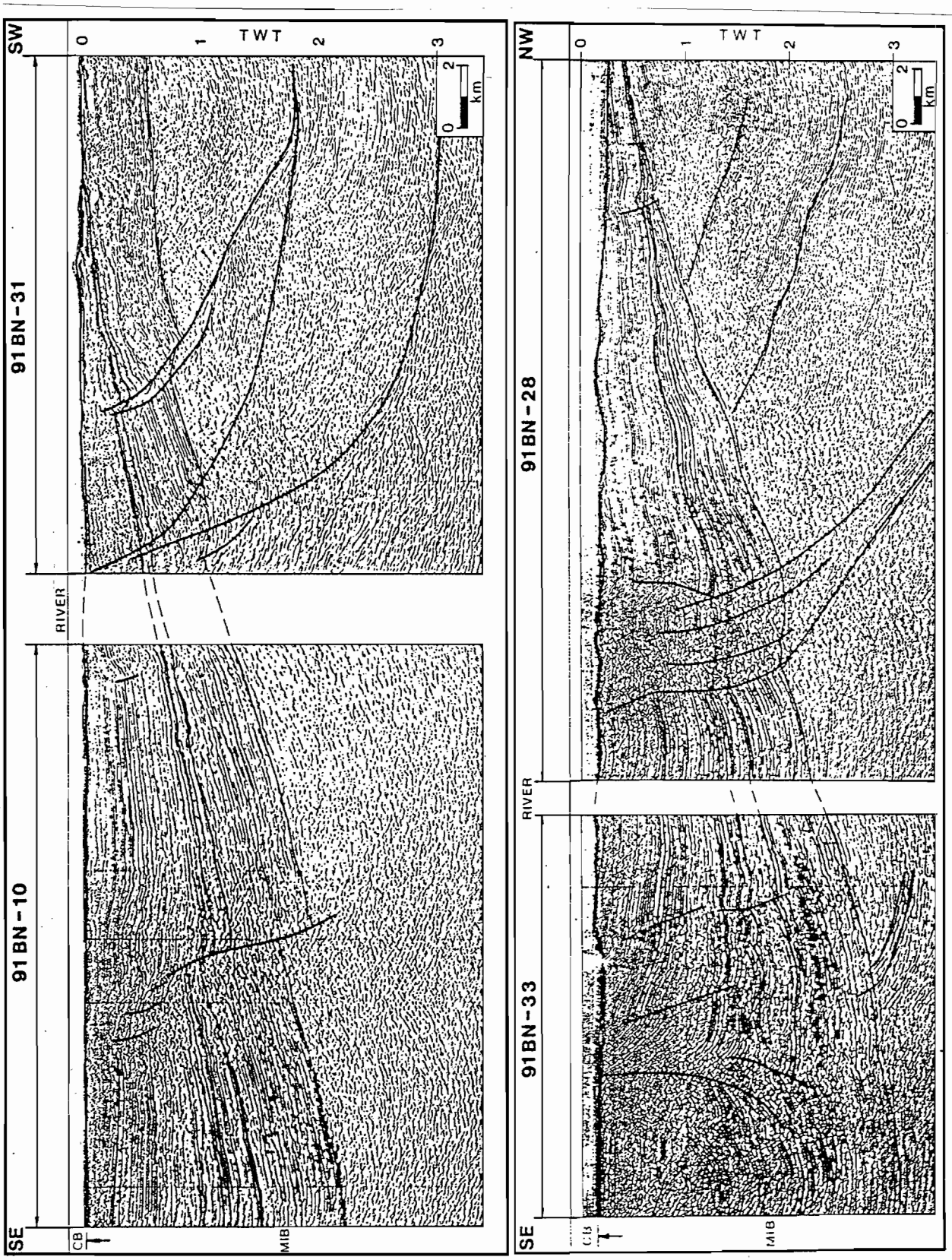

Figue 6—Seismic profiles for line 31–10 and 28–33 Lawn Hill, Amoco data.

are comparable with those from similar cover sequences in the Isa Inlier. More detailed review in the HYC region of the Batten Trough suggests that the upper part of the McArthur Group is more massively dolomitic and denser (about 2.77–2.78 t/cu m).

Lower densities have been employed for the Cambrian and Cretaceous cover sequences (2.5 max, and 2.35 t/cu m max respectively).

Values assessed in this way have been used throughout the interpretation. Many are unconfirmed but all are credible and reasonable and lead to no unexplained effect.

In summary, however, only two sequences are significantly magnetically; the felsic and mafic associations buried deep in the basin and which are only rarely exposed (felsics). Gravity analysis must, in contrast, consider the interactive effects of all sources. For this reason the magnetic data have been used to provide basic restraints on deep options, volcanic inferences and lateral variations and the gravity data have been applied to test feasibility and to derive information relevant to cover and basement variations.

Previous work

Some work within this study area has been reported previously (Leaman, 1993d). Much of the Wearyan Shelf review was terminated at the map sheet boundary which is very close to the southern margin of the Murphy Inlier. Only two profiles extended a moderate distance into the Mt Drummond region and one of these was displayed in the earlier report.

The presence of a major structure at the limit of general assessment was the source of some concern and it was suspected that the conclusions at the southern margin of the Wearyan study may have been affected.

The earlier interpretation suggested that many sequences onlapped a much rejuvenated inlier block and that the granites north of the inlier exposures were at least partly truncated by a major compressive structure — projected to surface at the Fish River Fault approximately. This view also led to a compound appraisal of the volumes of the deeper volcanic sections. The limited analysis south of the Fish River Fault confirmed that the volcanic units persisted either across, and certainly south of, the inlier. The relationships south of the fault were most uncertain but could be explained in terms of a limited inlier overthrust.

The seismic data, see Figures 4, 5 and 6, is limited to the region east of the principal exposures of the South Nicholson Group, south of the Fish River Fault, but some profiles terminate on or near exposures of the Cliffdale Volcanics or granites of the inlier.

Profiles 31–10 and 28–33 which are approximately N–S extend from the inlier axis and show that the Nicholson, and other, cover sequences thicken rapidly to the south. Note that one second of two-way time is equivalent to a minimum of 2.5 km in thickness. Thus line 33 includes at least 8 km of Proterozoic section.

Although the sections have been reproduced from McConachie *et al* (1993), and shows their interpretation (which in my view is not generally sustainable — below) it is clear that a typical basin sequence, with onlaps and unconformities, is present.

Line 31 ends at exposure of the Cliffdale Volcanics (as far as can be judged) and this is a typical failing of petroleum explorers. Amoco has not considered it worthwhile to extend the profile onto the inlier and, in failing to do so, has greatly diminished its chances of understanding the *entire* section. Even so some irregular piling can be observed in the northern half of the line above the "basement" interface — which, it should be noticed, is undefined and unconfirmed. Some irregular lumpiness in reflectors can be seen on other sections. About 1.5 km of Cliffdale Volcanics, at least, is implied at the north end of line 31 if the line does indeed end on these rocks. Alternatively this piling may represent the Westmoreland Conglomerate.

Some faulting is indisputable but the overall extension of the faults in depth shown in the sections is unsupportable — especially when some

clear, non multiple, character may be observed within the so-called basement. This is particularly clear in lines 3, 5 and 28. The dip opposes the overlying basin onlap and there is clearly a major angular unconformity. This shows that any granite basement must lie at depths in excess of 7 or 8 km in the region of the survey.

The published seismic data do support the authors' arguments about the general basin view which should be taken of this region but important underlying issues have been avoided or simply not recognised. There is also a change in basement character between lines 28 and 31.

The Peters Creek Volcanics can also be traced into these seismic sections as the very strong reflection extending south from surface in line 31 to the mid section anomaly at the river and in line 10. This boundary can be recognised in line 28 where no outcrop is possible. The entire sequence exposed south from the inlier can be identified in line 31–10; from north to south (right to left) — Cliffdale Volcanics (either as pile or as basement), Westmoreland Conglomerate, Peters Creek Volcanics, Fickling Group and Nicholson Group and negligible more recent cover. The shallow (< 1 km) trough fill of the Nicholson Group can be seen as an irregular basin between the river and the fault zone in line 10 where the thickest basin development is about 6 km south of the river.

The Peters Creek Volcanics thicken southward and may exceed 1000 m at the end of line 10 but there is no indication of what the 3 km of underlying unit may be comprised. It is either pinched out or onlaps the basement or conglomerate piles. And, as noted above, it is not certain whether the piling seen in line 31 represents Cliffdale Volcanics or conglomerate. The geological basemap would suggest the former.

Seismic data, therefore, provide (actually confirm) information about the style of the sequence and structuring but certainly do not answer all questions. The nature of the survey coverage has, to the contrary, added ambiguity.

Some of the issues: Is the basement Cliffdale Volcanics or is it non magnetic? Is the pile composed of conglomerate or is it magnetic and therefore volcanics? Is there space to fit the thick lower mafic sequences implied in all previous interpretations of this series? Are there two felsic volcanic sequences; one part of the cover sequence, and one older?

The present analysis, essentially focussed on the region east of the inlier, or south of it, has offered an opportunity to appraise the setting of the inlier and review the limits of the previous work and to develop the implications of the seismic data. The Murphy Inlier has been made the centrepiece for the present interpretation.

Interpretation

The interpretation has utilised the properties defined above in accordance with the interpretation criteria defined by Leaman (1993c) and the implications of previous work where wider ranges of exposures have produced convincing linkages between exposed materials and interpreted units.

Thirty four new regional profiles across the Murphy Inlier region have been assessed using 2D methods. These were oriented in a manner which allowed numerous intersection tests and also sample all aspects of the regional fields. 3D interactions and interference effects are inevitable but most such effects can be recognised and do not upset the interpretation in terms of gross relationships and source continuity.

Possible limits imposed on sensitivity and precision have been discussed by Leaman (1992, 1993d, 1994). These mainly relate to the use of simple methods, regional data and coarse observation and sampling intervals. Any solution provided is indicative only, or an integration which yields styles of structures and relationships and is certainly capable of greater detail given further analysis or improved data.

Model results for seven typical profiles are shown in Figures 8 to 14. The location of these profiles is shown in Figure 7. Three profiles correspond to seismic lines 5, 31–10 and 28–33.

The models illustrate the variability of pre Nicholson Group geology. There are substantial

thicknesses of mafic and felsic volcanics as described by Leaman (1993b). All modelling has used property values which are higher than determined for these rock associations based on near surface responses or measurements (see notes above). The susceptibility of the felsic and mafic sequences has been based on values of 0.003 and 0.005 cgs (0.045 and 0.065 SI) respectively. These are clearly extreme contrasts in terms of what is known in the McArthur Basin but are by no means atypical for the rock suites envisaged — if Isa Inlier comparisons are accepted. Use of such values does, however, mean that the interpretation may be considered to use virtual maximum contrasts and consequently recover minimum thicknesses. Given that the thicknesses implied, even with such contrasts, are large any reduction would seem to lead to incredible thickness estimates. Not necessarily unbelievable or incorrect, simply incredible. Should the contrasts employed prove to have been inappropriate then the result would be to change implied thickness, or dips within the units but would not affect the overall implications of relationships or lateral variations.

The profile interpretations provided are the result of combined analysis of both data sets.

Line 103 (Figure 8) displays quite smooth fields which require delicate balancing. The magnetic field is dominated by the thick felsic sequences which are exposed across the inlier. The discontinuity across the inlier reflects the loss of exposure due to outcrop of granite and metamorphics. The relative podding of the Cliffdale Volcanics near the inlier is clearly indicated. Overlying mafic sequences which may be directly correlated with the Peters Creek Volcanics (south) or Seigal Volcanics (north) thicken away from the inlier. The model also indicates the scale of Nicholson Group deposition and this is consistent with seismic data.

The gravity model introduces some new elements to interpretation of the region. First, the granites north and south are compositionally different whether or not these form the basement. Secondly allowance for different properties and magnetic constraints on upper sections has led to an alternative view of how to present basement away from the uplifted inlier. If we assume that the cover sequences were deposited in a rift-extension environment initially then we would also expect that the upper crustal basement sections would also be thinned and locally rotated as part of the primary extension. It is, consequently, unrealistic to portray granites as classical plutons at the margins of large basins where these might originally have been part of the stretched basement. Thirdly, different root depths are required for the granites north and south of the inlier. This is partly a function of implied contrast but the possibility of gross mantle depth change cannot be eliminated at this stage. These three effects interact to yield the model displayed which is different, in these basement terms, from previous models across the inlier. The new models could be considered to offer an alternative solution for the gross displacement model for the inlier. It is now the preferred option given the entire setting of the sequence and this more refined interpretation.

Line 104 (Figure 9) provides a first review of the seismic data (line 28–33). The model has a style comparable to line 103 but demonstrates that the lower section of the seismic profile with its strong dip character is magnetic and that the apparent basement for some of the seismic sections does include the Cliffdale Volcanics. The disturbed reflections above 2 seconds in line 28 would appear to be due to this formation. A major unconformity is implied. The mafic component can be traced into the Peters Creek Volcanics with little difficulty but the magnetic responses show that at least half of the onlapped sequence beneath the top volcanic marker must also be composed of mafic rocks. There is no possibility of fitting the magnetic field without use of the average bulk contrast applied (0.005 cgs) or with a thinner formation. The direct implication is that the unit may be thicker but there is no problem fitting extra volcanics within the seismic constraints. The regional dips implied magnetically and seismically are consistent.

The correlation between the two data sets provides some confidence in both the interpretation of either and an acceptance that the thick,

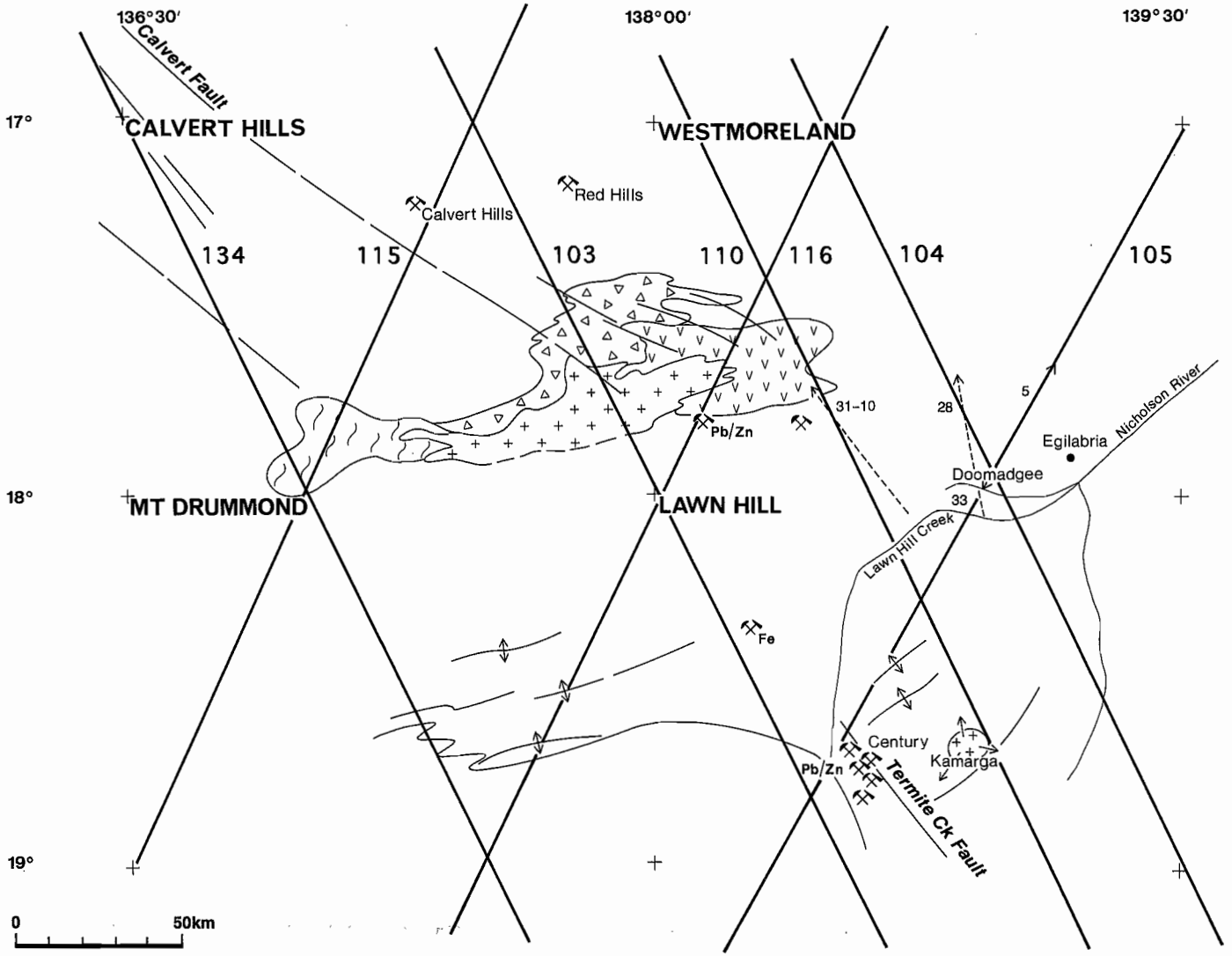

Figure 7—Locations of modelled sections Murphy Inlier — Lawn Hill region.

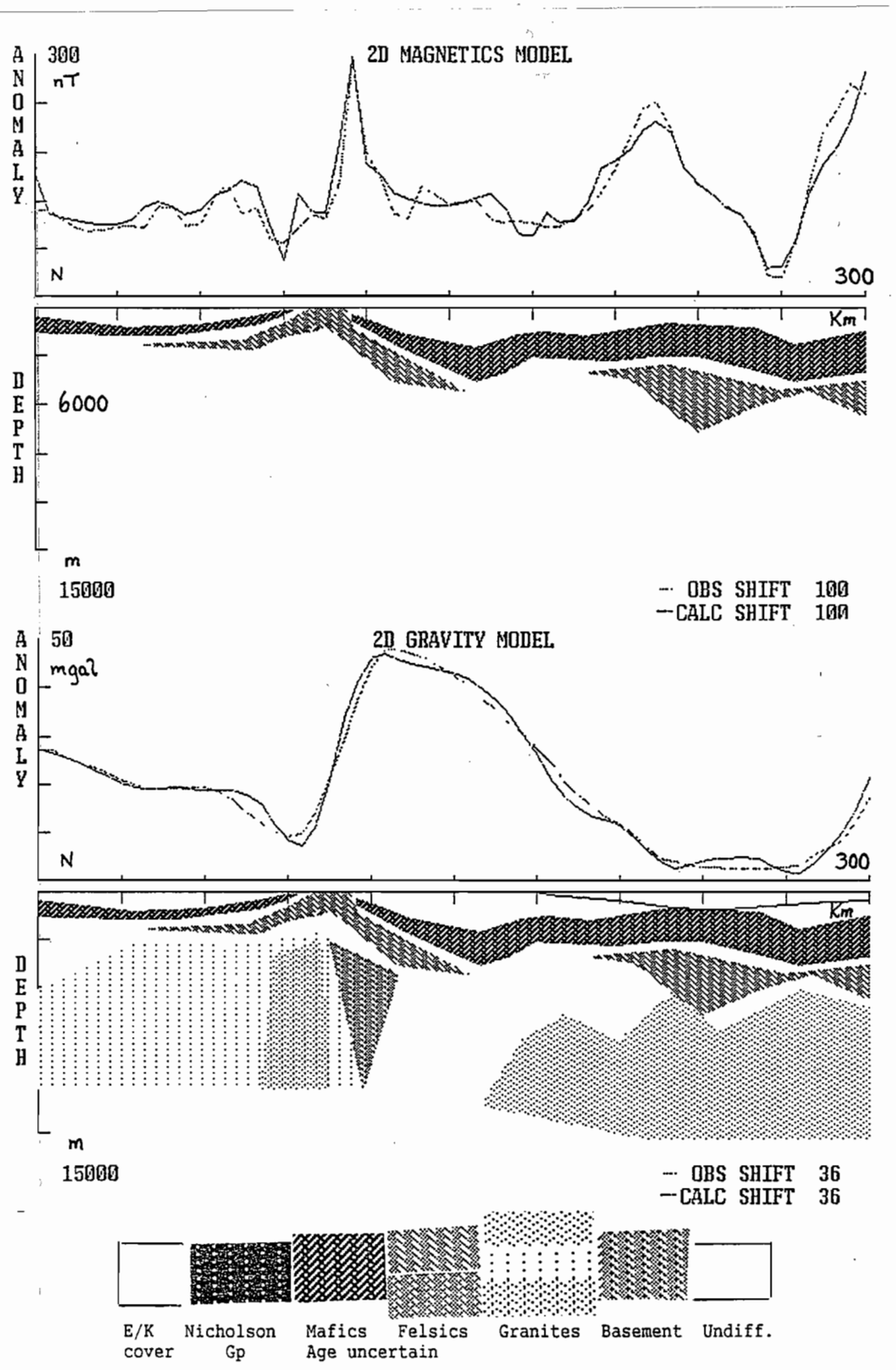

Figure 8—Gravity and magnetic models for line 103 Murphy Inlier — Lawn Hill region.

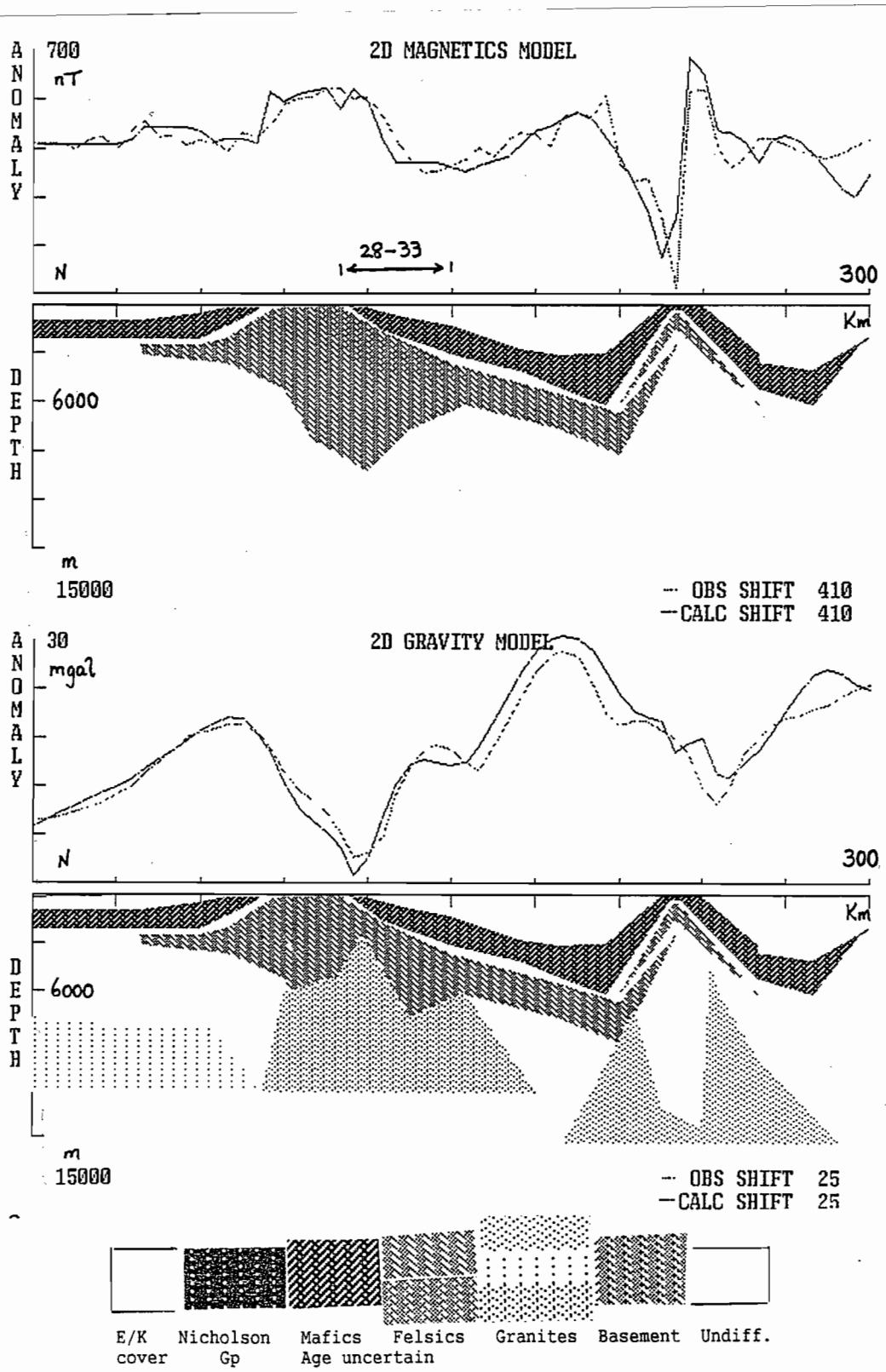

Figure 9—Gravity and magnetic models for line 104 Murphy Inlier — Lawn Hill region

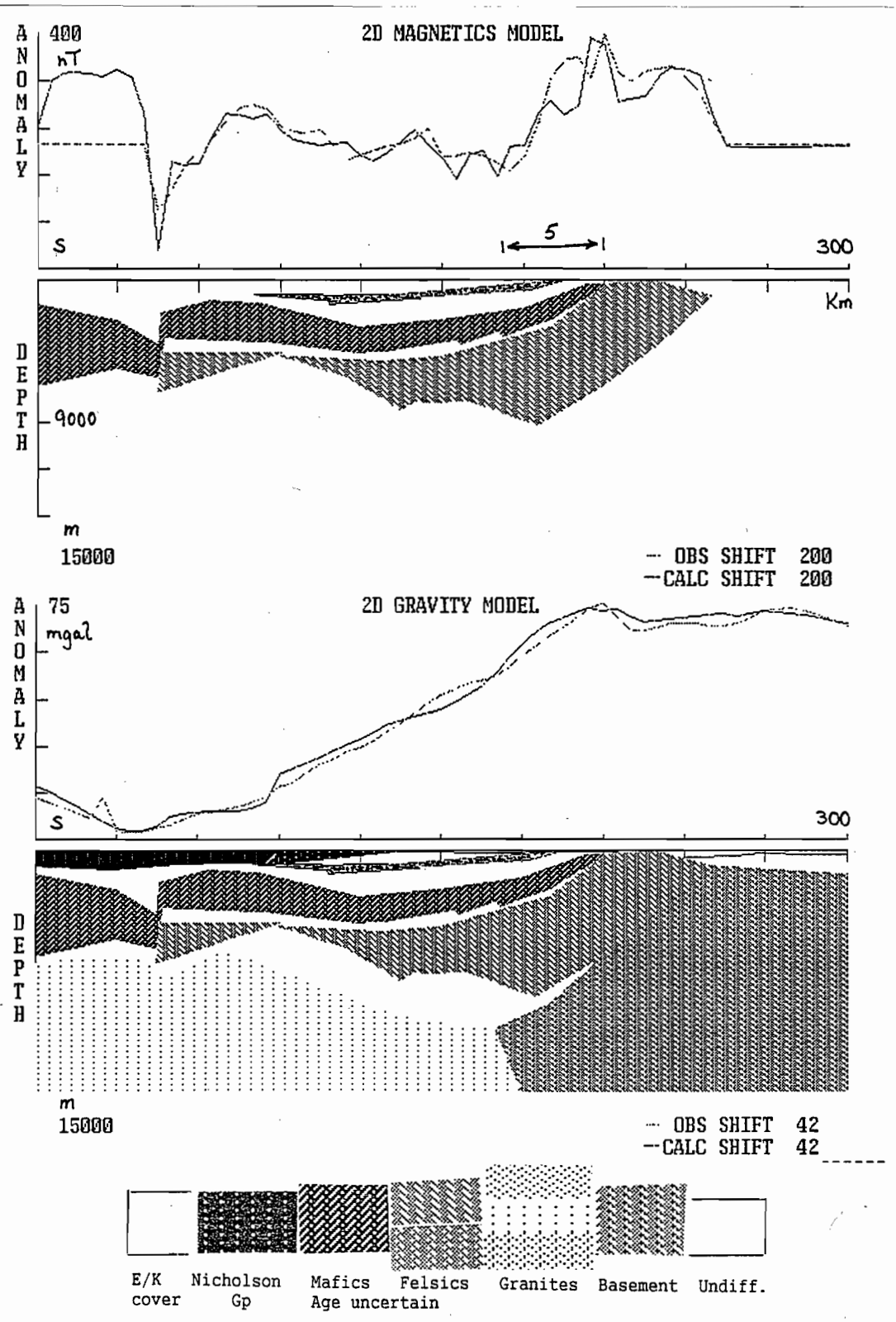

Figure 10—Gravity and magnetic models for line 105 Murphy Inlier — Lawn Hill region.

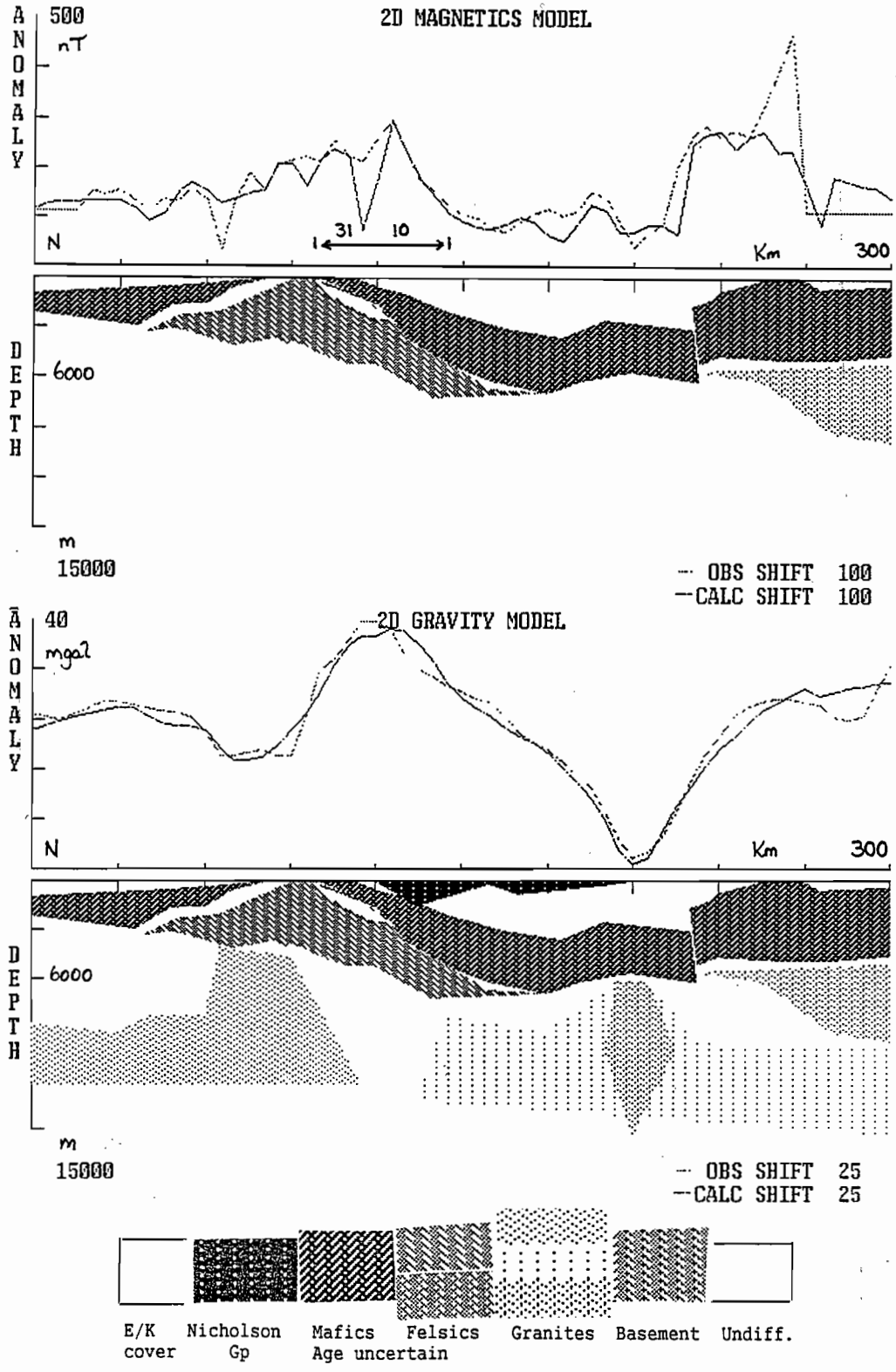

Figure 11—Gravity and magnetic models for line 110 Murphy Inlier — Lawn Hill region.

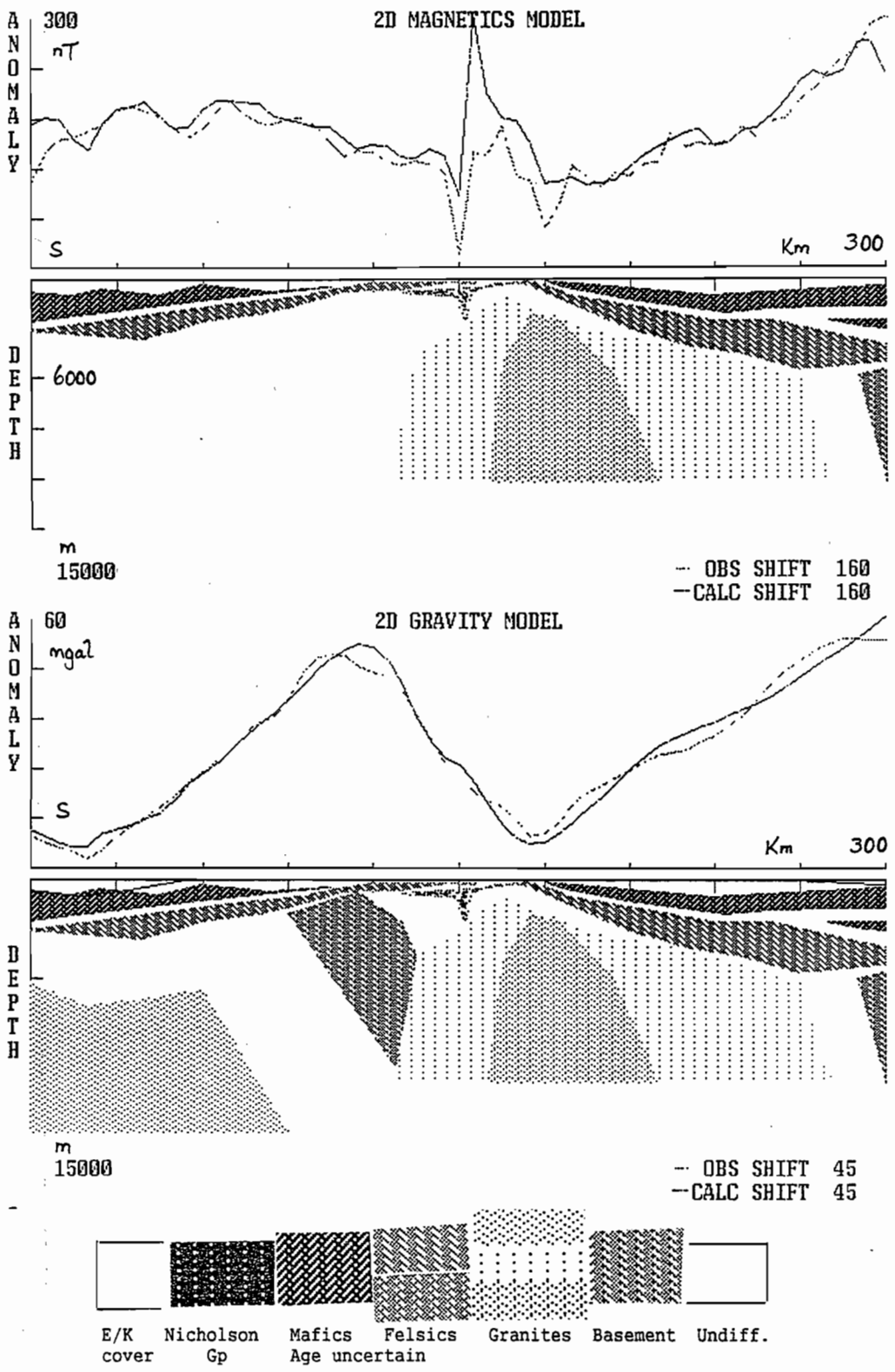

Figure 12—Gravity and magnetic models for line 115 Murphy Inlier — Lawn Hill region.

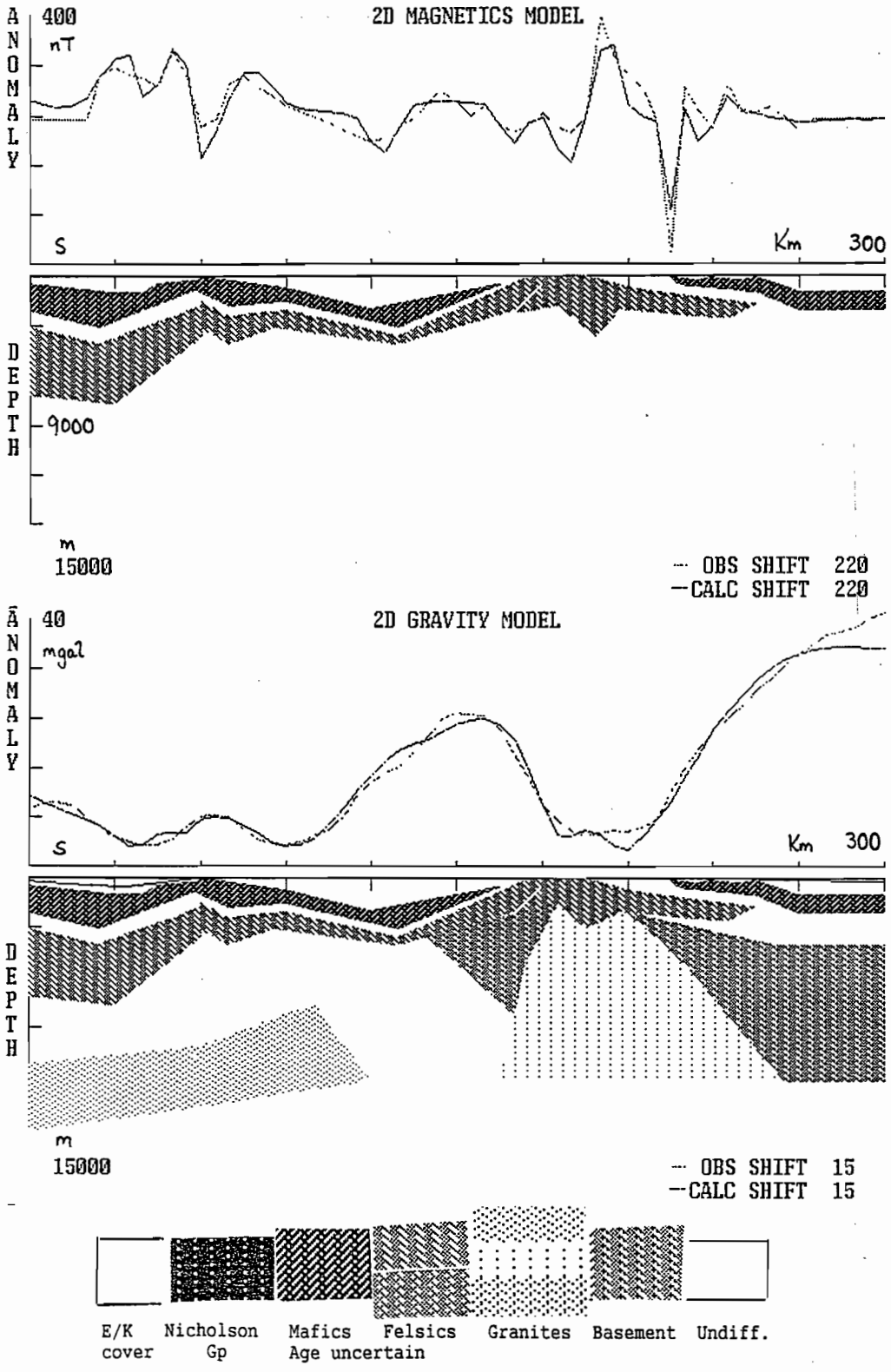

Figure 13—Gravity and magnetic models for line 116 Murphy Inlier — Lawn Hill region.

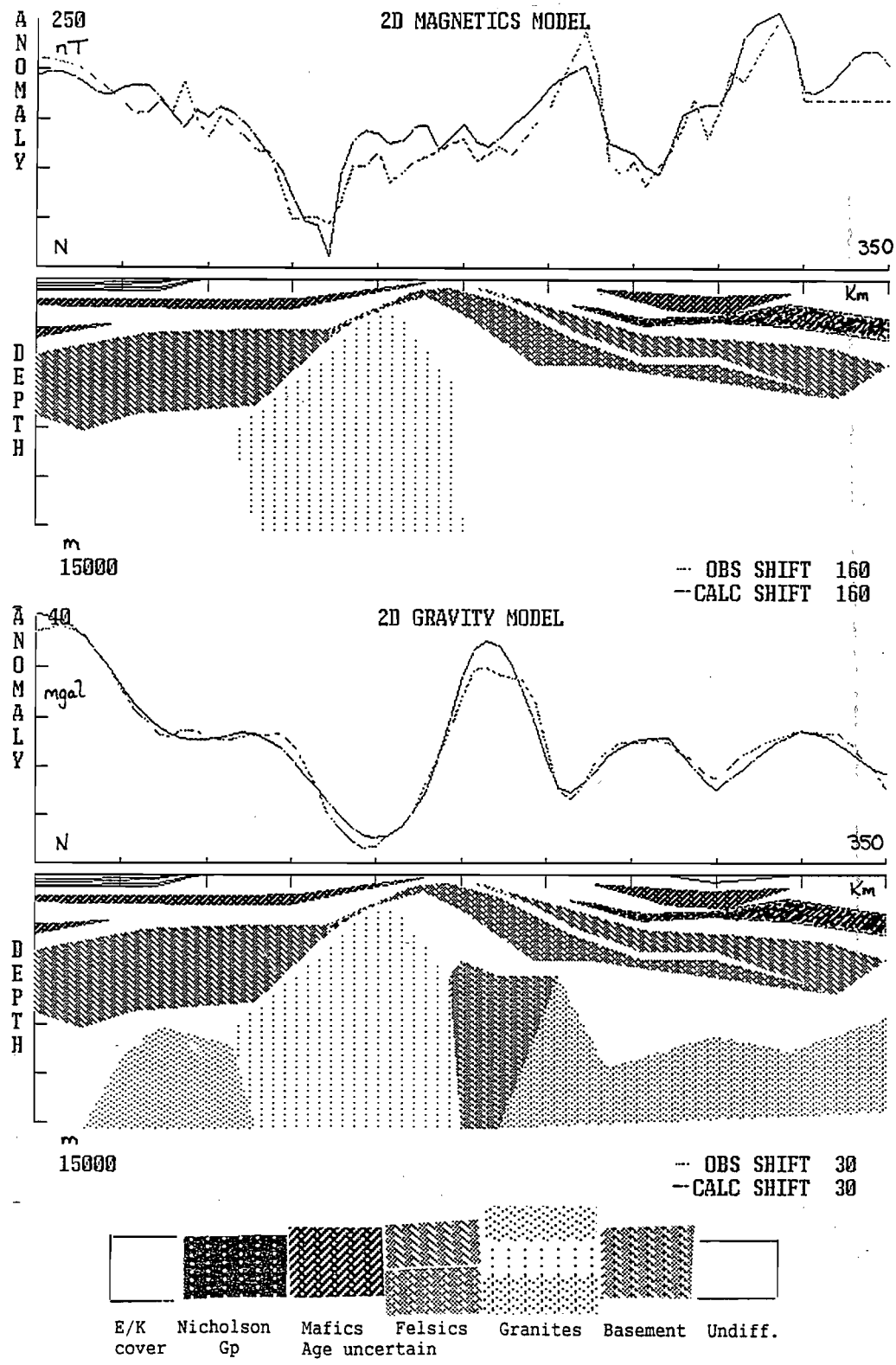

Figure 14—Gravity and magnetic models for line 134 Murphy Inlier — Lawn Hill region.

apparently conveniently onlapped, mafics are indeed present and are part of the basin sequence.

Differences in the granites are also confirmed by this section. The volumetric constraints offered by the seismic data when coupled with the magnetic data allow sufficient control to enable the gravity data to resolve the granitoids.

The two data sets draw attention to the possibility that the volume of felsics is both compound and difficult to properly appraise. This is evident just south of the inlier where the gravity model requires that part of the magnetic volume include granite. This complex relationship produces a section with mid level mafics, deeper felsics and perhaps a largely felsic basement intruded by granitoids. This is consistent with all the seismic inferences.

Line 105 (Figure 10) provides a correlation with seismic line 5. This section confirms the nature and composition of the seismic basement; Cliffdale Volcanics. It also shows how the Peters Creek Volcanics vary away from outcrop near the Fish River Fault.

This model is also important since it samples only the southern granites and shows that the basement to the north is denser than elsewhere. It may be argued that appropriate balancing of granites and dense basement could occur elsewhere and might not be resolved. This is a valid argument which might be applied to an individual section but many sections show that there is rarely the space to balance alternate masses with credible density contrasts along the length of the section. The interpretation, as a whole, has only found this possible either at the inlier itself or far to the north and east — as in line 105.

The model also includes some shallow, magnetic sources. These could be included in all sections and some examples are provided below. These sources correlate with the thin and variable volcanic members of the Tawallah Group and are not significant in terms of the regional models discussed here. These sources, however, are largely responsible for the localised high relief and high frequency character often noted in the magnetic maps (e.g. Calvert Hills, Figure 2).

The seismic data along line 5 display several half graben forms and these are required to satisfy the magnetic field. The correlation between structural geometry and magnetic response confirms the suggestion made for line 104 that the bulk of the lower basin sequence is composed of mafic volcanics.

Line 110 (Figure 11) can also be compared with seismic data (line 31–10).

This model has some important consequences since it includes the well-displayed basal pile within the basin sequence and this is shown to be magnetic. The properties are not consistent with the Westmoreland Conglomerate and are more typical of the Cliffdale Volcanics. Since the underlying "basement" is also magnetic it is likely that this section has captured the two variations of the felsic volcanics exposed on the inlier and that there is a major interval between their formation.

All models show that the basal volcanics are piled near the inlier and must once have been very thick if the persistent rejuvenation of the inlier has occurred. Nor should it be assumed that the lower volcanics are not part of the rift onset sequence simply because there is a major discontinuity between them and the distinctive cover packages. A similar relationship may exist within Bass Basin between various parts of the Cretaceous section and the overlying Tertiary cover sequences. The suggestion of regular dip, is not inconsistent with such a view.

The model also suggests the nature of thickness variations within all volcanic members including the Peters Creek Formation. Major changes are evident in the Kamarga region and the section is transformed across the nominal position of the Termite Creek Fault (230 km on the section).

The model also stresses differences in granitoids across the inlier.

Line 115 (Figure 12) essentially confirms the implications of previous models even though displaced nearly 150 km to the west. The exposed inlier forms an important component in the gravity model. All other features are consistent.

The volumetric subdivision of both the thickened felsic and mafic suites may be queried. It is

possible to exchange part of the volume of one for the other and still fit any given profile. The models shown, however, must also satisfy tie line conditions and these constrain the volumes which can be exchanged. The compositional and contrast balance also restricts alternatives. The models indicate realistic and consistent proportions and accurately portray thickness trends while not necessarily delivering precise thickness estimates. The gravity solution is important in that it may exclude many extreme or strongly variant options. If the thickened mafic element at the north end of this line were replaced by a uniform thickness of mafics and an increased thickness of felsics then the volume required would not allow any consistent fit, regardless of depth of roof, for the underlying granite which is known to approach surface off section along the inlier. Such a solution may, therefore, be excluded.

Line 116 (Figure 13) interlocks several other sections and shows how the underlying granitoids must be balanced with basement contrasts — including those across the inlier itself. This section shows that no special pleading is required to explain all characteristics of both fields and the geology of the inlier. It effectively excludes the inlier displacement model.

Line 134 (Figure 14) across the Carrara region of the Mt Drummond sheet allows some appraisal of the inlier and the continuity of the volcanic suites. It shows that the lower felsic volcanics are variable in thickness and variable in magnetic contrast and can be distinguished from the upper units.

All modelled profiles interlock consistently, in so far as resolution and 2D effects allow, and a series of structural contour surface maps have been produced for each major unit or variation Isopachs have also been extracted for both felsic and mafic piles. These isopach maps are presented as Figures 18 and 21 but it should be noted that these depend on judgments about best estimates at each line intersection and may not be fully consistent with the differences implied between the maps showing upper and lower surfaces. All contour maps are smoothed or integrated versions of the inferences of the interpretation and may locally be uneven in reliability.

The implied relief on the roof of the basement granites is shown in Figure 15. This diagram also shows the variation in granite type and the location of very low density, obviously highly siliceous and possibly young, phases. It also suggests the limit of basement density changes and the approximate depth to basement in areas of anomalous basement. No part of the basment complex, with the exception of the northern granite, is significantly magnetised.

The depth to the upper surface of the main mafic unit is shown in Figure 19. This map may include some deviation due to inclusion or omission, or confusion with, some of the thin, shallower volcanic members. The important aspect of this map relates to the differences north and south of the inlier. The disrupted nature of the unit, and the structure as a whole, south of the inlier can be contrasted with the regular forms to the north across the Wearyan region.

Similar character is evident in the form of the basal surface (Figure 20) which also shows that the thickness of the unit is much more variable to the south. This change must reflect both a primary change in thickness and a very active erosional and structural history. The thickness of the mafic column increases rapidly to the SE (Fig. 21) and the link, yet to be absolutely established between Peters Creek and Eastern Creek Volcanics, seems ever more likely.

The nature of the upper surface of the felsic volcanics, treated as a single entity for simplicity, is shown in Figure 16. This has a character very similar to the base mafics. The nature of the base felsics (Figure 17) is quite distinctive. It is regionally irregular and of very high relief. This is consistent with the formation of these piles within primary rift stages and substantial local preservation. Maximum thickness estimates are very similar regardless of sub region. The contrasts and similarities between surfaces suggests that the major erosional events preceded the mafic units and this is wholly consistent with the seismic implications.

It is also probably significant that some of the

thickest felsic accumulations remain along strike from the more emergent part of the Murphy Inlier. Other thick accumulations occur NW of the inlier in the region of the present Calvert Fault, but the form of the deposits remaining bears little relationship to its orientation, and in the region SW of the Termite Creek Fault.

Figure 22 presents a summation of cover (Cambrian and post Cretaceous) variations.

Some consistent trends may be recognised in these diagrams. Figure 23 presents a compilation of all trends recognised either in raw data or the surfaces interpreted.

The granite surface is dominated by the sub E–W trend now occupied by the inlier and the controlling structure clearly extends beyond the area reviewed. Few other trends can be unambiguously identified.

The major basement change is oriented normal to the granite grain (NNW) and this might suggest that these two trends are primary and original in the crust of the region. This gross change has a trend which can be traced north to the gulf and was previously shown to mark the margin of the granitic part of the basement to the Wearyan Shelf. This NNW trend is also parallel to the Emu Fault system and is clearly an important regional control.

The base of the felsic volcanics also reflects both these trends. Several NNW segments are evident. Only one significant NW–SE feature is apparent in Figure 17 and this extends right across the region. The upper felsic surface is dominated by the sub E–W elements and the NNW or NW features are muted. The thickness map recovers both trend systems while stressing an additional sub E–W trend south of the inlier. The inlier itself is not defined by this presentation.

The base of the mafic volcanics do not reflect clearly any trend system other than sub E–W although the region south of Lawn Hill station does reveal some NNW trends. This is the zone in which thick felsics and mafics have been preserved. The upper mafic surface, while much more disrupted — clearly by low relief folding and faulting which is much younger — does suggest some NE elements and one significant NW trending element in the region of the Termite Creek Fault. This latter trend is anomalous within the context of all character mapped by this interpretation.

Mafic thickness variations, however, tend to stress both the sub E–W regional forms and, south of the inlier, older NNW trends.

These patterns present some very interesting correlations with younger structuring, such as the post Nicholson Carrara Range folds which disrupt the region south of the inlier. The zone in which the felsics are thinnest corresponds exactly to the most disrupted portion of the Carrara region.

The Fish River Fault system is a rejuvenation of the major boundary between basement and granite systems and the limits to the uplift of the inlier have been prescribed by the position of the main NNW change in the basement complex. This change also limits the downwarped portion of the area which now carries the Cretaceous cover and restricts the extension of the E–W fold systems to the east.

Figure 23 also suggests the differences in fracture patterns across the inlier and that whilst several can be traced across all have been modified in intensity and orientation. This reflects the gentle and persistent uplifts which have marked this zone.

Direct controls on younger basin development are also evident, including the Nicholson region and the much younger Georgina and Carpentaria structures. These present shapes and patterns which are consistent with slow uplift and subsidence in association with the major elements described above.

Mineralised sites have been marked on all diagrams and it is evident that the major base metal deposits of the Kamarga–Century area are not some random occurrence. The Silver King–Century zone in particular has been active and is marked by a concentration of major fractures, a fan of trend changes, and lies adjacent to major volcanic systems — each of which was controlled by structures active during formation. This is especially true of the felsic suite. The Termite Creek Fault is a rejuvenation, or a flower projection, of this underlying structural net.

Other mineralisation (such as Constance Range)

is related to the projection of this fracture system and the Carrara axis or the intersection of the primary basement change and the Fish River system near the southern face of the inlier.

These relationships are too clear to be ignored or random but their style and type is unlikely to occur anywhere in the Calvert Hills sheet, further north in the Westmoreland sheet or across much of the Mt Drummond sheet. Some critical intersections may exist in the Lawn Hill sheet — such as along the Carrara trend — but these do not possess the volcanic history of the Century zone. It is assumed here that the felsic history is the more important for Pb–Zn mineralisation although it is possible that Cu mineralisation may be related to the basement boundary zone which is associated with active changes in mafic volcanism.

This interpretation includes a revision and an update of previous analysis in the vicinity of the Murphy Inlier. This reflects the inclusion of much more data and the application of tighter constraints which have been suggested by other parts of the McArthur Basin study. The revised solution is considered more realistic. These comments also caution about a common status in interpretation; that the first solution is assumed to be wholly correct. There is always a case to review and revise as more data are included and where direct links can be made to solid geological control. The generally flat-lying McArthur Basin rocks do not provide this form of control directly and this interpretation sequence began at the heart of the basin. However, the restraints imposed from the western and eastern margins suggest that the entire body of the analysis is generally supportable and viable irrespective of this lack of control at its heart. Moral: all interpretations should be subject to review and revision and the present status of this work should be accepted on its declared basis as indicative.

References

Leaman, D.E., 1992. Regional geophysics — basin architecture #1. Report 1, Amira P384.

Leaman, D.E., 1993a. Batten Trough region, update and further analysis. Report 2, Amira P384.

Leaman, D.E., 1993b. Do volcanic piles really exist? Report 2, Amira P384.

Leaman, D.E., 1993c. Criteria for evaluation of potential field interpretations. Report 2, Amira P384.

Leaman, D.E., 1993d. Regional geophysics—basin architecture #3. Report 2, Amira P384.

Leaman, D.E., 1993e. Issues: basin correlations and overall architecture. Report 2, Amira P384.

Leaman, D.E., 1993f. Regional geophysics — basin architecture #4. Report 4, Amira P384.

Leaman, D.E., 1994. Application of magnetics to basin structures. Report 6, Amira P384.

McConachie, B.A., Barlow, M.G., Dunster, J.N., Meaney, R.A., & Schaap, A.D., 1993. The Mount Isa Basin — Definition, structures and petroleum geology. *APEA Journal*, 33, 237–256.

Plumb, K.A., 1988. Geology of the McArthur Basin. 1: 1 000 000 map. BMR.

Plumb, K.A., & Derrick, 1975. Geology of the Proterozoic rocks of the Kimberley to Mount Isa region, in *Economic Geology of Australia and Papua New Guinea, Vol 1, Metals* (Ed. C.I. Knight), pp. 217–252 (The Australasian Institute of Mining and Metallurgy, Melbourne).

Plumb, K.A., & Wellman, 1987. McArthur Basin Northern Territory. Mapping of deep troughs using gravity and magnetic anomalies. BMR Journal Geology and Geophysics. 10, 243–252.

Plumb, K.A., Ahmad, M., Wygralak, A.S., 1990. Mid Proterozoic Basins of the North Australian Craton — Regional geology and Mineralisation. *In* Hughes, F.E. (ed.) *Geology of the Mineral Deposits of Australia and New Guinea.* Aust. I.M.M. 881–902.

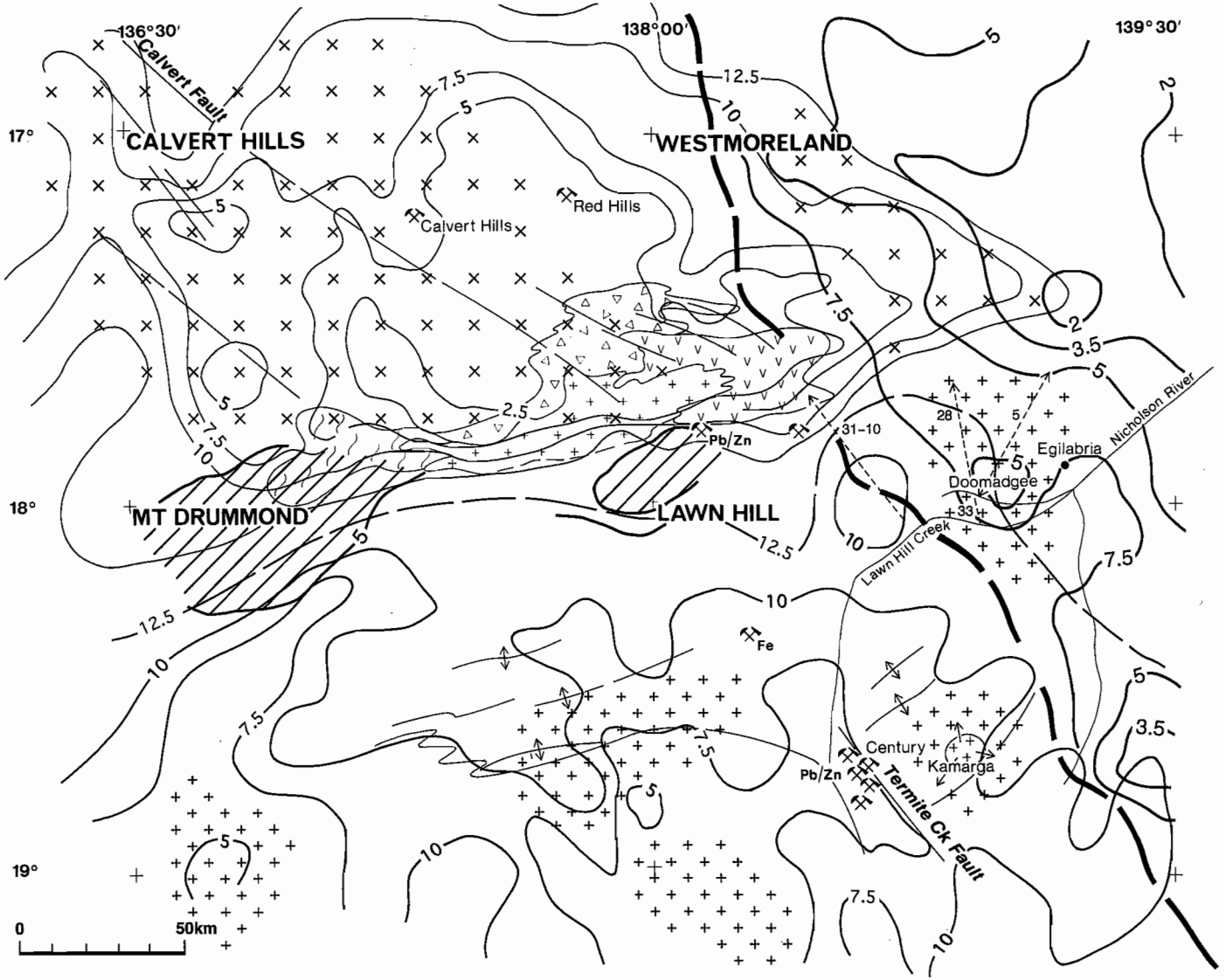

Figure 15—Distribution and form of basement and other granitoids and primary change in basement composition. Contours in km. Murphy Inlier — Lawn Hill region

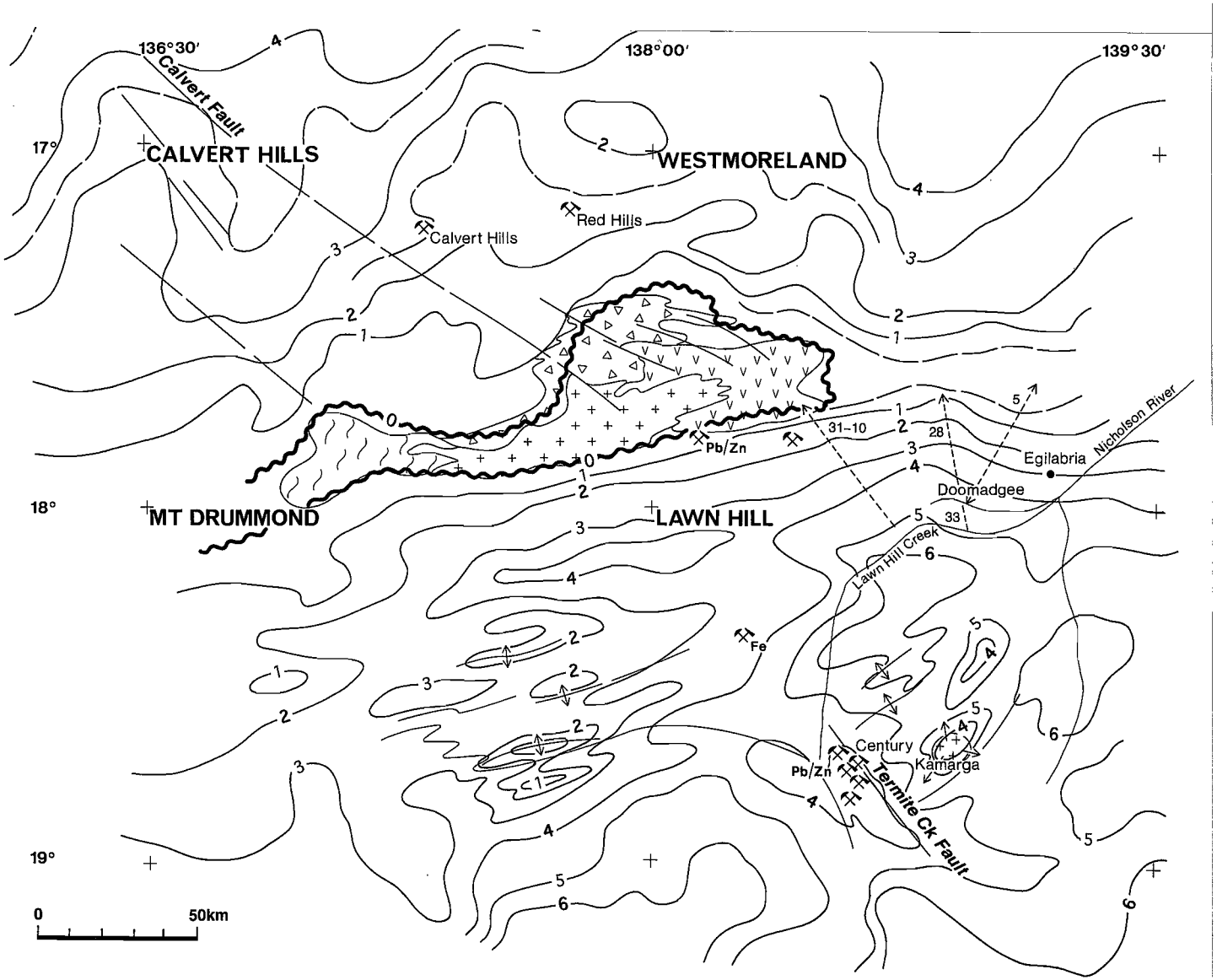

Figure 16—Indicative depth of upper surface of felsic volcanic sequence (contours in m) Murphy Inlier — Lawn Hill region

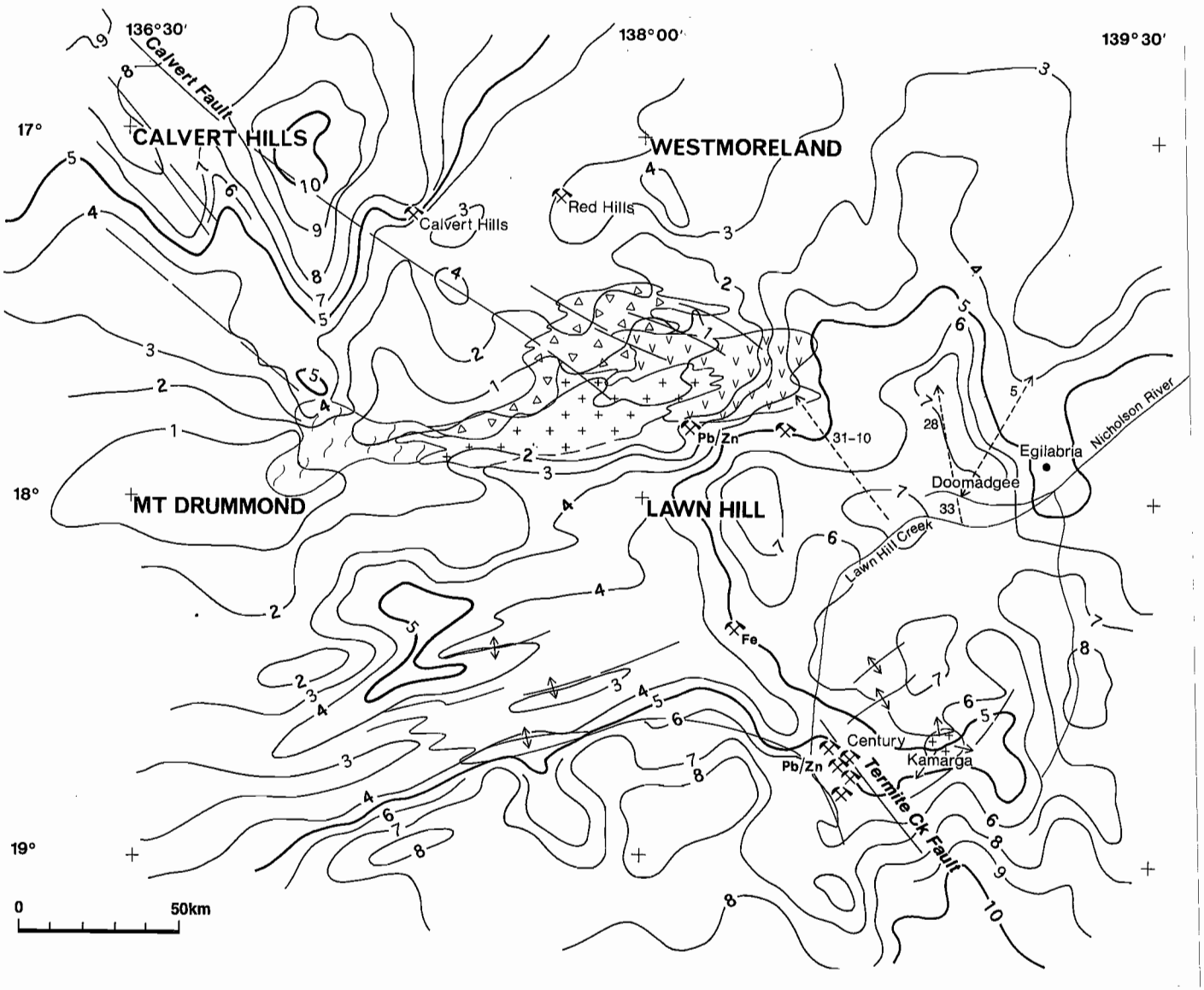

Figure 17—Indicated depth of lower surface of felsic volcanic sequence (contours in m) Murphy Inlier — Lawn Hill region

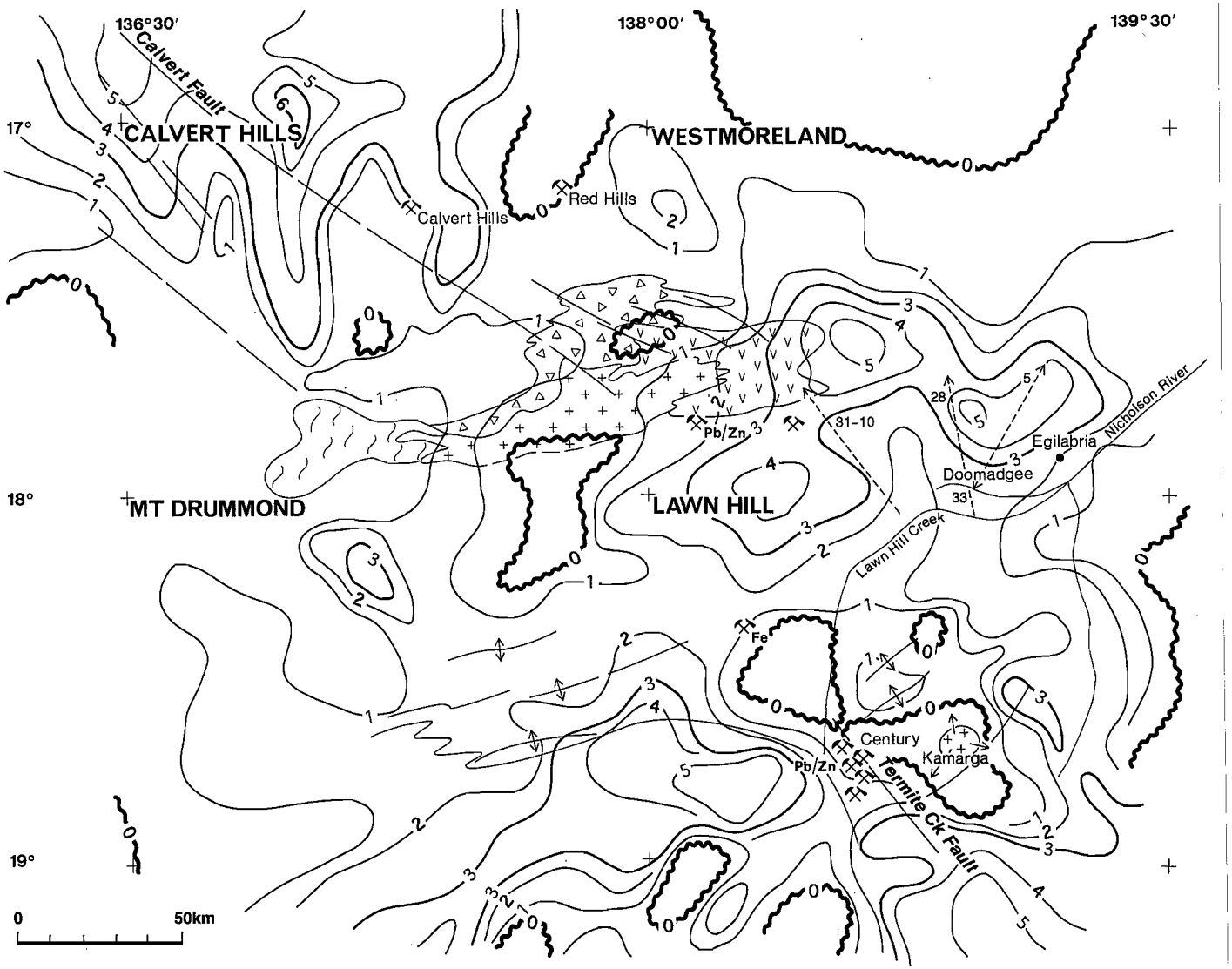

Figure 18—Estimated bulk thickness of felsic volcanic sequence (contours in m) Murphy Inlier — Lawn Hill region

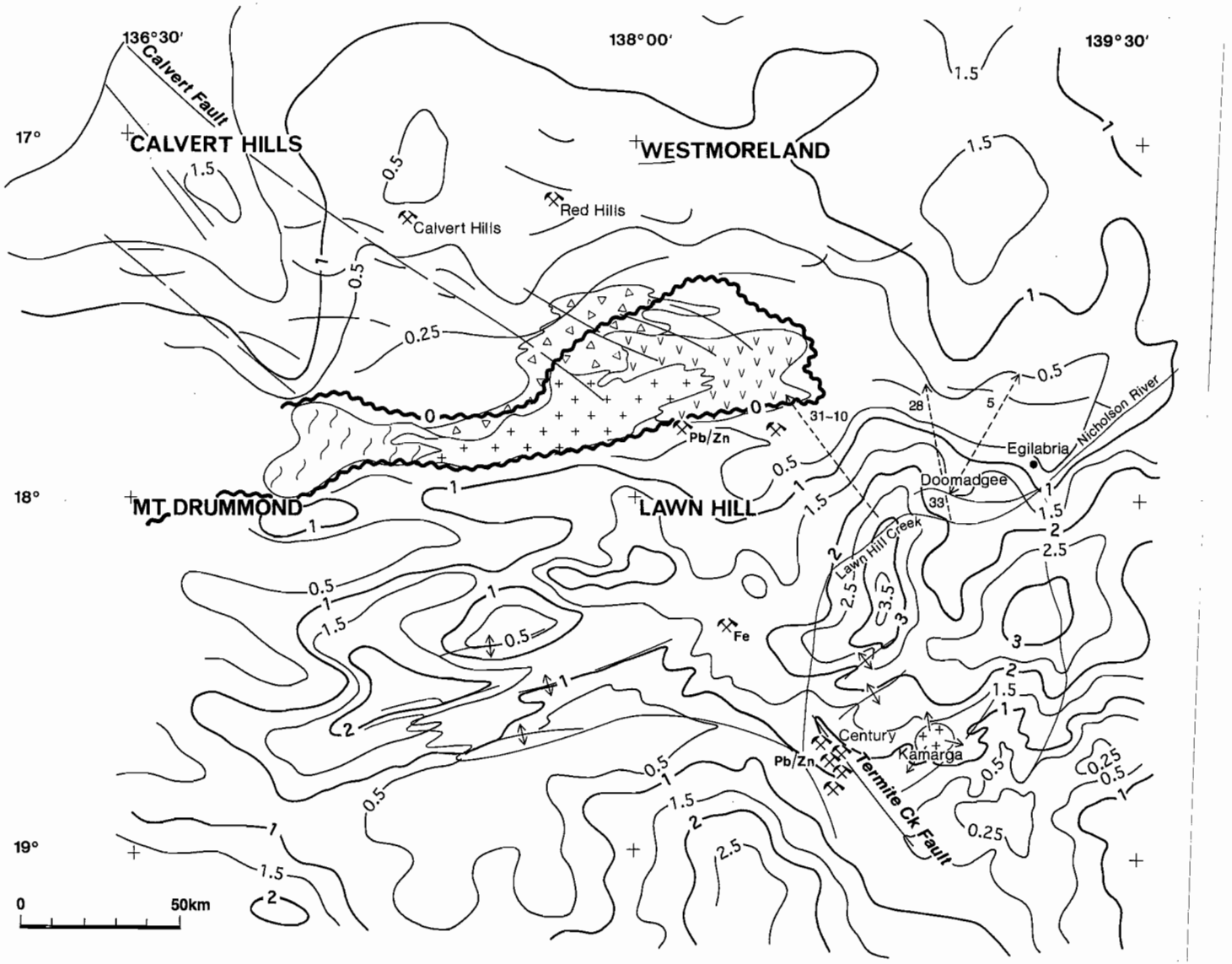

Figure 19—Indicated depth of upper surface of mafic volcanic sequence (contours in m). Main mafic pile only; subsidiary, thin high level mafic units have been excluded wherever possible. Murphy Inlier — Lawn Hill region

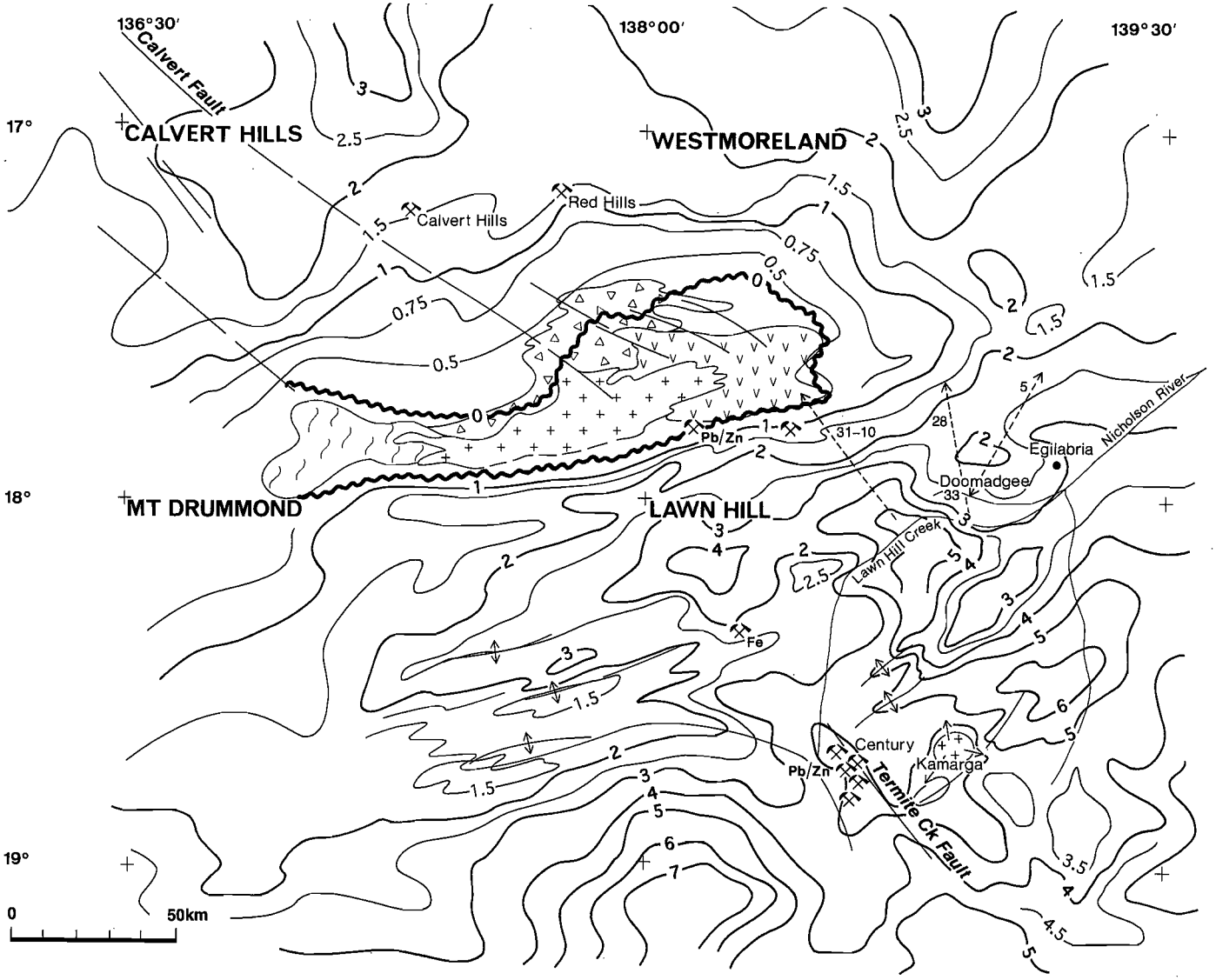

Figure 20—Indicated depth of lower surface of mafic volcanic sequence (contours in m). Murphy Inlier — Lawn Hill region

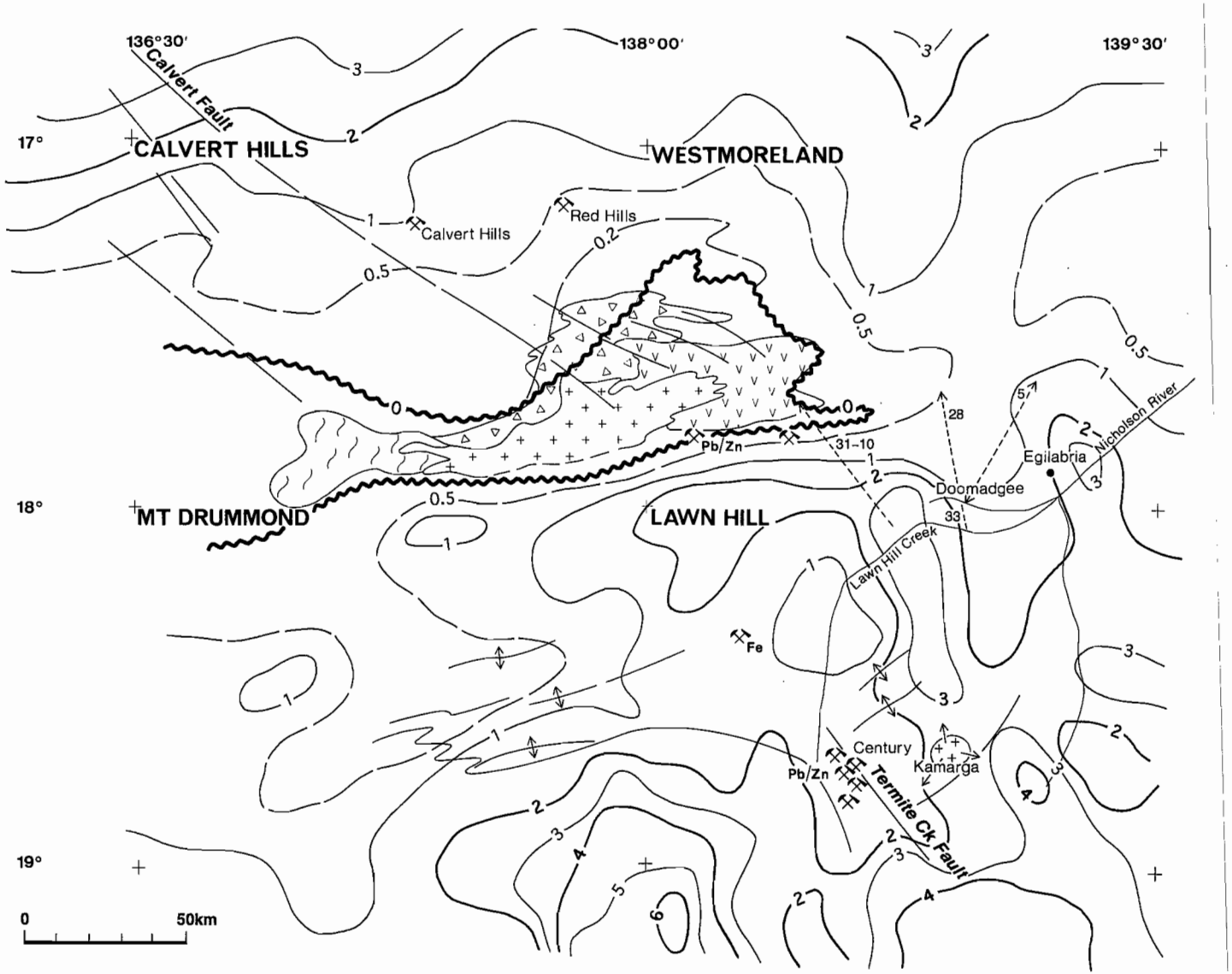

Figure 21—Estimated bulk thickness of all mafic rocks in section (contours in m) Murphy Inlier — Lawn Hill region

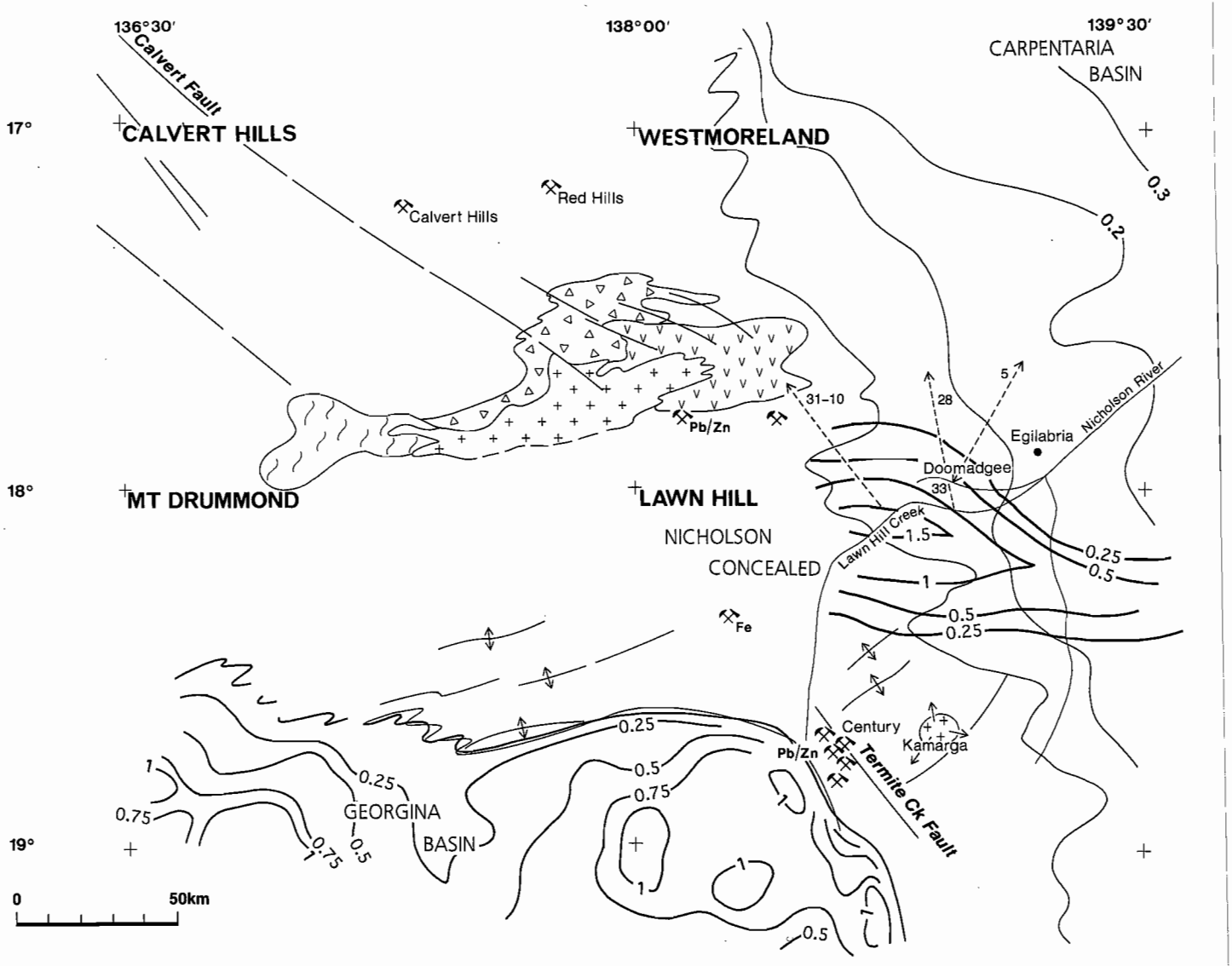

Figure 22—Interpreted distribution of younger cover sequences. Thickness estimates (depth to base from surface) in m. Murphy Inlier — Lawn Hill region

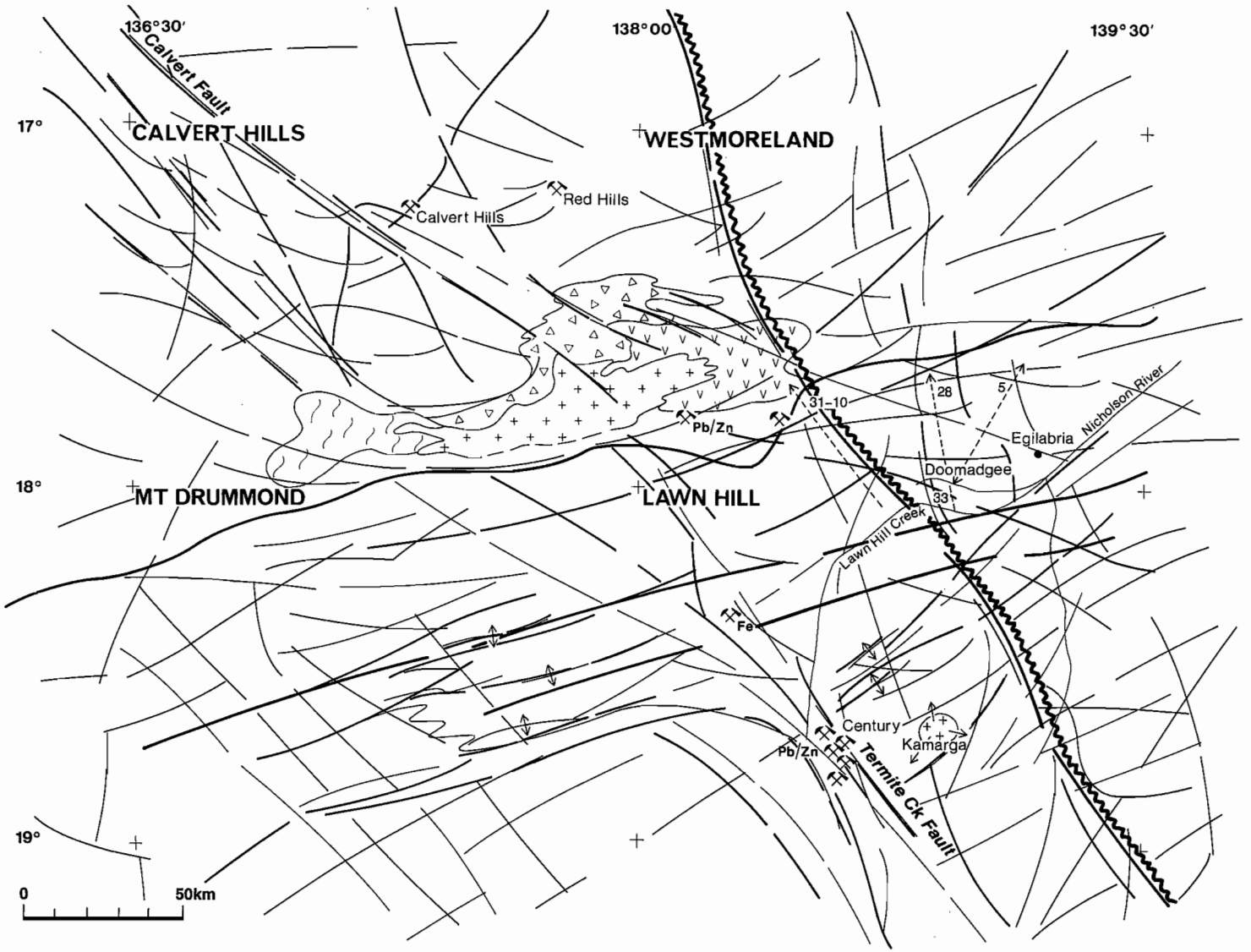

Figure 23—Trends and structural controls interpreted for Murphy Inlier — Lawn Hill region.

A preliminary structural analysis of the Riversleigh Fold Belt (formerly Lawn Hill Platform) with special reference to structures around the Lady Loretta deposit.

Richard A. Keele
Centre for Ore Deposit and Exploration Studies

Introduction

The Riversleigh Fold Belt (formerly the Lawn Hill Platform) has been sub-divided into three regions based on differences in structural style and history (Figure 1); these include:

1. Lady Loretta high strain zone which is principally due to E–W compression; this zone has been in the past incorrectly referred to as the Paradise Creek Graben.
2. Redie Creek Platform which is dominated by a number of W to WNW–trending thrusts.
3. Fiery Creek Dome which had largely been protected from the effects of the Isan orogeny by two major orthogonal wrench faults.

Regional compression in the region has been transferred away from the Lady Loretta high strain zone along an (as yet) unnamed NE dextral wrench fault and the Termite Range Fault (Figure 1). The age of the compression in the Fiery Creek Dome is unconstrained since it does not involve thrusting; however, as it bisects the measured D_1–D_2 stress directions for the rest of the fold belt, it can be assumed that this direction was relatively stable whilst the Isan Orogeny was busy elsewhere.

A regional axis, defined by the culmination of N- and S-directed thrusts, passes just south of the Lady Loretta Pb–Zn deposit and through the Lady Annie Cu deposit (Figure 2). North of this axis folds plunge to the north; south of it they plunge to the south. The axis is offset northwards as it passes across the high strain zone indicating that it was affected by all subsequent deformations. Consequently, one of the principal causes of F_2 plunge reversal is the region is the presence of this early axis. A D_1 structure (e.g. Redie Creek Fault, Leopard Fault and an offset on the Russell Creek Fault) may be traced for a distance of 50 km across the region. The potential for early E–W structures to focus mineralising fluids is highlighted by the spatial association between ore occurrences and this axis.

Sequence of Events

Three main periods of deformation are recognised. The first comprises extensional faults, with their mildly inverted equivalents, related to the changeover from a rift to a passive margin setting on the platform (Dunster and McConachie, in prep). This period covers the boundary between the Leichhardt and McArthur Events and Sequences (Etheridge and Wall 1994). The second comprises a NW–SE compression event, also present in the southern McArthur Basin (Keele 1993), that corresponds to inflexion (I_2) in the polar wandering curve for Proterozoic northern Australia (Loutit et

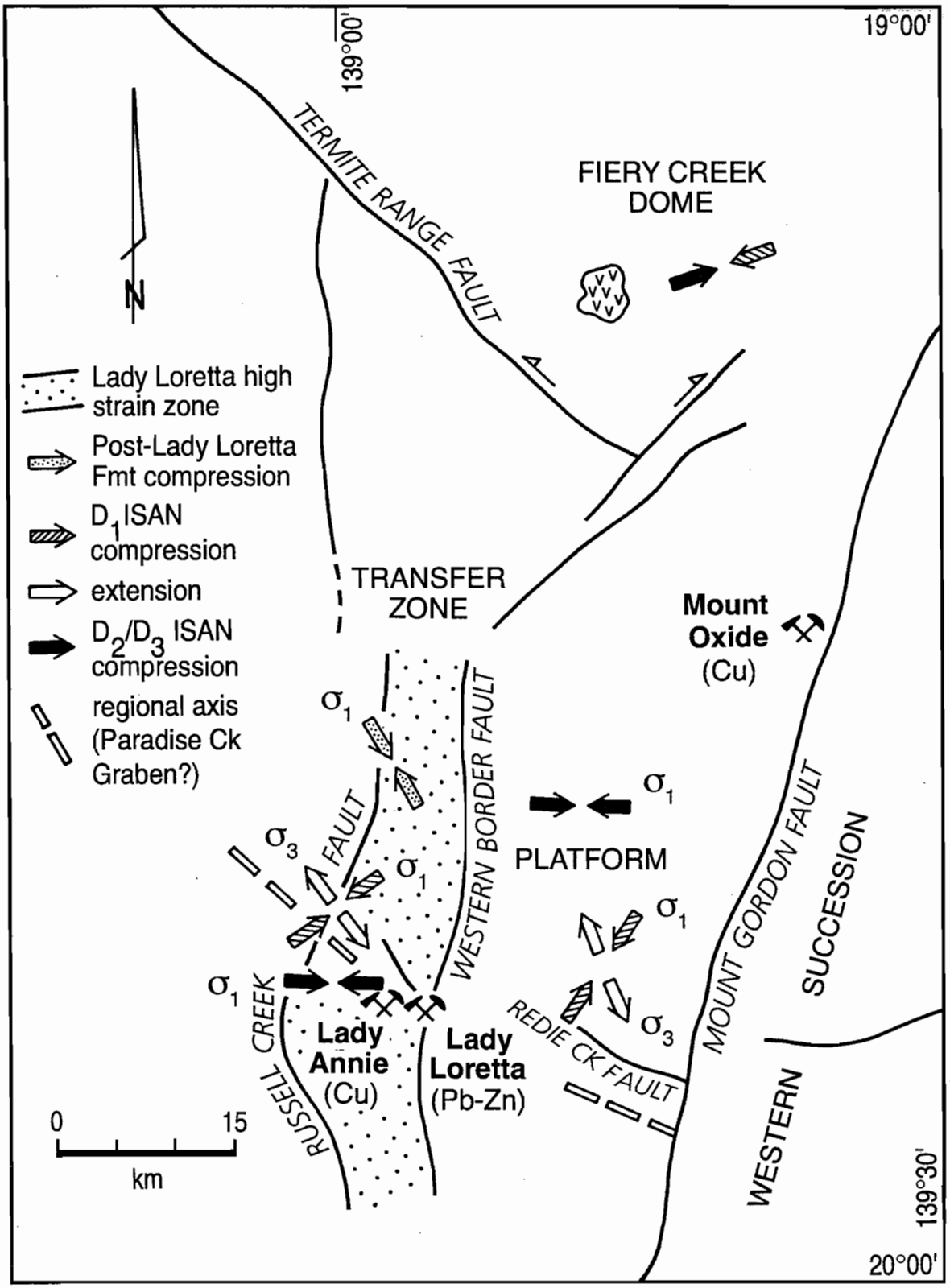

Figure 1—Structural sub-divisions in the Riversleigh fold belt. The calculated palaeo-stresses directions in three domains are shown by the arrows. The earliest brittle faulting event (NW-SE compression) has only been observed in the Lady Loretta high strain zone. This event is tentatively placed between the Lady Loretta Formation and the Shady Bore Quartzites.

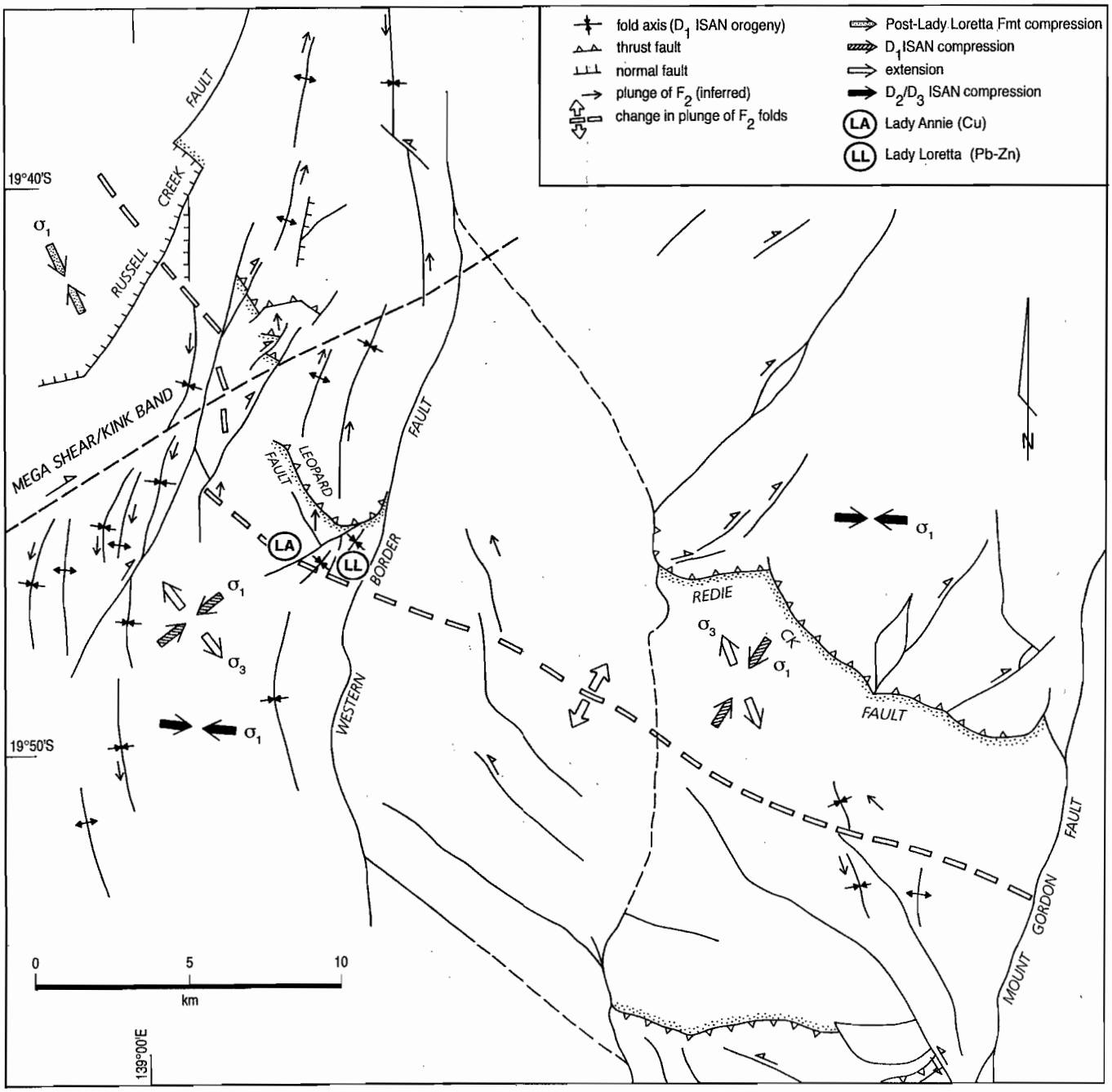

Figure 2—Simplified map of structures in the Lady Loretta region. The WNW-trending culmination axis that passes through the Lady Annie copper deposit is related to D1 thrusting during the Isan Orogeny. A thrust lying to the north of the axis (highlighted by stipples) may be traced across the whole region.

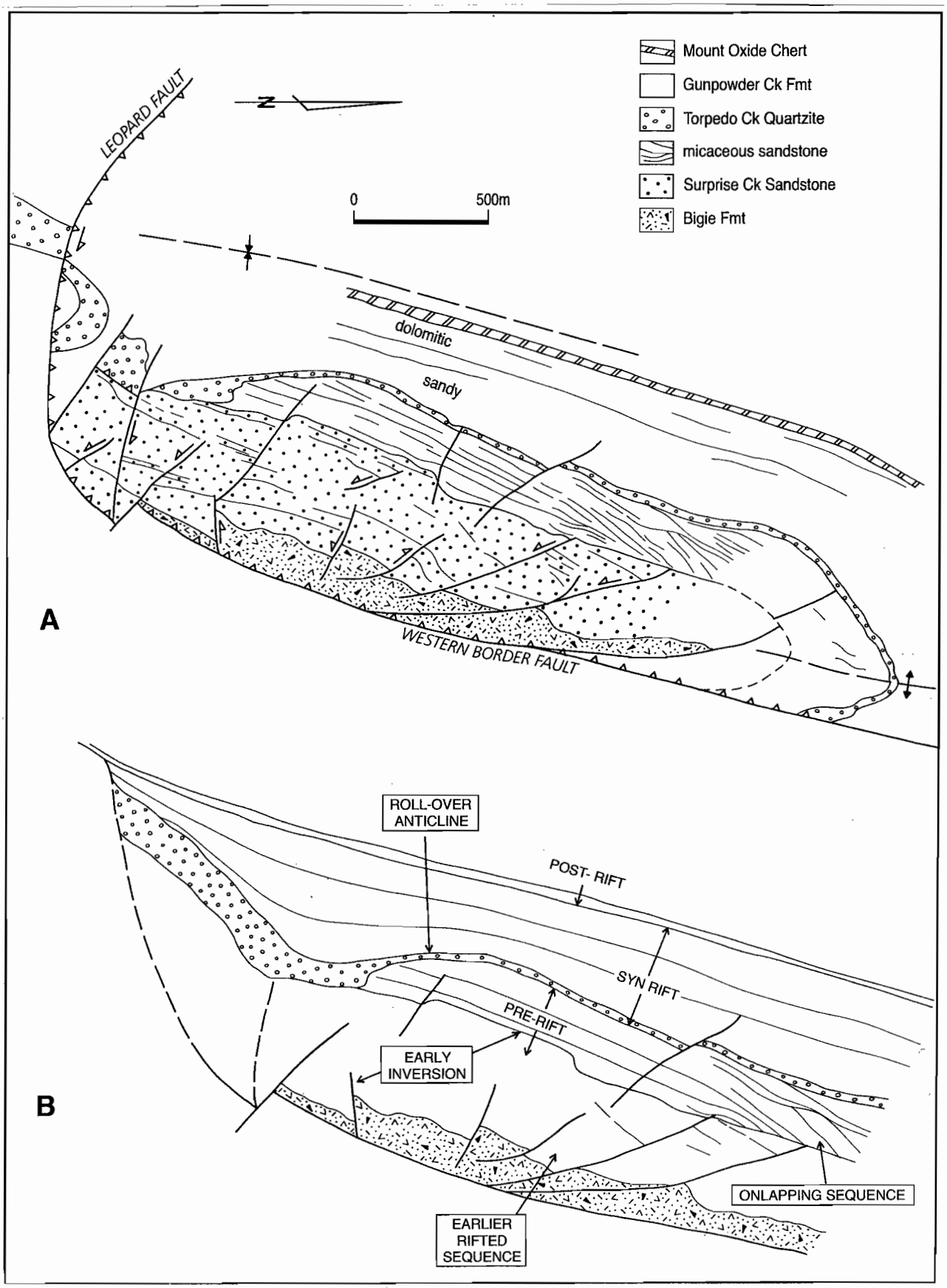

Figure 3—(A) Photo-geological interpretation of the quartz sandstone outcrops north of Lady Loretta. The Leopard Fault is folded into a syncline although only the east limb is shown. The stratigraphy ranges from the Bigie Formation as the base to the Mount Oxide Chert at the top. (B) Partial reconstruction of interpreted growth faulting on the Leopard Fault. Note the roll-over anticline and the minor inversions on the early rift faults.

al. 1994). This period also corresponds to the sinistral transpressive movements on the Emu Fault which were responsible for the HYC Pb–Zn mineralisation (Hinman et al. 1994). The third group relates to the Mount Isa Orogeny (Blake and Stewart 1992).

1. Leichhardt/ McArthur Boundary Event

There are a number of lines of evidence linking the Leopard Fault to the *break up unconformity* that developed during the changeover from rift to passive margin settings at the end of Surprise Creek times. They are:

- Significant erosion of the Surprise Creek sandstones near the fault (Figure 3).
- A marked thickening of the conglomerates of the Torpedo Creek Quartzite immediately adjacent to the fault.
- Evidence for a rapid dying out of rifting in the lower Gunpowder Creek Formation sandstone beds.

A folded wedge of quartzites, conglomerates and sandstones just north of the Lady Loretta Pb–Zn deposit provides a unique opportunity to study a cross section (albeit a slightly oblique one) through the volcano-sedimentary units adjacent to the Leopard Fault (Figure 3). Although folding has exposed the rift sequences equally on both limbs, only the eastern limb is considered.

Photo-interpretation shows that the neither the volcaniclastic sandstones at the base of the formation (Bigie Formation) nor the overlying reddish sandstone unit are markedly affected by the Leopard Fault. For example, the reddish sandstone does not change its thickness across the section, nor do the volcanics appear to be spatially related to the fault. On the other hand, the overlying micaceous flaggy sandstone unit is strongly eroded next to the fault and the Torpedo Creek Quartzite (and overlying Gunpowder Creek Formation) thicken into a roll-over anticline.

The extensional faults in the reddish sandstones are truncated by the overlying flaggy sandstone unit giving clear evidence that this unconformity surface marks the end of a rifting event. These faults, which are mildly inverted, may have formed as a set of antithetic normal faults to the Leopard Fault; however, evidence for this is not entirely compelling. Note that the flaggy sandstones are markedly onlapping at the northern end of the outcrop implying that they were sourced from some distance to the south.

One fault that is observed to cut the Torpedo Creek Quartzite can be traced at least as far as the Mount Oxide Chert marker bed, even though it shows no displacement. This indicates that the changeover from rift to passive margin was transitional in the sense that it continued at least to the end of Gunpowder Creek times.

2. Inflexion 2 (I_2) Event

This event is a NW–SE compression (in wrench mode) that pre-dated the Isan Orogeny. Little is known of this event. However its similar timing and orientation to the HYC deposit (Hinman et al. 1994) suggests that a tectonic event (with hiatus) may exist between the Lady Loretta Formation and Shady Bore Quartzite. This may have important implications for the Pb–Zn mineralisation.

3. The Isan Orogeny

- NNE–SSW compression. This brittle-style event, which is the D_1 Isan Orogeny, represents the first regional-scale inversion of early basinal faults. The Leopard Fault suffered major inversion during this period.
- After a period of stress relaxation, N-trending close to tight folds formed in the D_2 Isan Orogeny. A NE-trending mega-shear band, paralleling the Carlton Fault, formed late in this event. It cuts across the belt 5 km north of

Lady Annie rotating and offsetting fold axes in a dextral sense.

- The next event was the brittle style E–W compression of the ***D_3 Isan Orogeny*** with wrench faulting on NW and NE conjugates. This event is well developed in the Redie Creek Fault area to the east.
- The final tectonic event is a local fault-related ***NW–SE compression (D_4)*** that activated a series of small E–W dextral faults in the Big and Small Synclines at Lady Loretta (Hancock and Purvis 1990).

Implications for exploration and further work

1. Fault striae analysis has been shown to produce consistent and meaningful results in the Riversleigh fold belt. This is in line with recent research in SE Asia and N Africa/Europe where the adjacent platforms tend to record compressive stresses related to the orgenic events better than the orogens themselves (Angelier 1994). The results from this work will have implications for the controls on inversion-related copper mineralisation (e.g. Mt Isa D3 Cu) and Pb–Zn mineralisation.

2. The existence of extensional faulting during the Surprise Creek Sandstone times and growth faulting (e.g. Leopard Fault) during Torpedo Creek Quartzite times, confirms that crustal extension took place during the early rift cycle. Further work should involve detailed mapping north of Lady Loretta of faults in the sandstones and conglomerates sequences adjacent to the Leopard Fault and an extension of the pilot study into remaining areas of the platform. The study will focus on Isa D_1 thrusts as the inverted basinal growth faults and the possibility that the sub E–W trending culmination axes (e.g. Lady Annie axis) are inherited features dating back to the earliest parts of the basin history.

Acknowledgments

My sincere thanks go to Pancontinental Mining for their logistical support in the field.

References

Angelier J., 1994. Fault slip analysis and palaeostress reconstruction. *In:* Continental Deformation (ed. P.L.Hancock), 53–100. Pergamon Press 421 pp.

Blake D. H. and Stewart A. J. 1992. Stratigraphic and tectonic framework, Mount Isa Inlier. In (eds. A.J. Stewart & D.H. Blake) Detailed Studies of the Mount Isa Inlier. Bureau of Mineral Resources Bulletin **243**: 1–12.

Dunnet D. 1976. Some aspects of the Panantarctic cratonic margin in Australia. *Philospohical Transactions of the Royal Society* **A280**, 641–654.

Dunster J.N. and McConachie B.A., (in prep). Basin evolution of the northern Mount Isa Basin and its implications for stratiform sediment-hosted base metal mineralisation.

Etheridge M. and Wall V.(1994). Tectonic and Structural Evolution of the Australian Proterozoic. *Geol. Soc. Aust., Abstr.* No **37**, pp 102–103.

Hancock M.C. and Purvis A.H., 1990. Lady Loretta Silver–Lead–Silver Deposit. In Geology of the Mineral Deposits of Australia and Papua-New Guinea (Ed. F.E.Hughes), pp 943–948. (The Australasian Institute of Mining and Metallurgy:Melbourne).

Hinman M., Wall V. and Heinrich C., 1994. The interplay between Sedimentation, Deformation and Hydrothermal activity at the McArthur Pb–Zn(–Cu) Deposit. Geological Society of Australia, Abstracts No. 37:176–177.

Keele R.A. 1993 Histories of some faults in the southern McArthur Basin: evidence for an end-Tawallah uplift and a preliminary analysis of stresses related to post-McArthur and post Roper compressions, Codes:AMIRA/ARC Project P.384 - Proterozoic sediment-hosted base metal deposits, Report No 4: 55–86.

Loutit T.S., Wyborn L.A.I., Hinman M.C. and Idnurm M., 1994. Palaeomagnetic, Tectonic, Magmatic and Mineralisation Events in the Proterozoic of Northern Australia. In "Australian Mining Looks North - The Challenges and Choices' (ed. C.P.Hallenstein) The Australasian Institute of Mining and Metallurgy Publication Series No 5/94:123–128.

Appendix 1 — Summary diagram of calculated stress directions displayed on an area by area basis and through time.

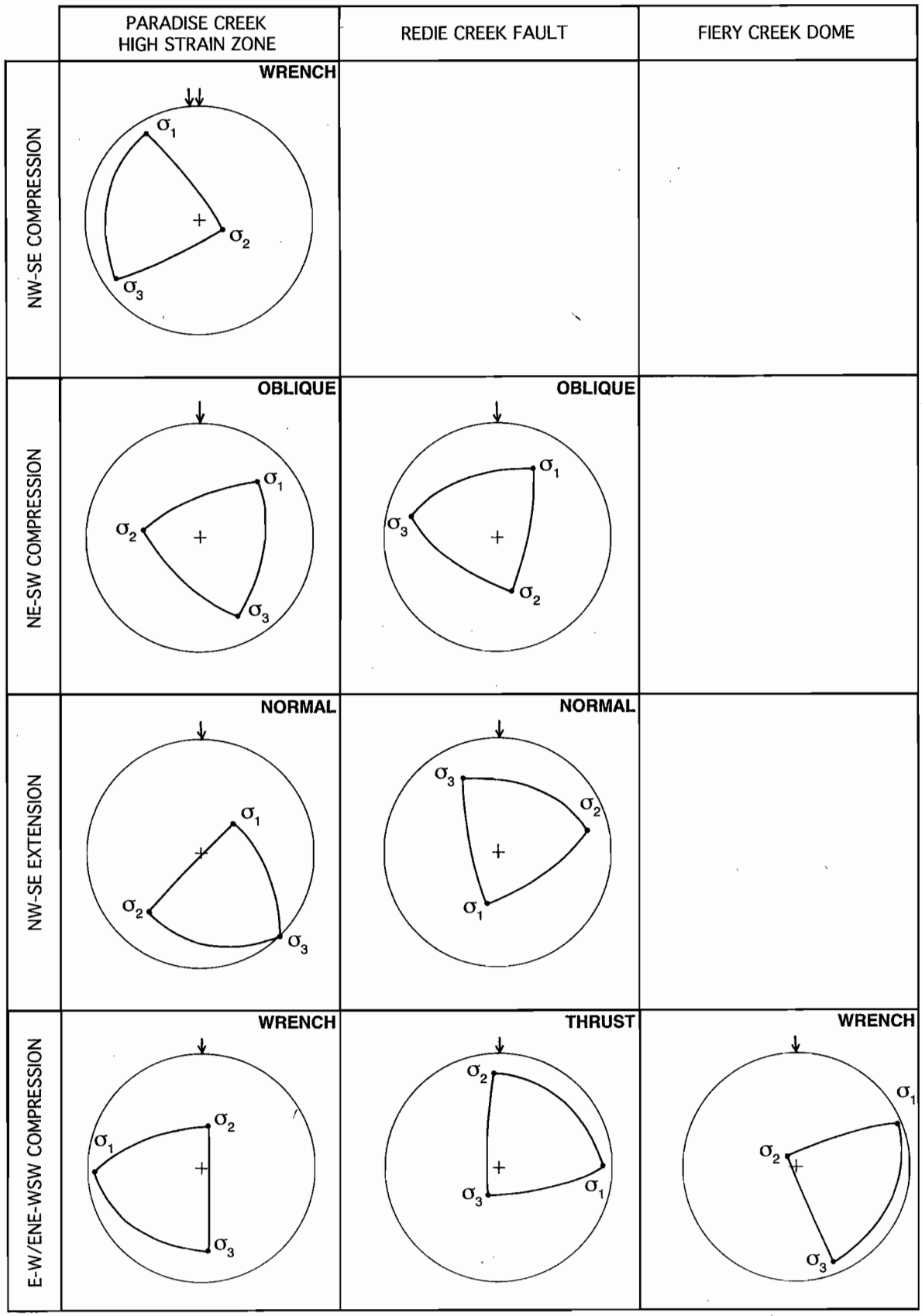

Appendix 2 — Structural data base.

Unique No.	Field No.	Rock Type	Form name	AMG E	AMG N	Bedding Dip	Bedding DipDir	Cleav Dip	Cleav DipDir	QV dip	QV dip dir	Fault str	Fault dip	Fault dip dir	pitch	pitch dir	sense
1	LH1	dolslst		295500	7814225	60	299	85	95	79	177						
2	LH2	qtzsst		295625	7813875	50	305			60	90	189	60	W	2	S	SIN
												96	75	N	0	W	SIN
												8	42	E	12	N	SIN
												182	71	E	25	S	DEX
												220	80	W	25	S	DEX
3	LH3	qtzsst		296025	7813850	69	59			69	59	285	19	N	20	W	X
												260	23	N	40	W	NOR
4	LH4	slst		293250	7814750	50	60	73	280								
5	LH5	fgsst		293550	7814250	61	0										
6	LH6	FZ		292800	7814800					40	306						
7	LH7			292500	7815350	61	76										
8	LH8	slst/mdst		294050	7819900	48	248										
9	LH9	qtzsst		294250	7820100	60	350			39	317	15	90	E	20	N	SIN
												254	73	S	20	W	DEX
												254	73	S	45	E	X
												178	83	E	10	S	SIN
10	LH10	mdst/slst		293050	7820350	53	253	81	278								
11	LH11	slst/fgsst		293400	7820500	45	270	85	110								
12	LH12	slst/mdst		293750	7820700	38	302	50	254								
13	LH13	sst/congl	TCQ	293900	7820650	18	129			84	40	262	59	N	15	W	DEX
14	LH14	fgsst/slst		292350	7822100	11	228	90	90								
15	LH15	slst/mdst		291900	7821650	25	140	77	91								
16	LH16	slst/fgsst		291600	7821600	67	118	71	96								
17	LH17	dol		291400	7821650	40	102	80	102								
18	LH18	sst		291150	7821600	63	127					222	30	E	80	S	NOR
												61	70	E	80	N	NOR
19	LH19	qtzite		290850	7820950	5	75					302	81	N	85	W	NOR
												200	30	W	75	S	NOR
												200	73	W	90	S	NOR
												298	61	S	15	W	DEX
												263	29	N	55	W	
20	LH20	qtzite	SBQ	290700	7821250	19	134										
21	LH21	qtzite	SBQ	290000	7821650												
22	LH22	slst/mdst		293375	7822650	60	308	87	290								
23	LH23	dol slst/fgsst		293600	7822350	87	303										
24	LH24		TCQ	293800	7822200	27	290			65	162	95	87	S	20	E	DEX
												110	73	N	30	E	SIN
25	LH25			296000	7812350	44	44			40	255						
26	LH26	sildol		296250	7812450	47	98			47	52						
27	LH27			298350	7813100	69	77										
28	LH28	qtz sst		297850	7813150	45	297			77	166	110	79	S	42	W	X
29	LH29	qtz sst		297300	7813400	67	13			57	81	140	51	S	42	W	REV
												32	59	W	40	S	REV
												174	33	W	80	S	REV
												40	67	E	12	N	DEX
												84	30	S	0	E	SIN
												133	65	E	30	S	SIN
												24	70	E	2	N	DEX
												24	40	W	90	N	REV
30	LH30	fg mic sst		308000	7814450	15	30			28	212	197	61	E	0	N	X
31	LH31	qtz sst		307750	7814300	79	176			81	173	326	67	S	80	W	NOR
												273	77	S	35	W	SIN
32	LH32	qtz sst		308950	7812650	23	0					102	34	N	77	W	REV
												123	19	N	50	E	NOR
33	LH33	qtz sst		308950	7812100							160	45	E	12	S	DEX
												135	39	E	45	S	REV
34	LH34	slst/fg mic sst		309650	7811650	15	34										
35	LH35	qtz sst		317850	7806350	18	100			77	175	158	43	W	75	N	REV
36	LH36	qtz sst		317550	7806600	3	252			87	98	110	81	N	90	W	REV
												50	17	W	35	N	REV
												53	43	W	20	S	DEX
												166	58	E	65	S	REV
37	LH37	qtz sst		317000	7806850	21	24					22	52	W	77	S	NOR
												118	87	N	15	E	DEX
38	LH38	dol slst/fg sst		316000	7807000	57	260										
39	LH39	qtz sst		314400	7807900	47	15			76	148	32	67	W	15	N	DEX
												44	26	W	45	S	REV
												100	38	N	37	E	SIN
												40	59	W	80	S	NOR
												59	27	W	25	S	DEX
												59	27	W	40	N	REV
												135	88	S	37	W	DEX
												90	69	S	20	W	SIN
40	LH40	chty dol		312550	7808950	55	227					142	51	N	40	E	NOR
41	LH41	qtz sst		312950	7809300	85	66					50	45	W	15	N	DEX
												177	61	W	50	S	REV
												172	49	W	80	S	REV
42	LH42	mdst/slst		319000	7805850	72	58			85	252	154	61	E	30	S	SIN
43	LH43	qtz sst		319250	7806150	42	60			70	10						
44	LH44	dol slst/fgsst		315400	7806600	84	34			18	41						
45	LH45	slst		293350	7872150	80	247			90	180	100	60	S	35	W	X
												143	90	W	0	N	SIN
46	LH46	pink,qv sst		296864	7873758	16	269			88	187	111	90	S	25	W	SIN
47	LH47	qtzite		297950	7872850					80	217	68	29	S	60	E	NOR
												134	22	S	15	W	SIN
												149	67	S	5	W	DEX
48	LH48	sst		298100	7873665					48	206	97	90	S	15	W	X
												159	43	E	80	S	REV
												99	20	S	20	W	DEX
49	LH49	qtz sst		308650	7868750	61	188			80	339	85	55	N	25	W	SIN
												50	77	N	5	E	DEX
												141	16	S	40	E	NOR
												128	23	S	25	W	REV
50	LH50	Qv		312350	7869050	45	197			65	340						
51	LH51	silicFZ		303350	7873506					33	105	163	31	E	15	N	DEXT

Modelling the relationship between sedimentary facies and Alteration Index and resolution of the "shale factor"

Ross R. Large
CODES Key Centre

Introduction

Previous research on AMIRA Project P384 (see Reports 3 and 4) has outlined the development of the "sedex alteration index" which can be used as a geochemical vector to assist exploration for stratiform sediment-hosted Pb–Zn deposits. When combined with zinc geochemistry and the calculated percentage of MnO in dolomite (MnO_D), the AI vector becomes a powerful tool for the discrimination of the sedimentary facies favourable for stratiform Pb–Zn mineralisation.

$$\text{Sedex AI} = \frac{(FeO + 10MnO)\ 100}{(FeO + 10MnO + MgO)}$$

Background values for Proterozoic dolomitic sediments in the McArthur Basin vary from 0 to 40, (Large, 1994), while sediments in the halo to Pb–Zn mineralisation at Lady Loretta and HYC increase from 40 to 100 approaching mineralisation, both along strike and across strike (Large & McGoldrick, 1993). These relationships are summarised in figures 1 to 5.

Factors controlling the Sedex AI

Our research has indicated that the following chemical and lithofacies factors control variations in Sedex AI:

- An increase in the Mn and Fe content of dolomite within the sediments causes an increase in Sedex AI. This is the **key factor** in using the Sedex AI as a vector within the halo of stratiform Pb–Zn deposits (Large & McGoldrick, 1993). In the extreme case (e.g. Lady Loretta) the Fe,Mn dolomite is replaced by siderite within the inner halo of the deposit.

- An increase in the pyrite content of sediments causes an increase in Sedex AI. This factor responds to the bedded pyritic halo around many Proterozoic lead zinc deposits (e.g. Lady Loretta and HYC).

- An increase in the shale/dolomite ratio causes a decrease in MgO of the sediments and consequently leads to an increase in Sedex AI. This is a useful trend as the major Australia Proterozoic stratiform Pb–Zn deposits are all located in shale-rich facies.

- Other lithofacies changes which cause an increase in FeO and/or decrease in MgO within the sediments will also cause increasing Sedex AI. For example, pure sandstone facies will have high Sedex AI due to their lack of MgO, while hematite- or magnetite-bearing sediments may also have high Sedex AI due to increased FeO levels. To date, these facies have not been

not been sampled due to their absence in the McArthur Group and on the Lawn Hill Platform. However, it is important to remember that the Sedex AI vector approach should be restricted to carbonate-bearing sedimentary basins and **is not applicable to siliclastics** and may not work in red-bed sequences.

Variations in shale/dolomite facies — the shale-factor

Previous research on the background of Sedex AI in the McArthur Basin (Large, 1994) has shown an increase in Sedex AI with increasing shale content of the sediments. In figure 6 it is apparent that shales (with less than 25% dolomite) have a mean AI of 40, compared with dolomites (with less than 25% mica and quartz) which have a mean AI of about 10.

Consequently, shales by themselves may give rise to anomalous AI values irrespective of whether they are related to Sedex Pb/Zn or not i.e. the index cannot discriminate "barren" shales from potentially fertile shale host rocks. Although it is useful to have a shale-factor built into the AI, because of the importance of shale facies in hosting stratiform Pb–Zn, it is not desirable for the shale-factor to become dominant to the extent that any shale in a dolomitic sequence is given high priority. For this reason, we have investigated ways to reduce the effect of the shale-factor on the alteration index.

Modelling dolomite–shale facies effect on Sedex AI

Computer modelling has been undertaken to assess the effect of varying shale/dolomite ratios on the Sedex AI. A relatively pure dolomite from the Barney Creek Formation was selected from the BGR database to use as a typical background dolomitic sediment, well removed from mineralisation. The partial analysis of this sample is shown in Table 1. An analysis of Post Archean Shale (PAS) from McLennan and Taylor (1985) was selected as a typical shale (Table 1). These two sediment analyses were mixed in 10% increments from pure dolomite to pure shale. The changing Sedex AI and MnO_D associated with this mixing are plotted in figure 7. It is apparent from this model that mixtures of greater than 50% shale give rise to anomalous values of Sedex AI (>40) and MnO_D (>0.5%). Samples with greater than 70% shale plot in the second priority zone for follow-up as defined by Large (1994). The apparent anomalism of PAS is due to its low MgO and high FeO and MnO values compared to the background dolomite (Table 1).

Eliminating the shale-factor

In order to counterbalance the shale-factor in the model outlined above, a series of modifications to the alteration index were attempted. Two of these modifications were found to be successful and are given below.

$$\text{AI Mark 3} = \frac{100(FeO + 10MnO)}{(FeO + 10MnO + MgO + Al_2O_3)}$$

$$\text{AI Mark 4} = \frac{100(FeO + 10MnO)}{(FeO + 10MnO + MgO + (SiO_2/10))}$$

An increase in the shale/dolomite ratio in a sediment package is accompanied by decreasing MgO and increasing Al_2O_3, SiO2 and K_2O. Consequently, introducing Al_2O_3 or SiO_2 into the denominator of the AI provides a counterbalance to the effect of shale on the index.

The mixing model path for AI Mark 3 (shown in figure 8) clearly demonstrates the strongly reduced effect of the Post Archean Shale on the new index. The dolomite to shale mixing line varies from AI Mark 3 values of 7 to 27 and remains within the background field.

Table 1—Partial chemical analyses of samples used in the sediment mixing models.

Lithology	Background Dolomite	W-Fold Shale	HYC Ore	Pyritic Shale	Post Archean Shale	Sideritic Shale	Ankerite
Designation	BGR 188	DDH Te 115/468.8	DDH Te 115/404.4	DDH Te 115/80.5	McLennan & Taylor	Lady Loretta 4Pi	Deer, Howie & Zussmann
SiO_2	6.17	56.3	21.6	25.0	62.8	48.46	-
Al_2O_3	1.01	11.90	4.48	5.18	18.9	6.58	-
FeO*	0.75	6.20	16.20	29.80	6.50	16.48	12.06
MnO	0.07	1.48	0.04	0.05	0.11	0.35	0.77
MgO	19.13	2.87	1.09	2.77	2.20	0.94	12.85
CaO	28.58	4.95	1.04	3.36	1.30	0.07	29.23
K_2O	0.72	4.98	1.84	2.99	3.7	3.54	-
Zn	10	1200	187,000	9400	85	9630	-

Al Mark 3 (Al_3) background values in McArthur Basin

Previous research indicated that there is a consistent negative correlation between % dolomite and Sedex AI in McArthur Basin sediments (Fig. 9a). This effect is caused by the "shale factor" discussed above. By using AI Mark 3, this negative correlation disappears as seen in Fig. 9b, and the background population for dolomites and shales is shown to have AI_3 values from 0 to 30. Six samples have $AI_3 > 30$ and these are considered to be anomalous.

Mixing models of Al_3 using typical halo samples

A series of computer models have been run which involve mixing background Barney Creek dolomite with various mineralised and halo facies samples. Partial analyses of the end members are given in Table 1.

- Manganiferous shale (Fig. 10) — progressive mixing of dolomite with Mn-shale from the W-fold member, immediately footwall to the HYC ore body, shows a trend of increasing AI_3 and MnO_D, reaching values of 60 AI_3 and 10% MnO_D.
- HYC ore (Fig. 10) — progressive mixing of dolomite with typical HYC Pb–Zn ore gives rise to a flatter trend with maximum AI_3 values of 75 and MnO_D values of 1%.
- Pyritic shale in HYC halo (Fig. 10) — mixing of dolomite with a hangingwall pyritic shale produces a flat trend which reaches AI_3 values of about 80, and MnO_D values of 0.5%.
- Sideritic shale in Lady Loretta halo (Fig. 11) — mixing of dolomite with Lady Loretta sideritic shale produces a path which is almost identical to the dolomite/HYC ore mixing path.
- Ankerite (Fig. 11) — mixing of dolomite with pure ankerite ($Ca_2MgFe(CO_3)_2$) produces a steep path reaching an AI_3 value of over 60 and MnO_D of about 4%.

On the basis of these mixing models, three priority zones are defined on the AI_3 vs MnO_D plot.

Priority 1: $AI_3 > 50$, $MnO_D > 1\%$ – very close to ore.

Priority 2: $AI_3 > 40$, $MnO_D > 0.5\%$ – close to ore.

Priority 3: $AI_3 > 30$, $MnO_D > 0.2\%$ – potential distal horizon for Sedex Pb/Zn.

Application of AI_3 to Lady Loretta & HYC

Comparison of the AI_3 and Sedex AI patterns for both the Lady Loretta halo and HYC halo are shown in figures 12 and 13. These demonstrate that AI_3 shows a systematic relationship to both Zn and MnO_D for both the Lady Loretta and HYC halo data. In both cases, AI_3 gives lower values (than Sedex AI), with the background values 0–30 and the ore values from 60 to 100. Even within or close to the Pb–Zn ore zones, the AI_3 values rarely exceed 80.

Background versus Anomalous ranges

Of the three sediment geochemistry data sets available for the McArthur Basin, (see Large, 1994), only the BGR set has Al_2O_3 analyses which enable AI_3 calculations. This data is plotted in figure 14 and indicates that over 95% of the samples plot in the background field with $AI_3 < 30$. Of the eight anomalous samples, two are in the first priority field and two in the second priority field.

Comparison of the HYC halo data (from DDH Te115) with the BGR data set (Fig. 15), and the modelled mixing paths discussed earlier in this paper (Fig.16) indicates the following:

- The Mn-shales in the W-fold member immediately footwall to the ore lenses show a steep trend which is an extension of the background data trend.
- The HYC ore trend and pyritic shale trend are flatter features which merge with the background data set over the interval of 20 to 30 AI_3.

These patterns should prove very useful when evaluating data from grass roots and partly drill tested prospects.

Application to DDH BMR 2

Previous research on the geochemistry of DDH BMR 2 (Large & McGoldrick, 1993, and Large, 1994) have defined two potential ore horizons based on AI and MnO_D data. A comparison of the down hole Sedex AI and AI_3 variations is shown in figure 18. This plot shows that the two anomalous horizons are clearly defined by the AI_3 data, although somewhat more subdued. Sedimentological studies on DDH BMR 2 by Stuart Bull (this volume) have shown that some of the samples with anomalous Sedex AI values (e.g. 14.8m and 15.9m) are from a quartz–muscovite sandy facies with little dolomite. These samples fall within the background population for the AI_3 plot (Fig. 15c). However, even though the down holes values are seen to be of lower value, there remain four samples with anomalous values of greater than 30, within the favourable forizon from 78 to 105m. Further information on the relationship between AI_3 and sedimentary facies is provided by Bull (this volume).

Conclusions

A study of sediment mixing models for the HYC and Lady Loretta areas has enabled the development of a refined alteration index called AI Mark 3 (AI_3) which utilises Al_2O_3 wt%, in addition to FeO, MnO and MgO wt%. This refined geochemical index vector reduces the "shale-factor" that was prevalent in the Sedex AI, which gave high priority

to low carbonate bearing shales, but could not discriminate between barren shales and potentially fertile shale host rocks. Further testing of AI_3 will be required to assess its full potential as a robust exploration vector.

References

Large, R.R. and McGoldrick, P., 1993. Primary geochemical halos related to Proterozoic sediment-hosted Pb-Zn deposits and applications to exploration. AMIRA Project P384, Report 3: 63-126.

Large, R.R. and McGoldrick, P., 1994. Refinement of the Sedex Alteration Index and MnO_D vectors. AMIRA Project P384 Report 5: 17-22.

Taylopr S.R. and McLennan, S., 1985. The continental crust: its composition and evolution. Blackwell.

LADY LORETTA HALO MODEL

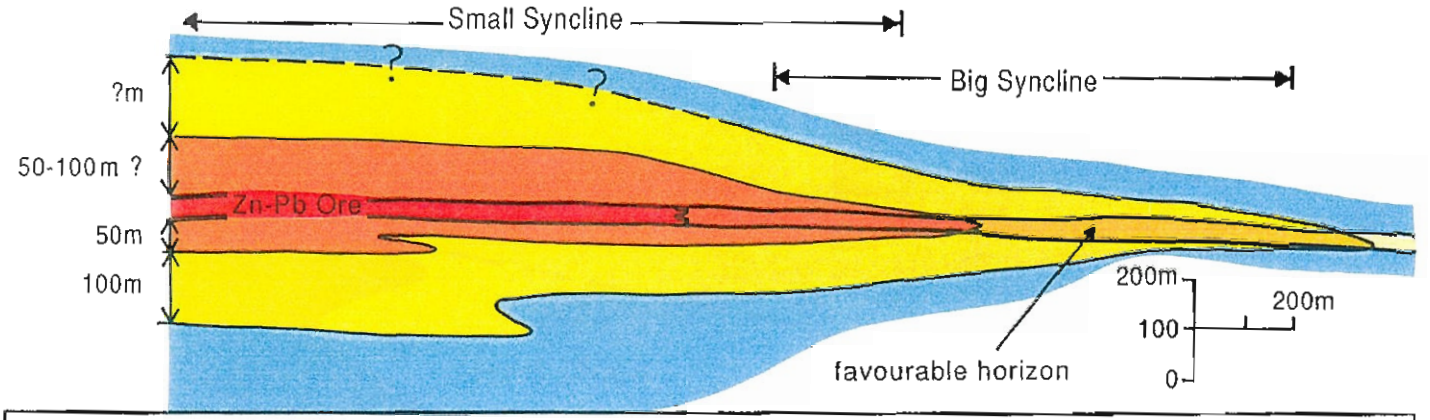

	Zn	Pb	dominant Carbonate	Tl	MnO	CaO	Sr	K_2O
Zn-Pb ore	>5%	>1000ppm	siderite	>50ppm	0.01-0.4%	0-1%	100-1000 ppm	↑
Siderite zone	100ppm to 5%	10-1000	siderite	2-50	0.01-1%	0-1%	10-500	no pattern
Tl halo	20-200ppm	<70	dolomite	2-50	0.01-0.4%	1-30%	<100	
Dolomite background	<50ppm	<30	dolomite	<4	<0.02	1-30%	<100	↓

LADY LORETTA HALO MODEL

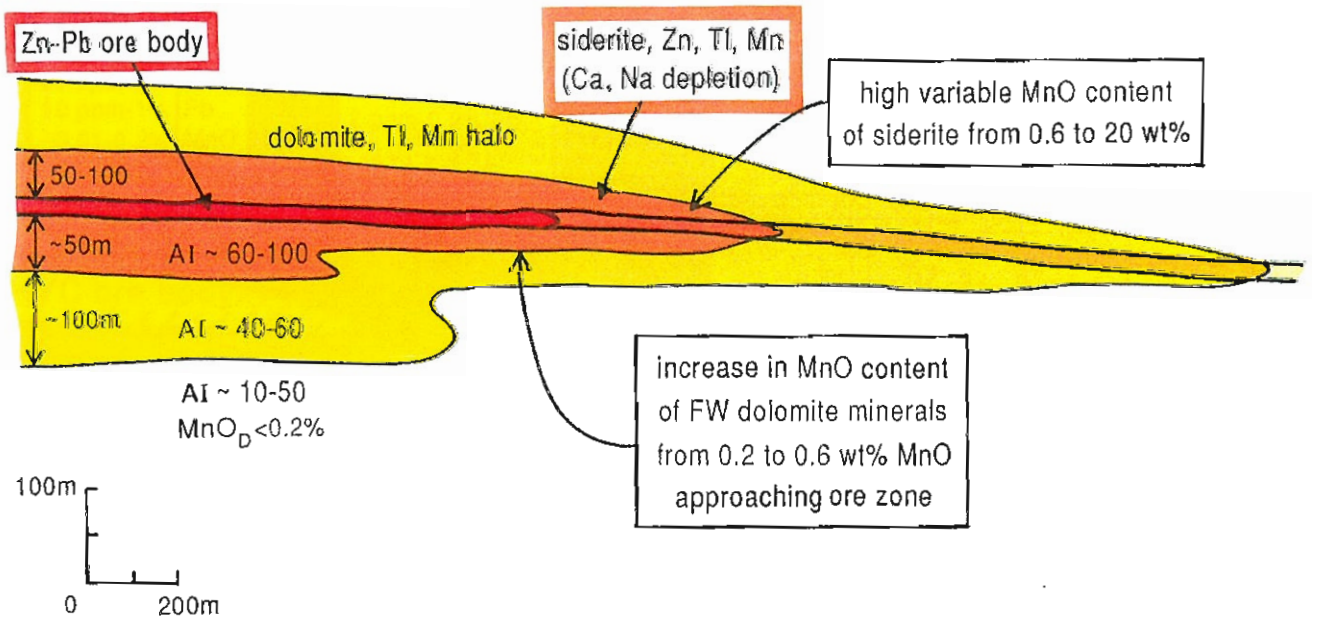

Figure 1—Geochemical halo model defined for Lady Loretta (Large & McGoldrick, 1993).

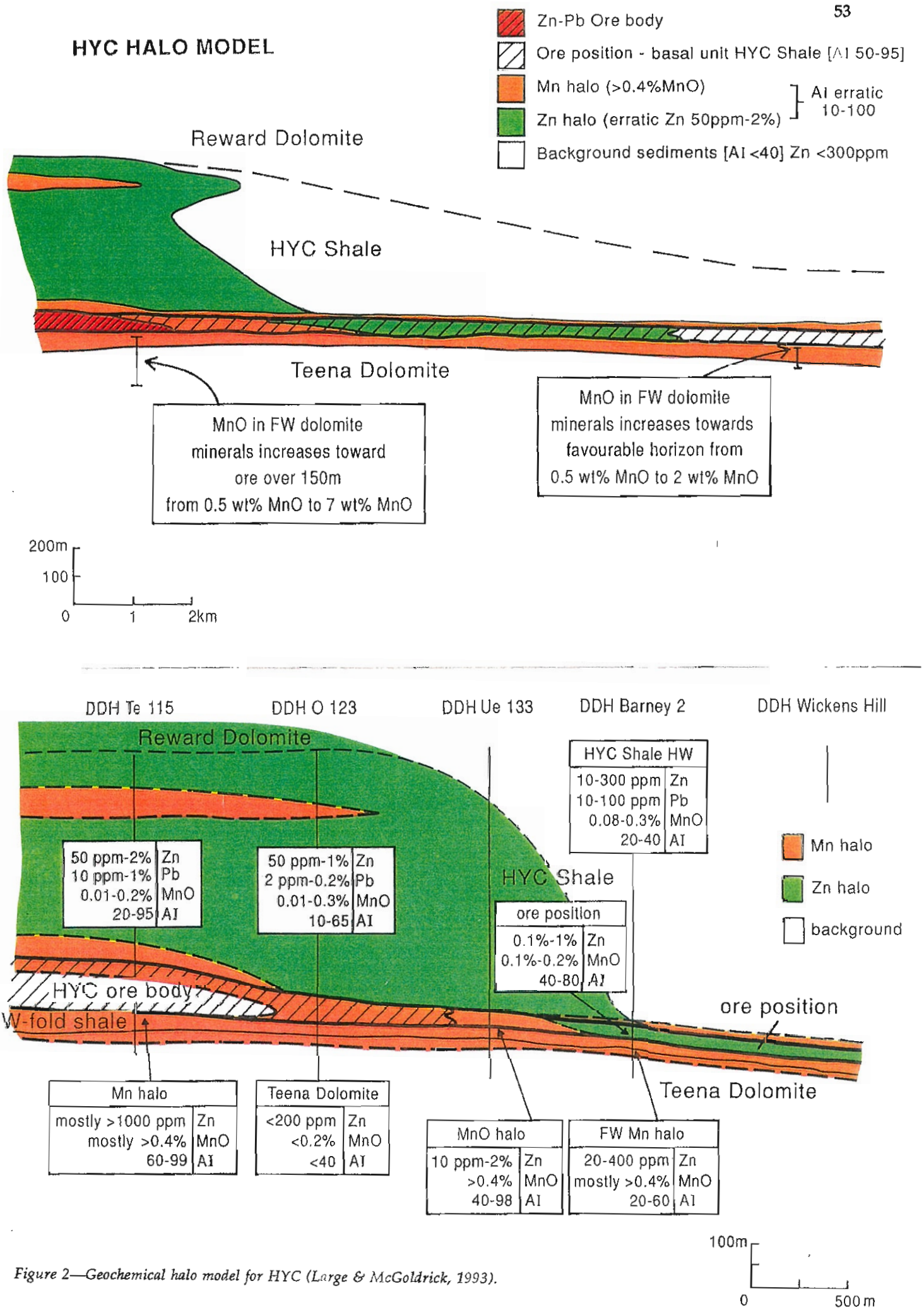

Figure 2—Geochemical halo model for HYC (Large & McGoldrick, 1993).

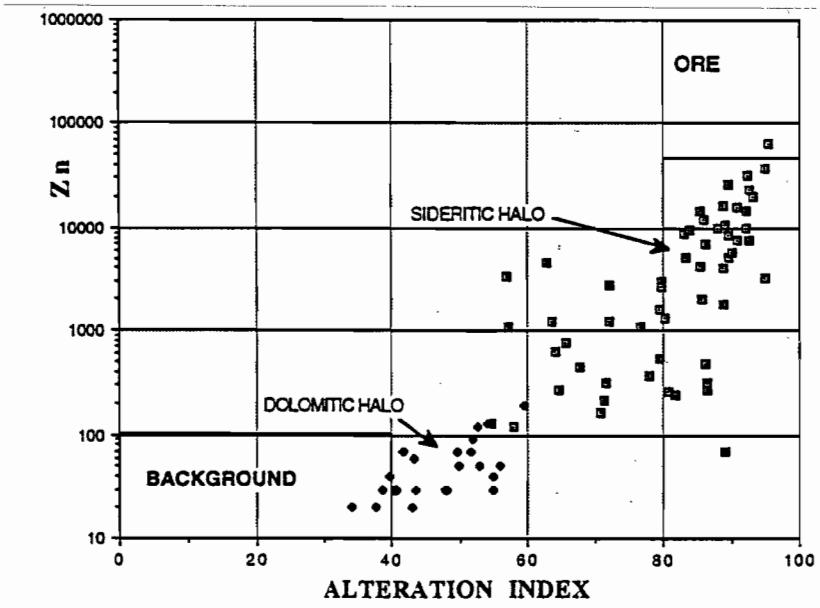

Figure 3—Trend between alteration index and zinc content for sediments in the Small Syncline, Lady Loretta.

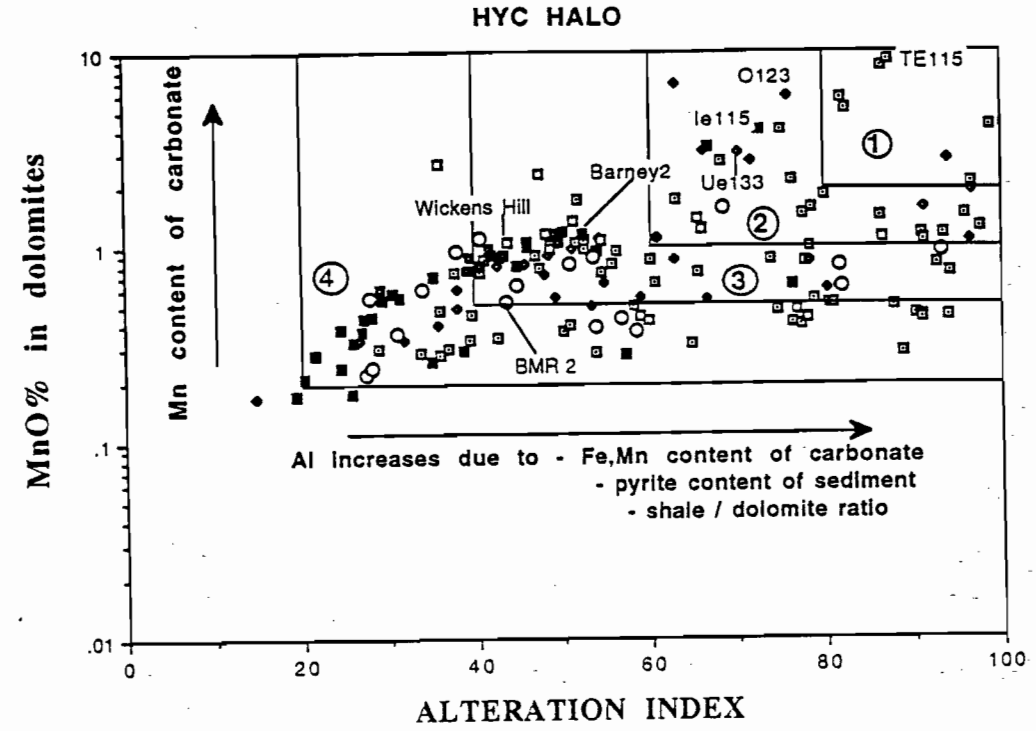

Figure 4—Trend of HYC samples showing increasing Al and increasing MnO_D for drill hole samples approaching the ore body (Large & McGoldrick, 1993).

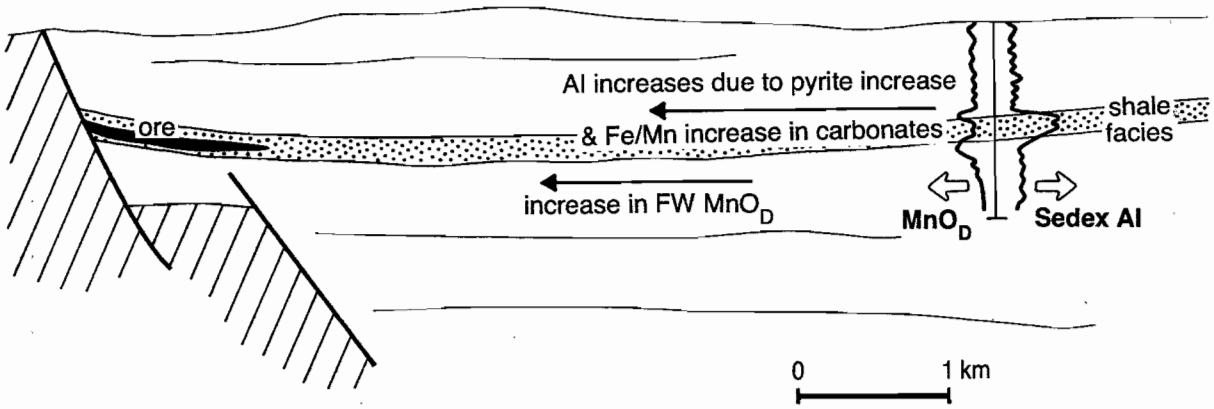

Figure 5—Sketch outlining use of the Al and MnO_D vectors during the initial exploration phase of a sedimentary basin.

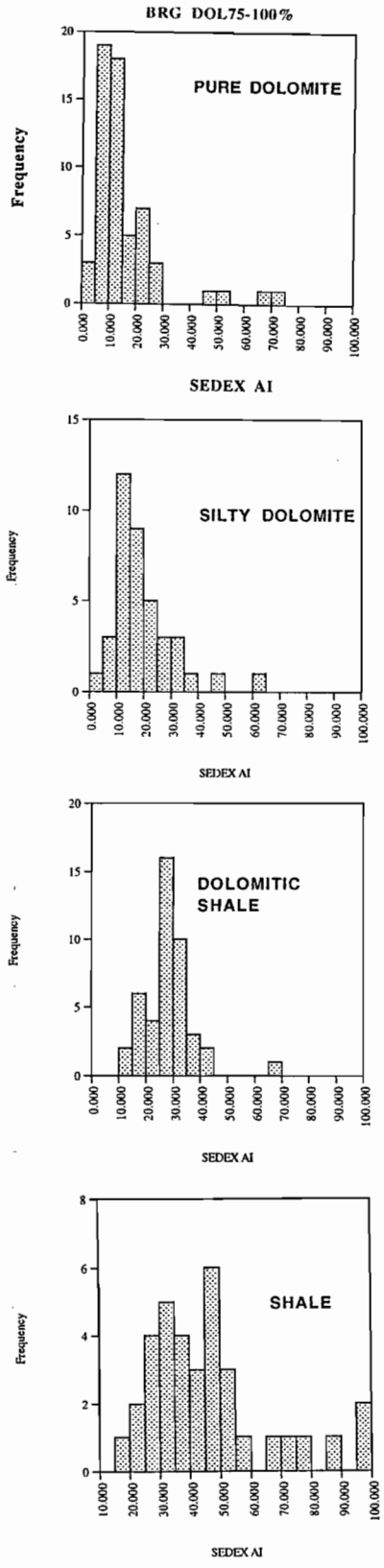

Figure 6—Histograph plot of Sedex AI for the four facies of sediments in the BRG data set. Pure dolomites contain 75 - 100% dolomite, silty dolomites 50-75% dolomite, dolomite shale 25 - 50% dolomite and shales <25% dolomite. Note the increase in mean Sedex AI passing from pure dolomite to shale.

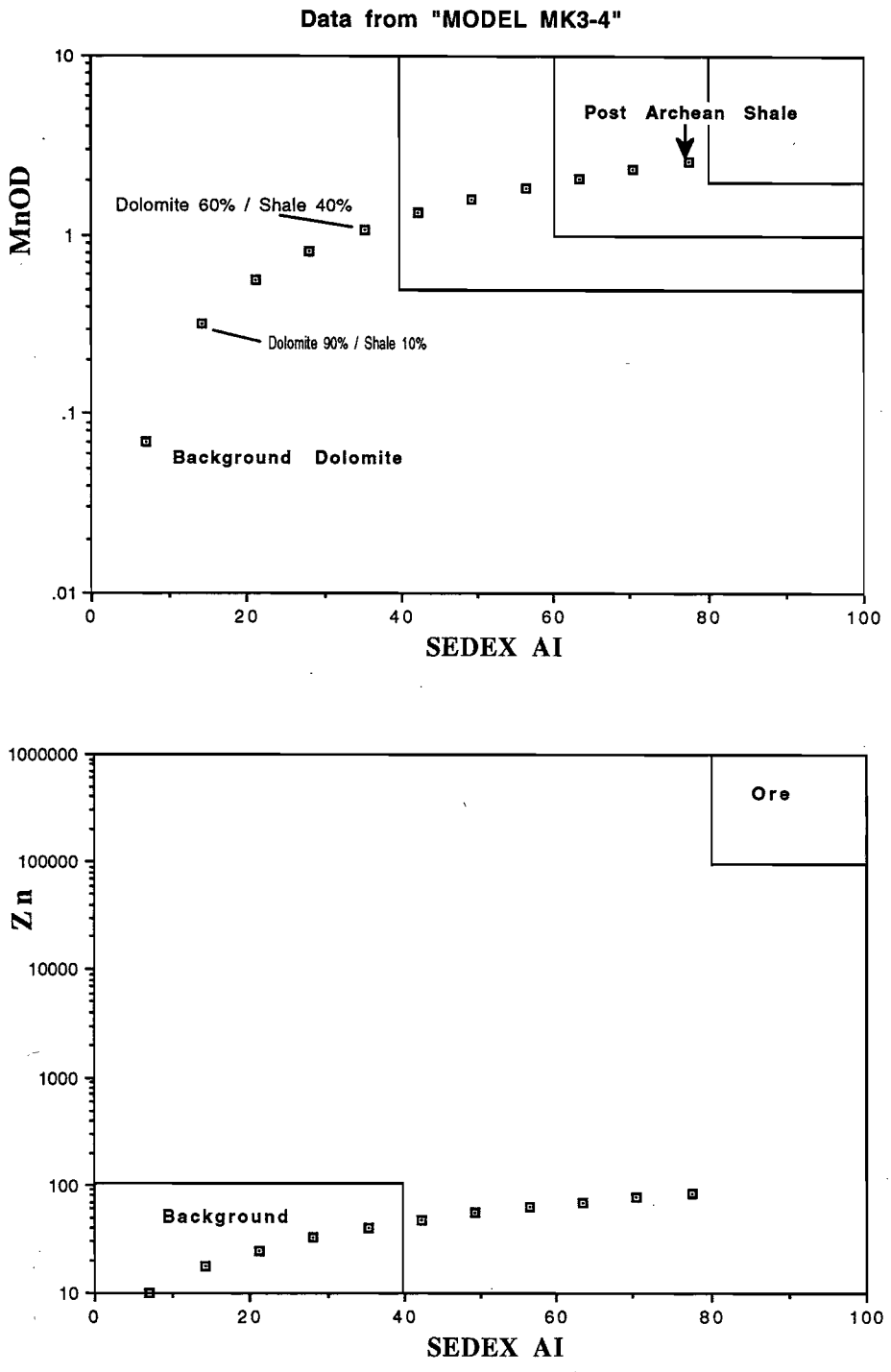

Figure 7—Mixing lines generated by mixing a background dolomite with Post Archaean Shale (PAS). Note that samples with greater than 50% shale plot in the anomalous zone.

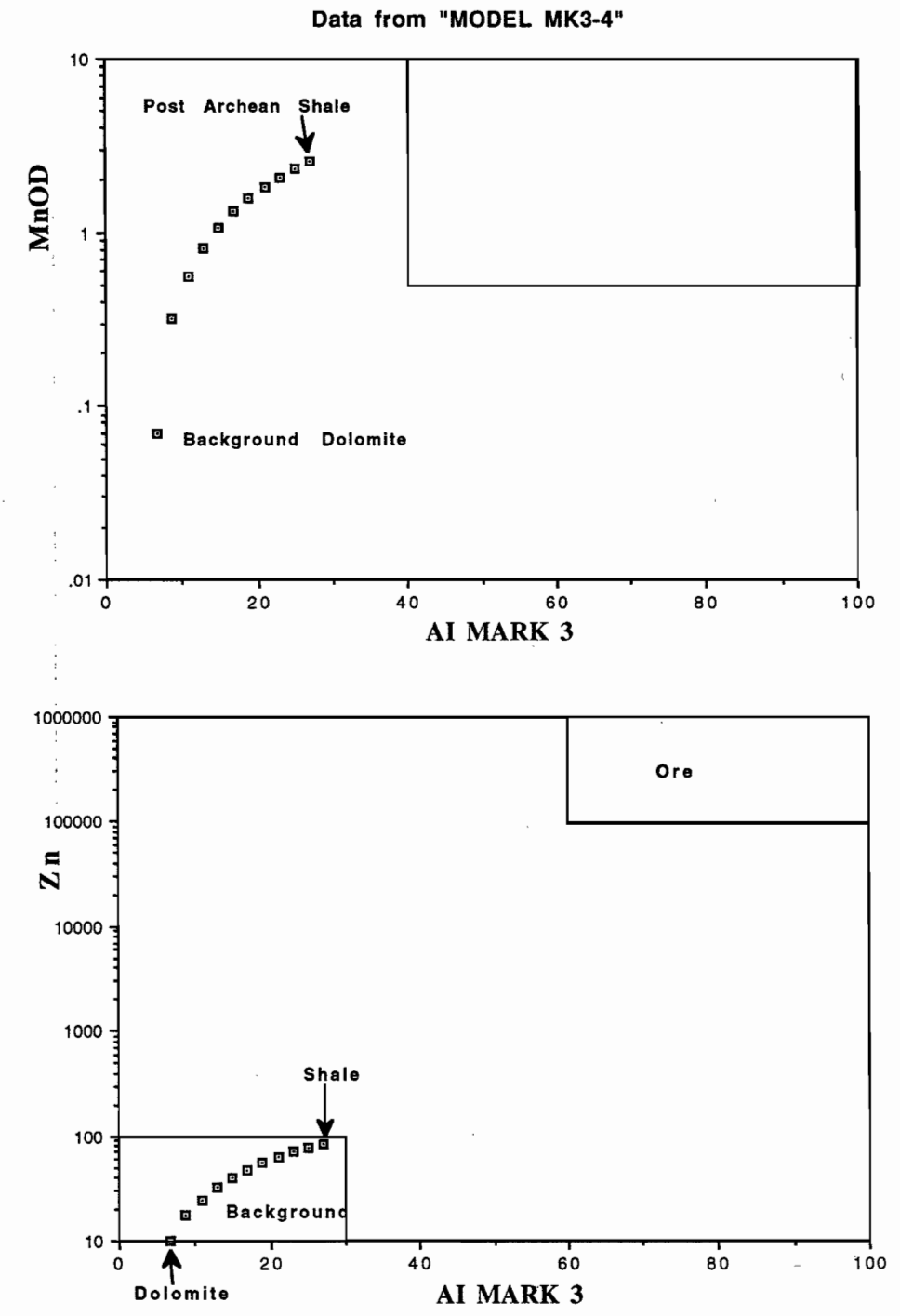

Figure 8—Mixing model (dolomite/shale) using the new alteration index, AI Mark 3. Note that the mixing path remains in the background zone.

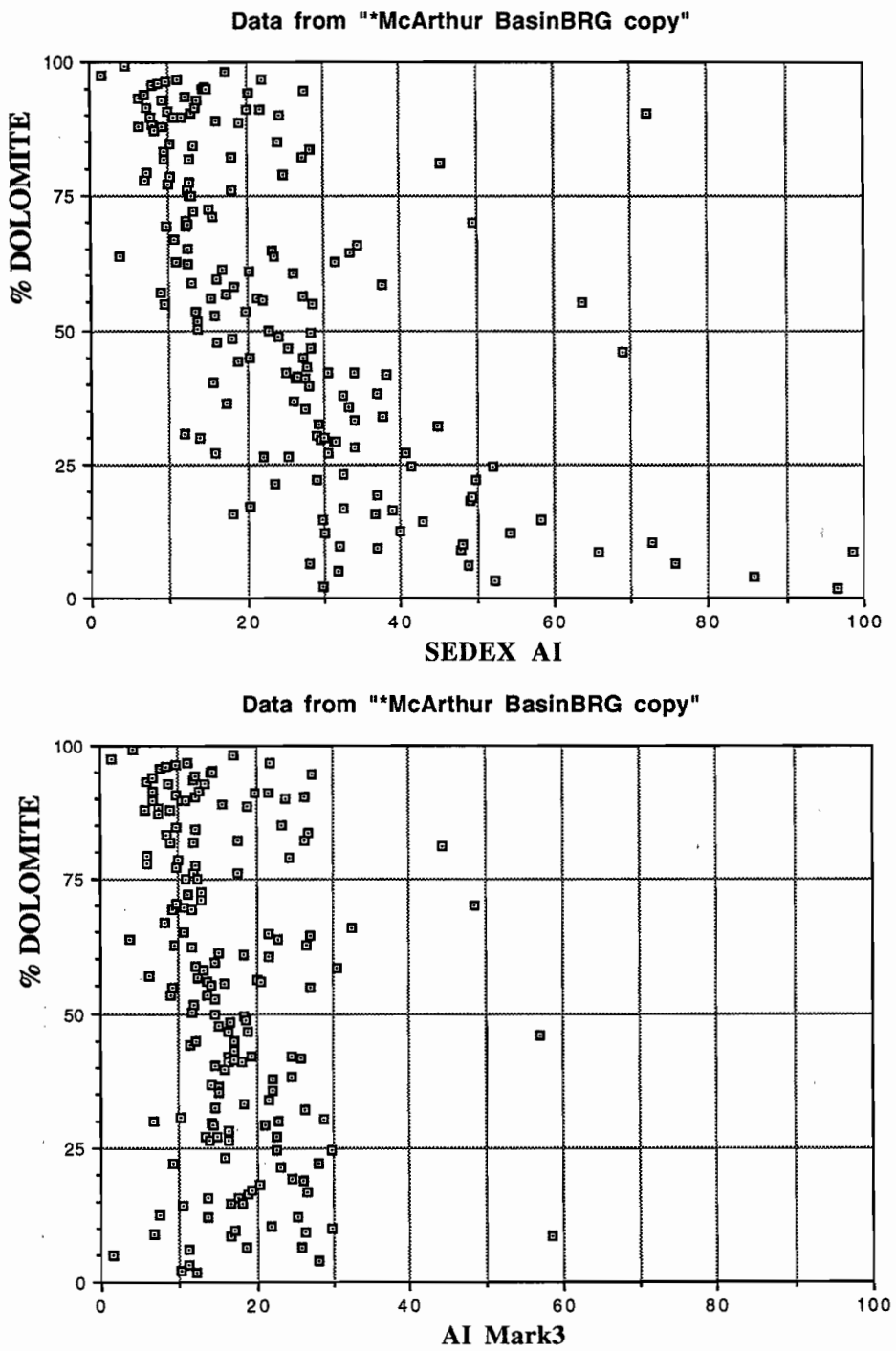

Figure 9—Plots of alteration index vs calculated % dolomite for the BGR data set. Note that the shale-factor is eliminated by using the AI Mark 3 index.

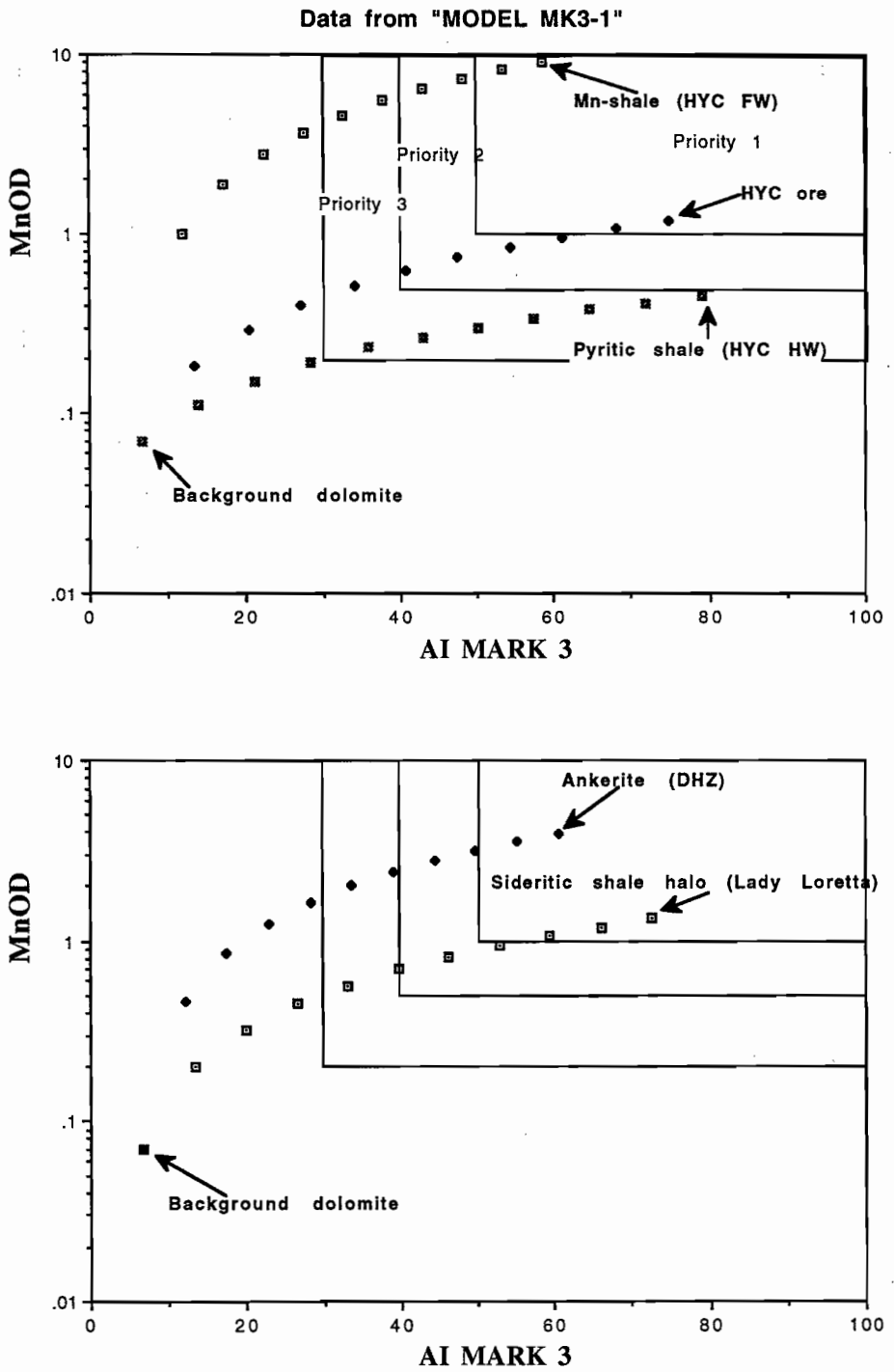

Figure 10—(a) Mixing models for HYC: (1) mixing background dolomite with W-fold shale, (2) mixing background dolomite with HYC ore, (3) mixing background dolomite with pyritic shale. (b) Mixing models for Lady Loretta: (1) mixing background dolomite with Ankerite, (2) mixing background dolomite with seritic shale from Lady Loretta inner halo.

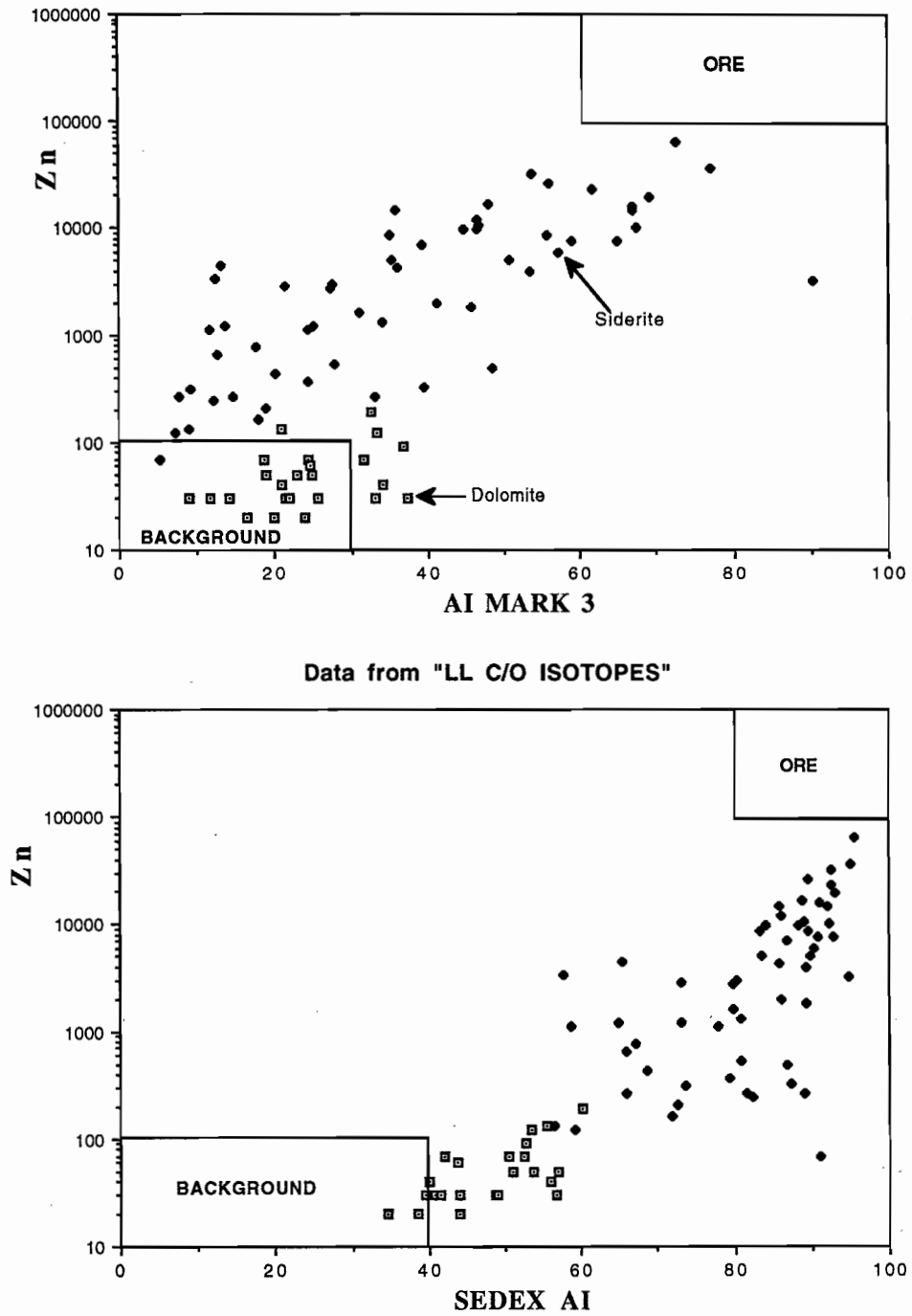

Figure 11—A comparison of AI Mark 3 with Sedex AI trends for the Lady Loretta halo data set.

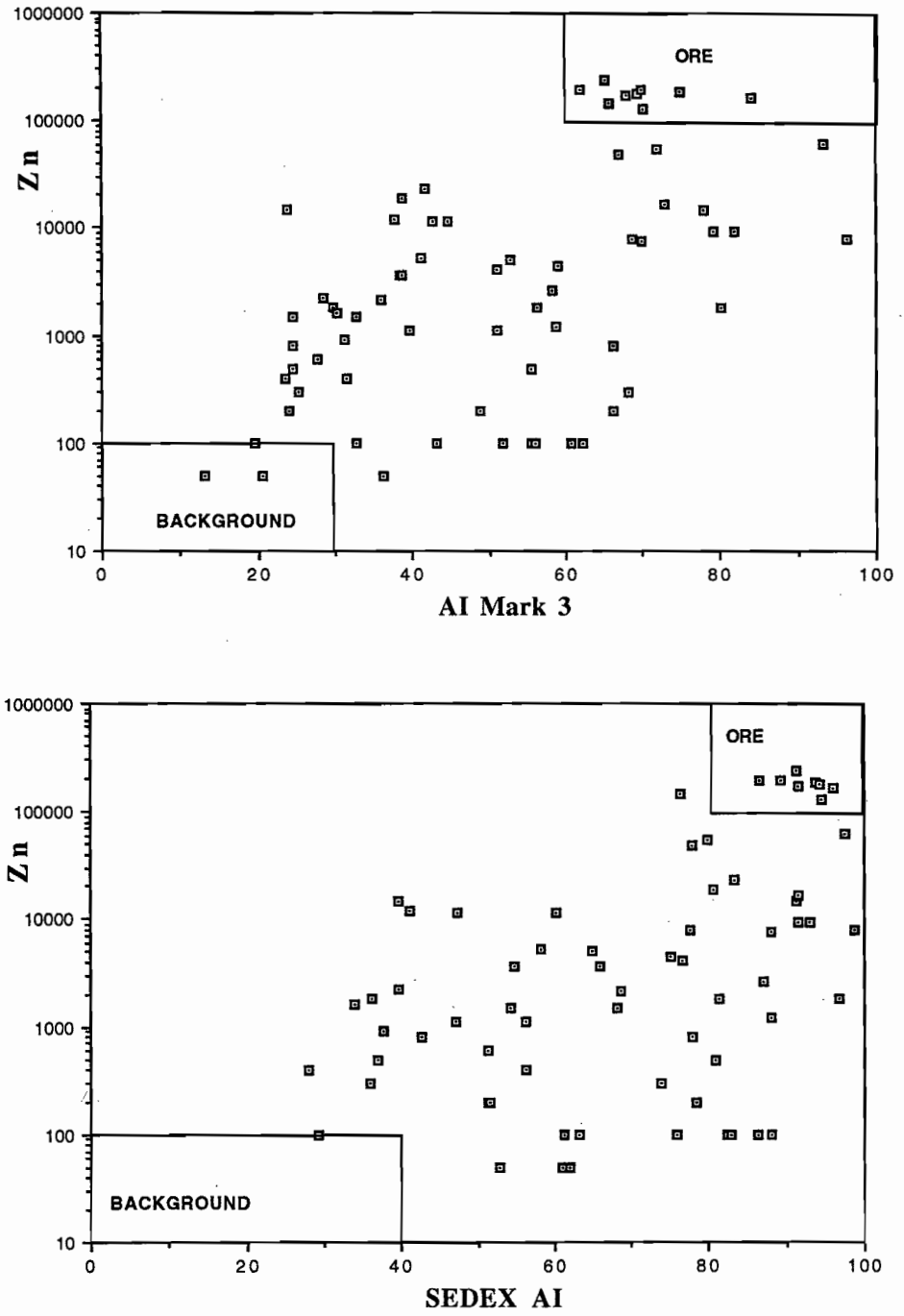

Figure 12—Comparison of AI Mark 3 with Sedex AI for the HYC halo and ore data (DDH Te 115)

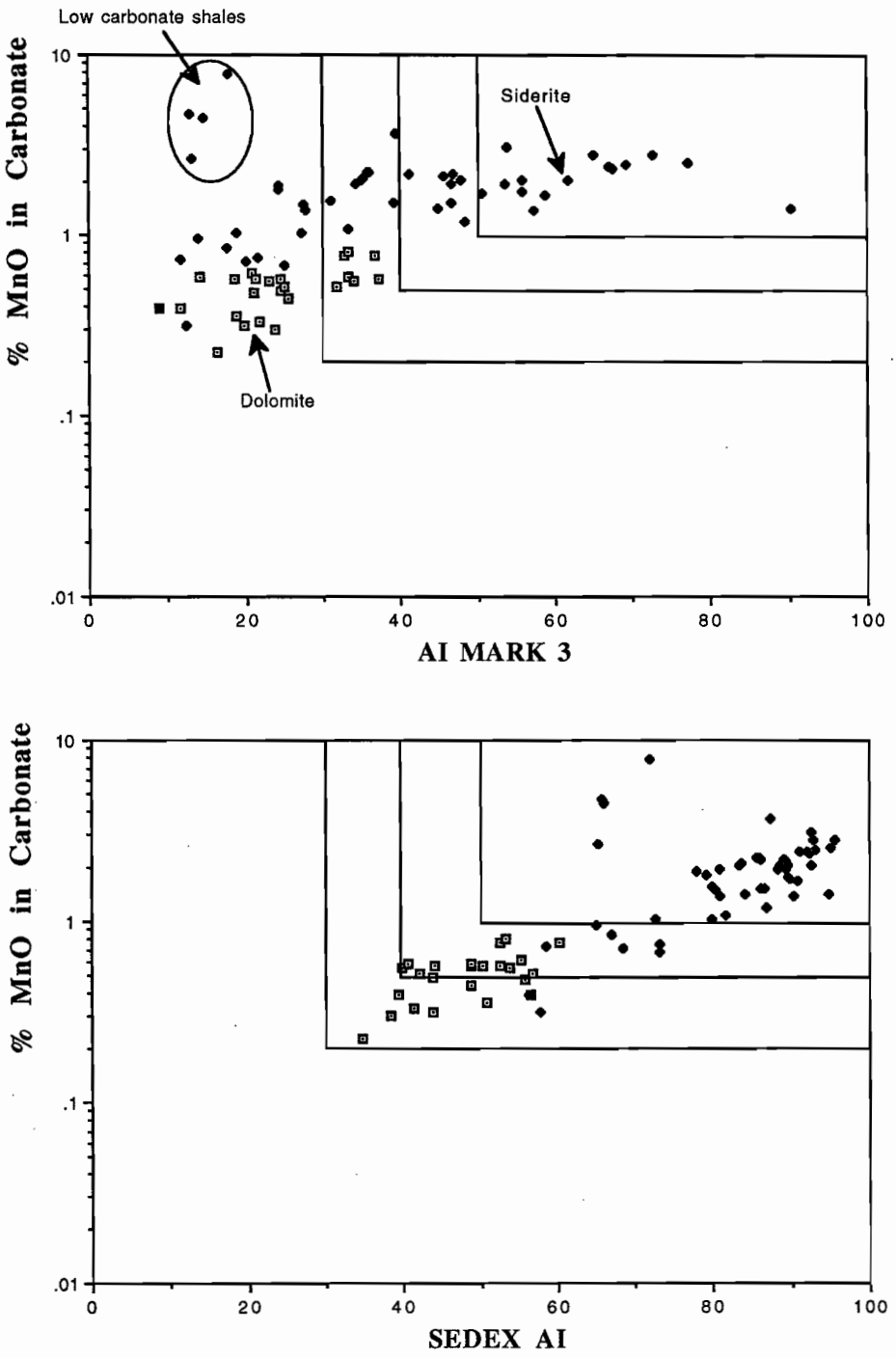

Figure 13—Comparison of AI Mark 3 with Sedex AI using the standard AI vs MnO_D plot. Data from Lady Loretta halo study.

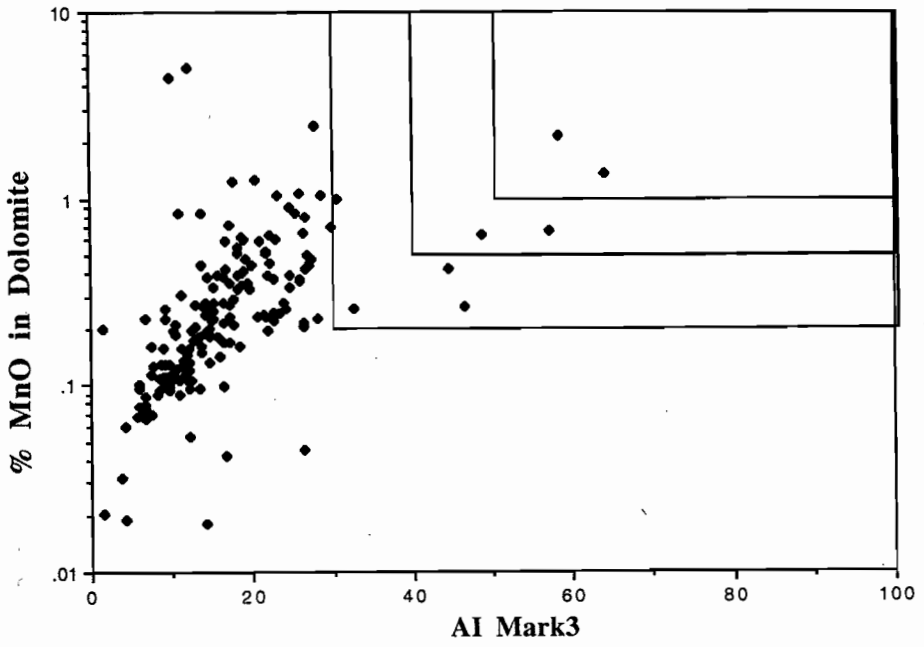

Figure 14—The BGR sediment dataset for the McArthur basin plotted on an AI_3 vs MnO_D diagram. Note that 2 samples plot in the high priority box and two in the second priority box.

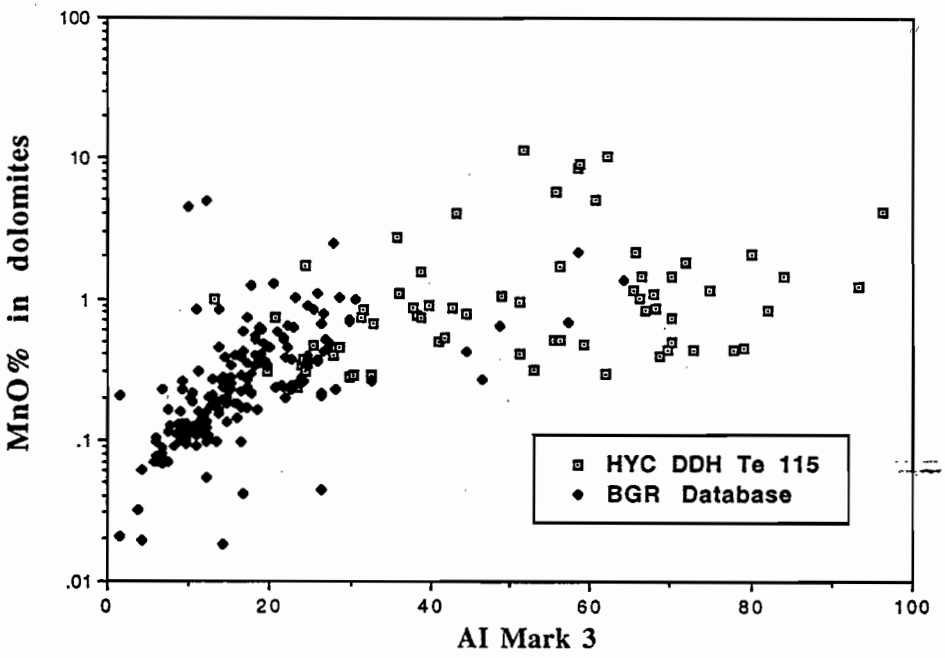

Figure 15—HYC ore body and halo data (DDH Te 115) compared with the BGR background data set.

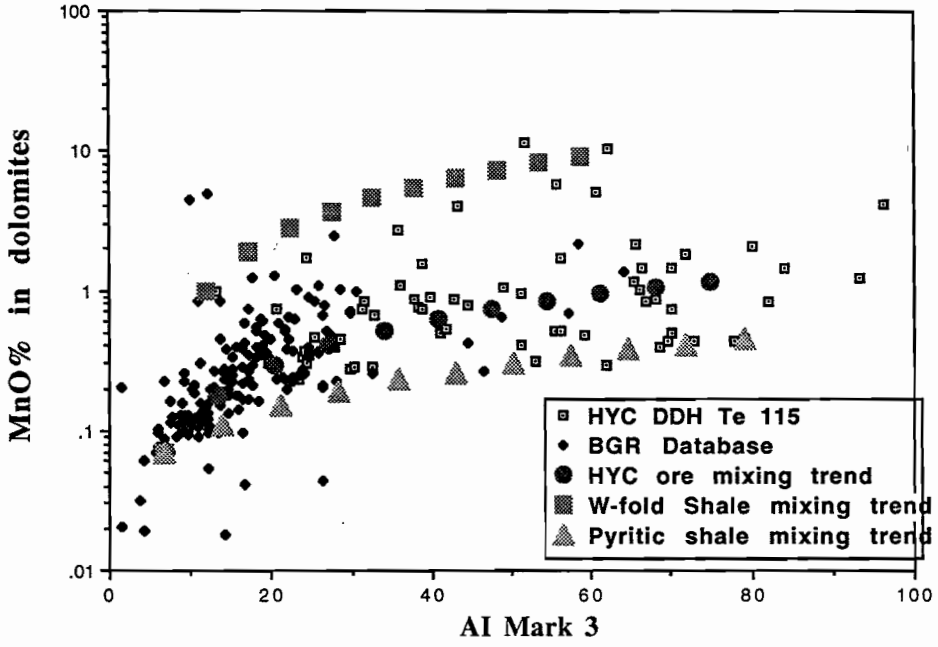

Figure 16—Mixing models for HYC superimposed on the BGR and HYC halo data.

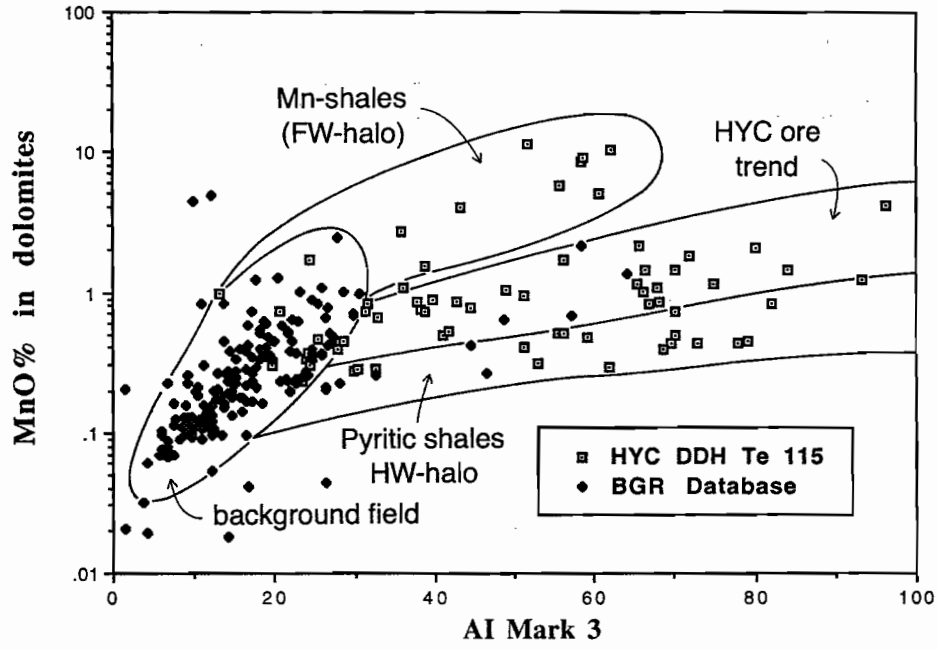

Figure 17—Trend fields for the McArthur Basin Barney Creek Formation based on the mixing models and HYC data sets.

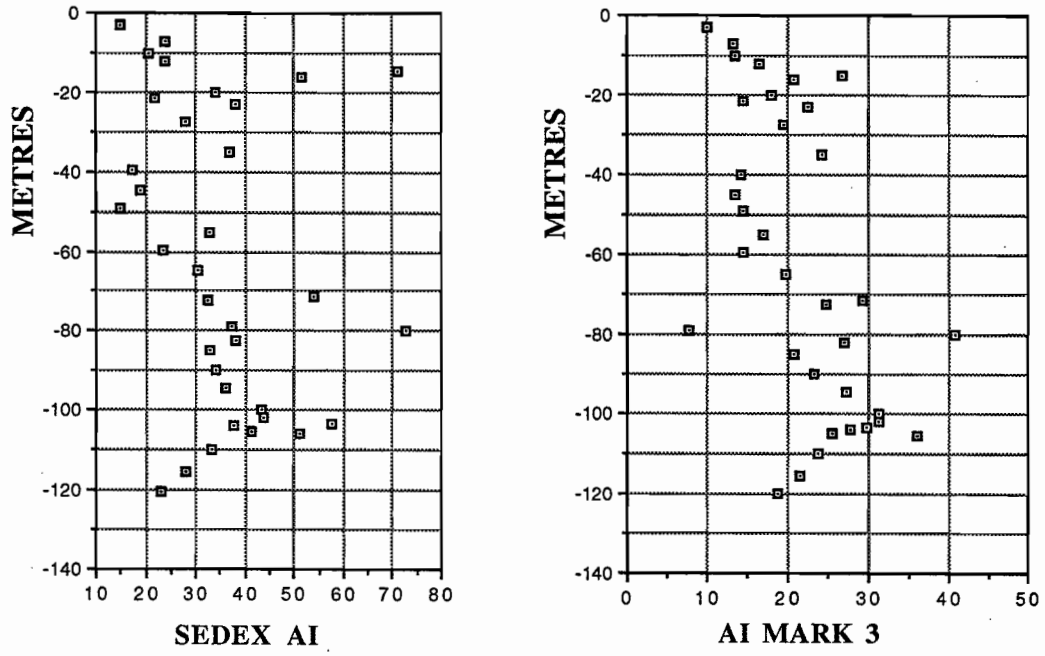

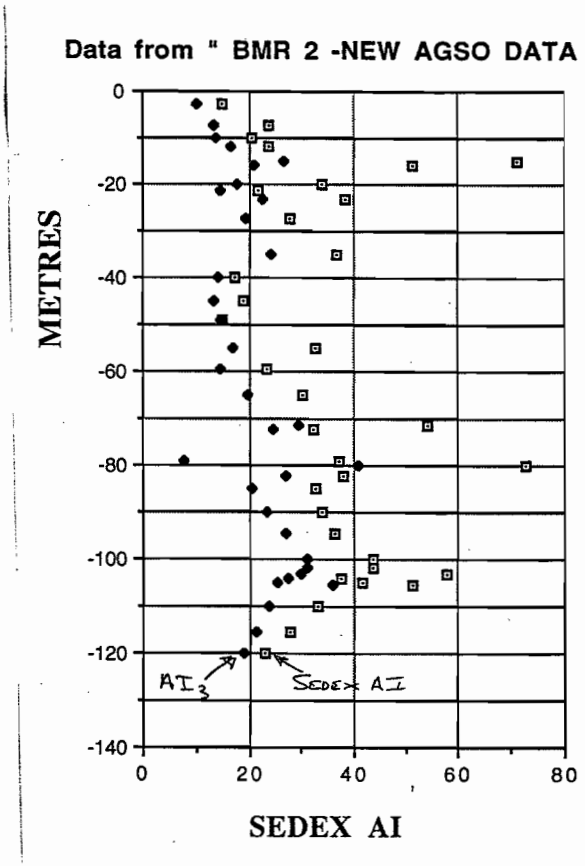

Figure 18—Comparison of down hole plots of Sedex AI and AI3 for the DDH BMR 2 sampling (based on the 1994 AGSO analyses).

Microprobe analysis of carbonate phases at Lady Loretta

Nathan Duhig
Centre for Ore Deposit and Exploration Studies

Introduction

The MnO_D and MnO_S vectors have been shown to be useful indicators of alteration proximity to sediment hosted mineralisation (Large & McGoldrick, 1993). These vectors are based entirely on whole rock analyses and make certain assumptions about the geochemistry and mineralogy, e.g. that all the CaO and MgO is present in carbonates and that all the Fe is taken up in the sulphides and carbonates. In order to test these assumptions it was decided to undertake a reconnaissance program of microprobe analyses of the carbonates from dolomitic sediments in the footwall and the siderite halo around the Lady Loretta, Small Syncline mineralisation.

Method

A number of compounding factors contributed to the sample selection. The best microprobe results are obtained from crystals >10μm diameter, preferably >25μm for single grain traverses. It is possible to probe crystals of 5μm diameter but this requires that the crystal is at least 5μm deep and has a good polished surface, oriented normal to the incoming beam. Unfortunately, carbonates of that grain size are more likely to volatilise during analysis.

Consequently the silts or silty shales were chosen preferentially. Secondly, the samples had to contain enough CO_2 to have carbonate present in appreciable quantities. This was determined to be about 4wt% by comparing the analyses with the thin sections. Higher CO_2 values in the shales correlate with increased abundance of organic carbonaceous matter.

Additionally, a number of polished thin sections (PTS) had already been cut and to minimise delay these were used if they met the above criteria. It was originally hoped to probe about 20 samples, representing a good range from deep in the footwall, though the ore horizon and into the hanging wall. Thus a number of extra PTS were prepared. Because of problems with the probing (see later), satisfactory results were obtained from 10 samples. These are shown in Figure 1.

The PTS were examined under the transmitted microscope and areas with coarse carbonates were marked with ink rings. An image capture card using a video camera hooked to the microscope and a monitor linked to a Mac IIcx computer, "grabbed" the images of the rings which were later output to a colour printer. These are invaluable for fine grained rocks, where the alternative is trying to hand draw enough detail. Depending on the sample a number of areas (1–5) would be mapped this way. Carbonates in the ground mass were chosen in preference to vein or pressure shadow

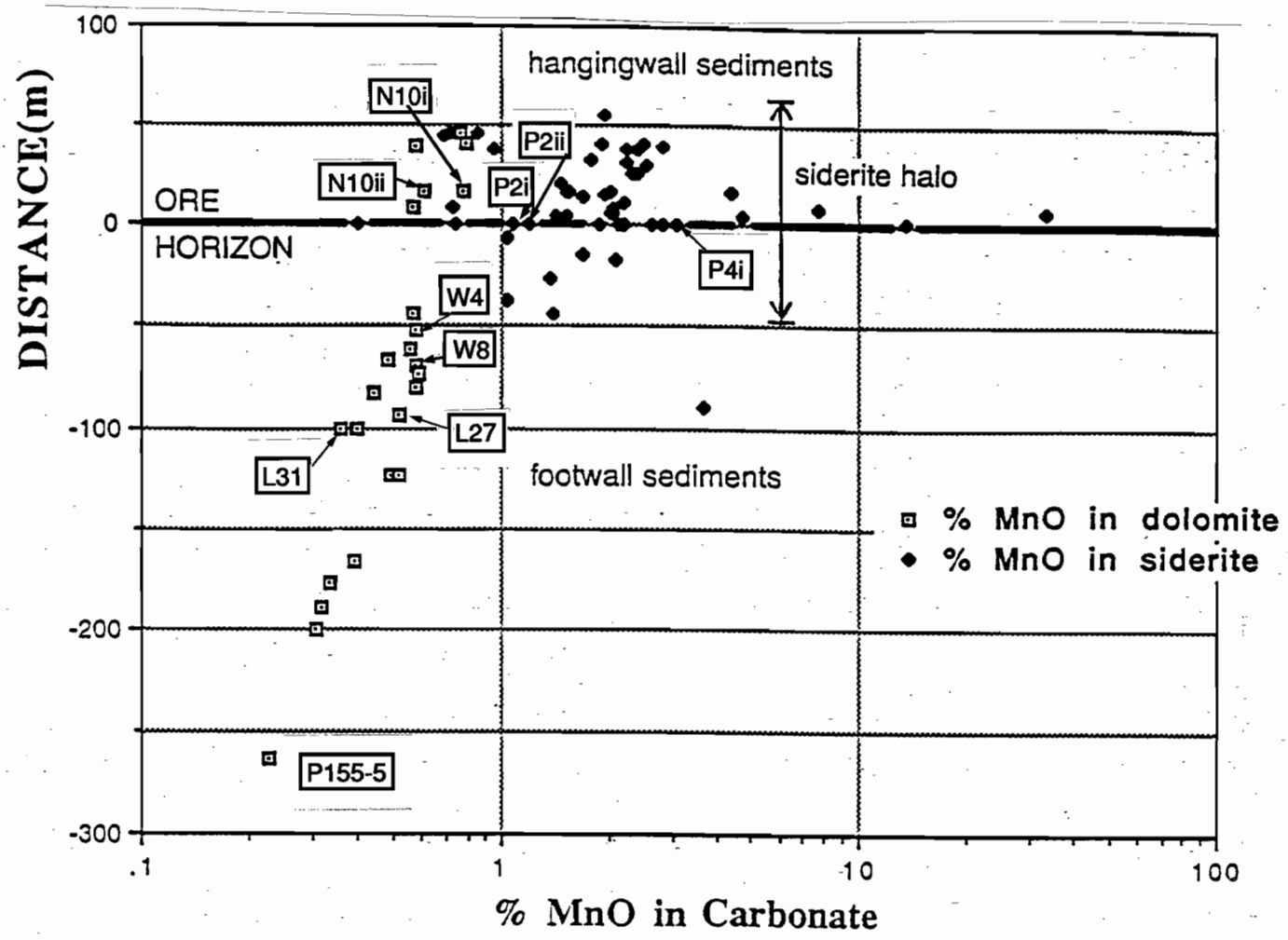

Figure 1— %MnO in carbonate vs distance from ore, showing the samples from which good mircroprobe analyses were obtained.

occurrences. The PTS were carbon coated by Wis Jablonski and all the analysis done on the Cameca SX 50 microprobe, with the guidance of Wis, Russell Fulton and Andrew McNeill. Wis must also be thanked for developing a new label (i.e. routine for the probe, upon which the analysis depends), on short notice. The standard carbonate label analyses for Ca, Mg, Fe, Mn, Ba, Sr and Zn and the new "Carbhigh" label omits Ba, but adds Si, Al, K, Ti and Na for reasons explained later. Results are reported from the probe as percentages of the relevant end member carbonates, i.e. $CaCO_3$, $MgCO_3$, $ZnCO_3$, etc.

After probing, analyses with poor (<95%) totals or excessive contamination (usually ≥5% combined $Si(CO_3)_2$ and $Al(CO_3)_2$) were rejected. Totals were then normalised and a least squares regression technique was used to reduce the Si, Al and K contents to 0%, hence raising the average totals for major cations. This technique was applied to groups of analyses with comparable major cation totals eg. Ca:Mg for the dolomites. It produces an **average** results for the group of analyses. Where this was not possible, an arithmetic mean was calculated.

The normalised MnO contents of the probed carbonates are presented as histograms on a log scale (Figs. 2a - j). On each figure the calculated MnO_D or MnO_S is shown, as is the arithmetic mean or regressed average.

Problems

Grain Size and Intergrowth

As previously indicated, grain size, polish and surface orientation are critical. As grain size drops below 10-15μm the polish quality generally deteriorates and the surface orientation becomes more variable. These constraints become critical as the dolomite and, more particularly, the siderite grains are not monocrystalline, but aggregates of 2-10μm crystals intergrown with fine quartz and muscovite. The grain size problem was surmounted in a brute force manner; try to obtain as many analyses as possible and discard the ones with unsatisfactory totals. The intergrown quartz and muscovite in the aggregates was combated by developing the Carbhigh label and regression method. The omission of Ba from the new label was a misunderstanding.

Despite these techniques, it was difficult to obtain good totals for some of the siderites. They are generally composed of aggregates of finer grains than the dolomites and ankerites. However, even some rare coarse siderites gave low totals. Re-examination of the thin sections revealed that the siderite frequently has a ?limonitic or ?goethitic stain, particularly near the grain boundaries and sometimes contains hematite crystals as inclusions. The presence of a ?hydrous iron oxide will reduce the totals, as the carbonates are assumed to be anhydrous. In one sample, P4i, the possible presence of Pb and/or Ba, which were not analysed for, may have affected the totals.

Discussion

As can be seen from a cursory examination of Fig. 2, most samples have a fairly tight spread. P155-5 (Fig. 2a) had very little groundmass carbonate coarse enough to analyse, so the analyses represent two veinlets and pressure shadows around ?diagenetic nodules of micritic dolomite in a foliated micritic-dolomite matrix. L31 (Fig. 2b) is characterised by the presence of both dolomite and ankerite and L26 (Fig. 2c) is almost entirely ankeritic. W8 and W4 (Figs. 2a and d) are both ferroan dolomite. P4i (Fig. 2f) is a mineralised sample (6.3% Zn, 1% Pb and 5.6% Ba) and contains extremely manganiferous (2.8 → 14 wt% $MnCO_3$) and zincian (0.7 → 14.4 wt% $ZnCO_3$) siderites and sideroplesites (5–30 wt% $MgCO_3$). The Mn and Mg are positively correlated and inversely correlated to Zn and Fe. This sample contains insufficient sulphur for all the zinc to occur as sphalerite, assuming that the Pb, Ba and 80% of the Fe is taken up by the respective sulphide, sulphate and siderite. P2i and P2ii (Figs 2g and h)

contain sideroplesite, both very close to the ore horizon, with P2ii being relatively zincian (~0.5 wt% $ZnCO_3$).

N1Oi (Fig. 2j) again is ankeritic, unusually for a sample from the siderite halo. However, the PTS is extremely carbonate rich and the MnO_D and alteration index values are extremely high for dolomitic sediments.

N1Oii (Fig. 2i), 10cm stratigraphically below N1Oi, gives a fascinating result. Only one ring was sampled in the basal silt of an upwards fining silty ankerite immediately above a 2mm pyrite band. The carbonates ranged in composition from almost pure dolomite (one analysis) through ankerites and the magnesian siderites, sideroplesite and pistomesite. One interpretation is that pyrite band expelled iron during diagenesis, transforming "primary" dolomite to ankerite and ultimately siderite.

Alternatively the pyrite band forming process may be analogous to the ore forming processes and the siderite formation is an integral part of this. Microscopically, there appears to be multiple generations of carbonate and cathode luminescence studies may help to unravel the paragenesis.

Conclusions and recommendations

Microprobe analysis on selected samples indicates a good correlation between the calculated MnO_D values based on whole-rock analysis and the mean microprobe MnO analysis of carbonate grains (Figure 3). However, ankerite, not dolomite, is the dominant carbonate away from the siderite halo. Is this reflecting an ankerite halo? The MnO distribution basically matches the predicted values, except in and around the ore horizon, where zinc becomes important. Siderite compositions are variable with varying substitution between Mg and Mn with Fe and Zn (where Zn is available).

It is recommended to incorporate the analyses from Carr (1981) from host rocks and ore and where appropriate further probe ore siderites. Cathode luminescence studies of some samples, especially N1Oii, may reveal something of the carbonate paragenesis. This technique, combined with etching the ore minerals may also be useful in the ore environment from a paragenetic perspective.

To test whether the siderite halo is a result of later fluid dispersion, probing carbonates immediately adjacent to pyrite bands away from mineralisation may be instructive, to determine whether an Fe ± Mn dispersion halo can be detected. The presence of ankerites within the siderite halo is puzzling but as the MnO_D and alteration index of this sample are both very high, they indicate proximity to an ore forming environment, possibly reflecting similarities to the HYC situation.

References

Carr, G.R., 1981: The mineralogy, petrology and geochemistry of the zinc-lead- silver ores and their host sedimentary rocks at Lady Loretta, north west Queensland. University of Wollongong, Ph.D. thesis (unpublished).

Large, R.R. and McGoldrick, P., 1993: Primary geochemical halos related to Proterozoic sediment-hosted Pb-Zn deposits and applications to exploration. AMIRA P384, unpublished report 4:63-126.

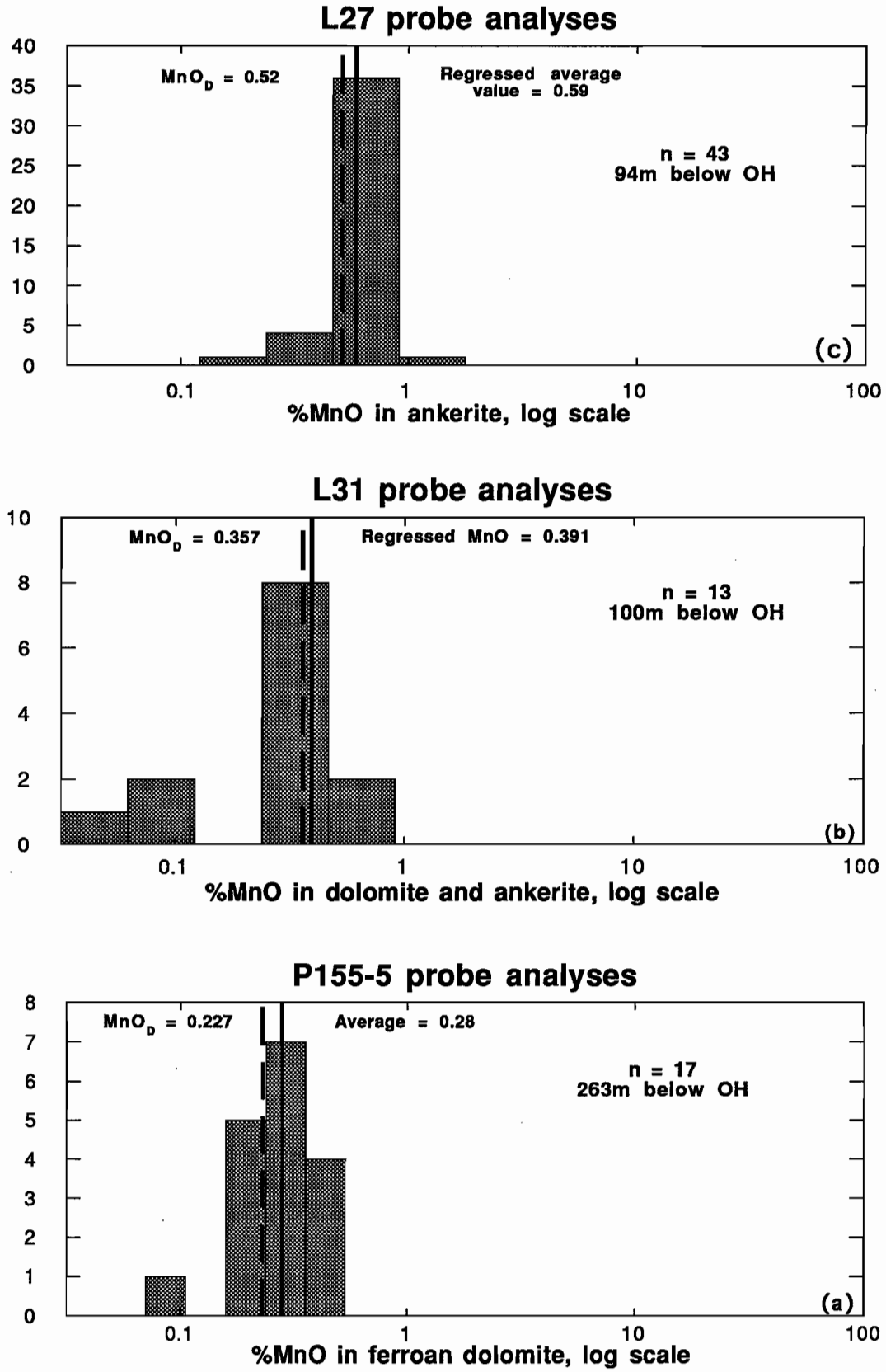

Figure 2—Histograms of %MnO in carbonate from microprobe analyses, using a log scale. The order 2a–j represents a 'traverse' from deep in the footwall, up into the hangingwall.

Figure 2 cont.

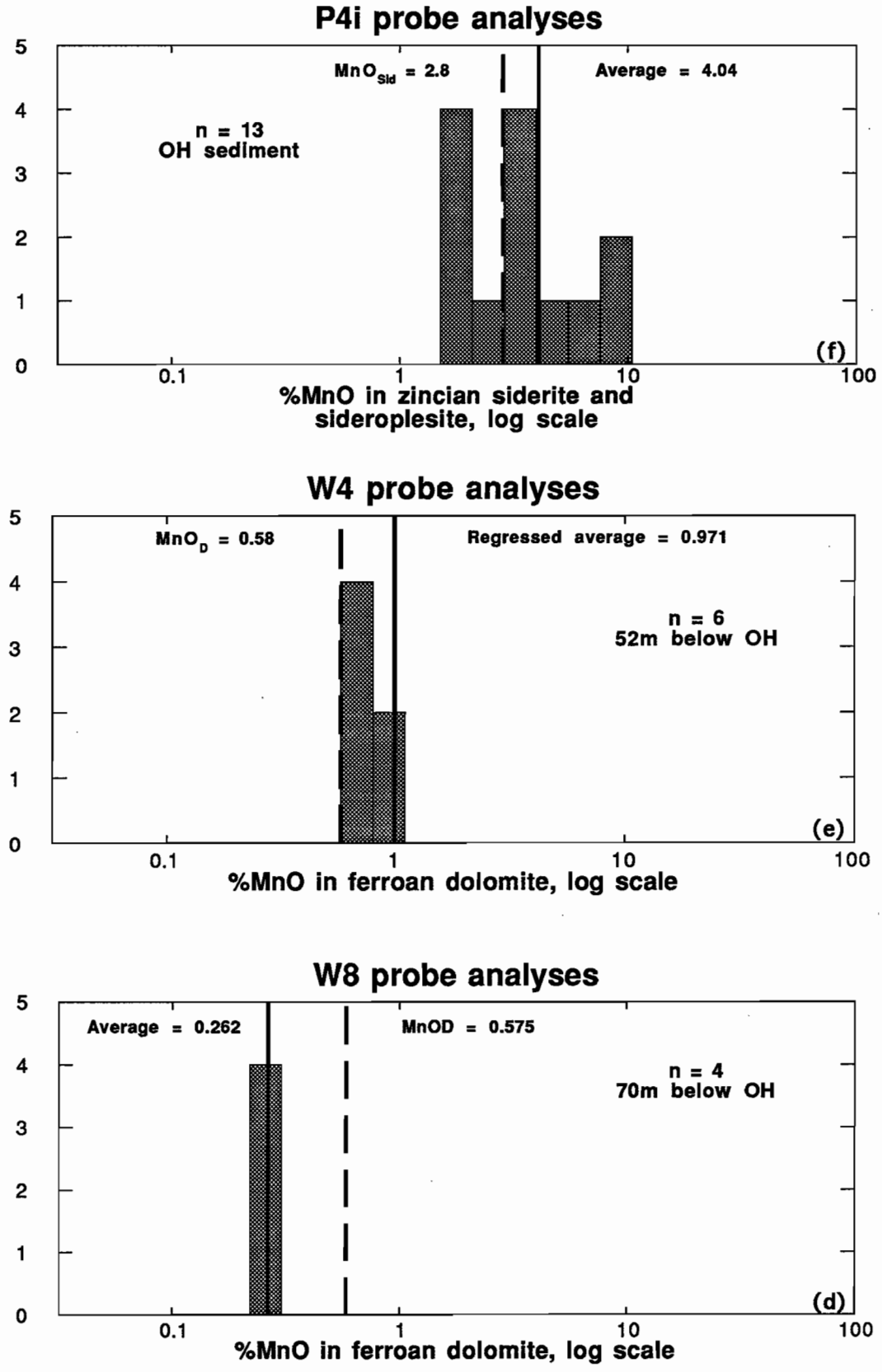

Figure 2 cont.

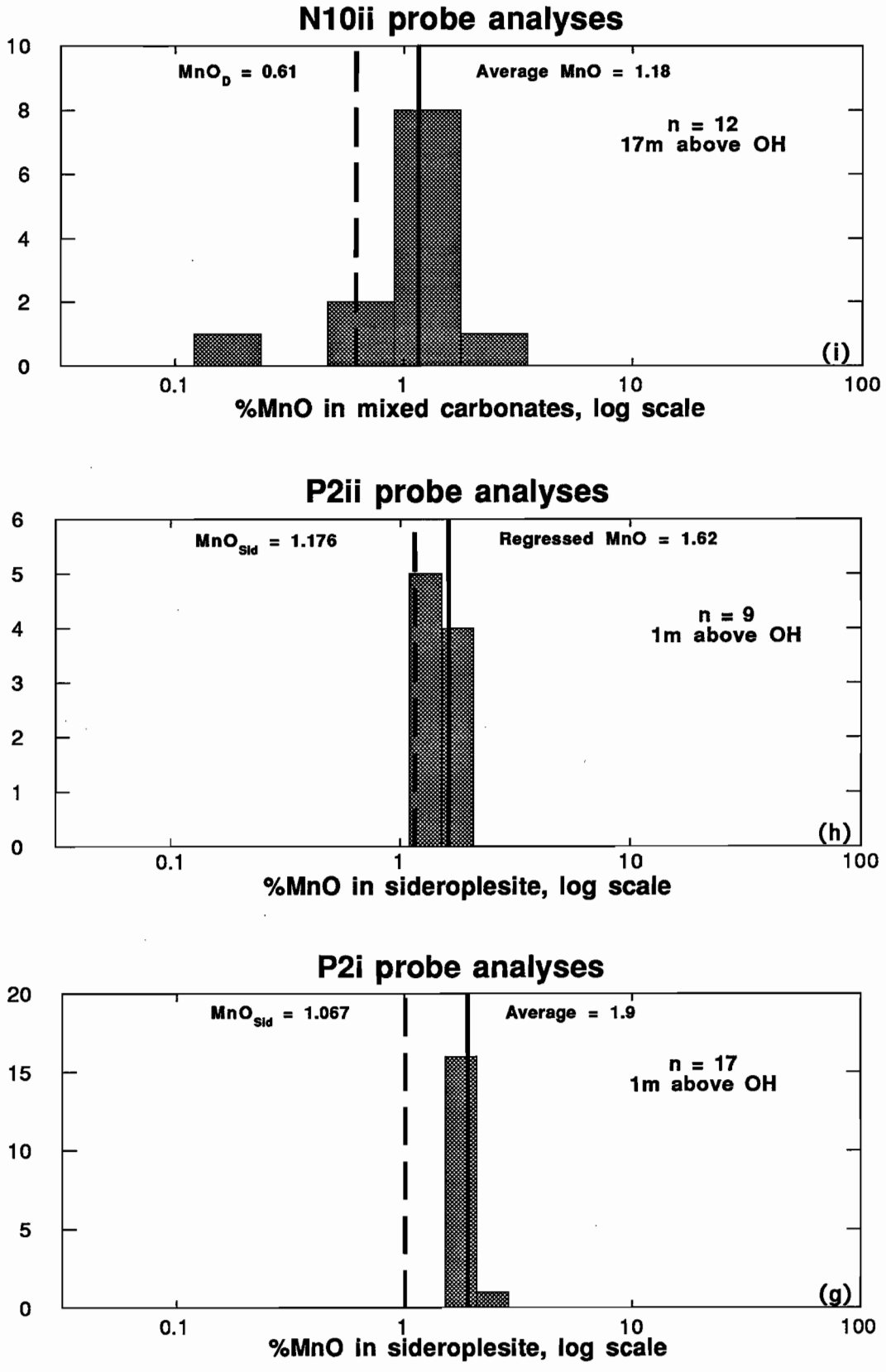

Figure 2 cont.

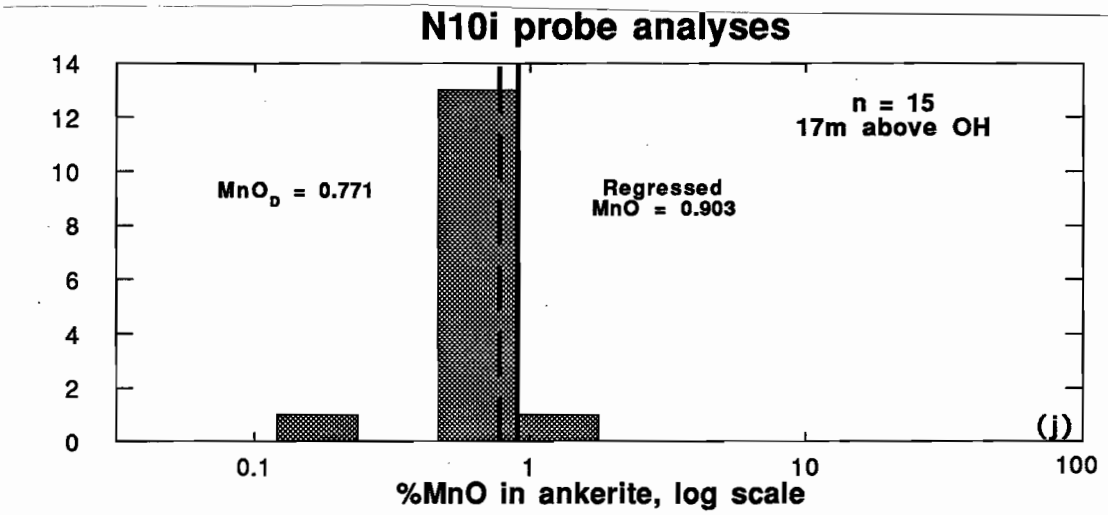

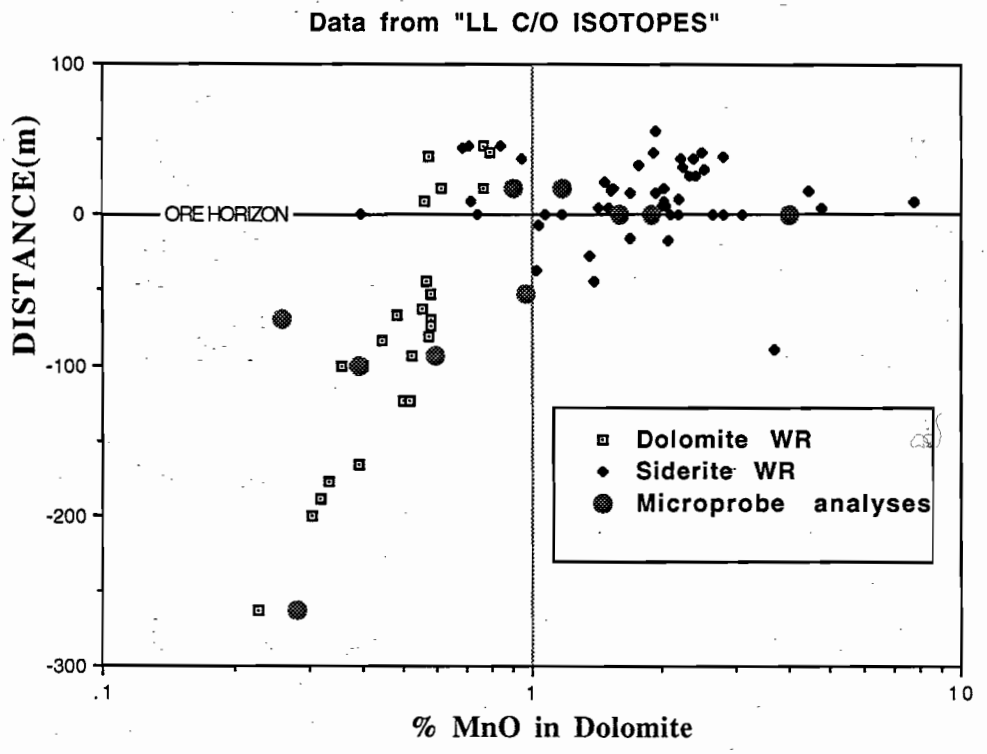

Figure 3—Mean microprobe %MnO in carbonate grains compared with whole-rock MnO_D values for the Lady Loretta data set.

Petrology and tectonic setting of the Tawallah Group igneous rocks

Jamie Rogers
Centre for Ore Deposit and Exploration Studies

INTRODUCTION

The Middle Proterozoic Tawallah Group is recognised as the basal stratigraphic package of the southern McArthur Basin (Jackson et al., 1987), being unconformably underlain by the Early Proterozoic Scrutton Volcanics (1857 ± 30 Ma; Rawlings et al., 1993), and records a period of intracontinental rifting within the northern Australian Craton. Consequently, geochemical characteristics of igneous units within the Tawallah Group have the potential to provide useful information regarding the role of mantle processes that were active during early basin development.

In the study region, the Tawallah Group contains four distinct igneous units; the Seigal Volcanics, Settlement Creek Volcanics, Gold Creek Volcanics and Tanumbirini Rhyolite all of which are considered by Rawlings (1994) to have developed in a continental intraplate setting. This study aims to better define the geochemical traits of these rocks and to determine their magmatic affinities and possible emplacement mechanisms with respect to the tectonic processes controlling basin formation.

GEOLOGICAL SETTING

The Tawallah Group may be divided into two main stratigraphic successions (Rogers and Bull, 1994). The lower succession is dominated by alluvial/fluvial clastic sediments overlain by shallow marine carbonates and include the Seigal Volcanics. These comprise a thick (-250m) and regionally extensive sequence of sheet-like basic lava flows suggested by Rawlings (1994) to have erupted during a period of (largely) subaerial flood volcanism.

Separating the lower succession from the upper succession of the Tawallah Group is a compressional tectonic event (Mid-Tawallah Inversion of Rogers and Bull, 1994) that may have had important influences on the genesis of subsequent magmatic events and their products. Together with lacustrine and high-energy fluvial sediments, the upper succession contain the three youngest Tawallah Group igneous units.

The Settlement Creek Volcanics were emplaced predominantly as shallow intrusive doleritic sills and commonly display upper brecciated (? auto-brecciated) and/or chilled contacts with the overlying Wollogorang Formation. The unit has been previously regarded as a bimodal volcanic sequence (Pietsch et al., 1991), however on closer inspection, many of the 'rhyolites dykes' within the unit are hornfels probably after rafts of

dolomitic siltstone or dolomite that were incorporated during intrusive emplacement at the base of the Wollogorang Formation. Although true rhyolite dykes exist in places (Rawlings, 1994), they comprise a volumetrically small percentage and the Settlement Creek Volcanics may be regarded as a primarily mafic unit.

The Gold Creek Volcanics consist of a series of very high level dolerite sills and minor basalt flows with individual intrusions ranging from 20 to 30 m in thickness. Sills typically display coherent bases that become increasingly vesicular and/or amygdaloidal towards the top, particularly in the upper 10 m. Pépéritic textures developed along upper sill margins are a regionally diagnostic feature of the unit and have been described in detail by Rawlings (1993). The Gold Creek Volcanics intrude what are considered to be the upper sandstone dominated section of the Wollogorang Formation.

The youngest volcanic unit of the Tawallah Group, the Tanumbirini Rhyolite was emplaced as series of localised subaerial lave domes and flows (Pietsch et al., 1991). Recent dating by R.W. Page (AGSO) using SHRIMP analysis of single zircons has revealed an age of 1713 ± 6 Ma for the unit (Rawlings et al., 1993). Rawlings (1994) incorporates the Tanumbirini Rhyolite into the Fagan volcanic phase, a regionally widespread and predominantly felsic magmatic phase that includes the Peters Creek Volcanics (Lawn Hill Platform) and Fiery Creek Volcanics (Mount Isa Inlier).

PETROLOGY

Thirty one representative and relatively unaltered samples of the Tawallah Group volcanic units were analysed for major and trace element geochemistry by XRF spectrometry (Table 1). Of these, three samples from each unit were analysed for rare earth elements using the ionic exchange analytical procedure of Robinson *et al.* (1986), Ta, Hf and Th using instrumental neutron activation analysis. Analysed Tanumbirini Rhyolite Gold Creek Volcanics, and the majority of Settlement Creek Volcanics samples are from surface exposures in the Scrutton Range. An additional three Settlement Creek Volcanics samples were collected from BHP drillhole GSD2 located on Kiana Station within the Emu Fault Zone. Seigal Volcanic exposures in the southern Tawallah Ranges were sampled for petrographic study although are highly altered and not considered useful for geochemical analysis. Relatively fresh drillcore samples of the unit collected by D. Rawlings from the CRAE Namalangi uranium deposit are therefore utilised in this study. Existing analyses from Pietsch *et al.* (1991) and Haines *et al.* (1993) have also been incorporated.

Petrography

Seigal Volcanics

The Seigal Volcanics have a phenocryst and microphenocryst assemblage of subhedral plagioclase (An_{70}-An_{74}; Darby, 1986), relict clinopyroxene (augite), olivine and amphibole and display an intergranular to subophitic texture.

Alteration assemblages include sericite-carbonate-clay ± hematite replacing plagioclase and augite, hematite ± clay completely replacing olivine and chlorite-hematite-sericite ± carbonate ± quartz in the groundmass. Vesicles are ubiquitous with amygdules typically filled with chalcedony, celadonite, calcite, quartz and in places alkali feldspar and sericite.

Settlement Creek Volcanics

The analysed samples show coarse to medium grained ophitic to porphyritic textures although cryptocrystalline and microcrystalline examples have been described by Rawlings (1993). Petrographic examination reveals a mineralogy comprising 60 to 70% sub- to euhedral plagioclase laths (An_{52}; Darby, 1986), 10-20% partially altered augite, 10 to 20% magnetite and accessory hornblende. Porphyritic varieties contain plagioclase as the dominant phenocryst type with augite

Sample No.	94-923	94-924	94-926	93-069	93-071	93-072	93-078	93-079	93-080	93-081	93-082	93-088A	93-088B	94-099	94-100	94-101
Formation	Pts	Pts	Pts	Pte	Pte	Pte	Pte	Pte	Pte	Pte	Pte	Pte	Pte	Pte	Pte	Pte
SiO_2	47.67	48.68	48.16	48.97	48.57	47.10	48.68	48.96	45.29	48.52	45.87	45.45	44.97	50.06	51.08	50.30
TiO_2	1.14	1.09	1.13	2.20	2.15	2.28	2.15	2.12	2.22	2.17	2.19	2.16	2.17	2.03	2.29	2.39
Al_2O_3	15.39	15.18	15.05	13.64	14.36	14.52	13.84	14.02	14.28	13.41	14.09	14.07	14.15	12.67	13.48	13.81
Fe_2O_3	11.43	11.38	12.60	16.16	14.77	14.78	15.52	15.18	12.17	15.81	12.99	13.90	13.95	12.98	12.28	13.53
MnO	0.13	0.16	0.08	0.45	0.35	0.24	0.39	0.28	0.33	0.37	0.32	0.31	0.34	0.11	0.10	0.08
MgO	9.00	8.49	7.83	5.95	5.35	3.97	5.37	5.13	4.02	5.63	5.75	5.22	5.13	6.96	6.96	8.05
CaO	7.70	7.41	6.09	3.96	4.28	5.44	4.23	5.00	8.31	4.91	5.27	5.78	5.98	2.96	2.51	1.15
Na_2O	1.72	1.77	1.60	2.03	2.43	2.34	2.34	2.21	2.38	2.37	1.88	2.16	1.88	2.32	4.40	3.93
K_2O	1.75	2.18	2.44	2.67	3.43	2.89	2.88	3.07	2.38	2.84	3.47	3.19	3.14	2.85	1.58	1.78
P_2O_5	0.15	0.15	0.15	0.44	0.41	0.40	0.43	0.42	0.44	0.43	0.45	0.43	0.42	0.37	0.40	0.39
L.O.I.	4.00	3.51	5.07	3.97	3.77	5.81	4.05	3.60	7.98	3.65	8.13	7.58	7.51	6.35	5.69	5.28
Total	100.08	100.00	100.20	100.42	99.87	99.77	99.89	100.00	99.79	100.09	100.42	100.25	99.65	99.66	99.77	99.69
Zr	116	112	114	172	161	165	169	167	190	170	186	183	180	190	201	198
Nb	7	7	7	11	9	9	11	10	11	10	11	11	12	12	13	12
Y	29	28.5	27.5	35.1	33.8	35.2	36.1	35.5	39.9	36	42.5	42.5	43.1	37.5	42.5	37
Rb	54	59	84	90	127	100	101	125	80	108	97	97	97	110	14.5	15.5
Sr	114	120	99	167	161	163	170	190	157	171	90	129	134	97	52	44
U	1.05	1.60	1.75	1.90	1.40	3.00	2.00	1.40	2.20	2.80	0.80	1.70	2.00	2.70	2.90	1.90
Th	3.66	3.18	3.16	7.20	5.40	5.60	6.80	6.90	7.03	7.28	6.90	7.50	7.14	8.50	9.60	9.70
Ta	1.27	0.98	0.97	-	-	-	-	-	1.29	1.35	-	-	1.42	-	-	-
Hf	2.71	2.68	2.71	-	-	-	-	-	4.19	4.45	-	-	4.08	-	-	-
Ba	244	265	319	774	1246	1138	1068	1181	1271	955	671	839	914	1136	170	223
Sc	38	35	40	33	34	37	34	32	39	32	36	35	38	36	39	39
V	259	249	310	266	296	358	271	263	340	266	322	336	338	349	421	430
Ni	141.5	140.5	137.5	35.7	23.9	25.1	30.9	32.5	30.5	32.6	32.0	32.3	31.7	21.0	13.5	14.5
Cr	160	156	180	58	38	34	54	56	70	58	63	62	65	30	10	10
Cu	44	20.5	110	40	35	52	35	34	61	38	58	57	52	49.5	13	10
Pb	6.5	6.5	10.0	151.0	61.0	34.0	111.0	87.0	30.0	71.0	14.0	81.0	60.0	157.0	4.0	5.5
Zn	85.5	89.0	49.0	366.0	182.0	161.0	233.0	284.0	131.0	191.0	138.0	214.0	205.0	255.5	86.5	90.5
La	14.5	13.8	14.4	-	-	-	-	-	31.3	30.3	-	-	30.4	-	-	-
Ce	32.4	30.8	31.5	-	-	-	-	-	66.5	63.1	-	-	65.4	-	-	-
Pr	3.98	3.9	3.99	-	-	-	-	-	8.01	7.78	-	-	7.70	-	-	-
Nd	16.90	16.20	16.50	-	-	-	-	-	33.4	32.2	-	-	32.0	-	-	-
Sm	4	4.1	3.83	-	-	-	-	-	6.62	6.56	-	-	6.63	-	-	-
Eu	1.18	1.12	1.08	-	-	-	-	-	2.01	1.87	-	-	2.17	-	-	-
Gd	4.54	4.49	4.4	-	-	-	-	-	7.05	6.70	-	-	7.44	-	-	-
Tb	0.64	0.72	0.67	-	-	-	-	-	-	-	-	-	-	-	-	-
Dy	4.7	4.53	4.46	-	-	-	-	-	6.53	6.34	-	-	6.92	-	-	-
Ho	0.88	1	0.97	-	-	-	-	-	-	-	-	-	-	-	-	-
Er	2.77	2.86	2.78	-	-	-	-	-	3.80	3.92	-	-	4.16	-	-	-
Yb	2.51	2.52	2.48	-	-	-	-	-	3.26	3.21	-	-	3.47	-	-	-

Table 1. Wholerock analyses of selected samples from the Seigal Volcanics (Pts) and Settlement Creek Volcanics (Pte). Trace element concentrations in ppm.

Sample No.	94-035	94-036	94-037	94-038	94-039	94-040	94-041	94-042	94-043	94-044	93-111	93-112	93-113	93-114	93-115
Formation	Ptg	Ptg	Ptg	Ptg	Ptg	Ptg	Ptg	Ptg	Ptg	Ptg	Ptt	Ptt	Ptt	Ptt	Ptt
SiO_2	44.61	48.06	44.10	44.25	44.10	47.69	45.77	47.57	46.30	46.57	77.50	75.51	76.35	76.39	76.60
TiO_2	2.25	2.15	2.23	2.20	2.17	2.75	2.71	2.70	2.74	2.72	0.34	0.37	0.34	0.36	0.39
Al_2O_3	14.13	14.30	13.86	14.09	14.12	16.51	16.13	16.32	16.16	16.24	13.85	15.40	14.11	13.84	13.57
Fe_2O_3	12.80	12.63	14.69	13.01	13.38	13.12	15.58	14.94	15.36	14.54	3.32	3.88	3.53	3.65	3.86
MnO	0.15	0.12	0.14	0.19	0.18	0.15	0.13	0.12	0.14	0.13	0.01	0.00	0.01	0.01	0.01
MgO	9.56	7.64	8.07	8.66	8.38	5.46	4.50	4.01	4.87	5.06	0.06	0.05	0.05	0.05	0.05
CaO	4.71	3.96	5.00	5.39	5.41	2.53	3.24	2.76	2.60	2.74	0.00	0.00	0.00	0.00	0.00
Na_2O	2.97	3.40	3.50	3.68	3.72	4.56	4.03	5.10	4.58	4.48	0.32	0.03	0.08	0.13	0.12
K_2O	1.03	1.48	1.36	1.63	1.67	3.10	3.63	2.54	2.75	3.07	0.29	0.19	0.20	0.18	0.18
P_2O_5	0.30	0.27	0.30	0.27	0.27	0.43	0.42	0.41	0.43	0.42	0.04	0.05	0.05	0.06	0.05
L.O.I.	7.70	5.65	6.95	7.40	7.18	3.60	3.64	3.25	3.68	3.73	4.98	5.39	5.47	5.07	4.89
Total	100.21	99.66	100.20	99.77	99.58	99.90	99.78	99.72	99.61	99.70	100.71	100.89	100.18	99.74	99.71
Zr	194	172	189	174	176	268	267	266	271	269	381	414	385	402	407
Nb	19	18	20	17	17	26	27	26	26	26	22	24	24	25	26
Y	33	30	32	31	30.5	45	46	45.5	46	45	34.5	22.6	31	37.1	30.9
Rb	27	40	31	15.5	17.5	66	82	63.5	64	68	5	3	4	3	3
Sr	53	82	63	91	92	162	185	162	162	162	74	121	87	111	100
U	1.70	1.60	1.25	0.90	1.45	1.45	1.60	2.10	1.50	1.35	3.60	4.60	4.70	5.70	3.70
Th	3.85	3.10	3.90	2.76	3.75	4.75	4.50	4.90	5.40	4.62	40.10	38.30	40.60	42.40	40.20
Ta	-	-	-	1.26	-	-	-	2.42	-	1.95	-	2.34	-	-	1.87
Hf	-	-	-	4.01	-	-	-	6.08	-	6.17	-	9.93	-	-	10.00
Ba	155	184	204	150	150	696	774	474	601	651	61	57	52	60	68
Sc	34	33	34	34	36	24	23	23	22	24	7	7	7	7	7
V	278	271	271	266	272	220	229	225	216	209	10	17	15	15	15
Ni	251.5	207.5	239.0	230.0	229.5	55.0	55.0	56.0	57.5	55.5	1.3	2.5	2.5	1.8	2.0
Cr	346	355	312	322	331	10	9	11	10	9	2	2	2	2	1.9
Cu	22.5	8.5	9	10.5	10	16	10	9.5	10	11	3	2	5	2	2
Pb	6.5	9.5	7.5	10.0	10.5	9.0	13.5	10.0	11.0	11.0	14.0	25.0	30.0	27.0	32.0
Zn	138.5	101.0	105.5	136.0	131.0	171.5	138.0	129.0	158.0	143.0	16.0	11.0	27.0	18.0	24.0
La	-	-	-	21.7	-	-	-	34.5	-	34.3	-	77.4	-	-	94.3
Ce	-	-	-	52.7	-	-	-	81.7	-	79.8	-	146.0	-	-	165.8
Pr	-	-	-	6.9	-	-	-	10.7	-	10.3	-	13.69	-	-	17.06
Nd	-	-	-	29.9	-	-	-	44.7	-	43.3	-	40.2	-	-	50.1
Sm	-	-	-	6.63	-	-	-	9.52	-	9.12	-	5.16	-	-	6.35
Eu	-	-	-	2.0	-	-	-	2.8	-	2.6	-	1.29	-	-	1.39
Gd	-	-	-	6.52	-	-	-	9.37	-	8.99	-	3.18	-	-	4.03
Tb	-	-	-	0.89	-	-	-	1.31	-	1.29	-	-	-	-	-
Dy	-	-	-	5.50	-	-	-	8.05	-	7.83	-	4.61	-	-	5.98
Ho	-	-	-	1.06	-	-	-	1.77	-	1.65	-	-	-	-	-
Er	-	-	-	2.82	-	-	-	4.41	-	4.28	-	3.62	-	-	4.47
Yb	-	-	-	2.43	-	-	-	3.70	-	3.57	-	4.15	-	-	4.75

Table 1 (cont.). Wholerock analyses of selected samples from the Gold Creek Volcanics (Ptg) and Tanumbirini Rhyolite (Ptt). Trace element concentrations in ppm.

and/or hornblende microphenocrysts set in a groundmass of lath-shaped and sericitised plagioclase, interstitial magnetite and cryptocrystalline material.

Alteration assemblages consist primarily of interstitial chlorite and sericite, the latter predominantly replacing plagioclase, with minor quartz, dolomite, alkali feldspar, clay and hematite. Amorphous rutile is occasionally found in association with chlorite, ilmenite occurs as possible exsolutions of primary magnetite. Pyrite and chalcopyrite occur as disseminations, in microfractures and along plagioclase cleavage planes.

Rare instances of intergranular pumpellyite may suggest the former presence of a glassy groundmass prior to low grade metamorphism or burial. Amygdules within the Settlement Creek Volcanics are uncommon but when present contain quartz, celadonite, dolomite or chalcedony.

Gold Creek Volcanics

The analysed Gold Creek Volcanic samples display either micro- to cryptocrystalline or porphyritic textures. The porphyritic examples are dominated by partially sericitised plagioclase phenocrysts that are strongly aligned to develop flow textures. Subophitic and intergranular textures have been described for the Gold Creek Volcanics by Rawlings *et al.* (1993) and are olivine-pyroxene bearing. It is feasible that these minerals are present in the cryptocrystalline groundmass of samples analysed in this study.

Representative dolerites from the lower to middle portions of two separate sills were sampled. This was necessary as amygdule content increases dramatically towards the pépéritic upper margins. Amygdules are predominantly filled with celadonite, calcite and quartz. Alteration assemblages are again dominated by chlorite-sericite-carbonate although secondary pyrite and chalcopyrite are less abundant than analysed Settlement Creek Volcanic samples.

Tanumbirini Rhyolite

The Tanumbirini Rhyolite is strongly porphyritic containing quartz phenocrysts up to 15 mm in diameter in a fine to medium gained micropoikilitic quartz groundmass. High concentrations of lithic fragments, dominantly chert and ferruginous material, are common. Crystal margins are highly irregular with sericite developed in the interstices between grains. Randomly orientated feldspar laths are occasionally contained within individual quartz crystals. These features define a micropoikilitic texture that McPhie et al. (1993) ascribes to initial devitrification of a slowly cooling lava of silicic composition.

Alteration and element mobility

According to Rollinson (1993), 'any suite of rocks which has been subjected to hydrothermal alteration or metamorphism is likely to suffer element mobility'. The igneous rocks of the Tawallah Group have been subject to prehnite-pumpellyite facies metamorphic conditions and regional hydrothermal alteration events.

Alteration of the mafic units of the Tawallah Group has been well documented (Donovan, 1993; Pietsch et al., 1991) and is characterised by regional pervasive potassic alteration and localised sporadic propylitic alteration. Pietsch et al. (1991) suggest that the potassic alteration, which was accompanied by Fe^{2+} enrichment and depletion of Na, Ca, Mg and Fe^{3+}, developed during a period of regional metasomatism relating to intrusion of potassic-ultrapotassic plutons at depth. Donovan (1993), in a detailed geochemical and isotopic study of the Settlement Creek and Gold Creek Volcanics at Mallapunyah Dome, favours an early diagenetic timing for the potassic alteration whereby relatively oxidised basinal brines derived from nearby evaporitic sediments interact with the volcanics during early burial.

In either scenario, many authors (Floyd and Winchestor, 1975; Crawford and von Rad, 1994; Rollinson, 1993) suggest that under low grade alteration and metamorphic conditions such as these, high field strength elements (REE, Y, Th, Zr,

Hf, Ti, Nb, Ta and P) generally remain immobile in basaltic rocks. A simple check for element mobility is to plot high field strength elements against each other on binary variation diagrams (Stolz, 1992). Element mobility during alteration or metamorphism can then be recognised as dispersed data, showing no linear trend that projects through the origin. Linear trends for Zr based variation diagrams (figure 4) suggest that all high field strength elements have remained immobile in the analysed samples of this study. A possible exception however is Y, which displays minor deviations from the expected linear trend.

Major and trace element compositions

Seigal Volcanics

Major and trace element analyses of the Seigal Volcanics indicate a basaltic composition with SiO_2 contents of 47.67-50.60 %. Relative to the younger igneous rock types of the Tawallah Group and regarding only the immobile elements, these rocks have characteristically low abundances of TiO_2 (1.09-1.36 %), P_2O_5 (0.12-.15 %), Nb (7-11 ppm), Zr (112-155 ppm) and Y (22-29 ppm). Typically high Mg numbers (≈ 43) suggest that the basalts are moderately evolved.

High Y/Nb (1.9-3.3) and Zr/P_2O_5 (0.072-0.12) indicate a tholeiitic affinity for the Seigal Volcanics (figure 1) and plot in the andesite/basalt to sub-alkaline fields on the least-mobile element variation diagram Zr/TiO_2-Nb/Y (figure 2). Tectonic discrimination diagrams (figure 3) based on Ti-Y-Nb-Zr associations imply a within plate setting for these mafic rocks, although a few exceptions plot transitional to the mid-ocean ridge basalt field.

Settlement Creek Volcanics

Analysed Settlement Creek Volcanic samples are predominantly basaltic although more evolved rock types approach andesitic compositions so that SiO_2 abundances range between 43.1-51.0 %. Haines *et al.* (1993) has suggested however that some SiO_2 enrichment may be related to post-compactional metasomatism rather than true magmatic fractionation.

In contrast to the Seigal Volcanics, these rocks have comparatively higher immobile element concentrations with TiO_2 (2.03-2.39 %), P_2O_5 (0.37-0.45 %), Nb (9-13 ppm), Zr (161-201 ppm) and Y (33.8-43.1) enriched by a factor of approximately two relative to the older mafic sequence. Y/Nb (2-3.3) and Zr/P_2O_5 (0.04-0.05) are again indicative of a tholeiitic affinity (figure 1) however relatively low Zr/P_2O_5 values suggest a more alkaline nature than shown by the Seigal Volcanics, particularly in relation to TiO_2. This feature is also suggested by the Zr/TiO_2-Nb/Y variation diagram (figure 2) with most of the more mafic rock types plotting in the sub-alkaline field. Furthermore, generally lower Mg numbers (≈ 36) indicate that the Settlement Creek Volcanics contain more highly evolved rock types than the Seigal Volcanics.

With respect to tectonic discrimination, relative abundances of Ti-Y-Nb-Zr strongly imply a within-plate setting for the Settlement Creek Volcanics (figure 3). The single sample that falls within the mid-ocean ridge basalt field contains an unusually high abundance of Y and other incompatible elements (Pietsch et al., 1991) and consequently plots away from the observed fractionation trends of figure 4. This suggests some mobility of high field strength elements for this particular Settlement Creek Volcanic sample.

Gold Creek Volcanics

Analysed Gold Creek Volcanic samples are generally basaltic in composition with SiO_2 contents between 44.1-48.1 %. However, based on immobile major and trace element abundances, two distinct groups are recognised. Group 1 dolerites are highly evolved (Mg number; 23-32) with compositions characterised by increased concentrations of TiO_2 (2.7-2.75 %), P_2O_5 (0.41-.043 %), Nb (26-27 ppm), Zr (266-271 ppm) and Y (45.5-46 ppm) relative to the Settlement Creek Volcanics. Group 2 dolerites are moderately evolved (Mg number; 31-45) relative to group 1 and have lower concentrations of TiO_2 (2.5-2.25 %), P_2O_5 (0.27-0.3 %), Nb

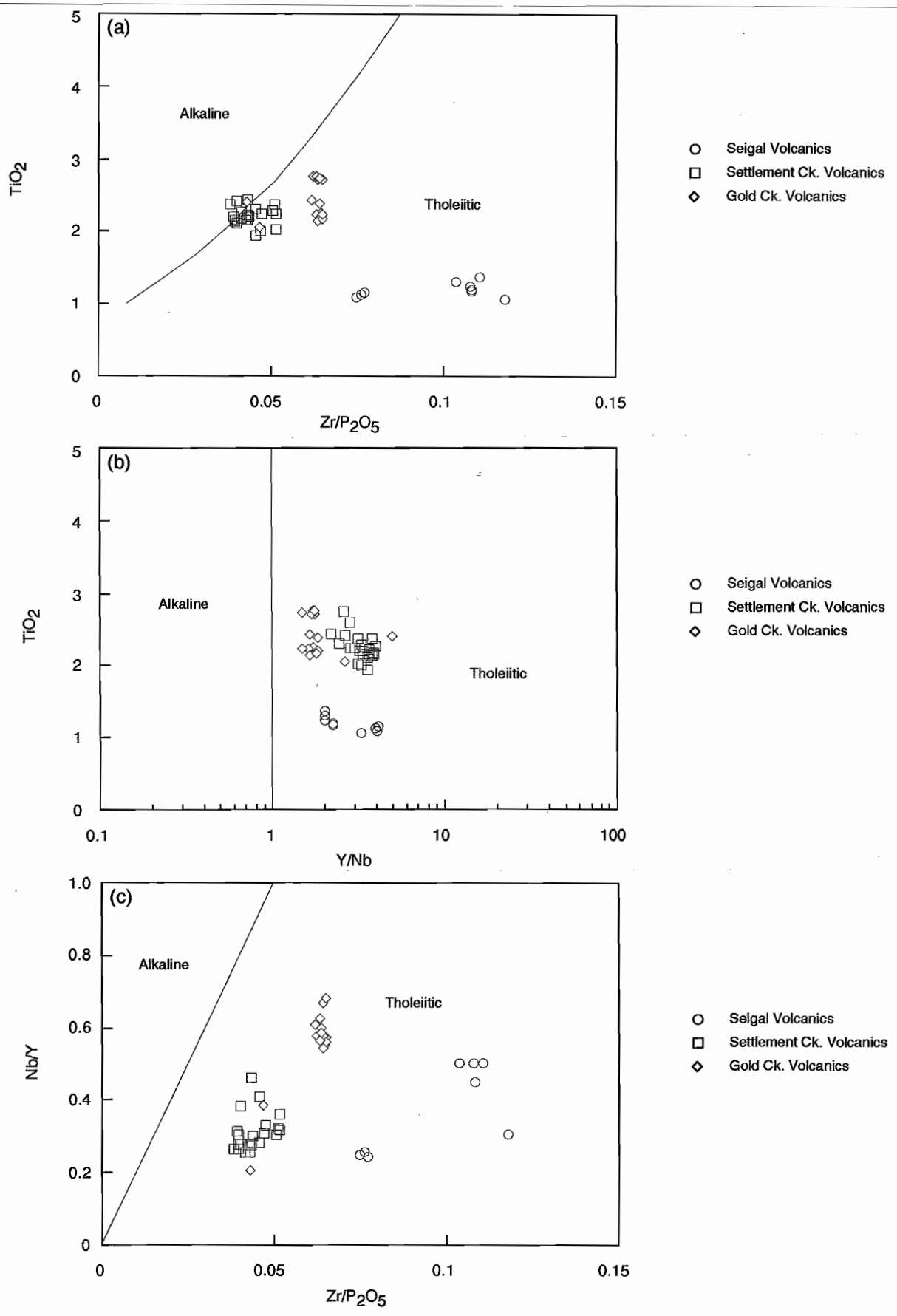

Figure 1. Plots of (a) TiO_2 versus Zr/P_2O_5, (b) TiO_2 versus Y/Nb and (c) Nb/Y versus Zr/P_2O_5 (Winchester and Floyd, 1976) for analysed sample from the Seigal Volcanics (circles), Settlement Creek Volcanics (squares) and the Gold Creek Volcanics (diamonds). Samples used for these plots are exclusively mafic/intermediate in composition.

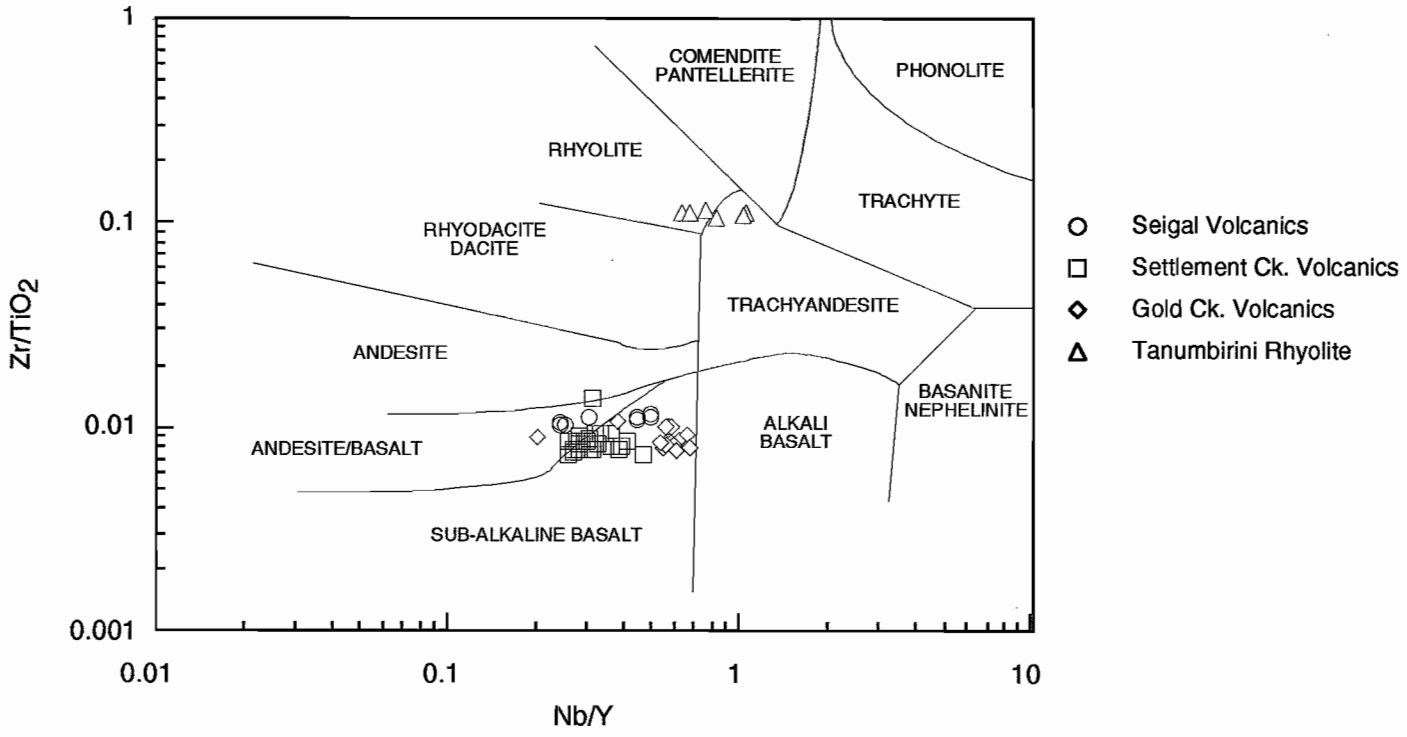

Figure 2. Plot of Zr/TiO_2 versus Nb/Y (Winchester and Floyd, 1977) for analysed samples of the Tawallah Group igneous units.

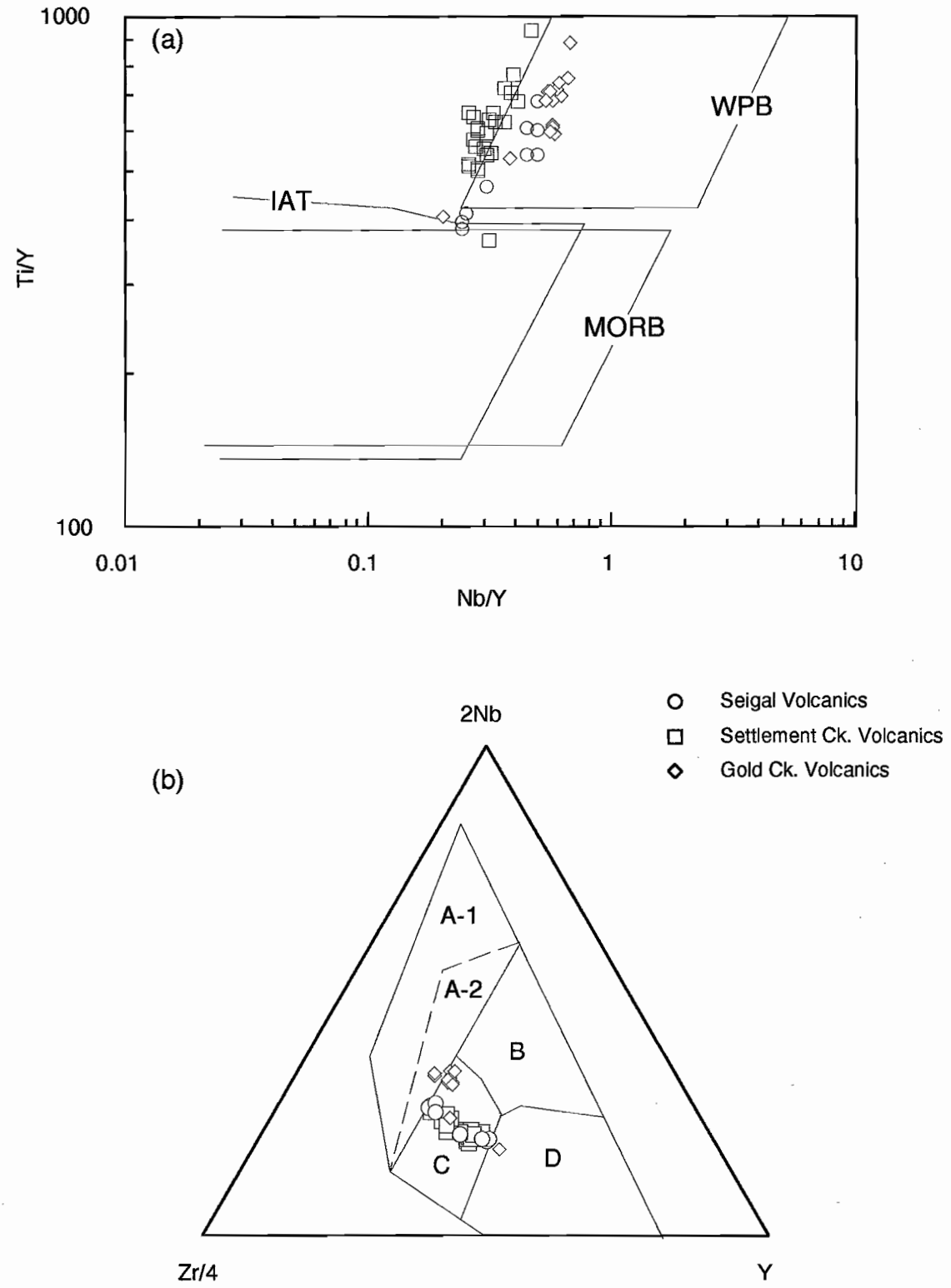

Figure 3. Trace element discrimination diagrams for basalts. Plot (a) Zr/TiO2 versus Nb/Y (Pearce, 1982) showing fields of within-plate basalts (WPB), volcanic-arc basalts (VAB) and MORB. Plot (b) Zr-Nb-Y (Merschede, 1986) showing fields of within-plate alkali basalts (A-1), within-plate alkali basalts and within-plate tholeiites (A-2), E-type MORB (B), within-plate tholeiites and volcanic arc basalts (C) and N-MORB and volcanic-arc basalts (D).

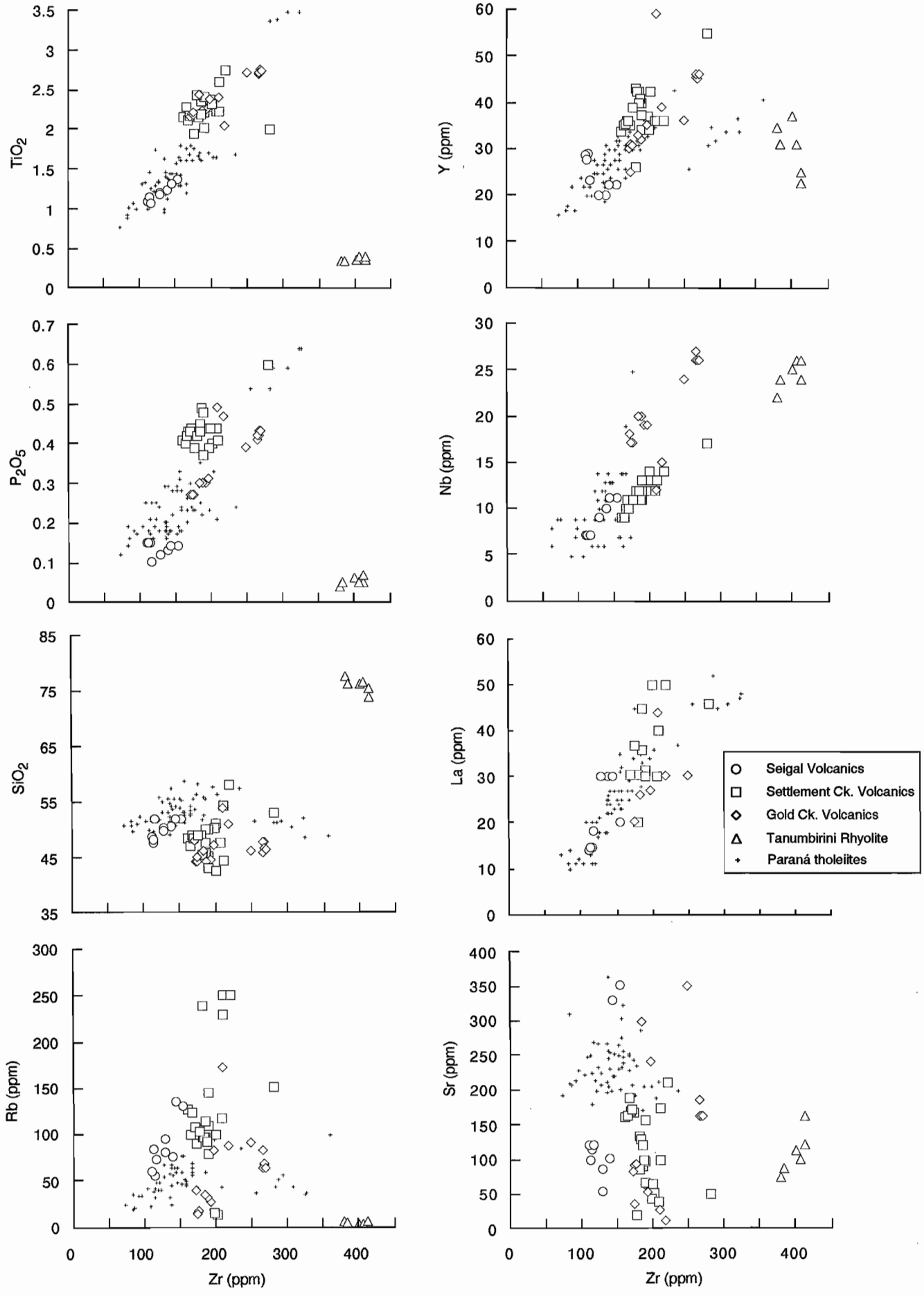

Figure 4. Variation diagrams showing the distribution of major (TiO_2, SiO_2, P_2O_5) and trace element (Y, Nb, La, Rb, Sr) distribution within the Tawallah Group igneous units. Selected tholeiitic basalts and andesites of the Paraná CFB province after Bellieni *et al.* (1984), Fodor *et al.* (1983) and Fodor and Vetter (1984).

(17-20 ppm), Zr (172-194 ppm) and Y (30-33 ppm). Immobile element variation diagrams (figure 4) would suggest that these compositional differences are controlled by variable degrees of fractionation. Interestingly, group 2 dolerites display very high abundances of Cr (312-355 ppm) and Ni (207.5-251.5 ppm) when compared to similarly evolved rock types from the older igneous units and while showing general similarities to Seigal Volcanic compositions, their relatively high TiO_2 and P_2O_5 content suggests a closer relationship to the Settlement Creek Volcanics in terms of the overall genesis of the Tawallah Group igneous rocks.

The Gold Creek Volcanics can be classified as tholeiitic dolerites as shown by their Y/Nb and Zr/P_2O_5 relationships (figure 1). Nb/Y ratios are somewhat higher than shown by Seigal and Settlement Creek Volcanic samples and accordingly plot within the subalkaline basalt field of the Nb/Y-Zr/TiO_2 least-mobile element variation diagram (figure 2). A further consequence of high Nb/Y ratios, in association with relatively high Ti and Zr values, is that Gold Creek Volcanic samples plot almost completely within the within-plate basalt fields for the tectonic discrimination diagrams of figure 3.

Tanumbirini Rhyolite

The Tanumbirini Rhyolite is typified by relatively high concentrations of SiO_2 (75.5-77.5 %), Zr (385-414 ppm), La (77.4-94.3 ppm), Ce (146.0-165.8 ppm), U (3.6-5.7 ppm) and Th (40.1-42.4 ppm) with low K_2O (0.18-0.29 %), Na_2O (0.03-0.32 %) and Rb (3-5 ppm) and plot within the rhyolite field for the Zr/TiO_2-Nb/Y variation diagram (figure 3). In terms of immobile element concentrations, this composition is typical of similarly aged Proterozoic felsic volcanic suites elsewhere within Australia (Wyborn *et al.*, 1987).

Wyborn et al. (1987) state that the felsic volcanics of this period are predominantly I-type and are sourced from granulitic lower crustal regions. Cox (1980) has proposed that the gabbroic deep crustal sill complexes that underplate continental crust to source flood basalt volcanism ultimately invert to granulite facies assemblages. Wyborn *et al.* (1987) suggests therefore that mafic material has underplated continental crust during earlier Proterozoic extension to generate progressively accreting I-type source regions. Consequently, the Tanumbirini Rhyolite may represents the product of lower crustal partial melts subsequent to production of the tholeiitic magmas.

Unusually low alkali contents of the Tanumbirini Rhyolite is likely to reflect a combination of alteration and surface weathering (silicification) resulting in the predominant quartz and minor sericite mineralogy and almost complete absence of K-feldspar.

Variation Diagrams

Comparisons between the igneous units of the Tawallah Group and overall geochemical trends can be identified by considering the bivariate diagrams of figure 4. SiO_2, MgO or FeO*/MgO that are usually selected as differentiation indicators for such diagrams, are mobile during low grade alteration and metamorphism of the Tawallah Group (Donovan, 1993; Pietsch et al., 1991) and consequently an alternative must be used. Zr has been shown to be immobile under these conditions, shows the greatest data range compared to other analysed high field strength elements and is incompatible. Zr is therefore adopted as a fractionation index for this study. Also shown on the variation diagrams of figure 4 are selected tholeiitic basalts and andesites from the Paraná continental flood basalt (CFB) province of southern Brazil.

Regarding the immobile elements, the Seigal Volcanics, Settlement Creek Volcanics and Gold Creek Volcanics show well defined fractionation trends with enrichment of TiO_2, P_2O_5, Y, Nb and La with increasing Zr. These strong enrichment patterns with increasing differentiation are typical of tholeiitic suites where characteristic olivine, clinopyroxene and plagioclase assemblages are the result of low pressure crystal fractionation

(Crawford and Hilyard, 1990) of MgO rich picritic parental magmas (Cox, 1980). The trends are mutually exclusive however, with subtle differences indicating that the Tawallah Group igneous units do not originate from progressive magmatic fractionation or partial melting of a homogeneous source. Alternatively some of the differences may be attributed to variable degrees of crustal contamination.

An important consequence is that compositional fields can be defined for the different igneous units of the Tawallah Group. For a given Zr value, the Seigal Volcanics are markedly depleted in TiO_2, P_2O_5, Y and La but are enriched in Nb relative to the Settlement Creek Volcanics. Similarly, the Gold Creek Volcanics, while showing similar TiO_2 and La contents to the Settlement Creek Volcanics are enriched in Nb yet slightly depleted in P_2O_5 and Y for a given Zr value. These features allow for recognition of the different mafic units which may be potentially useful in areas where exact stratigraphic position is otherwise poorly constrained.

The data in each case fall within the compositional fields defined by and show similar fractionation trends to the tholeiitic basalts and andesites of the Lower Cretaceous Paraná CFB province. The Paraná tholeiites were erupted during early continental rifting that preceded true oceanic (N-type MORB) magmatism associated with the opening of the South Atlantic Ocean (Bellieni et al., 1984; Fodor and Vetter, 1984; Fodor et al., 1985). The Paraná CFB tholeiites comprise two geochemically and isotopically distinct groups; those with high TiO_2 and P_2O_5 (HPT) and those with low TiO_2 and P_2O_5 (LPT; Bellieni *et al.*, 1984; Mantovani *et al.*, 1985; Fodor, 1987). This is a feature common to many other CFB provinces such as Karoo (Duncan, 1987), Etendeka province of Namibia (Marsh, 1987) and the Kirkpatrick basalts of Antarctica (Siders and Elliot, 1985). At Paraná, the groups are geographically distributed such that HPT tholeiites occur in the northern half of the province with LPT tholeiites in the south. The processes responsible for such a compositional distribution are the subject of much controversy in the literature. Whereas Bellieni *et al.* (1983) and Mantovani *et al.* (1985) favour mantle source heterogeneities to generate the HPT and LPT tholeiites, Fodor (1987) describes a model that involves varying degrees of partial melting and lower crustal temperatures that relate to proximity of mantle hotspot. The latter case involves a common mantle source that is relatively homogenous.

The Tawallah Group tholeiites can equally be divided as the Seigal Volcanics show pronounced compositional similarities to the Paraná LPT tholeiites and, while not as enriched as the HPT tholeiites, the Settlement Creek and Gold Creek Volcanics display markedly higher TiO_2 and P_2O_5 abundances. This distinction is not however, a geographical distinction as is the case in the Paraná CFB province, but a temporal one. Defining the processes responsible for this compositional variation is clearly beyond the scope of this study. However, considering that the change from low TiO_2/P_2O_5 to high TiO_2/P_2O_5 is temporal and that it is not defined by a single fractionation trend, a model involving chemically distinct mantle source regions (eg. Bellieni *et al.* 1983; Mantovani *et al.* 1985) seems more likely.

For each mafic unit, SiO_2 contents become slightly enriched with increasing Zr. Pietsch *et al.* (1991) however, suggest that the vertical data trends are associated with element mobility during alteration and metamorphism. This feature is also evident yet more pronounced for Rb and Sr.

Rare Earth Elements and Multi-Element Variation Diagrams

Rare Earth Elements

Thompson *et al.* (1984) propose that the majority of continental flood basalts (CFB) have elemental compositions that clearly indicate derivation from an ocean island basalt (OIB) source mantle, stating that instances of primary, unmodified mantle-derived magmas (N-MORB) erupting through

continental crust are rare. Figure 5 shows chondrite-normalised rare earth element (REE) patterns for analysed Tawallah Group mafic rocks compared to average MORB and OIB. In all cases, the Tawallah Group tholeiites show light-REE enrichment compared to average N-MORB and show close similarities to the pattern defined by average OIB. A slight but significant negative Eu anomaly occurs for all analysed samples and implies removal of plagioclase from the melt by crystal fractionation (Rollinson, 1993). Negative Eu anomalies such as these have been described for the majority of Paraná tholeiitic basalts and andesites (Mantovani *et al.*, 1985). Figure 5(c) shows increased REE concentrations for highly evolved group 2 dolerites (samples 94-042/044) of the Gold Creek Volcanics relative to the moderately evolved group 1 dolerites (sample 94-038).

Interestingly, a comparison of REE patterns for the Tawallah Group mafic units reveals that light-REE enrichment increases with time. The Seigal Volcanics display moderate light-REE enrichment ($La/Yb_N \approx 4$) while the Settlement Creek Volcanics ($La/Yb_N \approx 6.6$) and Gold Creek Volcanics ($La/Yb_N \approx 6.7$) are both very light-REE enriched relative to average N-MORB. This trend towards the average OIB pattern with time would indicate that Tawallah Group mafic units are derived from an evolving source region that is becoming progressively enriched in incompatible elements. Alternately, a deeper, more enriched mantle source may become more important with time.

Multi-Element Variation Diagrams

Rollinson (1993) suggests that multi-element variation diagrams normalised to N-MORB are most appropriate for evolved basalts and andesites. Figure 6 shows such a diagram for mafic Tawallah Group samples, the order of elements is that of Colwell et al. (1994). An important feature of each multi-element variation pattern is that marked negative Nb-Ta anomalies occur for all analyses. Thompson et al. (1983), in a detailed and comparative study of CFB multi-element variation patterns, suggests that many display a distinct trough at Nb-Ta and that such a feature contrasts the characteristic patterns of continental and oceanic alkali basalts which generally show a Nb-Ta peak. The generation of this Nb-Ta trough is generally considered to reflect equilibration of mantle-derived magmas within deep continental crust Thompson et al. (1984). The patterns also show a significant negative Sr anomaly that Thompson et al. (1983) attributes to plagioclase fractionation. Figure 6(d) compares multi-element variation patterns for the Seigal Volcanics, Settlement Creek Volcanics and Gold Creek Volcanics and suggests a general trend to become more evolved with time.

In Summary, REE patterns suggest that the Seigal Volcanics were derived from a less enriched source than the Settlement Creek and Gold Creek Volcanics in terms of incompatible elements. Furthermore, multi-element variation diagrams indicate that all Tawallah Group mafic rock types were emplaced in an intra-plate CFB setting as opposed to continental rift-zone volcanism.

MAGMATIC AFFINITIES

Relationships between Zr/Nb, Y/Nb and $(La/Yb)_N$ are widely used to interpret the source characteristics of mafic and intermediate rocks associated with extensional tectonic settings (Le Roex et al., 1983; Crawford and von Rad, 1994; Crawford and Hilyard, 1990; Fodor and Vetter, 1984). In the classification of Le Roex (1983), basalts with 'depleted' (N-type MORB) characteristics have high Zr/Nb (>17) and Y/Nb (>8) with low $(La/Yb)_N$ (0.9-1.2)while enriched basalts with 'plume' characteristics (P-type MORB) have low Zr/Nb (5.8-6.8) and Y/Nb (0.9-1.2) with high $(La/Yb)_N$ (4.8-6.9). Those basalts that fall between these compositions are termed transitional (T-type MORB). Figure 7 is an adaptation of the Le-Roex (1983) model for the generation of these different source types. Partial melting in the deep mantle (enriched OIB mantle source reservoir of Thompson et al., 1984) is initiated by a mantle plume or hotspot

during crustal and lithospheric attenuation (figure 7(b)). The rising mantle proceeds to form 'veins' in the upper mantle variably enriching it such that N-type MORB is derived from unveined mantle, P-type MORB from highly veined regions and T-type MORB from variable vein/mantle source regions (figure 7(c)).

Crawford and Hilyard (1990) suggest that the majority of CFB tholeiites have trace element compositions that fall between N-type MORB and P-type MORB tholeiites. Furthermore, Crawford and von Rad (1994), Fodor and Vetter (1984) and Crawford and Hilyard (1990) have shown that with time and as continental crust is attenuated, then ruptured and eventually oceanic crust is generated at an established spreading centre, basalt trace element geochemistry suggests a move from T-type MORB (CFB) towards steady-state N-type MORB volcanism. The igneous units of the Tawallah Group, while falling into the field defined by Paraná tholeiites, show a reverse trend such that the Seigal Volcanics and Settlement Creek Volcanics have Zr/Nb-Y/Nb-$(La/Yb)_N$ relationships typical of T-type MORB tholeiites while the Gold Creek Volcanics fall closer to the P-type MORB field (figure 8). This supports the overall changes observed in the REE patterns and may be interpreted in one of two ways.

One possibility is that sub-continental lithospheric source regions become progressively enriched with time. In the model proposed by Le Roex (1983), generation of T-type MORB may result from partial melting of mantle regions with variable vein/mantle ratios or alternately, mixing of P-type and N-type MORB during ascent. In either case it would seem that the geochemical characteristics of the Tawallah Group tholeiites record increasing input of relatively enriched deep mantle into the sub-continental lithosphere. A possible consequence is to 'dilute' the effects of N-type MORB in the system by reducing the amount of unveined mantle regions or increasing the abundance of P-type MORB that may mix with N-type MORB during ascent. An interesting aside is that the high TiO_2/P_2O_5 basalts of Gondwanaland (Paraná and Karoo provinces in particular) may develop during mantle contamination between 'primitive' and 'enriched' components, while low TiO_2/P_2O_5 basalts are more typically N-MORB in character (Bristow, 1990).

An alternative is that instead of erupting N-type MORB, expected with increased crustal extension and rupture, a more enriched, deeper mantle source region was tapped as the entire plume system relaxed to depth. This may be interpreted to reflect the fact that rifting in the southern McArthur Basin failed at an early stage. Substantial geological evidence supports the notion that initial rifting was halted by a compressional tectonic inversion event during Tawallah Group deposition (Rogers and Bull, 1994). This inversion event postdates eruption of the Seigal Volcanics yet predates emplacement of the Settlement Creek Volcanics, Gold Creek Volcanics and Tanumbirini Rhyolite. Crustal extension may have therefore occurred at lesser rates following early tectonic compression with rifting all but ceased by the time of Tanumbirini Rhyolite development. That rifting had ultimately failed is evidenced by deposition of the overlying carbonate and evaporite dominated McArthur Group in a non-volcanic sag-phase tectonic setting.

CONCLUSIONS

- The Tawallah Group igneous rocks have been subjected to varying levels of low grade alteration and metamorphism. In consequence, element mobility has occurred in all analysed samples. Geochemical interpretations are valid however when regarding only the high field strength elements which have remained immobile under these conditions.
- All mafic rock types of the Tawallah Group are tholeiitic in nature with the majority characterised by sub-alkaline compositions and importantly, have Ti-Y-Nb-Zr relationships that strongly imply a within-plate tectonic setting.
- Major and trace element variation diagrams

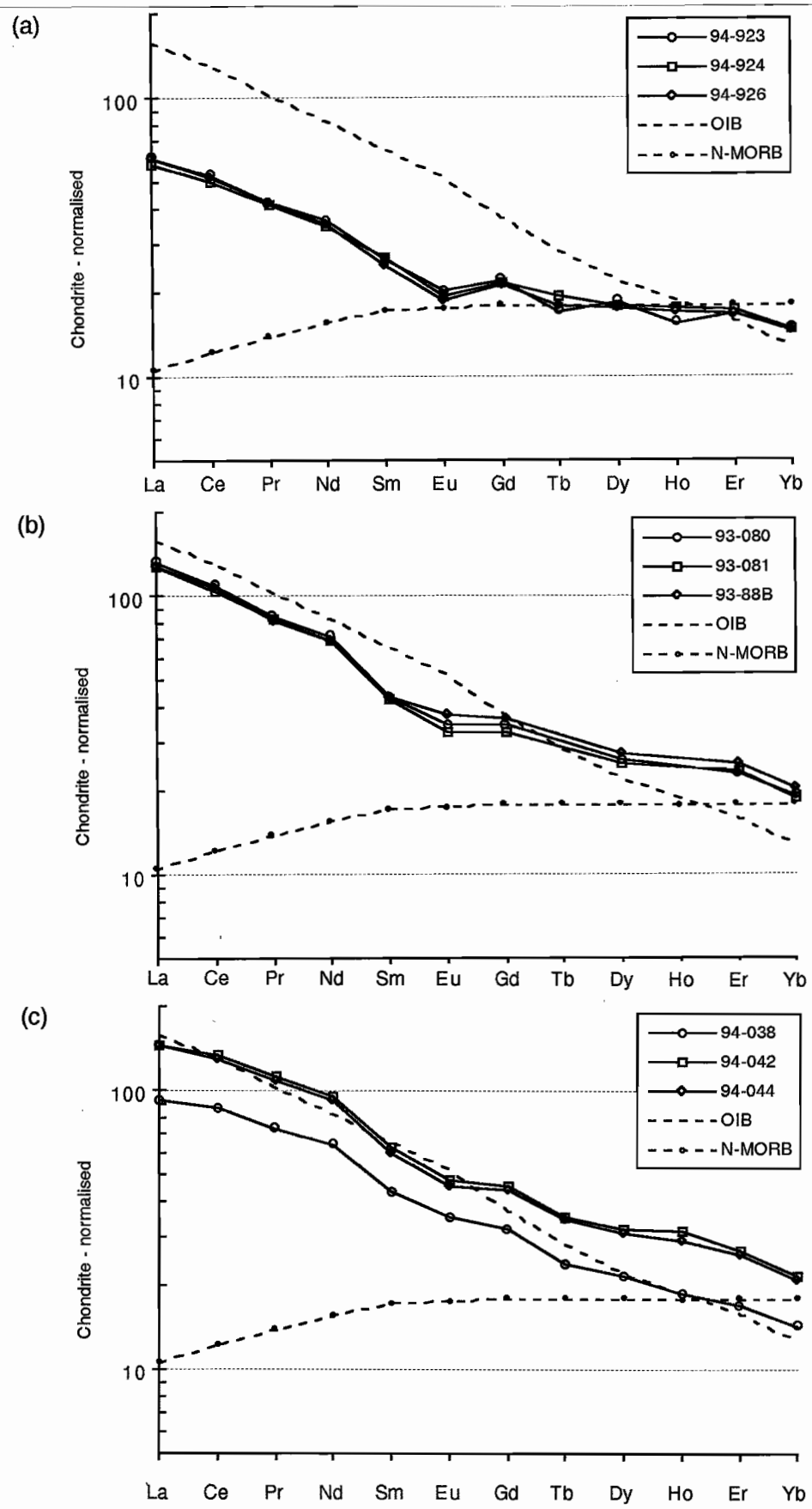

Figure 5. Chondrite-normalised REE diagrams for analysed; (a) Seigal Volcanics, (b) Settlement Creek Volcanics and (c) Gold Creek Volcanics compared to average OIB and N-MORB. Normalisation factors, average OIB and average N-MORB from Sun and McDonough (1989).

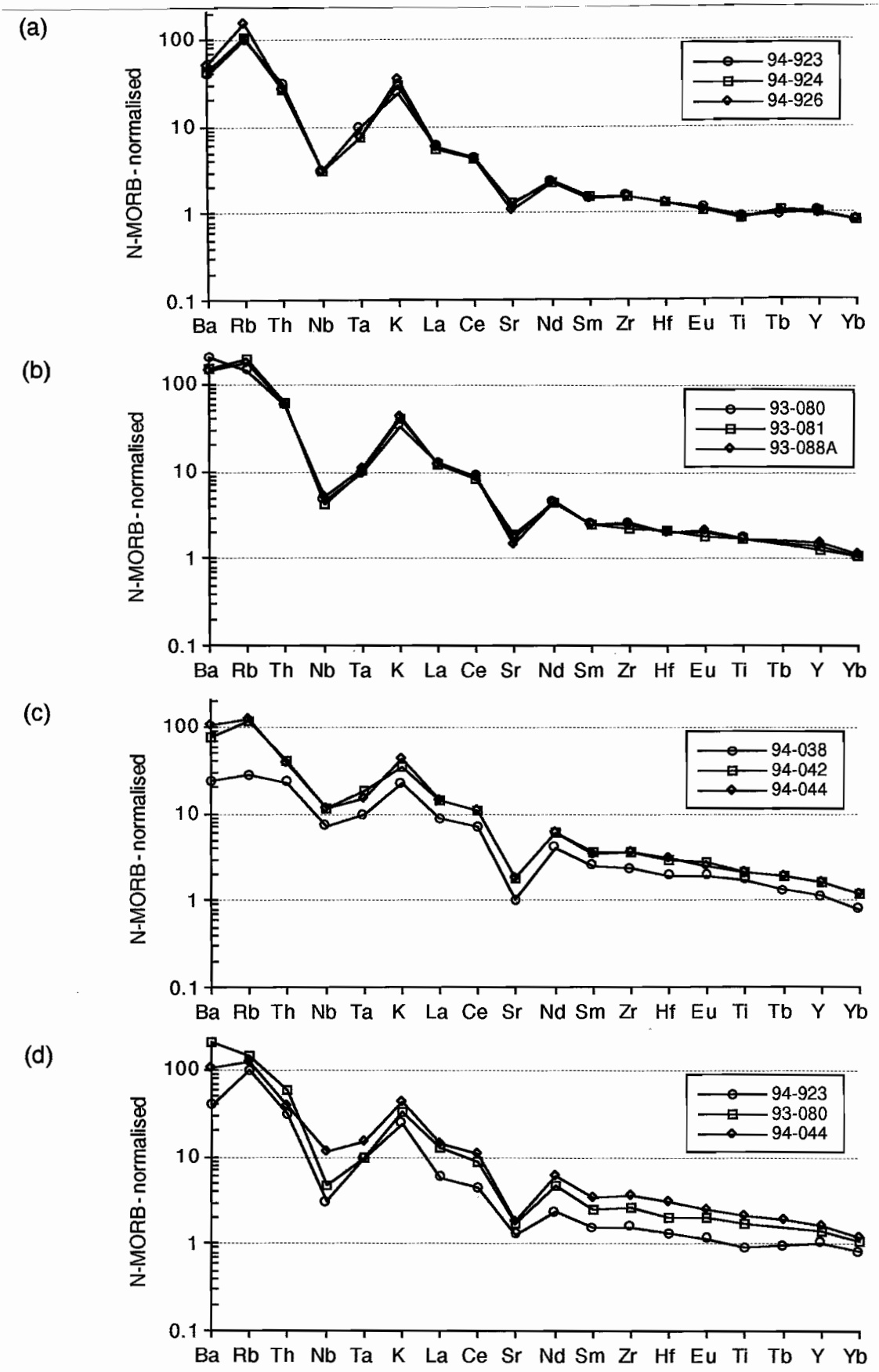

Figure 6. N-MORB-normalised multi-element variation diagrams for analysed basalts and dolerites of the: (a) Seigal Volcanics, (b) Settlement Creek Volcanics and (c) Gold Creek Volcanics. Plot (d) shows a comparison between the Seigal Volcs. (circles), Settlement Ck. Volcs. (squares) and Gold Ck. Volcs. (triangles). Normalisation factors from Sun and McDonough (1989).

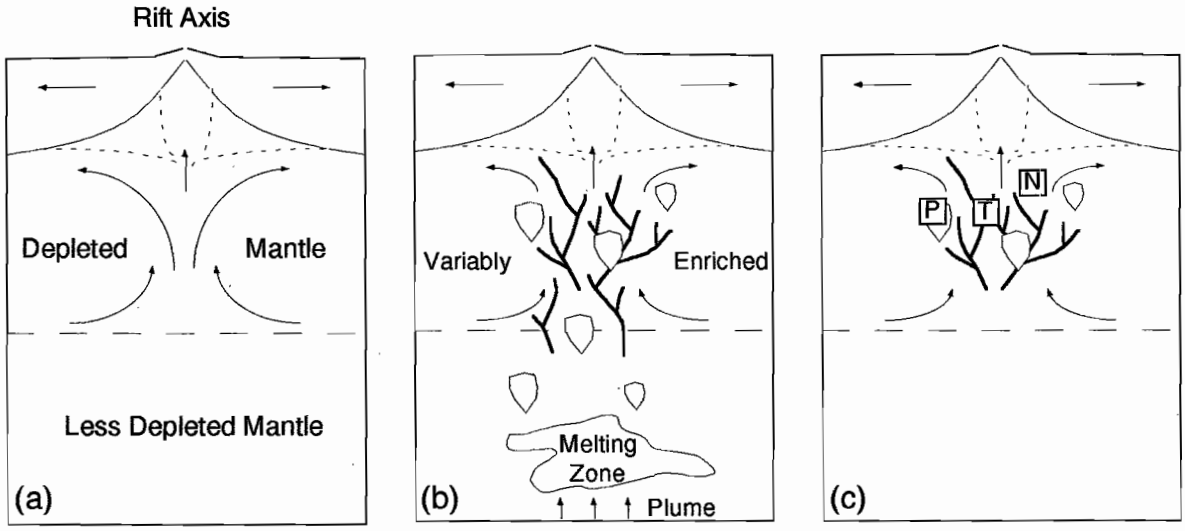

Figure 7. Genesis of P-type MORB, T-type MORB and N-type MORB (Le Roex, 1983). See text for discussion.

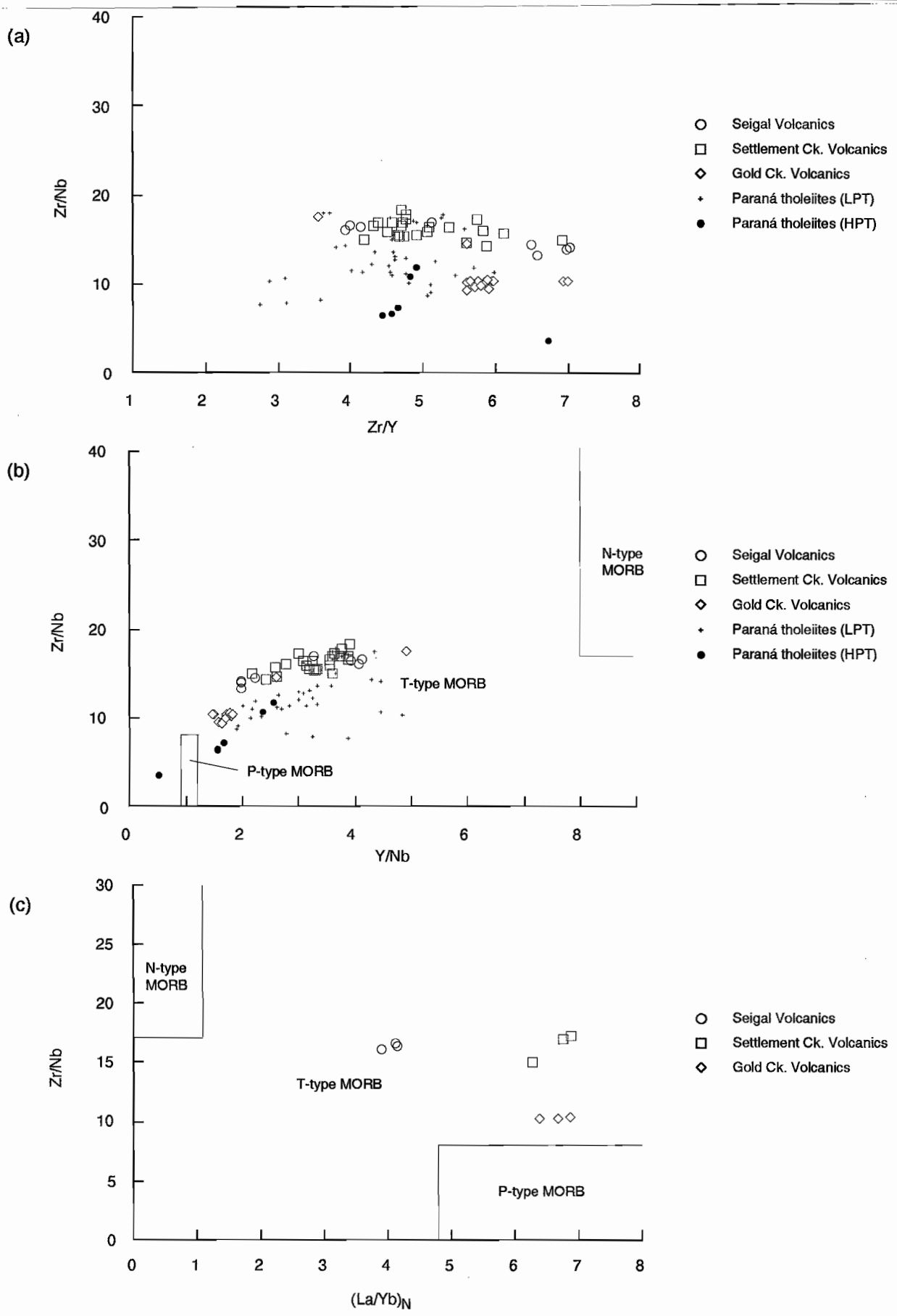

Figure 8. Plots of Zr/Nb versus (a) Zr/Y, (b) Y/Nb and (c) $(La/Yb)_N$ for basalts, basaltic andesites and dolerites of the Tawallah Group and selected tholeiites from the Paraná CFB province (Fodor *et al.*, 1985; Fodor and Vetter, 1984). N-type, T-type and P-type MORB fields after Le Roex *et al.* (1983). La and Yb normalised to chondrite (Sun and McDonough, 1989)

suggest that while crystal fractionation was an important process in the evolution of each individual Tawallah Group igneous suite, they are defined by distinct geochemical compositions. For similarly evolved rock types, the Seigal Volcanics are markedly depleted in TiO_2, P_2O_5, Y and La relative to the Settlement Creek and Gold Creek Volcanics. The Gold Creek Volcanics are distinguished from the Settlement Creek Volcanics by enriched Nb and slightly depleted P_2O_5 and Y abundances.

- Such immobile element compositions, although allowing for geochemical distinction of individual Tawallah Group mafic rock types, fall within the general trends defined by tholeiitic basalts and andesites of the Lower Cretaceous Paraná CFB province. Furthermore, multi-element variation patterns for all analysed mafic samples display a significant Nb-Ta trough. This feature can be used to distinguish CFB from other within-plate basalt types (Thompson *et al.*, 1983).
- Zr/Nb, Y/Nb and REE relationships suggest that the Settlement Creek and Gold Creek Volcanics are derived from a more enriched mantle source (T-type to P-type MORB) than the Seigal Volcanics (T-type MORB). Such a trend contrasts other CFB provinces that generally move towards N-type MORB volcanism as continental crust is attenuated, ruptured and oceanic crust eventually generated at an established spreading centre (Crawford and von Rad, 1994).

  One interpretation is that the Tawallah Group tholeiites record increased input of relatively enriched deep mantle into sub-continental lithospheric source regions. Alternatively, the deeper mantle source region becomes more important as the plume system relaxes to depth.
- In either case, it may suggest that rifting in the southern McArthur Basin failed at an early stage. This statement is supported by the existence of an early compressional tectonic event that postdates eruption of the Seigal Volcanics and predates Settlement Creek and Gold Creek Volcanic emplacement. Lesser extension rates may have followed the compressional event with rifting rapidly waning by the time of Tanumbirini Rhyolite emplacement. Rifting had ultimately failed with the deposition of the McArthur Group in a non-volcanic, sag phase tectonic setting.

ACKNOWLEDGEMENTS

Thanks go to Ian Brown and crew at the BHP Leila Creek exploration office for allowing access to drillhole GSD2. David Rawlings (NTGS) is thanked for the Seigal Volcanics core samples and for advice and comments in the field and elsewhere.

REFERENCES

Bellieni G., Brotzu P., Comin-Chiaramonti P., Ernesto M., Melfi A., Pacca I. G. and Piccirillo E. M., 1984. Flood basalt to rhyolite suites in the southern Parana Plateau (Brazil): palaeomagnetism, petrogenesis and geodynamic implications. *J. Petrol., 25* : 579-618.

Bristow J. W., 1990. Flood Basalts in new perspective.

Colwell J. B., Symonds P. A. and Crawford A. J., 1994. The nature of the Wallaby (Cuvier) Plateau and other igneous provinces of the west Australian margin. *AGSO J. Aust. Geol. Geophys., 15/1* : 137-156.

Cox K. G., 1980. A model for flood basalt vulcanism. *J. Petrol., 21 (4)* : 629-650.

Crawford A. J. and Hilyard D., 1990. Geochemistry of Late Proterozoic tholeiitic flood basalts. Adelaide Geosyncline, South Australia. In Jago J. B. and Moore P. S. (eds.): The evolution of a Late Precambrian-Early Palaeozoic rift complex: the Adelaide Geosyncline. *Geol. Soc. Aust. Spec. Publ. 16*: 49-67.

Crawford A. J. and von Rad U., 1994. The petrology, geochemistry and implications of basalts dredged from the Rowley Terrace-Scott Plateau and Exmouth Plateau margins, northwestern Australia. *AGSO J. Aust. Geol. Geophys., 15/1* : 43-54.

Darby P., 1986. Petrology and geochemistry of igneous rocks of the Tawallah Group, in the southern part of the McArthur Basin. *NTGS Technical Report, GS86/10*, (unpubl.).

Donovan S., 1993. *The geology of west Mallapunyah Dome, southern McArthur Basin, Northern Territory*. University of Tasmania, BSc hons. thesis (unpubl.).

Duncan A. R., 1987. The Karoo igneous province - a problem area for inferring tectonic setting from basalt geochemistry. *J. Volcan. Geotherm. Res., 32* : 13-34.

Floyd P. A. and Winchester J. A., 1975. Magma type and tectonic setting using immobile elements. *Earth Planet. Sci. Lett., 27* : 211-218.

Fodor R. V., 1987. Low- and high-TiO_2 flood basalts of southern Brazil: origin from picritic parentage and a common mantle source. *Earth Planet. Sci. Lett., 84* : 423-430.

Fodor R. V., Corwin C. and Roisenburg A., 1985. Petrology of Serra Geral (Paraná) continental flood basalts, southern Brazil: crustal contamination, source material and South Atlantic magmatism. *Contrib. Mineral. Petrol., 91* : 54-65.

Fodor R. V. and Vetter S. K., 1984. Rift-zone magmatism: Petrology of basaltic rocks transitional from CFB to MORB, southeastern Brazil margin. *Contrib. Mineral. Petrol., 88* : 307-321.

Haines P. W., Pietsch B. A., Rawlings D. J. and Madigan T. L., 1993. Mount Young - 1:250 000 geological map series. *NTGS explanatory notes, SE53-15.*

Jackson M. J., Muir M. D. and Plumb K. A., 1987. Geology of the southern McArthur Basin, Northern Territory. *BMR Bull., 220* .

Le Roex A. P., Dick H. J. B., Erlank A. J., Reid A. M., Fray F. A. and Hart S. R., 1983. Geochemistry, mineralogy and petrogenesis of lavas erupted along the southwest Indian Ridge between Bouvet triple junction and 11 degrees east. *J. Petrol., 24 (3)* : 267-318.

Mantovani M. S. M., Marques L. S., Sousa M. A. D., Civetta L., Atalla L. and Innocenti F., 1985. Trace element and strontium isotope constraints on the origin and evolution of Paraná continental flood basalts of Santa Catarina State (southern Brazil). *J. Petrol., 26 (1)* : 187-209.

Marsh J. S., 1987. Basalt geochemistry and tectonic discrimination within continental flood basalt provinces. *J. Volcan. Geotherm. Res., 32*: 35-39.

McPhie J., Doyle M. and Allen R., 1993. *Volcanic Textures.* CODES Key Centre: Hobart.

Meschede M., 1986. A method of discriminating between different types of mid-ocean ridge basalts and continental tholeiites with the Nb-Zr-Y diagram. *Chem. Geol., 56* : 207-218.

Pearce J. A., 1982. Trace element characteristics of lavas from destructive plate boundaries. In Thorpe R. S. (ed.): *Andesites,* (pp 525-548). Wiley: Chichester.

Pietsch B. A., Rawlings D. J., Creaser P. M., Kruse P. D., Ahmad M., Ferenczi P. A. and Findhammer T. L. R., 1991. Bauhinia Downs, Northern Territory - 1:250 000 geological map series. *NTGS explanatory notes, SE 53-3.*

Rawlings D. J., 1993. Mafic pépérite from the Gold Creek Volcanics in the Middle Proterozoic McArthur Basin, Northern Territory. *Aust. J. Earth. Sci., 40* : 109-113.

Rawlings D. J., 1994. Characterisation and correlation of volcanism in the McArthur Basin and transitional domain, NT. In Hallenstein C. P. (ed.): Australian mining looks north - the challenges and choices. *1994 AusIMM Annual Conference Tecnical Program Proceedings, Darwin*: 57-160.

Rawlings D. J., Madigan T. L., Pietsch B. A. and Haines P. W., 1993. Tawallah Range, Northern Territory - 1:100 000 geological map series. *NTGS explanatory notes, 6066.*

Robinson P., Higgins N. G. and Jenner G. A., 1986. Determination of rare-earth elements, yttrium and scandium in rocks by an ion exchange - XRF technique. *Chem. Geol., 55* : 121-137.

Rogers J. R. and S.W.Bull, 1994. A tectono-stratigraphic model for the southern McArthur Basin. *Geol. Soc. Aust. (abs), 37* : 382.

Rollinson H., 1993. *Using geochemical data: evaluation, presentation, interpretation.* Longman Scientific & Technical: Essex.

Siders M. A. and Elliot D. H., 1985. Major and trace element geochemistry of the Kirkpatrick Basalt, Mesa Range, Antarctica. *Earth Planet. Sci. Lett., 72* : 54-64.

Stolz A. J., 1992. *Compositional and Textural Alteration of Volcanic Rocks:*. MSc. Econ. Geol. Course Work Manual 10. CODES: 7-22.

Thompson R. N., Morrison M. A., Dickin A. P. and Hendry G. L., 1983. Continental flood basalts... arachnids rule OK? In Hawkesworth C. J. and Norry J. (eds.): *Continental basalts and mantle xenoliths* (pp 158-185). Shiva: Nantwhich.

Thompson R. N., Morrison M. A., Hendry G. L. and Parry S. J., 1984. An assessment of the relative roles of crust and mantle in magma genesis: an elemental approach. *Phil. Trans. Roy. Soc. Lond., 310* : 549-590.

Winchester J. A. and Floyd P. A., 1976. Geochemical magma type discrimination; application to altered and metamorphosed basin igneous rocks. *Earth Planet. Sci. Lett., 28* : 459-469.

Winchester J. A. and Floyd P. A., 1977. Geochemical discrimination of different magma series and their differentiation products using immobile elements. *Chem. Geol., 20* : 325-343.

Wyborn L. A. I., Page R. W. and Parker A. J., 1987. Geochemical and geochronological signatures in Australian Proterozoic igneous rocks. In Pharaoh T. C., Beckinsale R. D. and Rickard D. (eds.): *Geochemistry and mineralisation of Proterozoic volcanic suites,* (pp 377-394). Geol. Soc. Spec. Publ. 33.

Depositional attributes of the Barney Creek Formation in DDH BMR McArthur 2

Stuart Bull
Centre for Ore Deposit and Exploration Studies

INTRODUCTION

The 122 m long diamond core DDH BMR McArthur 2 was drilled in the early seventies to investigate the Barney Creek Formation. It was collared in Reward Dolomite on the northern side of the Carpentaria Highway approximately 23 km southwest of McArthur River Mine (Fig. 1). As far as can be ascertained, no sedimentological study of the core was ever carried out, however, geochemical analyses of samples from the hole were published by Corbett et al. (1975). This data was used as part of a study of the Barney Creek Formation for the geochemical halo module of the current project (Large and McGoldrick, 1993). Upon later examination of the hole at the AGSO core shed in Canberra, it was unclear where the samples used for the original geochemical analyses were obtained and as a result the hole was resampled by the author. The aim of this work was to provide a new geochemical data set in order to check the previous results (Large, 1994), and to study the effects of sedimentary facies on the alteration index.

SEDIMENTARY FACIES

The interval cored in DDH BMR McArthur 2 can be considered in terms of two broad sedimentological packages which are comprised of four distinct facies discussed individually below. The interval from the base of the hole at 122 m up to around 25 m below the top is characterised by abundant, thinly-bedded, grey, dolomitic siltstone to fine-grained sandstone beds (Fig. 2). These are interbedded with varying proportions of massive, carbonaceous ± pyritic black mudstone, and in the interval from 53 to 38 m, with thicker-bedded, graded dolomitic sandstone units. Overall, this lower interval is considered to represent the Barney Creek Formation proper. The interval from 25 m to the top of the hole also consists of abundant thinly-bedded, grey, dolomitic siltstone- to fine-grained sandstone beds, however, there is less intercalated mudstone and scattered ripples and flaser bedded zones are present (Fig. 2). This interval is interpreted to represent a gradational transition to the Reward Dolomite in which the hole was collared.

Thin-bedded dolomitic sandstone/ siltstone/mudstone facies

This facies dominates the Barney Creek Formation portion of DDH BMR McArthur 2 comprising approximately 88% of it by length. It is characterised by pale grey dolomitic siltstone/fine-grained sandstone beds which range in thickness

CODES: AMIRA/ARC Project P.384 — Proterozoic sediment-hosted base metal deposits. November 1994

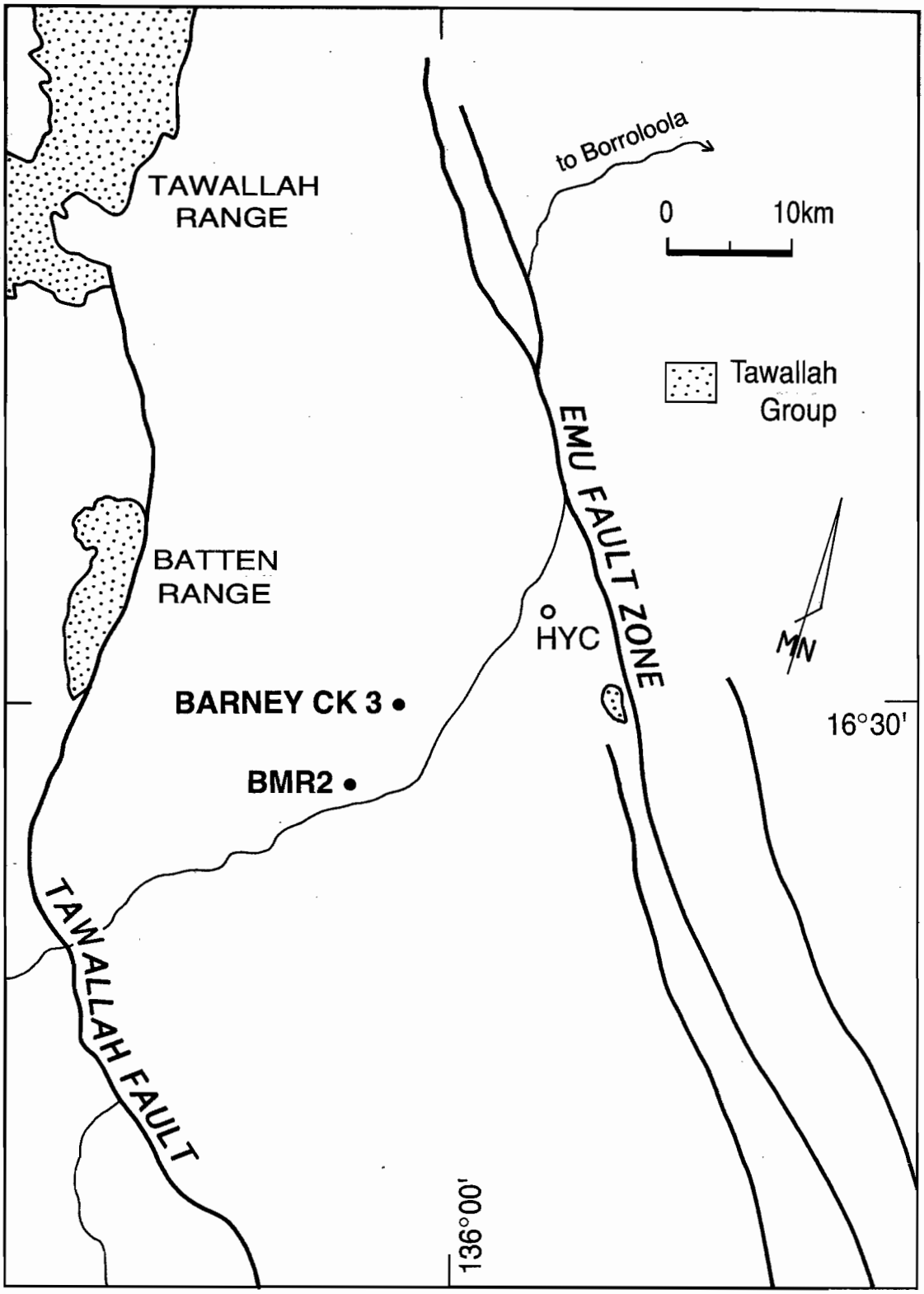

Figure 1—Location of DDH BMR McArthur 2 and DDH Barney Creek 3; geology after Pietsch et al. (1991).

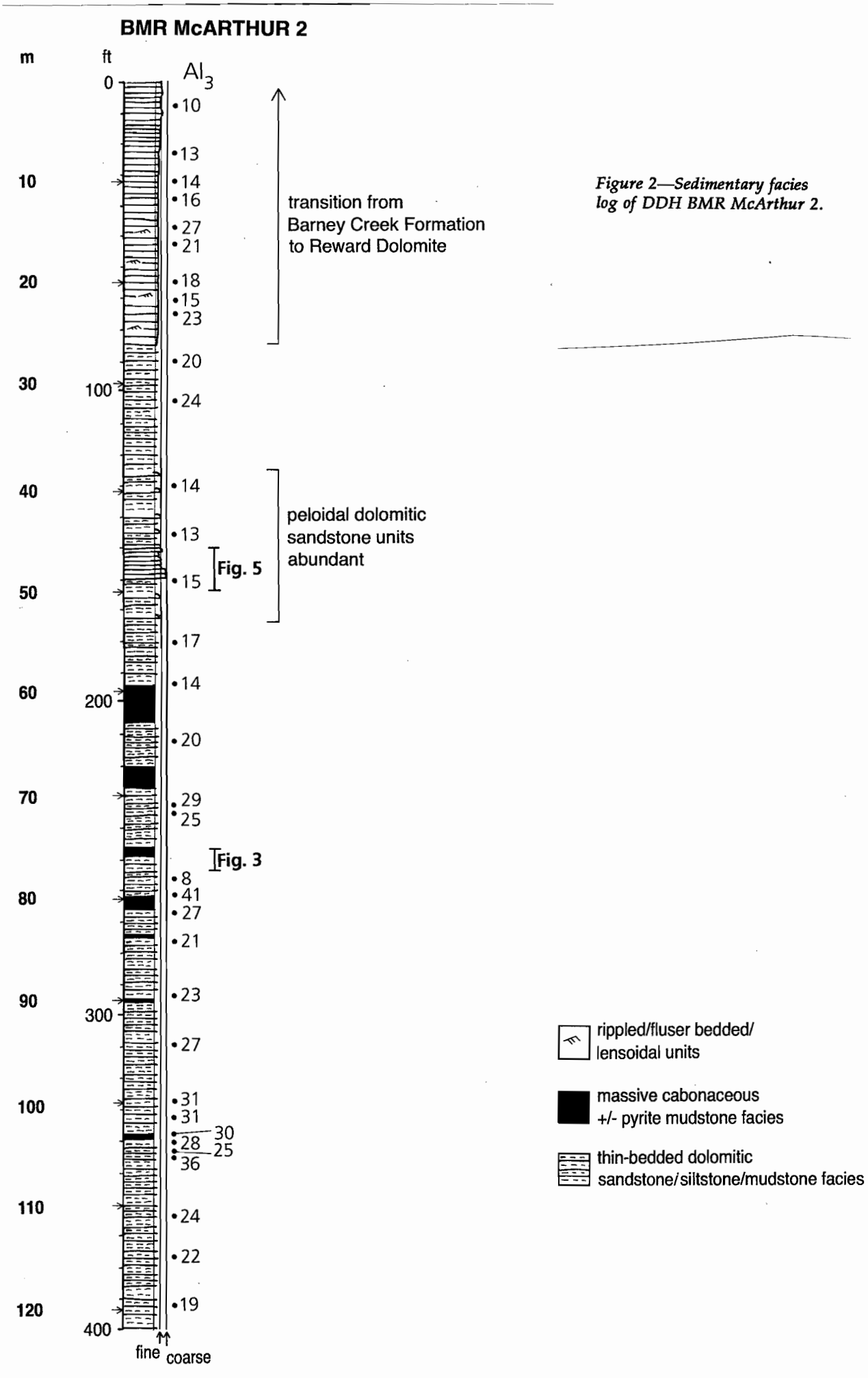

Figure 2—Sedimentary facies log of DDH BMR McArthur 2.

from < 1 cm to around 20 cm, with most in the range of < 1 to 6 cm (Fig. 3). Individual units have sharp bases which often exhibit scours with relief of up to 2 cm, loadcasts and flame structures (Fig. 3b). Incipient to well-developed stylolites are often developed along bed bases and to a lesser extent bed tops. Normal grading defined by an upward decrease in grainsize and increase in the proportion of carbonaceous mudstone matrix is common. Other sedimentary structures include planar and ripple cross-lamination. All of these features are consistent with deposition from small-volume, turbulent mass flow deposits.

In thin section, the thin-bedded dolomitic mass-flows characteristic of this facies consist of an interlocking framework of silt- to fine-grained sand-sized fragments of monocrystalline quartz and dolomite. Proportions of the two major components vary and both quartz-dominated and dolomite-dominated end members occur (Fig. 4a and b). Although the dolomite-rich areas appear crystalline, and to have a similar grainsize to the associated quartz fragments, in detail they are amorphous in crossed polars (Fig. 4a). They are, therefore, interpreted to represent a recrystallised dolomitic mudstone matrix. Towards bed tops increasing proportions of mudstone are present which first occur as discrete, bedding parallel stringers of carbonaceous material within the amorphous grey recrystallised matrix (Fig. 4c), and grade up into the grey/black mudstone. This massive mudstone which hosts the thin-bedded dolomitic mass-flows consists of an interlocking fine-grained mosaic of black carbonaceous material and dolomite, with varying proportions of dispersed silt-sized and finer quartz fragments (Fig. 4c). This facies is interpreted to represent ambient depositional conditions which consisted of accumulation from hemi-pelagic suspension of fine-grained material in a quiet-water (ie. sub-wave base), reduced subaqueous environment. The bedding parallel carbonaceous stringers may be transported fragments of algal mat, however, they could also represent incipient stylolites.

Massive carbonaceous +/- pyritic mudstone facies

Mudstone is interbedded with the thin-bedded dolomitic mass-flows characteristic of the *thin-bedded dolomitic sandstone/siltstone/mudstone facies* throughout the Barney Creek Formation interval in DDH BMR McArthur 2. However, seven discrete mudstone intervals which occur in the lower half of the drill hole, which together comprise approximately 12 % of the Barney Creek Formation interval, are thick enough to be considered as a depositional facies in their own right. The mudstone intervals range in thickness from 0.5 to 6.5 m and have gradational contacts with the adjacent *thin-bedded dolomitic sandstone/siltstone/mudstone facies* (Fig. 3a and c). They consist of massive, black (ie. carbonaceous) mudstone with occasional diffuse bands of fine-grained pyrite. Dolomitic siltstone units, if present, are a minor component and are generally < 1 cm thick. In some samples the facies exhibits a foliation in thin section which is defined by bedding parallel stringers similar to those which occur in the upper parts of graded sandstone beds (Fig. 4c).

The mudstone units which comprise the *massive carbonaceous ± pyritic mudstone facies* are interpreted in the same manner as the mudstone intercalated within the *thin-bedded dolomitic sandstone/siltstone/mudstone facies*. However, the massive nature of these intervals indicates that in this case hemi-pelagic sedimentation was largely uninterrupted by periodic mass-flows. Conditions also appear to have been more reduced during the accumulation of this facies, because the mudstone appears more carbonaceous and pyritic than the bulk of the mudstone intercalated in the *thin-bedded dolomitic sandstone/siltstone/mudstone facies*. It should be noted, however, that while total organic carbon values of up to 10.4% have been recorded from the Barney Creek Formation (Jackson et al., 1988), calculated dolomite percentages for the four samples of the *massive carbonaceous ± pyritic mudstone facies* analysed range from 20.85 to 52.52% with an average of 37.68%. This is not significantly

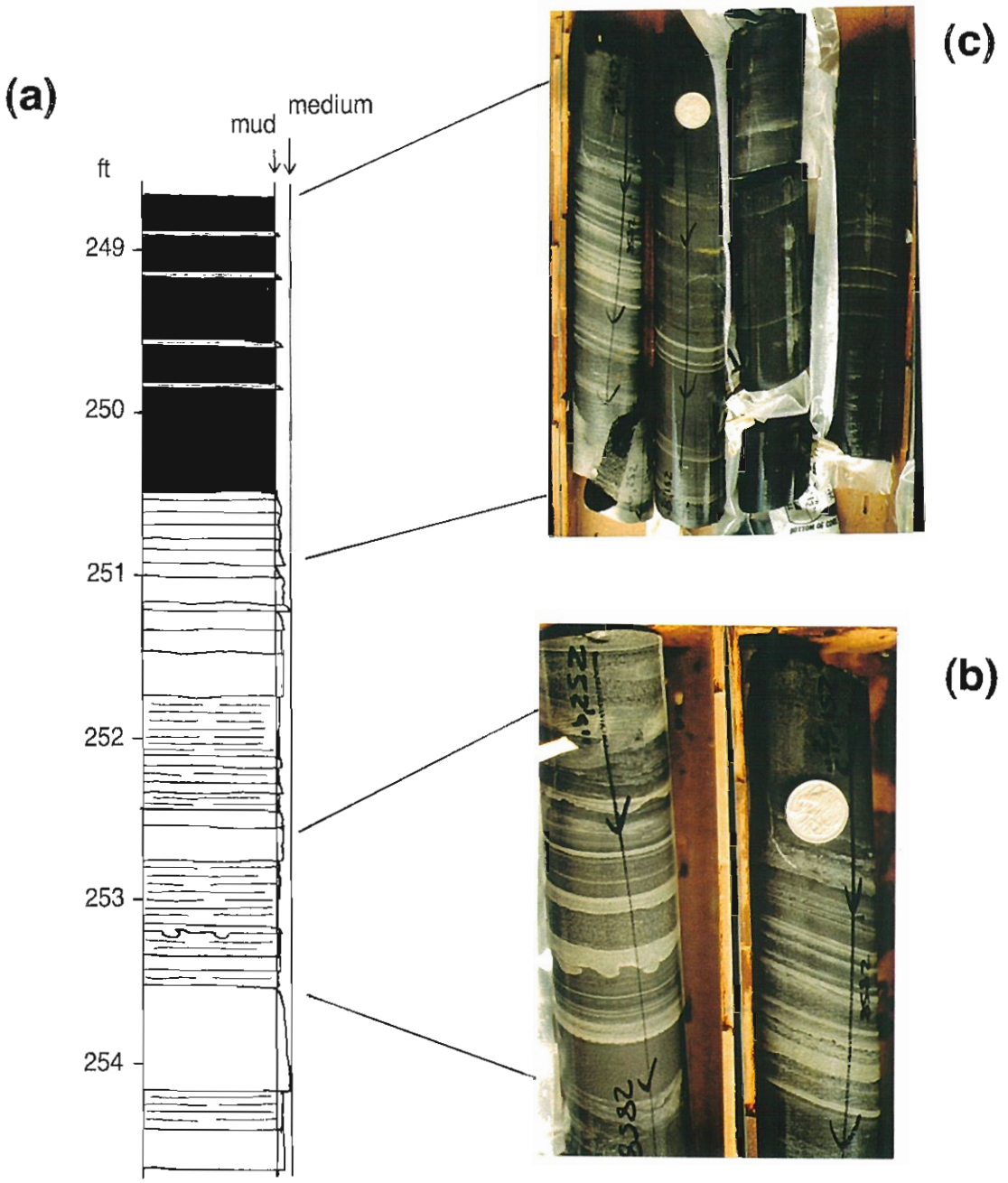

Figure 3— (a) Detailed sedimentary log of the interval 248'8" to 254'8" in DDH BMR McArthur 2 which incorporates the transition from the massive carbonaceous ± pyritic mudstone facies *to the* thin-bedded dolomitic sandstone/siltstone/mudstone facies *downhole. (b) Typical features of the* thin-bedded dolomitic sandstone/siltstone/mudstone facies*; note the loadcasted injected base in the middle part of the left hand core sample. (c) Gradational contact from between the* thin-bedded dolomitic sandstone/siltstone/mudstone facies *on the left and the* massive carbonaceous ± pyritic mudstone facies *on the right.*

OPPOSITE:

*Figure 4—(a) Photomicrograph (*2.5 crossed polars) of a typical dolomitic sandstone bed characteristic of the* thin-bedded dolomitic sandstone/siltstone/mudstone facies. *(b) Photomicrograph (*2.5 crossed polars) of a quartz-rich dolomite -poor sandstone bed from the* thin-bedded dolomitic sandstone/siltstone/mudstone facies. *(c) Photomicrograph (*2.5 plane polarised light) of the carbonaceous dolomitic mudstone which is intercalated with the sandstone beds in the* thin-bedded dolomitic sandstone/siltstone/mudstone facies. *Note the bedding parallel carbonaceous stringers throughout. (d) Photomicrograph (*2.5 crossed polars) of the peloidal dolomitic sandstone characteristic of the* thin/medium-bedded graded dolomitic sandstone facies. *Note the dolomitic siltstone peloid lower centre (arrowed) and the fine-grained dolomitic sandstone fragment upper right of centre (arrowed). (e) Flesh coloured weathering at 10.5 m which is typical of the uppermost 14 m of DDH BMR McArthur 2; note the clear crosscutting/overprinting relationship with typical grey dolomitic siltstone/mudstone. (f) Examples of rippled/flaser/lensoidal sandstone/siltstone units from around 16.5 m which are characteristic of the* thin-bedded laminated and rippled grey dolomite facies *which comprises the interval from around 25 m to the top of the hole. (g) One of the two platy intraclastic pebble breccia horizons in DDH BMR McArthur 2 (at 11.7 m) interpreted to have been formed by the disruption (?compaction-generated) of early diagenetic crusts.*

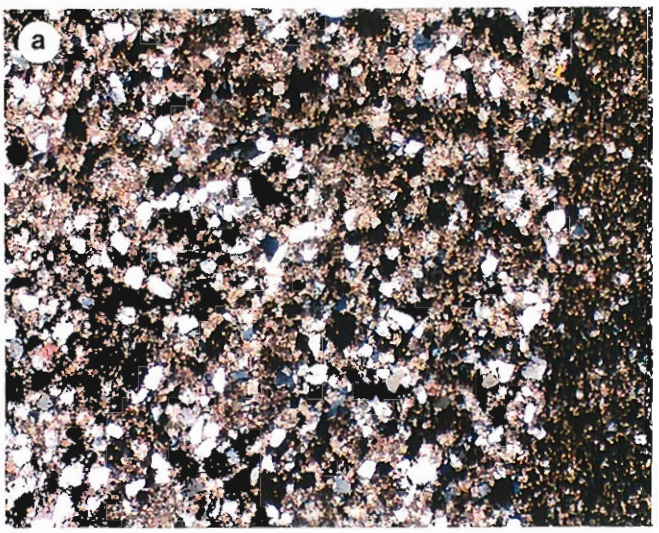
a

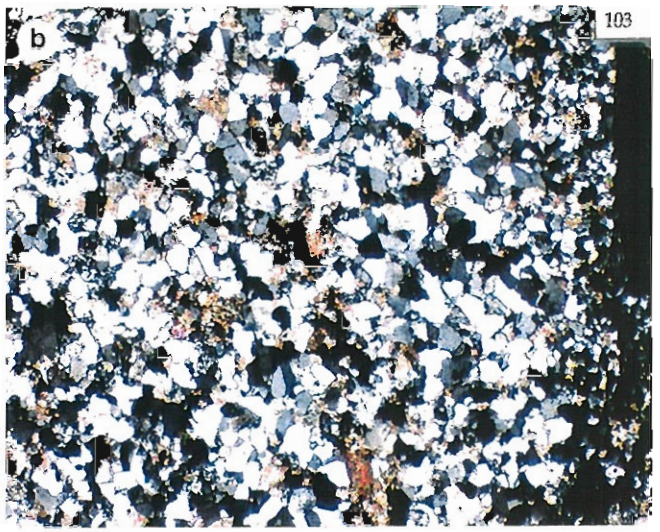
b


c

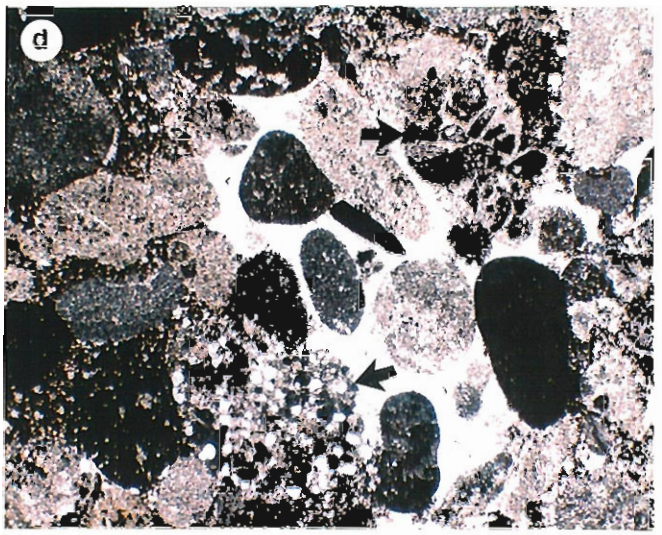
d


e
CORE PIECE
BOTTOM
OF WELL

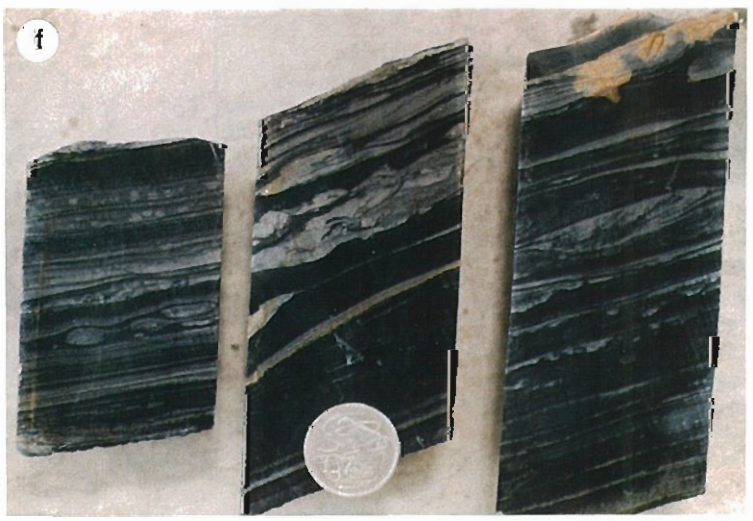
f

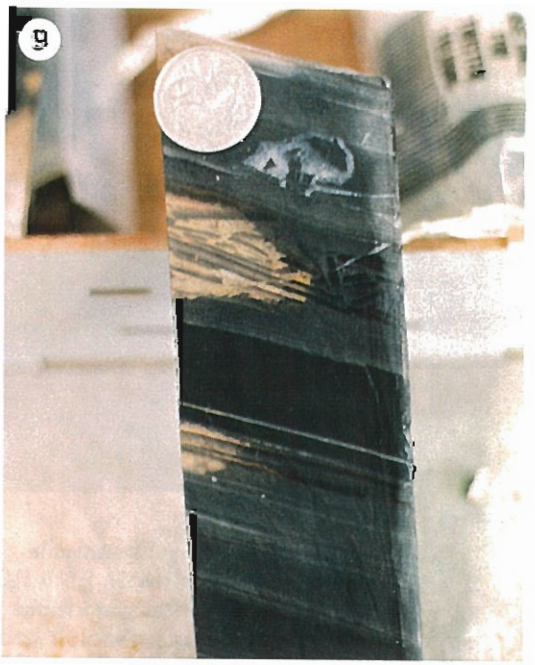
g

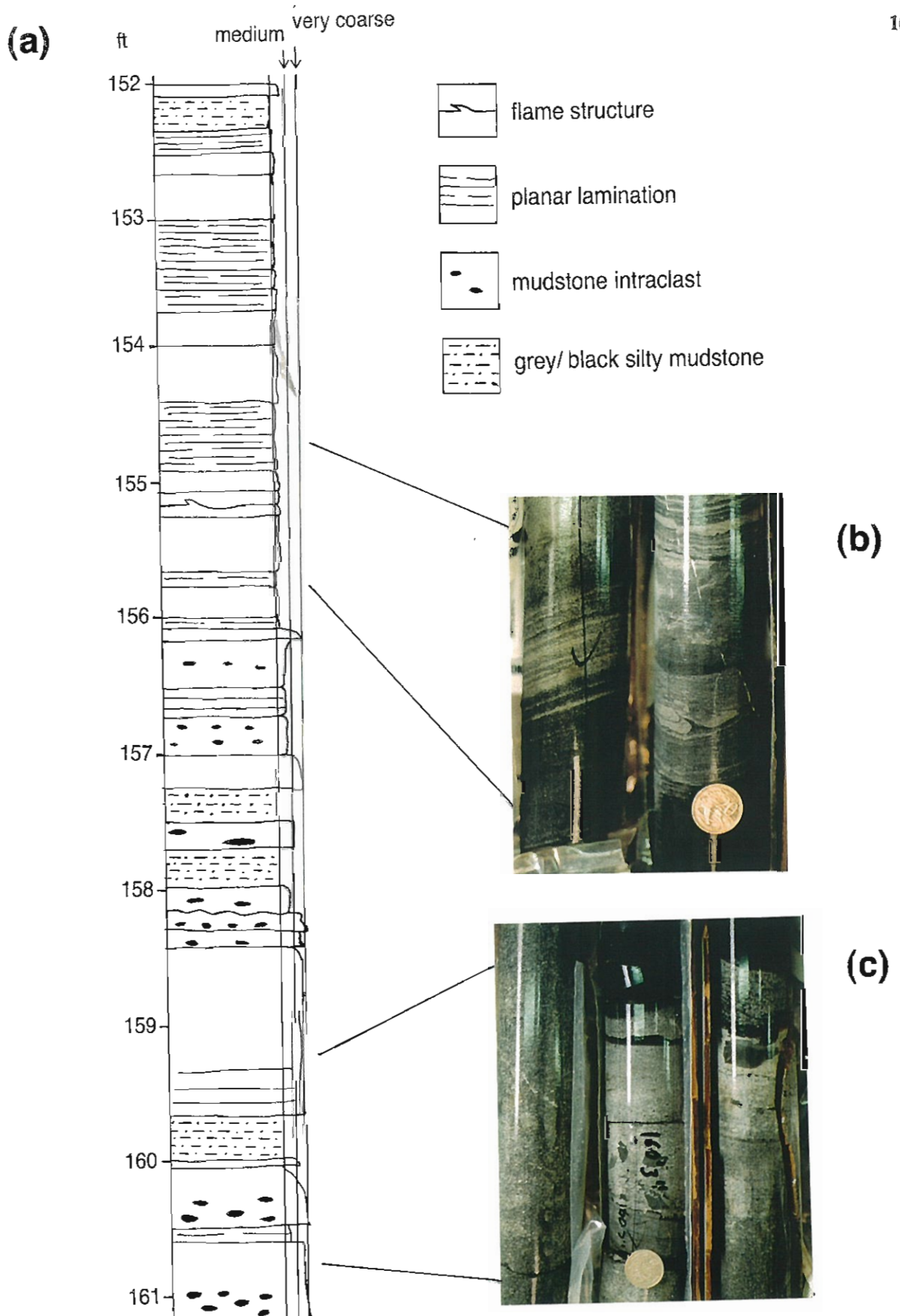

Figure 5—(a) Detailed sedimentary log of the interval 150'11" to 163' in DDH BMR McArthur 2 illustrating the nature of the units which comprise the thin/ medium-bedded graded dolomitic sandstone facies. *(b) Massive and stratified peloidal sandstone; note the flame structure in the lower middle region of the right hand core sample. (c) Typical massive bedded sandstone with normal grading accentuated by the presence of mudstone intraclasts in the basal part of the bed in the middle part of the middle core sample.*

different to the calculated dolomite percentages from twenty samples of the *thin-bedded dolomitic sandstone/siltstone/mudstone facies which* range from 27.52 to 64.76% with an average of 49.73%. Examination of thin sections under high power indicates that the dolomite is fine-grained and occurs in a interlocking mosaic with dispersed particles of similarly silt-sized quartz, carbonaceous material and pyrite. In order to accurately determine the range of organic carbon present in the BMR 2 samples they are currently being analysed for organic carbon.

Thin/medium-bedded graded dolomitic sandstone facies

In addition to the dolomitic mass-flows which characterise the *thin-bedded dolomitic sandstone/siltstone/mudstone facies*, thicker-bedded and coarser-grained units which are also clearly of mass-flow origin occur as scattered isolated beds throughout the Barney Creek Formation interval in DDH BMR McArthur 2. These are thickest (up to 0.5 m), coarsest (up to very coarse-grained sand-sized) and most abundant in the interval from 53 to 38 m (Fig. 2). They exhibit typical mass-flow features of sharp, scoured bases with occasional load and flame structures (Fig. 5a and b). Normal grading is common, often highlighted in this case by the presence of basal mudstone intraclasts (Fig. 5c).

In thin section, the medium- to very coarse-grained fragments which characterise the *thin/medium-bedded graded dolomitic sandstone facies* clearly consist of discrete peloids of dolomitic mudstone or sandstone (Fig. 4d). Fabrics range from close packed peloids with a dolomitic mudstone matrix and, in places, a clear, crystalline dolomitic cement (Fig. 4d), to dispersed in a matrix of fine-grained dolomitic sandstone similar to that which comprises the dolomitic mass-flows of the *thin-bedded dolomitic sandstone/siltstone/mudstone facies*. The peloids may be spherical or ovoid, but all are well rounded except where they show the effects of compaction generated deformation. Internally, they consist of massive dolomitic mudstone and, less commonly, dolomitic quartz sandstone (Fig. 4d; lower centre arrowed) and none exhibit concentric laminae. Rare examples consist of aggregates of finer-grained peloidal sandstone (Fig. 4d; upper right of centre arrowed) indicating a complex, multi-generational history for these fragments.

The peloidal fragments which characterise the *thin/medium-bedded graded dolomitic sandstone facies* are interpreted to represent intraclasts derived from erosion of dolomitic mudstone and sandstone units. The high degree of rounding of the peloids clearly indicates that the units being eroded were competent, and that the erosion occurred in an environment with relatively high hydraulic energy levels (eg. an agitated shoreline). The competency of the material being eroded suggests either that it comprised older, lithified sedimentary units which had been structurally uplifted during Barney Creek Formation deposition, or alternatively, that it represents erosion of shallow (exhumed) or surficial early diagenetic crusts.

Thin-bedded laminated and rippled grey dolomite facies

This facies comprises the interval from around 25 m to the top of the hole (Fig. 2). The interpretation of this upper part of the hole is complicated by a crosscutting, overprinting buff-coloured weathering feature (Fig. 4e), the main effect of which is to impart the apparent increase in grainsize shown on the log (Fig. 2). In general, however, the facies clearly has a similar structure to the *thin-bedded dolomitic sandstone/siltstone/mudstone facies* in that it also consist of thinly interbedded grey dolomitic siltstone/fine-grained sandstone and darker dolomitic mudstone. However, subtle but important differences include: (1) a smaller proportion of carbonaceous mudstone intercalated with the bedded dolomitic siltstone/sandstones; note also that no intervals of the *massive carbonaceous ± pyritic*

mudstone facies are present: (2) Rather than being of mass-flow origin, some of the dolomitic siltstone/sandstone beds consist of rippled, flaser bedded/lensoidal intervals (Fig. 4f) which often infill shallow scours. These features are rare in the underlying Barney Creek Formation and are considered to be consistent with a gradational contact between the Barney Creek Formation and the overlying Reward Dolomite.

DISCUSSION

Sedimentology

It has been reported previously (Bull, 1994), that although a number of depositional models have been proposed for the Barney Creek Formation which involved, at least in part, shallow water to evaporitic sabkha conditions (eg. Williams and Logan, 1981; Muir, 1983; Logan and Williams, 1984; Jackson et al., 1987) this interpretation has not been validated by the sedimentological characteristics of the unit away from the HYC deposit. An alternative model was proposed in which the bulk of the unit was deposited in a quiet (ie. below wave base), anoxic subaqueous environment via hemipelagic suspension deposition interrupted by periodic small volume mass flows. The facies described above from DDH BMR McArthur 2 are entirely consistent with this interpretation. In addition, the decrease in proportion of mudstone and increase in ripples and lensoidal bedding characteristic of the *thin-bedded laminated and rippled grey dolomite facies* which occurs at the top of the hole (Fig. 2), are all suggestive of gradually shoaling conditions towards the contact with the Reward Formation at this locality.

An important sedimentological feature which has not previously been described from the Barney Creek Formation is the presence of dolomitic peloids (Fig. 4d). Although they occur as detrital grains in some of the sub-wave base mass flow emplaced units, these grains must have originated by erosion of competent dolomitic units in co-existing agitated shoreline environment. In fact, lenses of pelletal sandstone interpreted as tidal channels have been described from the Reward Dolomite (Brown et al., 1978). This suggests that the Barney Creek Formation and the Reward Dolomite may be partially time equivalent.

In a model in which the Barney Creek Formation and the Reward Dolomite were partially time equivalent, some of the areas of the latter unit with shallow water characteristics would have been shoreline facies, which co-existed with areas of sub-wave base deposition represented by the Barney Creek Formation and overlying relatively quiet water Reward Dolomite facies. Such a model would explain the marked lateral facies changes recorded in the Reward Dolomite by Jackson et al. (1987). It would also explain the close relationship between the Barney Creek Formation and the Reward Dolomite described by the same authors, who noted that "the thicker sections, in which the rocks are mainly shale, coincide with the thick developments of the Barney Creek Formation; conversely, where the Barney Creek Formation is thin, so too is the Reward Dolomite."

The discrete nature of the interval from 53 to 38 m where the peloidal mass flow units in the Barney Creek Formation are anomalously thick, coarse and abundant (Fig. 2) suggests that a significant "event" occurred at this time. This could have involved a period of more restricted sub-wave base deposition, when the agitated shoreline environment which was the source of the peloidal units was relatively proximal. Alternatively, it could represent a tectonic event which uplifted older competent lithologies, the erosion of which was the source of the peloidal fragments. A major transpressional tectonic event which occurred during the deposition of the Barney Creek Formation in the area of the McArthur River Deposit has recently been documented by Hinman et al. (1994).

An ambiguous feature present at two places in the DDH BMR McArthur 2 core (11.7 and 35 m) are pebble breccia horizons comprised of platy intraclasts oriented roughly parallel to bedding (Fig. 4g). These superficially resemble intraclast flat-pebble

breccias which are widely interpreted, with a range of other sedimentary structures, as being indicative of shallow/emergent conditions (eg. Jackson et al., 1987). Such breccia units are commonly generated by of erosion of hardground by tidal- or wave-associated current activity, and as a result, they often comprise imbricated platy intraclasts bounded by basal scours. In detail, the breccias in the DDH BMR McArthur 2 core differ from "normal" flat-pebble breccias in that they are not associated with scouring and the platy clasts are not systematically imbricated. In fact the clasts are jigsaw-fit and have clearly been formed by relatively minor disruption of several thin (few mm), competent dolomitic mudstone laminae. These features are interpreted to have been formed by the disruption (?compaction-generated) of early diagenetic crusts and they are, therefore, not considered to have any application as indicators of palaeoenvironmental conditions.

New AGSO Analyses of BMR 2 Samples

The 34 samples collected by us from DDH BMR 2 have been analysed for a full suite of majors and traces at the AGSO laboratory. A tabulation of the results to date is given in Appendix 1. This data set now supersedes the partial analyses from ALS given in our previous report (Large, 1994).

Down hole plots of AI_3, MnO_D, Zn and dolomite % are given in figure 6. These confirm previous results that indicate a potential ore position in the Barney Creek Formation proper at 80 to 105 m and a less probable position in the gradational contact zone between the Barney Creek Formation and the Reward Dolomite at 10 to 20 m. The data in figure 7 indicate that four samples display an $AI_3 > 30$ and are clearly anomalous. All these samples are from the lower interpreted ore position.

The characteristics of the four anomalous samples are shown in table 1.

There is no clear relationship between % dolomite in each sample (calculated from CaO content) and the AI_3 (Fig. 8a), with anomalous samples varying from 19 to 47 wt% dolomite. Data in figure 8b, however, indicates a rough linear relationship between AI_3 and sulphur content (occurring as pyrite).

Effects of sedimentary facies on the alteration index

Application of the current alteration index (AI_3) to the AGSO geochemical data from DDH BMR McArthur 2 (Fig. 6) confirms the two peaks defined by analysis of the various geochemical datasets with the previous version of the index (Large, 1994). However, the relief on the upper peak, which occurs is the gradational contact zone between the

Table 1. Anomalous samples from DDH BMR 2

Meters	AI_3	% Dolomite	MnO_D %	Lithology
79.86	41	19	1.5	carb mudst
99.97	31	44	0.9	dolomitic siltst
101.86	31	47	1.1	dolomitic siltst
103.33	30	24	0.9	carb mudst
105.67	36	42	1.3	dolomitic siltst

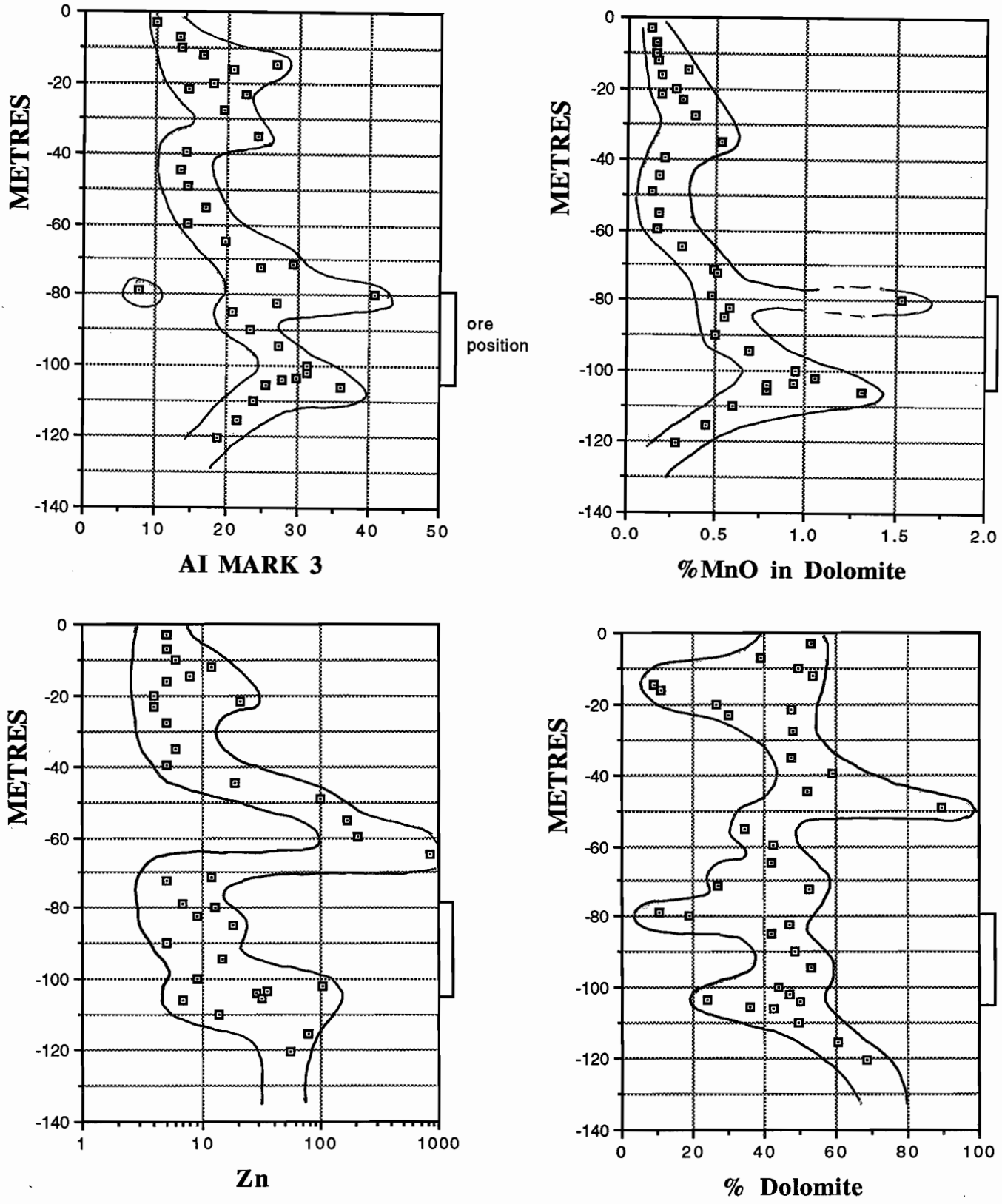

Figure 6—Downhole plots for DDH BMR McArthur 2 showing variations in AI_3, MnO_D, Zn and % Dolomite. Based on this data the interpreted ore position is 78 to 105 m. The data are from the new AGSO analyses given in Appendix 1.

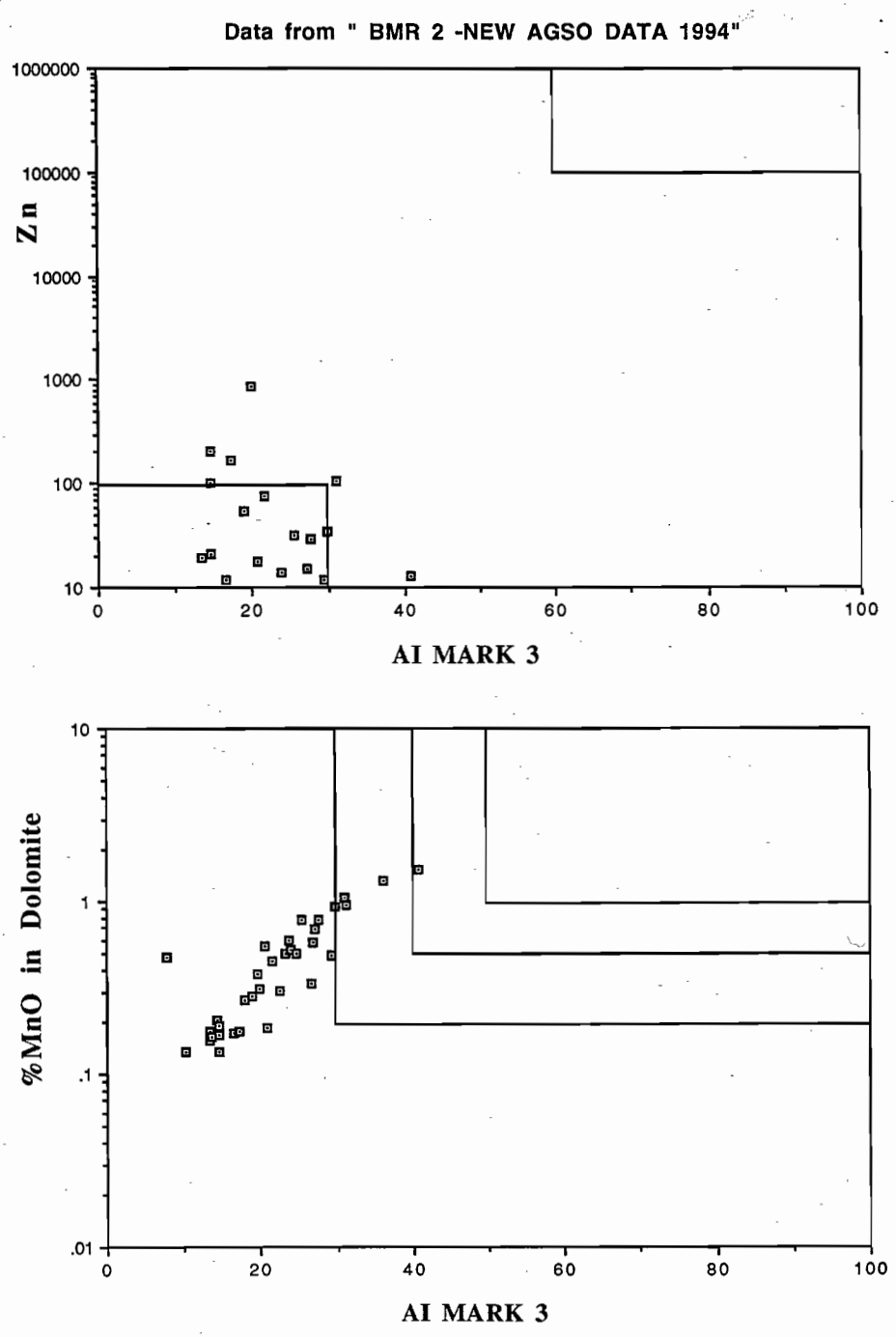

Figure 7—Alteration index plots for samples from DDH BMR McArthur 2 based on the new AGSO analyses (Appendix 1). Note one of the samples (~80 m downhole) plots in the priority 2 zone and a further three samples in the priority 3 zone.

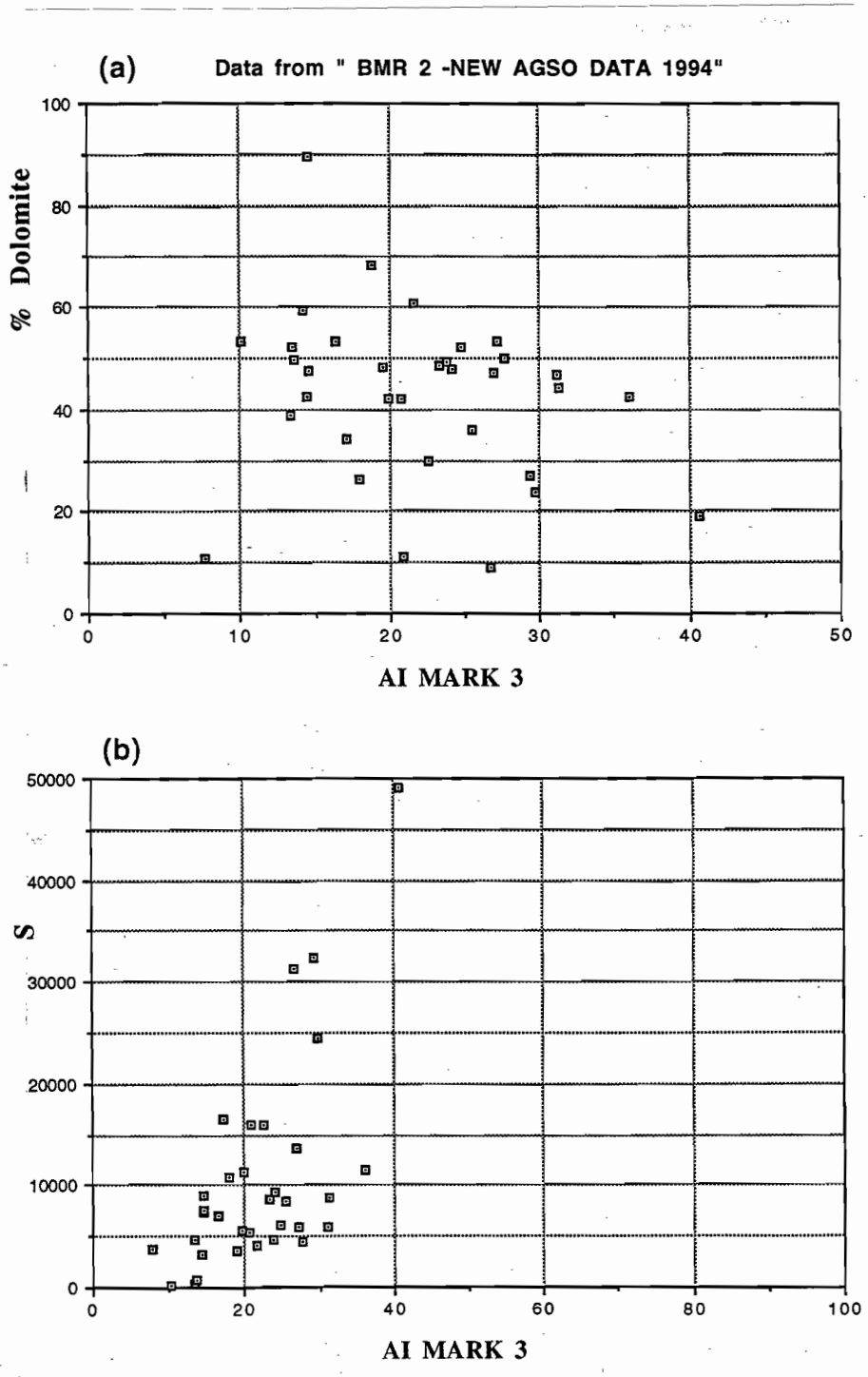

Figure 8—(a) Variation of AI_3 with % Dolomite. Dolomite content shows no correlation with AI_3 with the anomalous samples varying from 19 to 47% dolomite. (b) Variation of AI_3 sulphur. A rough correlation between sulphur (as pyrite) and AI_3 is evident.

Barney Creek Formation and the Reward Dolomite, is largely suppressed using AI_3.

Using the previous alteration index the upper peak in DDH BMR McArthur 2 was mainly defined by two samples which had alteration index values of greater than 50. Examination of the hand specimens and a thin section indicated that these samples were dominated by quartz-rich, framework supported sandstone, which had relatively minor dolomite (calculated values were around 10%) occurring as interstitial cement or recrystallised dolomitic mudstone matrix (Fig. 4b). These samples were clearly anomalous with respect to the generally dolomite-rich sediments intersected in DDH BMR McArthur 2. It was suspected that their anomalous alteration index values were due to the "shale effect" (Large, this volume), in which dolomite-poor samples gave relatively high alteration index values because they were low in MgO which is incorporated in the denominator of the alteration index equation. The current version of the alteration (AI_3) has Al_2O_3 added the denominator to balance the effects of samples with relatively high proportions of shale and low proportions of dolomite. The suppression of the upper alteration index peak in DDH BMR McArthur 2, which could clearly be related to anomalous dolomite-poor samples, validates the use of AI_3 in overcoming this problem.

Examination of the five samples from the lower alteration index peak in DDH BMR McArthur 2 which have AI_3 values of 30 or greater, indicates that three belong to the dominant facies defined in the hole, the *thin-bedded dolomitic sandstone/siltstone/mudstone facies* (at 99.97, 101.86 and 105.67 m), and two belong to the associated *massive carbonaceous +/- pyritic mudstone facies* (at 79.86 and 103.33 m). The highest AI_3 value recorded, 41, is given by one of the two samples from the latter facies. In general, high AI_3 values from this facies would be expected because the characteristic carbonaceous mudstone is often obviously pyritic in hand specimen and it will, therefore, be relatively iron-rich. Although only four samples from this facies were analysed from DDH BMR McArthur 2 because it only comprises 12% of the cored Barney Creek Formation by length, it should be noted that one sample (at 64.92 m) records a relatively low AI_3 value of 20. This, in combination with the fact that AI_3 values of 30 and greater also occur in the dominant *thin-bedded dolomitic sandstone/siltstone/mudstone facies*, suggests that apart from the "shale effect" addressed above, there is no direct relationship between alteration index and the sedimentary facies defined in DDH BMR McArthur 2.

CONCLUSIONS

Detailed sedimentological examination and geochemical resampling of DDH BMR McArthur 2 has indicated that:

1. A depositional model for the Barney Creek Formation in which the bulk of the unit was deposited in a quiet (ie. below wave base), anoxic subaqueous environment via hemi-pelagic suspension deposition interrupted by periodic small volume mass flows is valid.

2. The contact between the Barney Creek Formation and the overlying Reward Dolomite in the area where DDH BMR McArthur 2 was collared is gradational and represents gradually shoaling conditions.

3. The presence of peloidal sandstone beds throughout the Barney Creek Formation which are clearly sourced from an agitated shoreline environment, facies equivalents of which have been reported from the Reward Dolomite, suggests that the two units are at least partly time equivalent.

4. There is no direct relationship between alteration index and the sedimentary facies recognised in DDH BMR McArthur 2 (which are defined on the basis of dominant depositional mechanism and probably also organic carbon content) apart

from the "shale effect" which has been addressed by creating AI_3.

5. There is no clear relationship between % dolomite (calculated from CaO content) and AI_3 values, however, there is a crude relationship between AI_3 and sulphur content (occurring as pyrite).

FUTURE WORK

In order to confirm the relationship between AI_3 and sedimentary facies and to compare AI_3 values in spatially associated holes, it is proposed to carry out a similar integrated study on DDH Barney Creek 3. This hole was drilled by CEC in 1976 and was collared approximately 8 km NNE of DDH BMR McArthur 2 (Fig. 1) in Reward Dolomite. It intersected approximately 184 m of the HYC Pyritic Shale Member and was terminated in W-Fold Shale Member.

REFERENCES

Brown M. C., Claxton C. W. and Plumb K. A. 1978. The Proterozoic Barney Creek Formation and some associated units of the McArthur Group. Northern Territory. Australia Bur. Mineral Resources Rec. 1969/145 (unpubl.), 59p.

Bull S. W. 1994. Day 2 - Section of the Barney Creek Formation and adjacent units in the Top Crossing area. CODES: AMIRA/ ARC Project P384 Report No. 6, p. 33-40.

Corbett J. A., Lambert I. B. and Scott K. M. 1975. Results of analyses of rocks from the McArthur area, Northern Territory. CSIRO Tech. Comm. 57,.

Hinman M., Wall V. and Heinrich C. 1994. The interplay between sedimentation, deformation and hydrothermal activity at the McArthur River Pb-Zn(Cu) Deposit. Geol. Soc. Aust. Abst. 37, p. 176-177.

Jackson M. J., Muir M. D. and Plumb K. A. 1987. Geology of the southern McArthur Basin. B. M. R. Bull. 220. 173p.

Jackson M. J., Sweet I. P. and Powell T. G. 1988. Studies on petroleum geology and geochemistry, Middle Proterozoic, McArthur Basin northern Australia 1: Petroleum potential. APEA Journal, 28, p. 283-302.

Large R. and McGoldrick P. 1993. Primary geochemical halos related to Proterozoic sediment hosted Pb-Zn deposits and applications to exploration. CODES: AMIRA/ARC Project P384 Report No. 3, p. 63-126.

Large R. 1994. Case Studies: Application of the alteration index to selected areas in the McArthur Basin. CODES: AMIRA/ ARC Project P384 Report No. 5 p. 24-40.

Logan R. G. and Williams N. 1984. Sedimentary controls on the hydrothermal system that formed the H. Y. C. deposit at McArthur River, Northern Territory. In Geosciences and the Development of Natural Resources. Seventh A. G. C., Sydney, 1984. Geol. Soc. Aust. Abst. 12, p. 339.

Muir M. D. 1983. Depositional environments of host rock to northern Australian lead-zinc deposits, with special reference to McArthur River. Geol. Assoc. Can./Min. Assoc. Can. Annual Meeting, Victoria, Canada, May 1983, short course contribution, p. 141-174.

Pietsch B. A., Rawlings D. J., Creaser P. M., Kruse P. D., Ahmad P., Ferenczi P. A. and Findhammer T. L. R. 1991. Bauhinia Downs 1:250 000 geological map series. Northern Territory Geological Survey, Explanatory Notes SE53-3.

Williams N. and Logan R. G. 1981. Depositional environments of the sediments hosting the McArthur River stratiform Pb-Zn deposits. In Groves, D. I., McNamara, K., Brown, R. G. and Johnstone, M. H. (Editors)-Sediments Through the Ages. Fifth A. G. C., Perth, 1981. Geol. Soc. Aust. Abst. 3, p. 8.

Application of the Alteration Index and MnO_D to the Mount Isa and Hilton zinc-lead-silver deposits

Peter McGoldrick
Centre for Ore Deposit and Exploration Studies

SUMMARY

This report describes an assessment of the applicability of geochemical vectors to mineralisation developed for Lady Loretta and HYC to the giant Mount Isa and Hilton Zn–Pb systems. Several old public domain data sets have been used for this purpose. The data analysis indicates that the 'Sedex Alteration Index' (Large and McGoldrick, 1994), the 'Alteration Index Mk3' (Large, this volume), MnO_D (Large and McGoldrick, 1993) and Tl (McGoldrick, 1986) are all potentially useful vectors to the Mount Isa and Hilton deposits.

INTRODUCTION

The giant stratiform sediment-hosted (SSH) Zn–Pb–Ag deposits at Mount Isa ('Isamine') and at Hilton, 20 km to the north, had a pre-mining combined reserve of more than 200 Mt at about 13% Zn+Pb and 150 g/t Ag (Forrestal, 1990). At each deposit mineralisation comprises multiple stacked lenses in the upper 600 m of the Urquhart Shale. Individual orebodies are metres to a few tens of metres thick, but may be hundreds of metres in diameter, i.e. they have sheet-like aspect ratios. Hence, the deposits' geometry makes them ideal for testing the geochemical vectors to SSH Zn–Pb mineralisation developed previously for Lady Loretta and HYC (Large and McGoldrick, 1993; Large and McGoldrick, 1994). This report uses existing geochemical data for the Isamine and Hilton host sequences to test the utility of the Alteration Index and MnO_D for these deposits.

DATA SOURCES

The data used in this report are from three sources:

- a large (>1000 samples) multi-element suite from (Smith & Walker, 1970); these samples were analysed by carbon-rod spark-source emission spectroscopy at the BMR in the late 1960s
- twenty-seven samples analysed for major and trace elements by XRF and AAS at the CSIRO (Scott and Taylor, 1979)
- eighty-seven samples from (McGoldrick, 1986) analysed for major and trace elements by XRF at the University of Melbourne.

The Smith and Walker (1970) data set has a wider (both spatial and stratigraphic) coverage than the other two data sets, but the quality of much of it is difficult to assess. Nevertheless, the elements needed to calculate the various geochemical vectors appear to have been measured well enough, in most cases, for useful comparisons with the other data sets.

CODES: AMIRA/ARC Project P.384 — Proterozoic sediment-hosted base metal deposits. November 1994

MINE SEQUENCE SAMPLING AT ISAMINE

Sample locations

Most samples from McGoldrick (1986) were collected from underground development on 15B sub-level (Fig. 1). The twelve samples from the 7042 cross-cut are unmineralised 'shales' (the Urquhart Shale is mainly a carbonaceous, dolomitic, pyritic, siltstone ± base metal sulfides — Mathias and Clark (1975), but the use of the term 'shale' to describe these rocks is well entrenched and will be continued here). The 7042 cross-cut spans nine separate Zn–Pb orebodies. The remaining samples from McGoldrick (1986) are mostly ores and shales from 12 orebody and its along strike equivalents. The Scott and Taylor (1979) samples are from underground drill-core within and in close proximity to 8 and 11 orebodies (Fig. 2) and include ore-grade samples and unmineralised shales. The samples in the Smith and Walker (1970) collection came from four underground diamond drill holes and their locations are illustrated schematically on Figure 3. They are all from the southern end of the mine, and, while none penetrated Zn–Pb orebodies, G27W provides a 300 m section of Urquhart Shale approximately a kilometre along strike from the Zn–Pb orebodies. The drill hole W23C provides some additional unmineralised shale samples, but samples from the fringes of the silica dolomite envelope to 1100 Cu orebody have been excluded for the purpose of this study. W26W penetrated the upper 100 m of the Urquhart Shale and about 150 mem tres of the overlying Spear-Kennedy Siltstone. Drill hole PE36S provides samples of the underlying Native Bee Siltstone.

Results

For ease of presentation the data from McGoldrick (1986) and Scott and Taylor (1979) have been combined on Figures 4–7. The systematic approach to data analysis recommended in (Large and McGoldrick, 1994) has been utilised. Diagrams illustrating the spatial variation of important geochemical vectors in the 7042 cross-cut and from P70E drill-hole are also presented (Figs 8 and 9).

Figure 4 plots Ca and Mg for 114 samples and demonstrates that dolomite is the dominant carbonate mineral in most of the samples. Ten samples with less than one weight percent MgO or lying well away from the 'ideal dolomite' line have been omitted from subsequent plots.

Large (this report) recommends a modification to the 'Sedex Alteration Index' (AI) described in P384 Report No 5 (Large and McGoldrick, 1994). This modification incorporates Al_2O_3 into the denominator of the formula used to calculate the index, in order to remove the tendency for 'shaley' rocks to have anomalously high AIs. Both the original alteration index and the 'Alteration Index Mk3' (AI 3) have been calculated for the Isamine data set and they can be compared on Figure 5, and a good correlation is observed between the two indices. Where possible in this report both indices will be used for the purpose of data presentation.

Figure 6 shows the relationship between Zn and the two AIs for the 104 Isamine samples. Virtually all samples would be classified as anomalous (AI > 40, AI3 > 30) using either index, and even shale samples with less than 1000 ppm Zn have AI and AI3 values of up to 90 and 82, respectively.

Figure 7 depicts MnO_D and AI and AI3 for the Isamine samples. Most of the samples have anomalous MnOD values, with shale samples mainly scattered through the priority 2 and 3 fields of Large and McGoldrick (1994). The prominent outlier with an MnO_D value of less than 0.2 is a composite shale sample collected from drill hole collared about 10 km north of Isamine.

P70E profile: The 23 samples from drill hole P70E provide a useful insight into the AI and MnO_D patterns in close proximity to high-grade Zn–Pb mineralisation (Fig. 8). Sample spacing is of the order of a metre and samples include ore grade

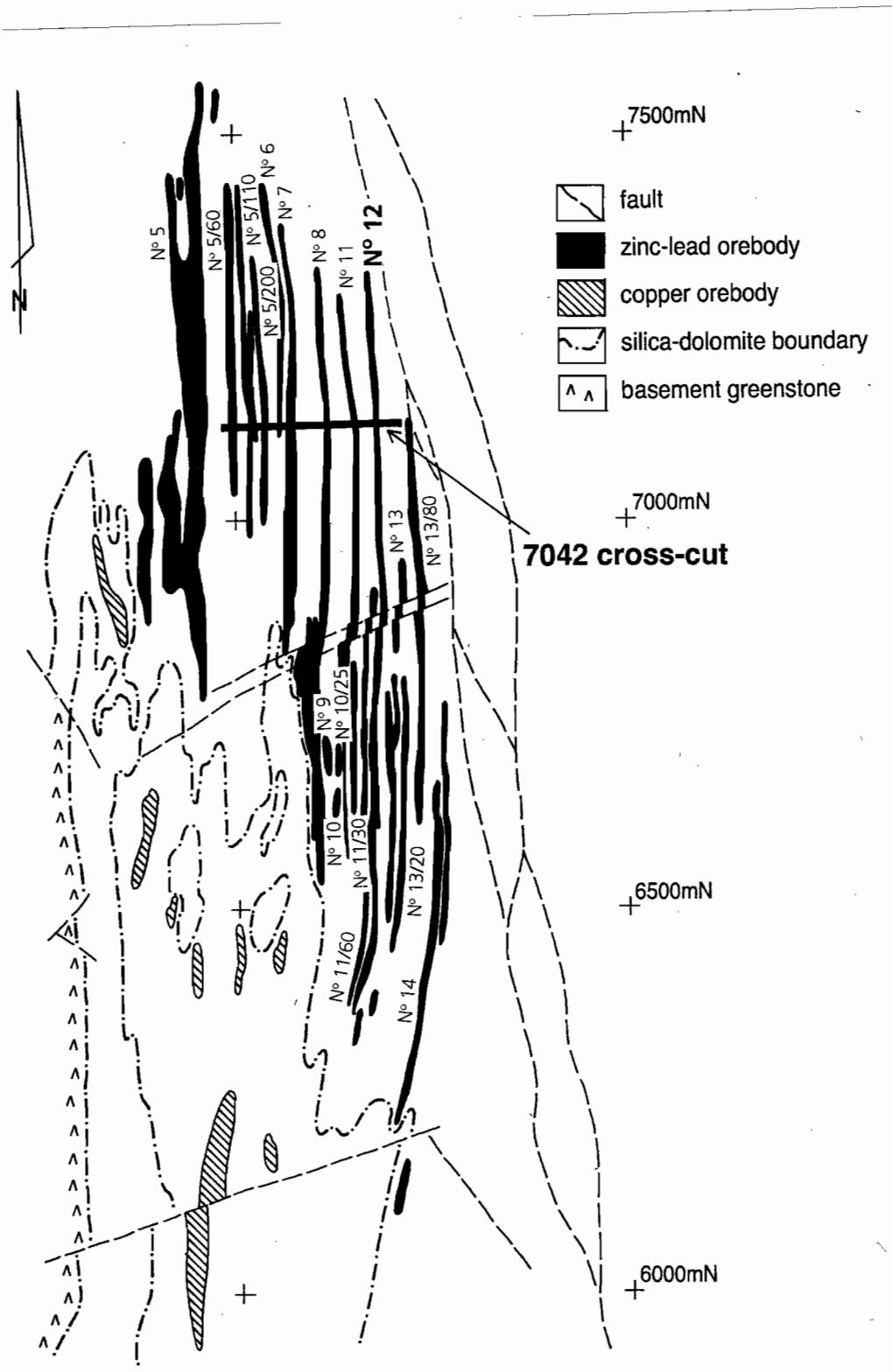

Figure 1 — Plan of the northern end of 15B sub-level from Isamine indicating the position of 12 orebody and the 7042 cross-cut.

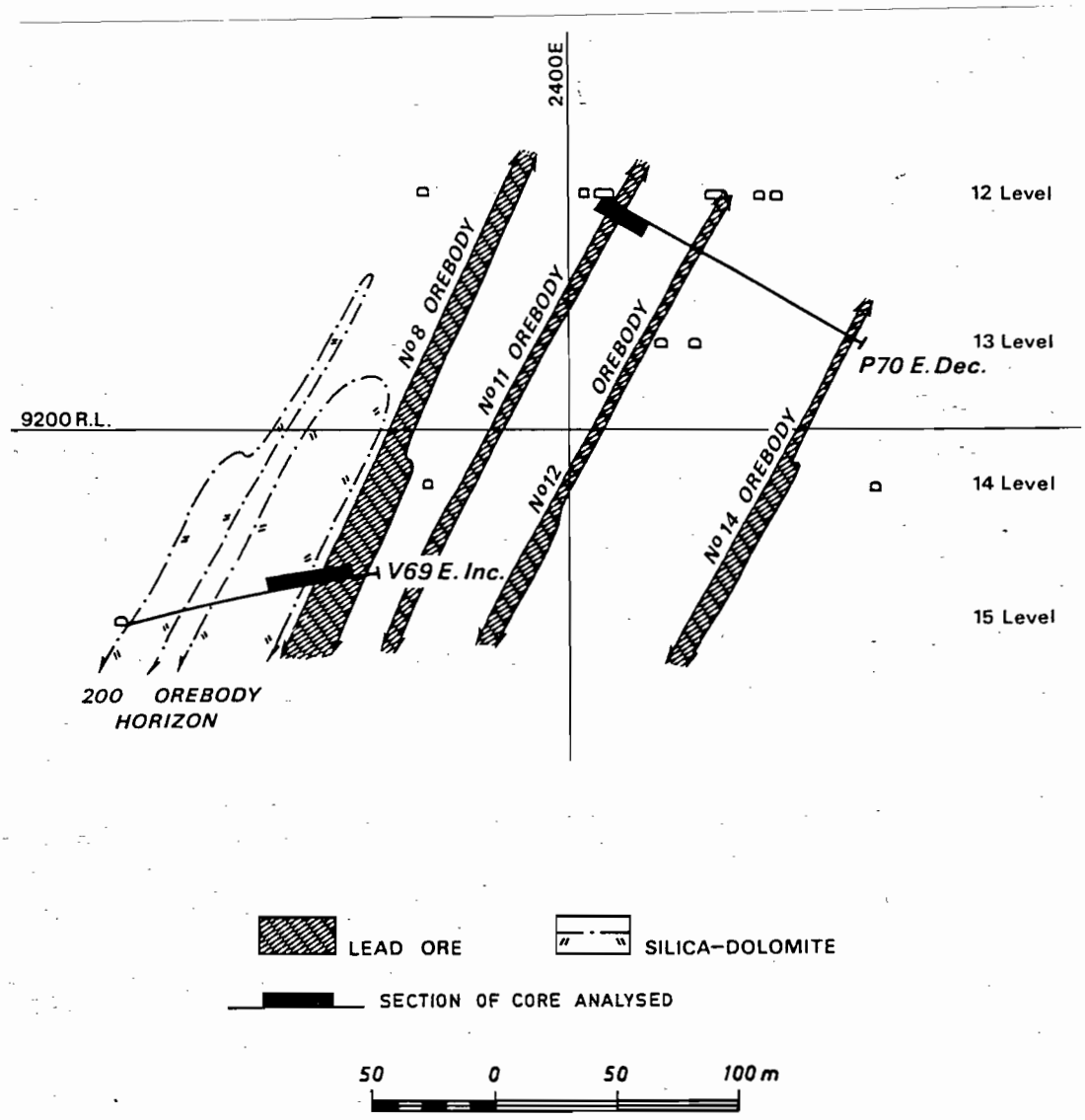

Figure 2 — Diagrammatic (east–west) section of part of Isamine (about 6600m N — mine grid) showing the location of drill holes P70E decline, and V69E incline and the intervals sampled by Scott and Taylor, 1979).

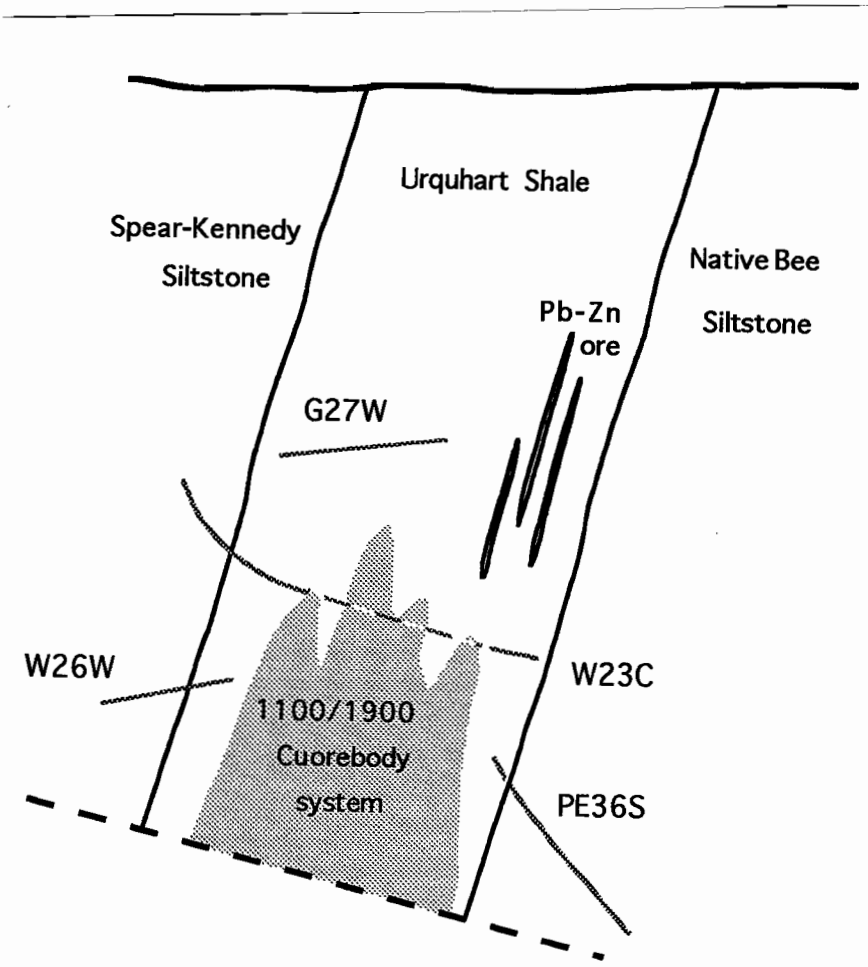

Figure 3 — Cartoon section of the southern end of Isamine showing the relative position of the drill holes samples by Smith and Walker, 1970, and nearby Cu and Zn-Pb orebodies.

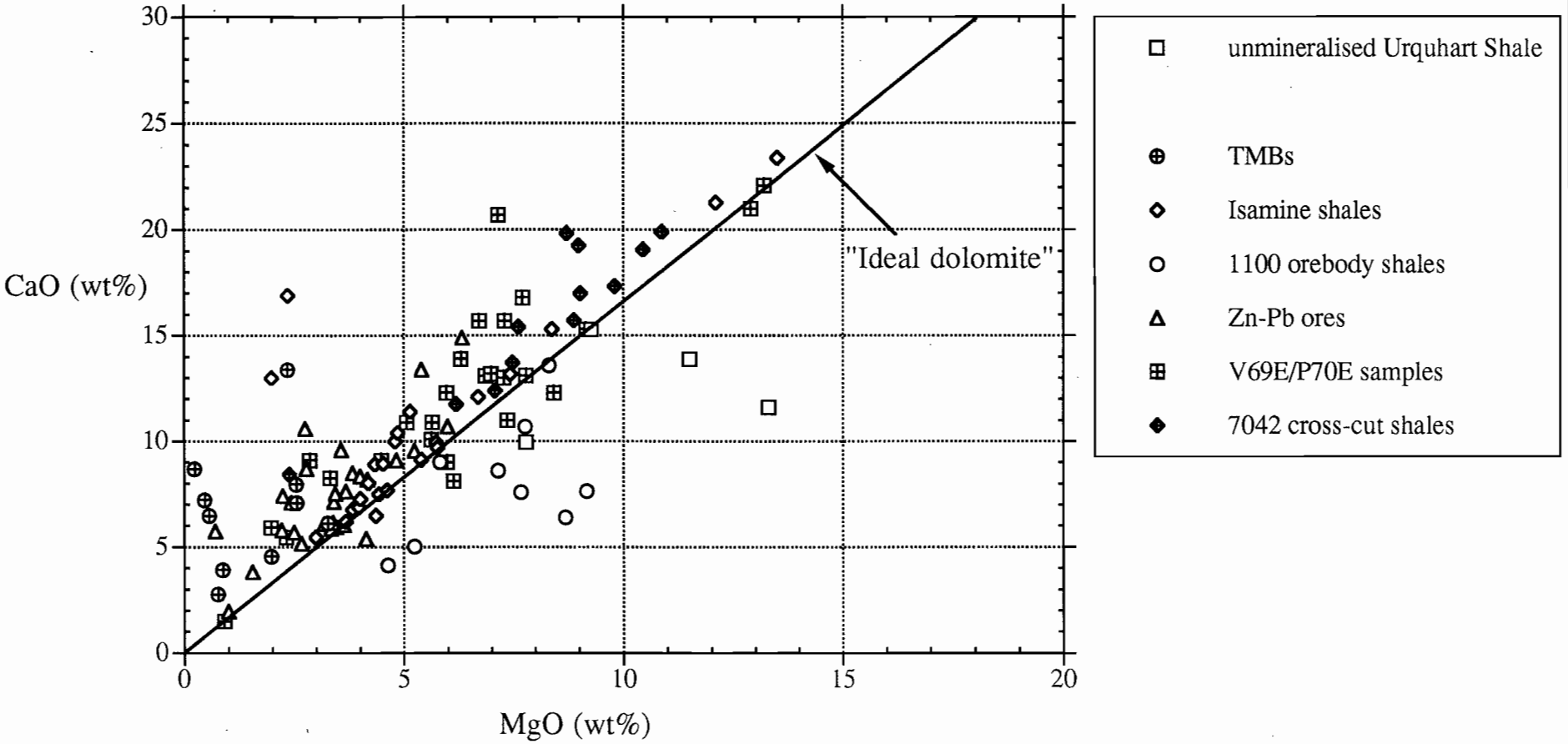

Figure 4 — CaO v MgO for all samples from Scott and Taylor (1979) and McGoldrick (1986). The line labelled 'Ideal dolomite' corresponds to the CaO:MgO proportions in stoichiometric dolomite; sediments in which dolomite is the only mineral containing Ca and Mg should plot close to this line.

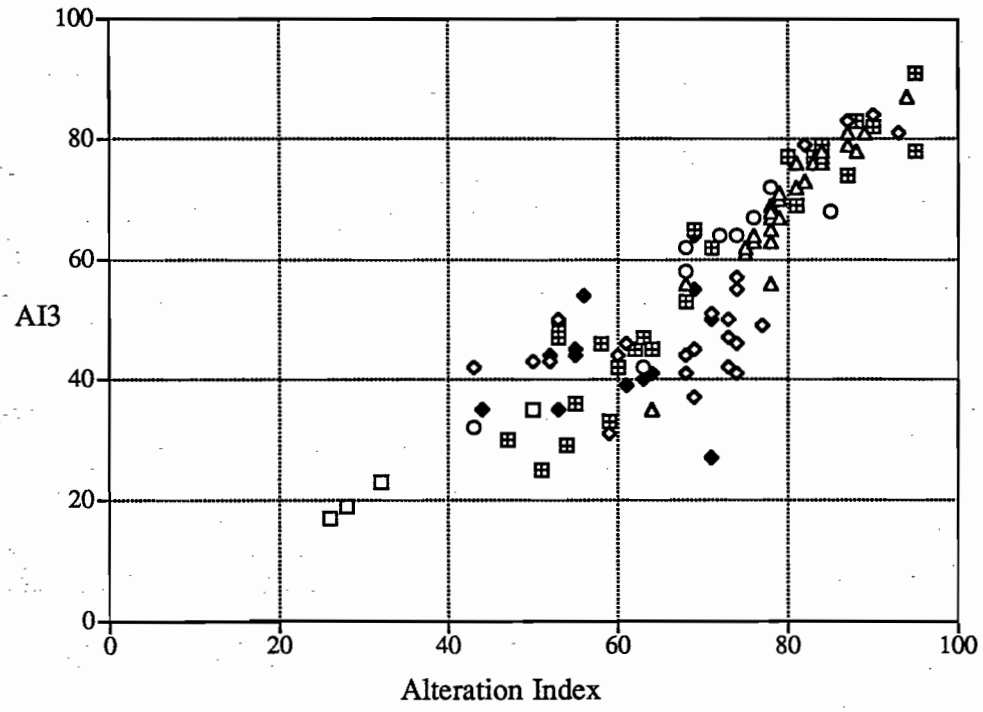

Figure 5 — A comparison of the 'Sedex Alteration Index' and the 'Alteration Index Mk 3' for samples from Isamine (same symbols as Figure 4).

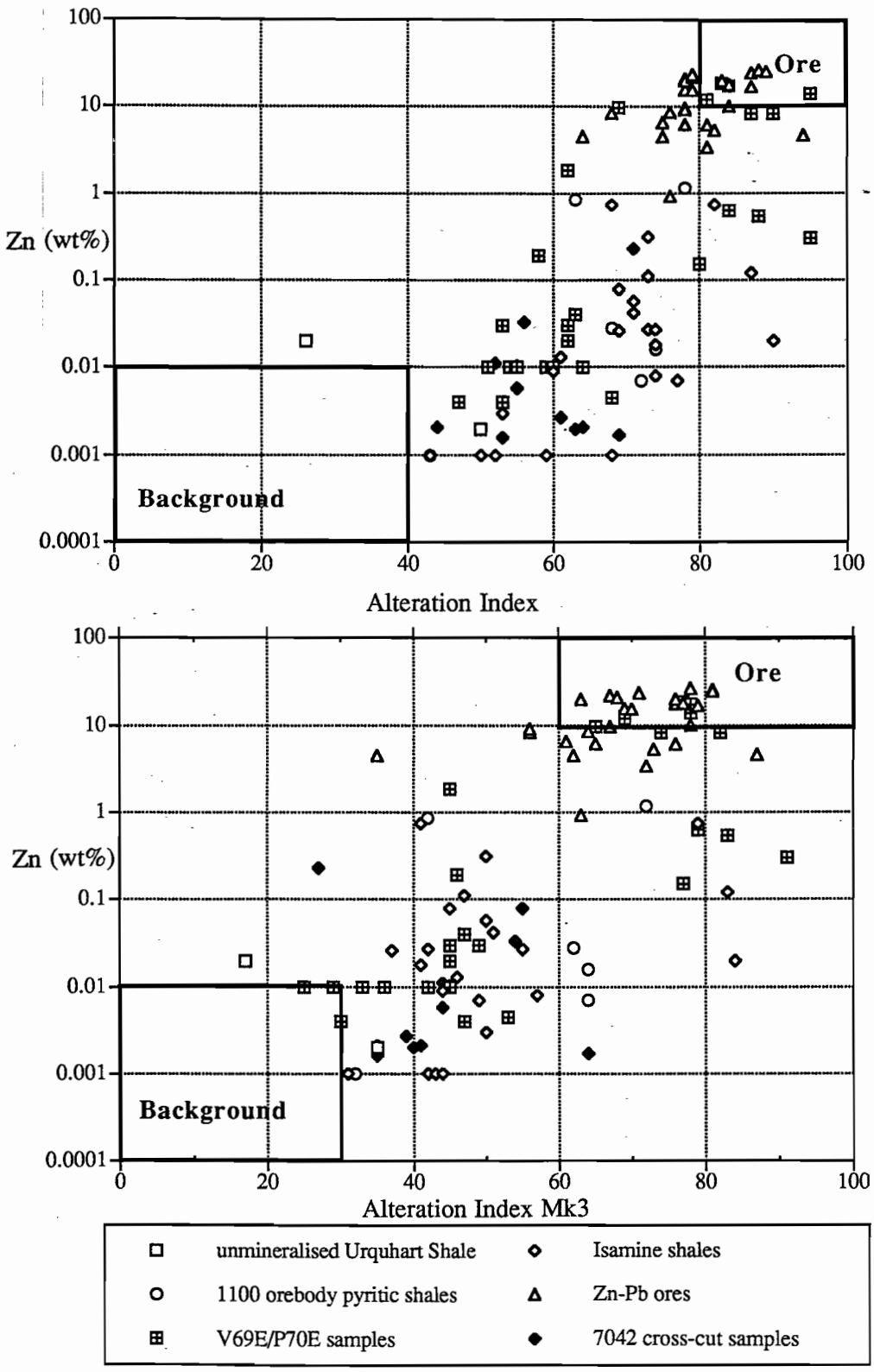

Figure 6 — Zn v AI and AI3 for 102 samples from Isamine and two remote 'unmineralised Urquhart Shale' samples.

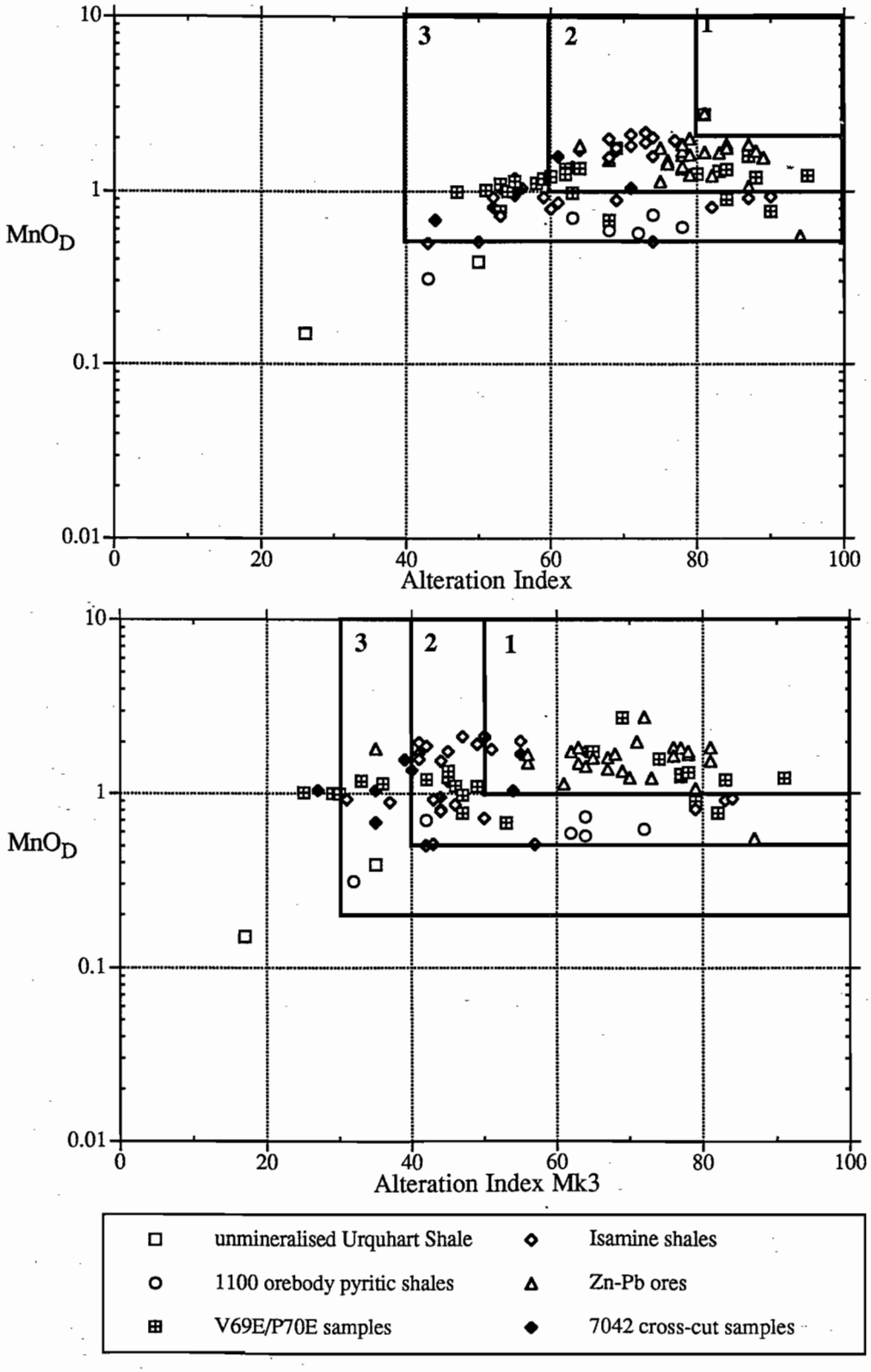

Figure 7 — MnO_D v AI and AI3 for 102 samples from Isamine and two remote 'unmineralised Urquhart Shale' samples.

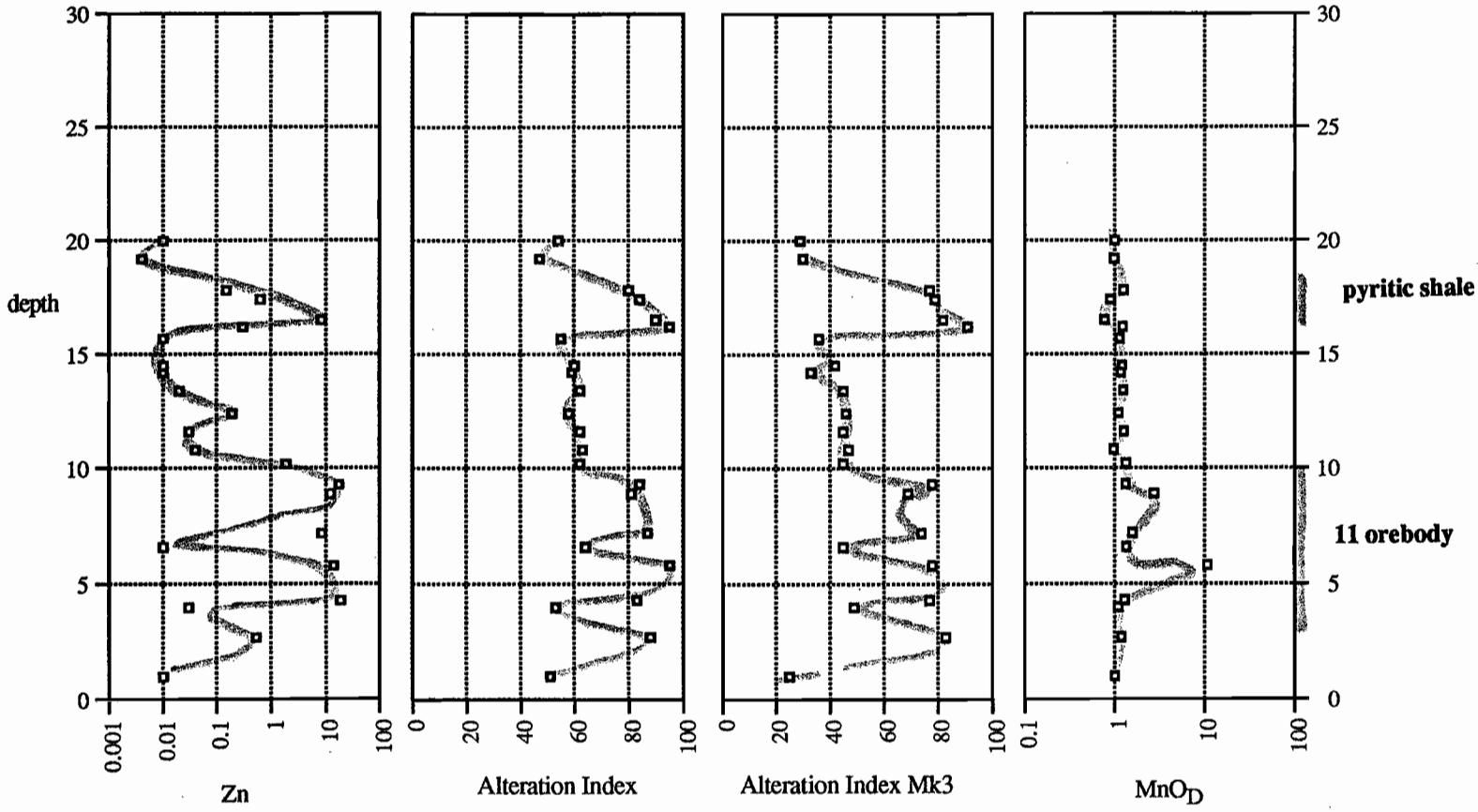

Figure 8 — The distribution of Zn, AI, AI3 and MnO_D in 23 samples from DDh P70E. The position of 11 orebody and a strongly pyritic band in the footwall are highlighted.

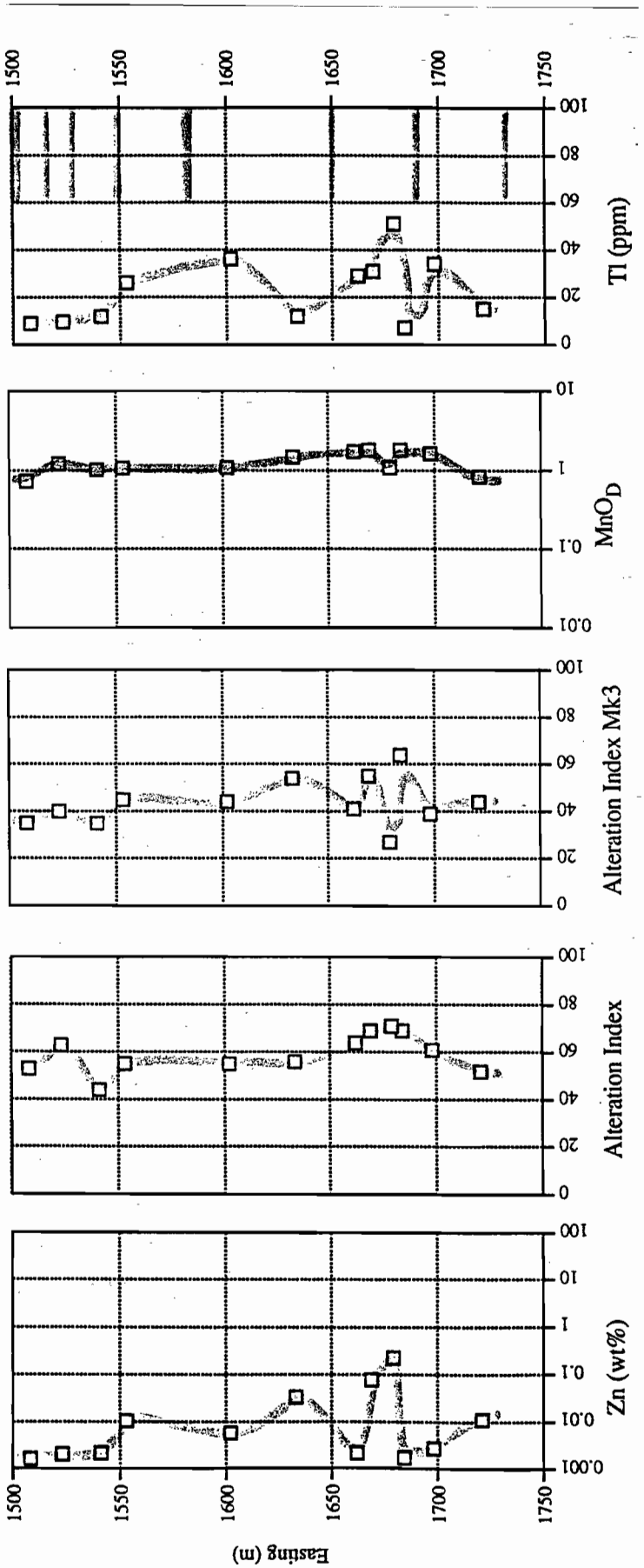

Figure 9—The distribution of Zn, AI, AI3 , MnO_D and Tl n 12 samples from 7042 cross-cut on 15B sublevel. The positions of Zn-Pb orebodies are highlighted. as horizontal bars on the Tl plot.

material from 11 orebody and shale and pyritic shale from the hangingwall and footwall. Zinc shows a spikey distribution with values of between 0.1 and 2 weight percent occurring in shales peripheral to 11 orebody. Values for the AI and AI3 peak in the orebody, but are still strongly anomalous in the shales on either side. The MnO_D values show a much smoother distribution than the AIs and Zn, and virtually all the samples are in the priority 1 or 2 category of Large and McGoldrick (1994).

7042 cross-cut: The twelve samples from 7042 cross-cut span approximately 200 m of true stratigraphic thickness in the upper half of the Urquhart Shale. Although, nine separate Zn–Pb orebodies are present in this interval on 15B sublevel, all the samples were collected from the unmineralised interore beds. Figure 9 illustrates the relationship through the sequence of Zn, the AI, AI3, MnO_D and Tl, and the location of the various Zn–Pb orebodies. Most of these samples contain little Zn, but all show anomalous AIs and prospective MnO_Ds. The Tl levels are also strongly anomalous (10 to 40 ppm cf 'typical shale' abundance of 0.5 to 2 ppm — de Albuquerque and Shaw, 1974; McGoldrick, 1986).

Smith and Walker (1970) data: All the Ca and Mg data for these samples are plotted on Figure 10. The scatter of points is much greater than that shown by the newer data. It is not clear if the scatter reflects the presences of carbonates other than dolomite in the samples, or, alternatively, greater analytical uncertainty for the emission spectrographic analyses. However, for the time being, these analyses are the most wide ranging data set (publicly) available for the Mount Isa deposits. For these reason no attempt has been made to screen out 'non-dolomite' samples and all the data are included in subsequent plots. Aluminium was not analysed by Smith and Walker (1970), so AI3 cannot be calculated for these samples.

Figure 11 plots Zn and MnOD against AI for these samples. While there is a wide range in both AI and MnO_D, a significant proportion of samples have high (more than 1%) MnO_Ds similar to the newer data sets, and many samples lie in or near the 'prospective' parts of the plots. Considering the drill holes individually is more revealing. Hole P36E samples 400 metres of Native Bee Siltstone stratigraphically below (Cu-mineralised) Urquhart Shale, and has unexciting, fairly uniform, AI and MnO_D values averaging about 40 and 0.5, respectively (Fig. 12). The first 100 m, or so, of the hole is in Urquhart Shale and these samples have slightly higher MnO_D values and more erratic AIs. Drill hole G27W intersected about 300 m of Urquhart Shale with sporadic uneconomic Zn mineralisation (the nearest stratigraphically equivalent Zn–Pb orebodies are about a kilometre to the north). The AI values in this hole are spikey, but commonly range between 40 and 80, and MnO_D values are somewhat anomalous ranging between about 0.5 and 1% (Fig. 13). Hole W26W penetrated a hundred metres of the top of the Urquhart Shale and a similar distance into the overlying Spear-Kennedy Siltstone. The AI values in Urquhart Shale in this hole resemble those in G27W, but drop off as the Spear-Kennedy Siltstone is approached and increase again toward the bottom of the hole (Fig. 14). The MnO_D index has a more systematic trend to higher values near the top of the Urquhart Shale with a sudden drop into Spear-Kennedy Siltstone, followed by a gradual increase back to values similar to Urquhart Shale.

Discussion

The data from McGoldrick (1986) and Scott and Taylor (1979) indicate that the AI, AI3 and MnOD are useful vectors to Mount Isa Zn-Pb mineralisation on the scale of a metres to a few tens of metres of sediment thickness (i.e. barren interore beds carry a strong AI, AI3 and MnO_D signature). Data from Smith and Walker (1970) suggest that these halos may persist for (at least) hundreds of metres along strike from high grade mineralisation.

Thallium (an important minor component of the Mount Isa Zn–Pb ores) is also present at high

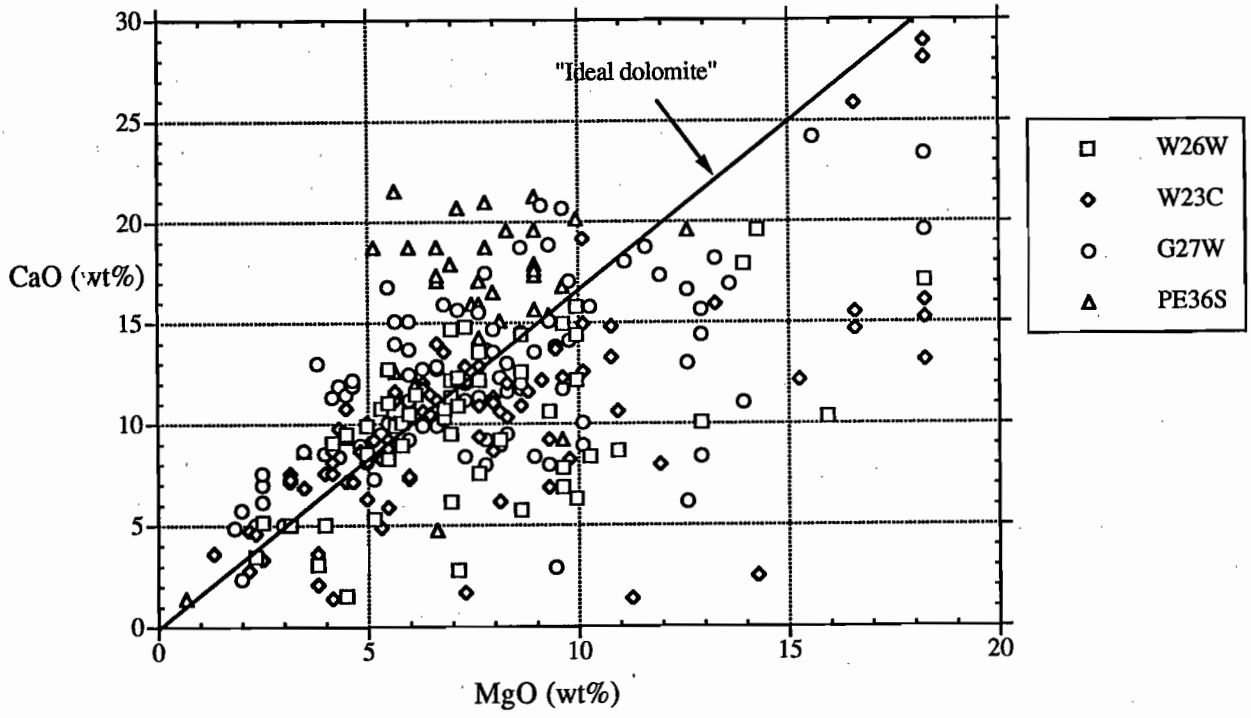

Figure 10 —The CaO v MgO relationship for all the Isamine samples from Smith and Walker (1970)

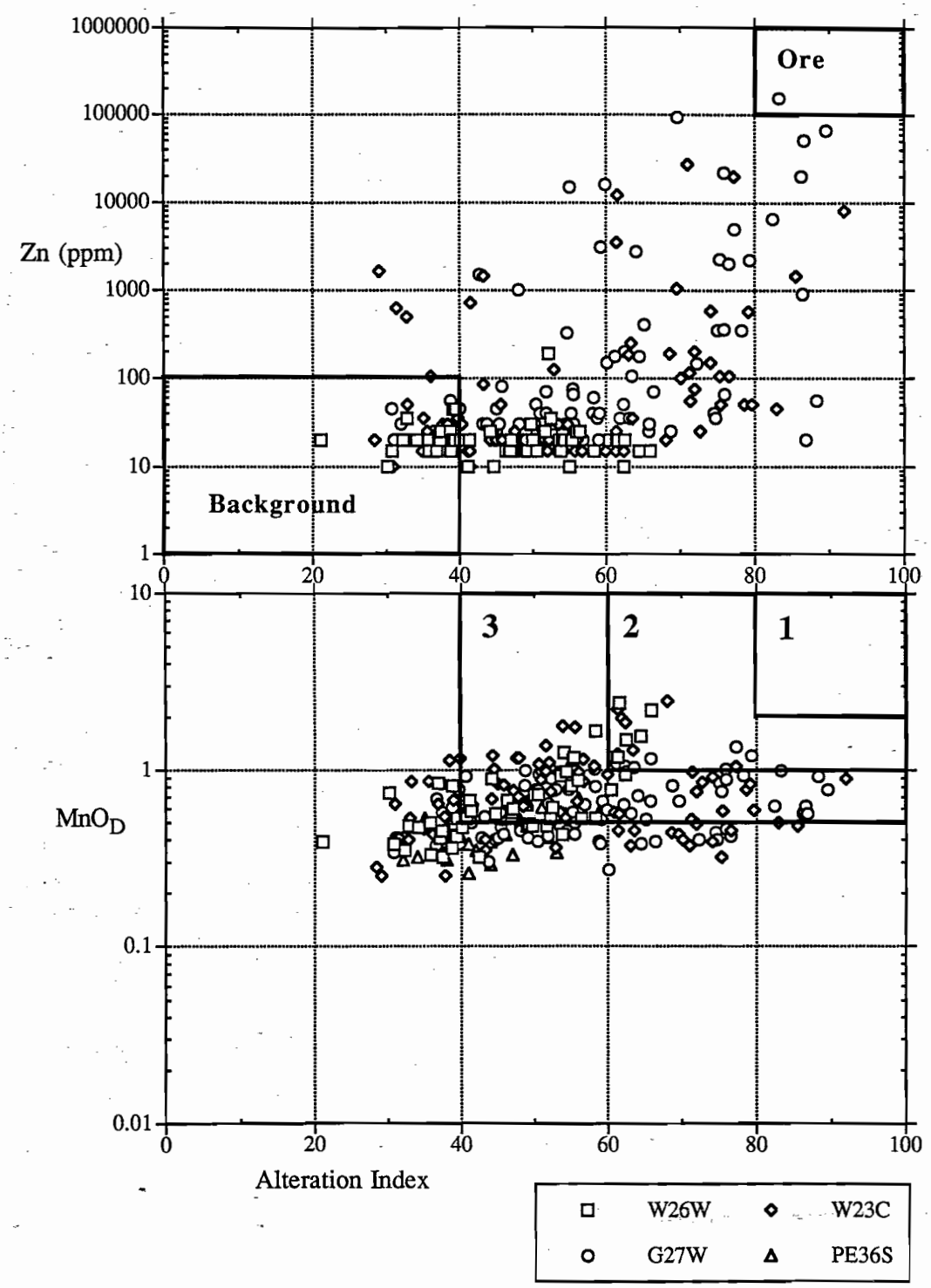

Figure 11—The AI v Zn and AI v MnO_D relationships for Isamine data from Smith and Walker (1970). Note that no Zn analyses were available for PE36S.

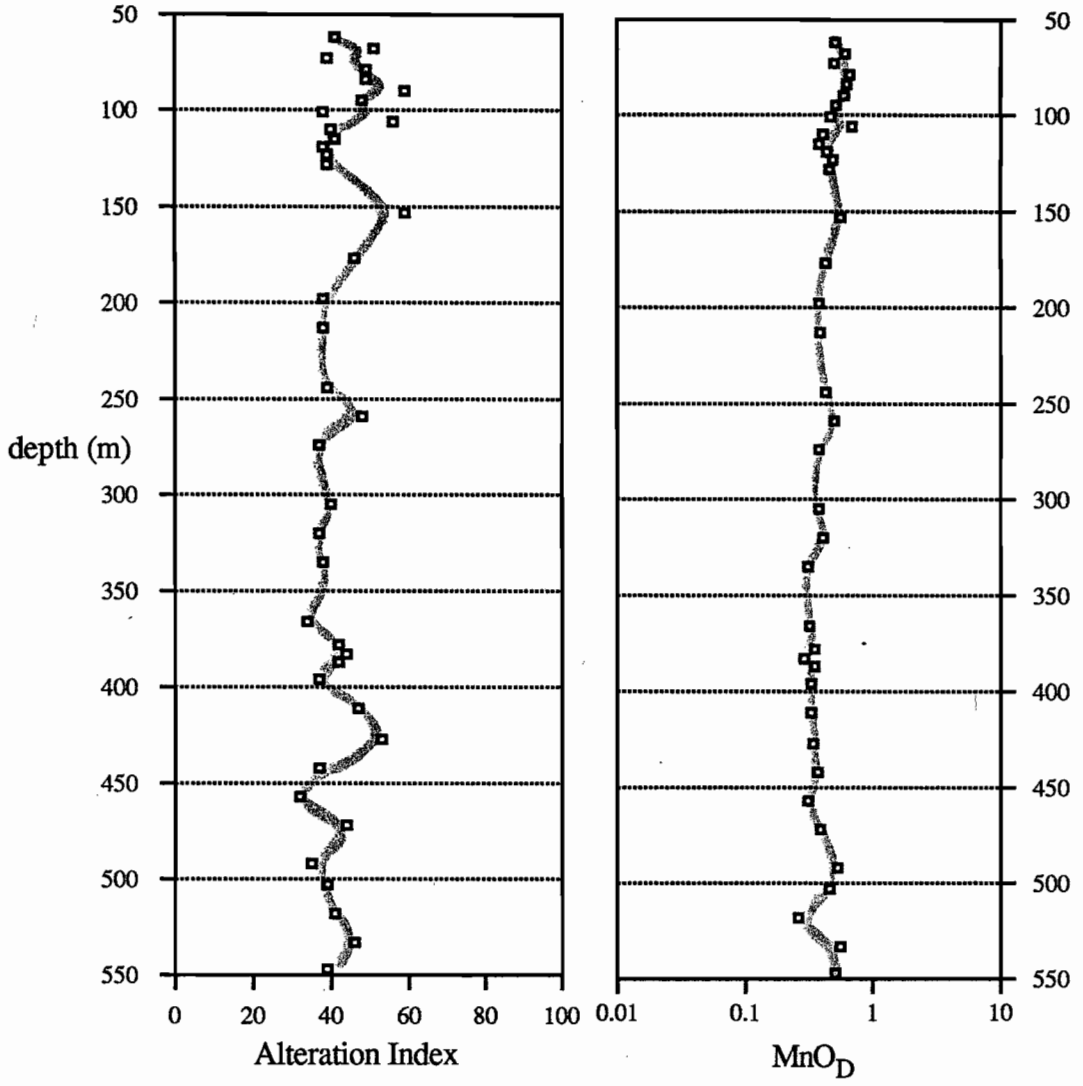

Figure 12—Down hole plots of AI and MnO_D for drill hole PE36S. Note that all samples, except those from about the first hundred metres, are from the Native Bee Siltstone Member which is stratigraphically below the Urqhuart Shale.

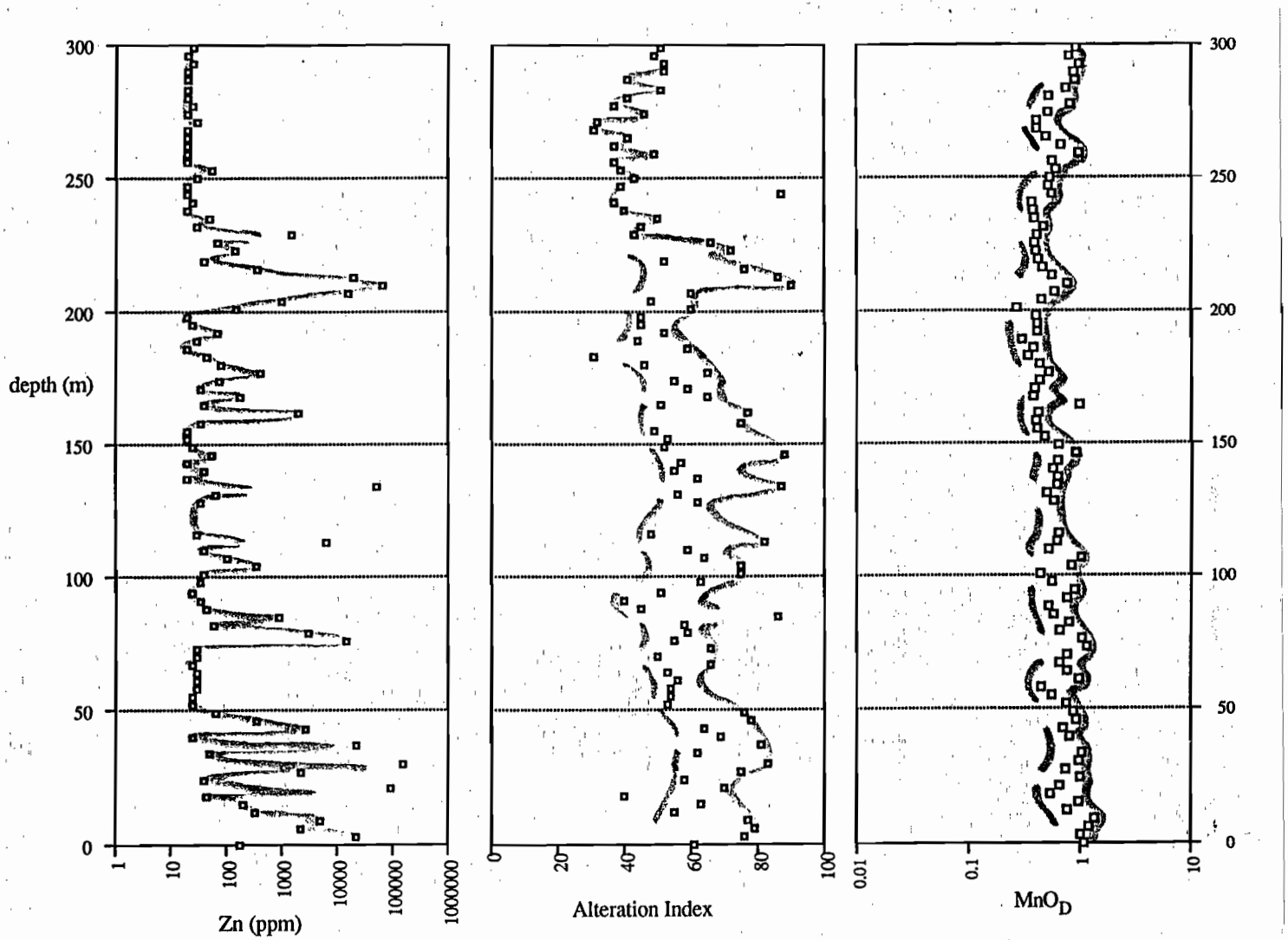

Figure 13—Down hole plots of Zn, AI and MnO_D for drill hole G27W which samples barren and weakly mineralised Urquhart Shale which is stratigraphically equivalent of the Zn-Pb orebodies about a kilometre to the north.

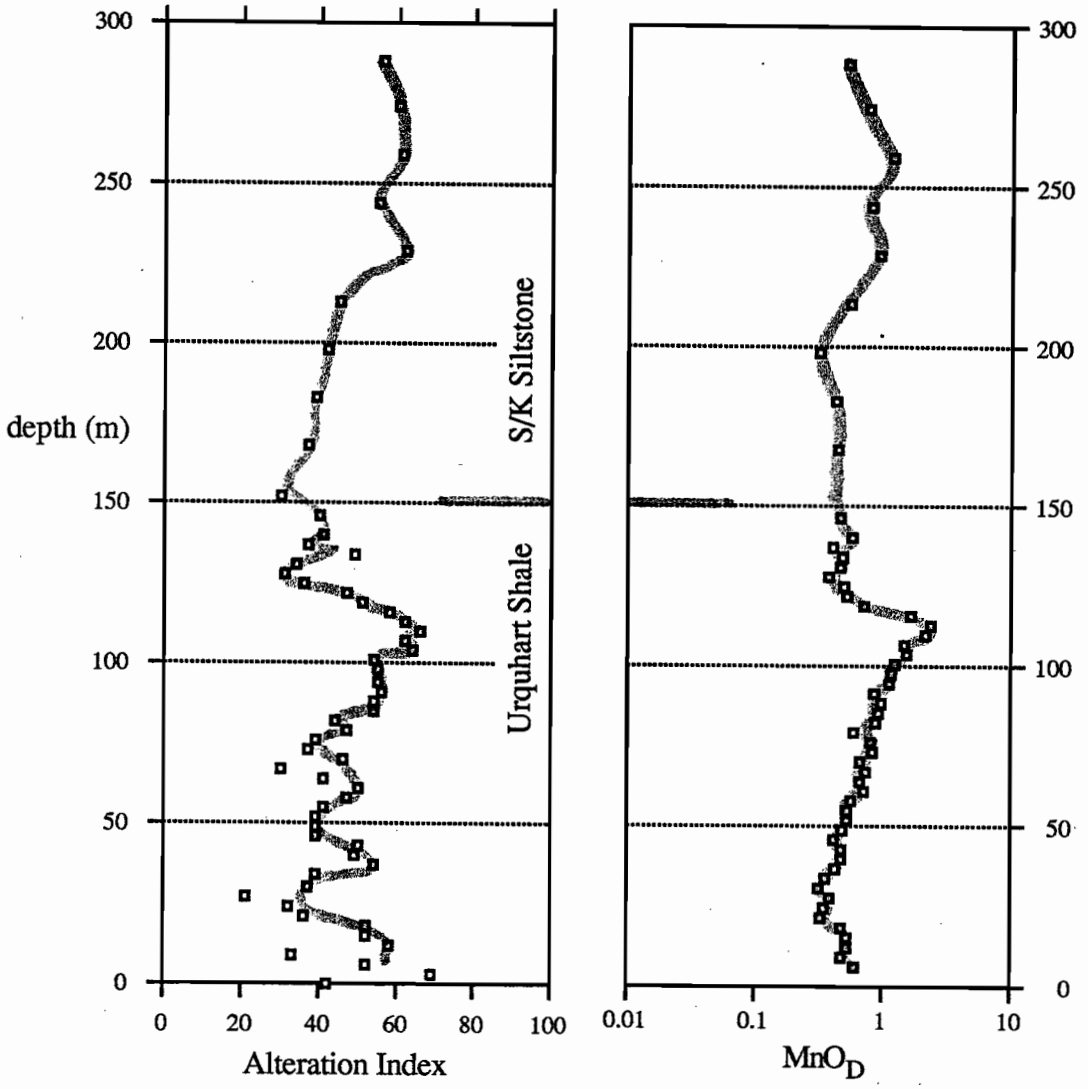

Figure 14—Down hole plots of AI and MnO_D for drill hole W26W. Note this hole was drilled 'up-sequence' with the approximately the first 150 metres in Urquhart Shale and the rest of the hole in Spear/Kennedy Siltstone.

levels in the unmineralised shale samples from the mine sequence. The observation that Tl is strongly correlated with K and only poorly correlated with S in these samples (Fig. 15) lends support to the interpretation that Tl is substituting for K in K-silicates (e.g. phyllosilicates and/or K-feldspar — McGoldrick, 1986) and not sulfides. This ability of Tl to substitute for K may make it an useful alternative to Mn as a vector to SSH Zn–Pb mineralisation hosted in carbonate-free, fine grained siliciclastic sequences.

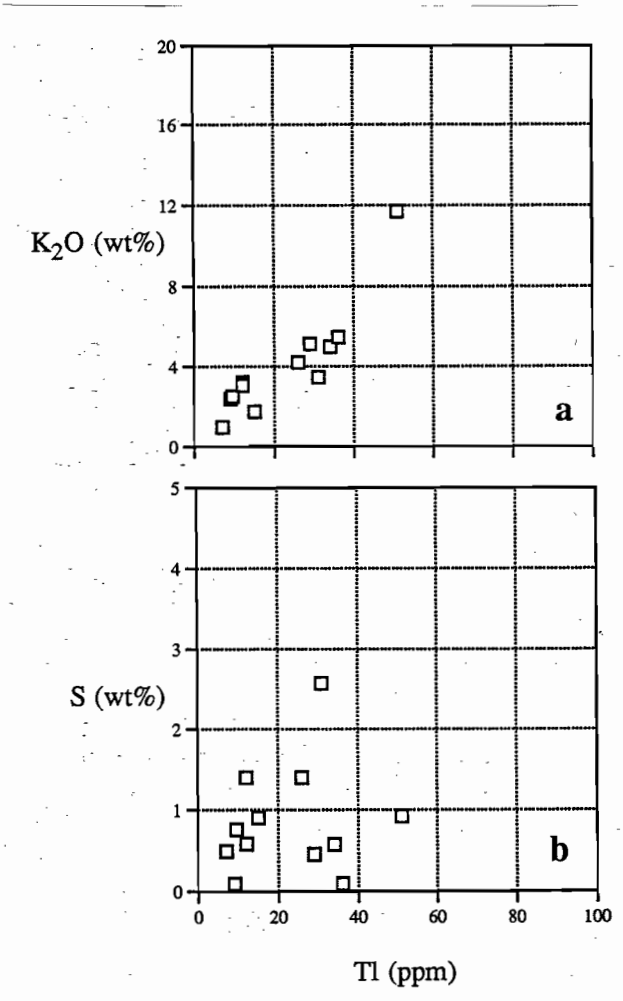

Figure 15— (a) The K_2O v Tl relationship for twelve unmineralised shales from 7042 cross-cut showing the strong correlation (r= 0.89) between these elements. b) The S v Tl relationship for twelve unmineralised shales from 7042 cross-cut showing the poor correlation (r= 0.15) between these elements.

HILTON

Smith and Walker (1970) present data from two deep surface holes that pass through the Spear-Kennedy Siltstone and the mineralised Urquhart Shale at Hilton Mine. Only one of these holes is considered here (NL 21/21A) because the other (NL14) was drilled through the leached part of the orebodies. Most samples are from the bottom half of the hole and would lie within Urquhart Shale. The bottom 250 m of hole penetrated four or five of the smaller stratiform Hilton orebodies (Fig. 16).

Calcium and Mg are plotted for the NL21 samples on Figure 17 and most show a 'dolomitic' character. A small number of samples are more Ca-rich samples and a few are devoid of Ca. No attempt has been made to discriminate these samples on subsequent plots.

Figure 18 shows the Zn–Al–MnO_D relationships for these samples. Few samples have more than 1000 ppm Zn but more than half have Al values greater than 50 and MnO_D values of more than one percent.

When the data are plotted down hole (Fig. 19) a very erratic Zn pattern is produced, however, both Al and (especially) MnO_D produce smoother patterns with a good correspondence of elevated values with the interval containing the orebodies.

Discussion

Although data from Hilton are limited to a single drill hole the observed Al and MnO_D distributions are very similar to those from the mine sequence and its environs at Mount Isa. It is likely, therefore, that both these indices would have anomalous values in unmineralised samples collected along strike from the Hilton orebodies.

Quartzite No 1

This hole was collared about 5 km south of Hilton Mine and penetrated 800 m of upper Mount Isa Group sediments (probably Spear-Kennedy Siltstone and Urquhart Shale). Smith and Walker (1970) present 116 analyses for this about hole and

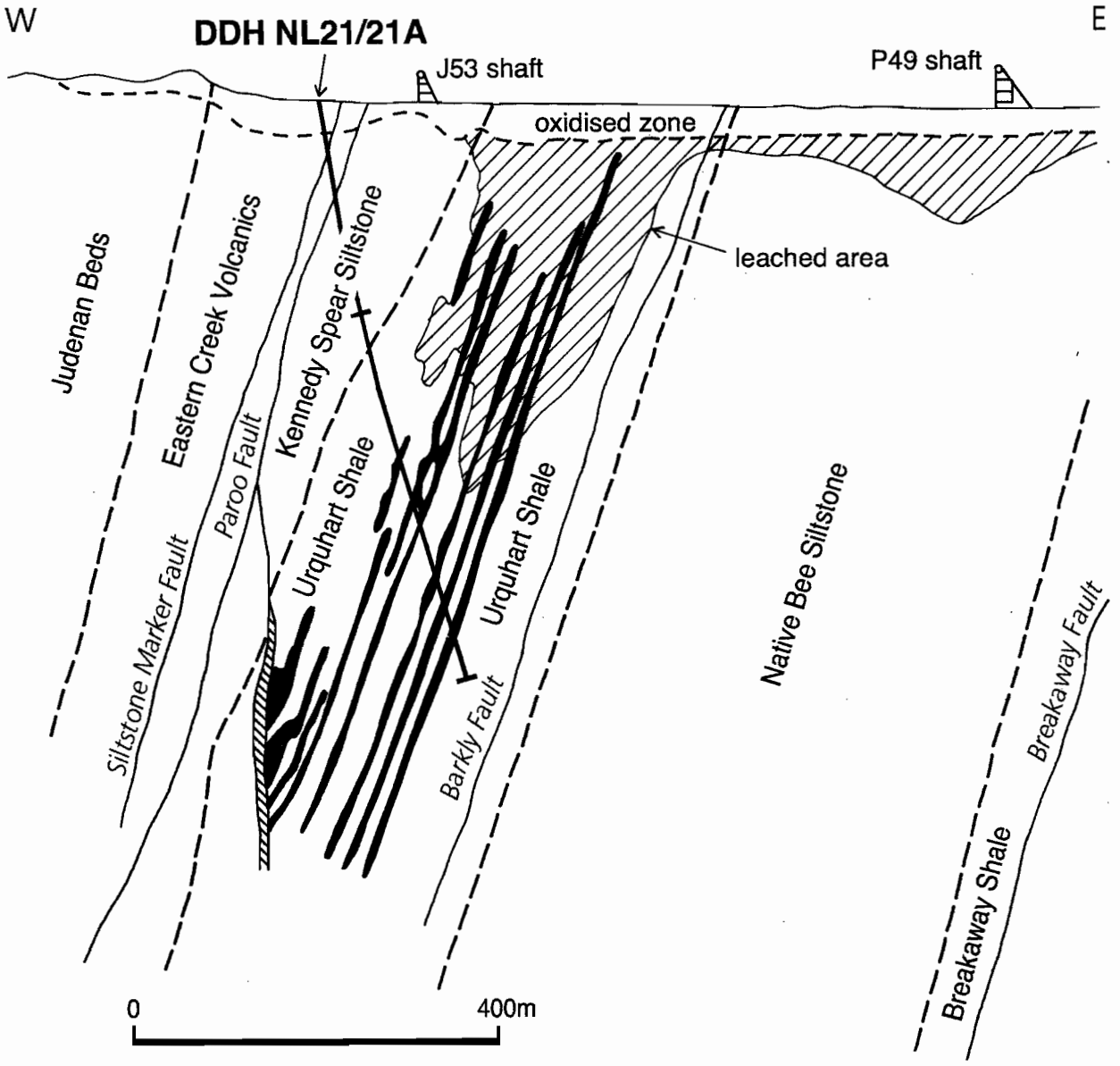

Figure 16 —Cross-section looking north at Hilton Mine showing the location of drill hole NL21/21A.

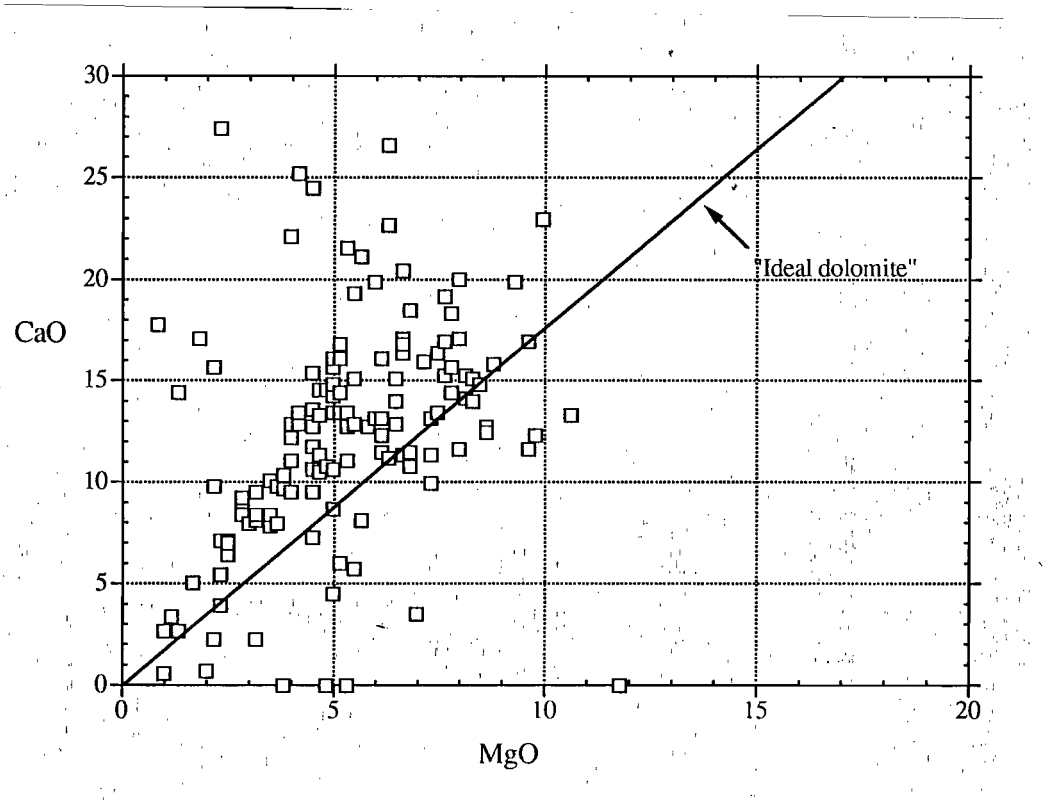

Figure 17—The CaO v MgO relationship for all samples from NL21/21A.

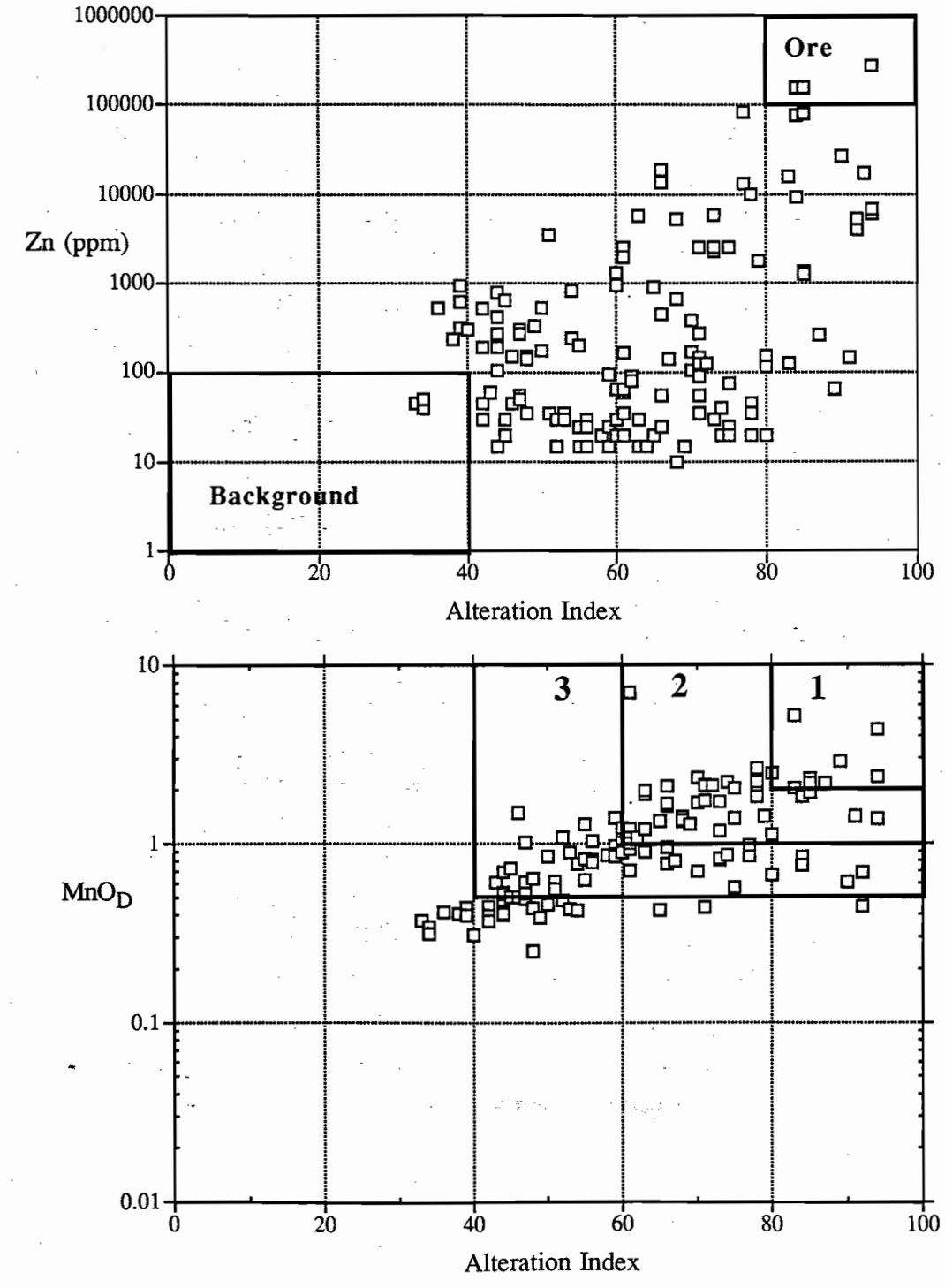

Figure 18—The AI v Zn and AI v MnO_D relationships for all samples from NL21/21A.

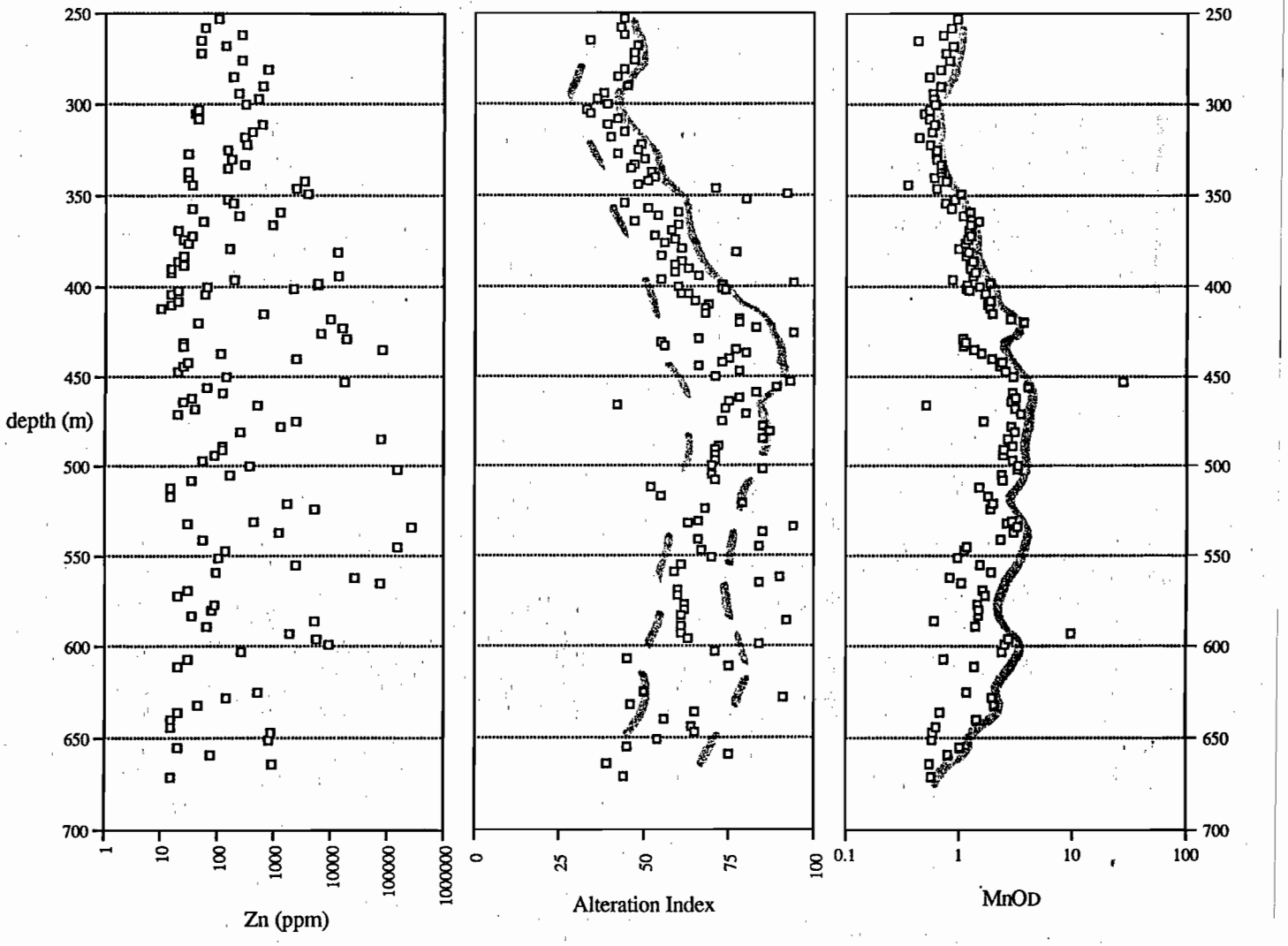

Figure 19—Down hole plots of Zn, AI and MnO_D for drill hole NL21/21A. Note that only the lower two thirds of the hole was sampled and the Hilton Zn-Pb orebodies are concentrated in the lower two thirds of the sampled interval.

their data are displayed in Figures 20– 22. The Zn values for most samples are at or near detection limit and are not very encouraging. However, a significant proportion of the samples have elevated AIs and MnO_Ds and down hole plots indicate that a zone between 100 and 400 m down the hole that is distinctly anomalous in both these indices. The along strike equivalent of this zone should be considered quite prospective within a kilometre north or south along strike.

IMPLICATIONS FOR THE GENESIS OF SSH Zn–Pb DEPOSITS

The origin of the Mount Isa and Hilton Zn–Pb lodes has been the subject of wide ranging speculation and debate(Finlow-Bates & Stumpfl, 1979) (Neudert, 1983) (Perkins, 1990) and McGoldrick, 1986). A detailed presentation of current genetic models is beyond the scope of this report. However, the observation that the host rocks to both Mt Isa and Hilton display chemical vectors to mineralisation essentially the same as those observed at Lady Loretta and HYC (Large and McGoldrick, 1993) must be reconciled in any genetic model for these deposits. Furthermore, it extends a long list of features common to all the SSH Zn–Pb deposits of the 'Carpentarian Zinc Belt' of northern Australia (McGoldrick, 1994) and reinforces arguments that these deposits can be grouped in a single genetic classification.

CONCLUSIONS

- Three different data sets for samples from Isamine and Hilton Mine indicate that the SSH Zn–Pb deposit alteration vectors ('Sedex Alteration Index', 'Alteration Index Mk 3' and 'MnO_D') developed for Lady Loretta and HYC can be applied to these giant deposits.
- Mine sequence samples (Scott and Taylor, 1979; McGoldrick, 1986) at Isamine indicate that unmineralised interore beds carry strongly anomalous AI and MnO_D signatures.
- The Hilton deposit appears to have a similar geochemical signature to the Isamine deposits.
- Thallium is elevated in the Isamine samples, and its unusual geochemical properties may make it an important mineralisation vector in siliciclastic dominated sequences.
- An older, poorer quality, data set (Smith and Walker, 1970) indicate that AI and MnO_D are elevated for hundreds of metres along strike from economic mineralisation.
- A deep 'stratigraphic' hole drilled about 5 kilometres south of Hilton Mine in the 1960s has AI and MnO_D values that suggest SSH Zn–Pb mineralisation may be present within a kilometre along strike.

REFERENCES

de Albuquerque, C. A. R., & Shaw, D. M. (1974). Thallium. In K. H. Wedepohl (Ed.), *Handbook of Geochemistry* Springer-Verlag.

Finlow-Bates, T., & Stumpfl, E. F. (1979). The copper and lead–zinc–silver orebodies of Mount Isa mine, Queensland: products of one hydrothermal system. *Annales de la Societe Geologique de Belgique*, 102, 497–517.

Forrestal, P. J. (1990). Mount Isa and Hilton silver-lead–zinc deposits. In F. E. Hughes (Ed.), *Geology of the Mineral Deposits of Australia and Papua New Guinea* (pp. 927–934). Melbourne: The Australasian Institute of Mining and Metallurgy.

Large, R. R. (1994). Case Studies. Application of Alteration Index to selected areas of the McArthur Basin. *CODES AMIRA/ ARC Project P384* — Proterozoic sediment-hosted base metal deposits Report No. 5, 23–40.

Large, R. R., & McGoldrick, P. J. (1993). Deposit Halos 5. Primary geochemical halos related to Proterozoic sediment hosted Pb–Zn deposits and applications to exploration. *CODES AMIRA/ARC Project P384* — Proterozoic sediment-hosted base metal deposits Report No. 3, 63–126.

Large, R. R., & McGoldrick, P. J. (1994). Refinement of the Sedex Alteration Index and MnOD vectors. *CODES AMIRA/ ARC Project P384* — Proterozoic sediment-hosted base metal deposits Report No. 5, 1–17.

Mathias, B. V., & Clark, G. J. (1975). The Mount Isa Copper and Silver–Lead–Zinc orebodies - Isa and Hilton mines. In C. L. Knight (Ed.), *Economic Geology of Australia and Papua New Guinea* (pp. 351–371). Australasian Institute of Mining and Metallurgy.

McGoldrick, P. J. (1986). *Volatile and precious metal geochemistry of the Mount Isa ores and their host rocks*. Unpub. PhD thesis, University of Melbourne.

Neudert, M. (1983). A depositional model for the Upper Mount Isa Group and implications for ore formation. In Ph. D., (pp. 324p).

Perkins, W. G. (1990). The Mount Isa Ag–Pb–Zn orebodies stratiform replacement lodes in a zoned hydrothermal system. *BMR Record*, 1990/95, 63–64.

Scott, K. M., & Taylor, G. F. (1979). Analyses of samples from DDHs P70E, V69E and M14E, Mount Isa Mines. *CSIRO Restricted Investigation Report*, 1021R, 12.

Smith, S. E., & Walker, K. R. (1970). *Mount Isa geochemical project - analyses of core samples* (Record No. 47). Bureau of Mineral Resources.

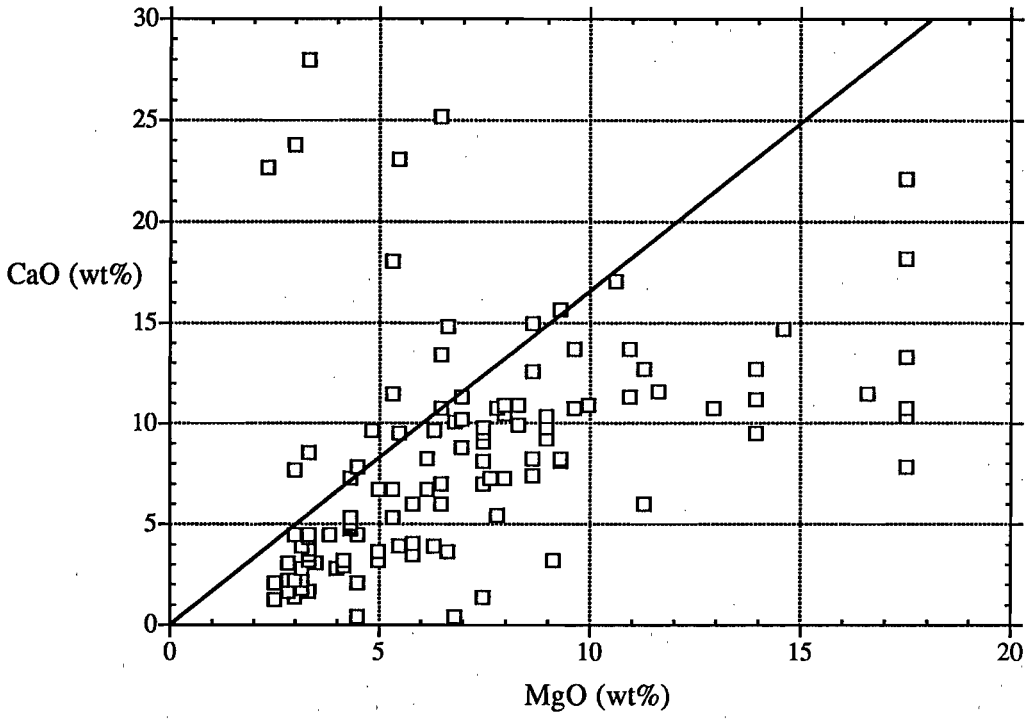

Figure 20—The CaO v MgO relationship for all samples from Quartzite No 1.

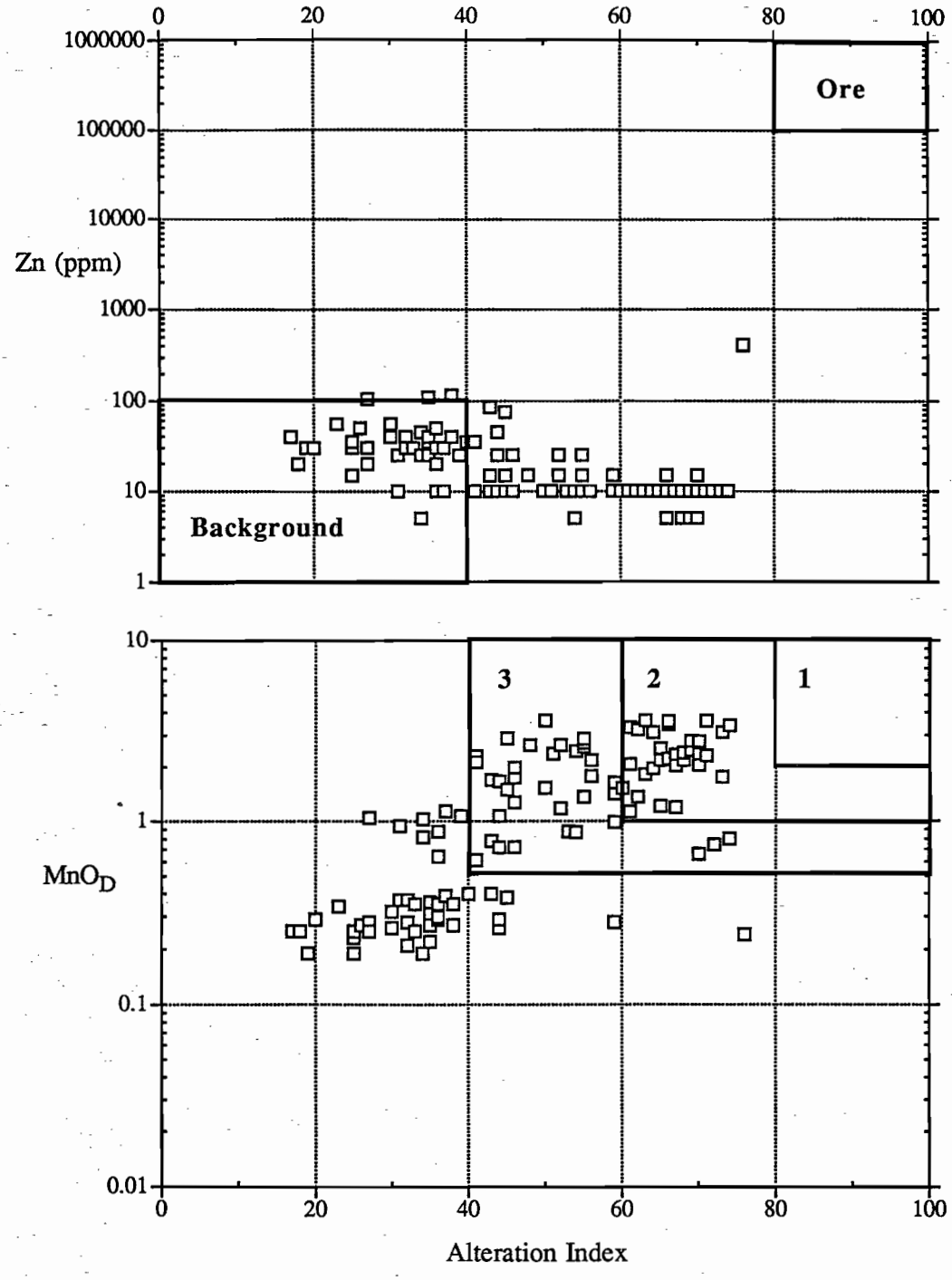

Figure 21—The AI v Zn and AI v MnO_D relationships for all samples from Quartzite No 1.

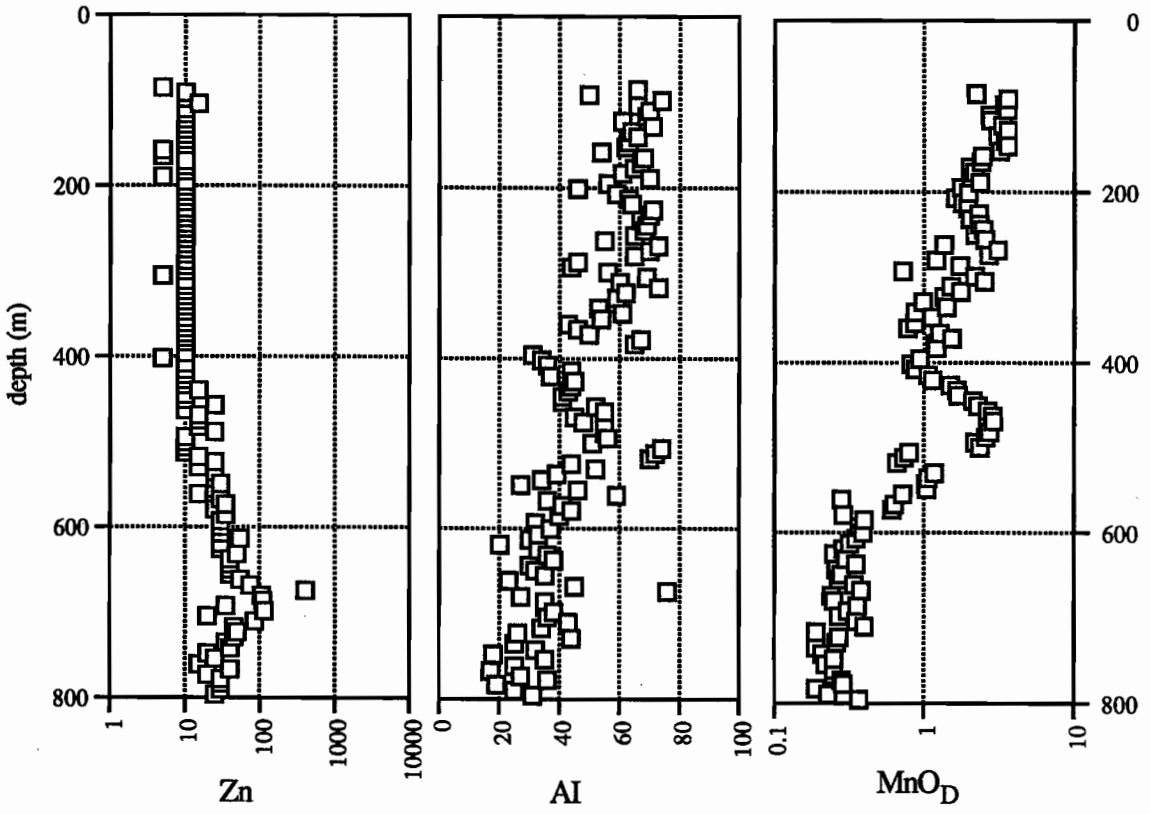

Figure 22—Down hole plots of Zn, Al and MnO_D for drill hole Quartzite No 1.

The geochemistry of 'barren' late Palaeoproterozoic sediments from the McNamara Group: background values for the 'SEDEX AI', 'AI Mk3' and MnO_D

Peter McGoldrick
Centre for Ore Deposit and Exploration

Summary

This preliminary report presents geochemical data for 43 samples collected from four stratigraphic drill holes through McNamara Group sediments in the Lawn Hill Platform/Riversleigh Fold Belt (McConachie et al., 1993). The geochemical vectors refined by (Large and McGoldrick, 1994) and Large (this volume) are calculated for these samples and the results are used to confirm 'background' values for these indices. This analysis supports intuitive arguments that these samples represent 'typical' compositions for unmineralised fine grained sediments in the McNamara Group.

Introduction

Fundamental to any lithogeochemical exploration techniques is the recognition of 'background' and 'anomalous' values for the elements or indices being used. With very large data sets rigorous statistical methods can be used to define these parameters. However, no large multi-element data sets suitable for this approach are available for Australian Palaeoproterozoic sediments. Furthermore, subtle lithological variations may have profound effects on sediment composition (e.g., Large, this volume). An alternative approach, suitable for dealing with small data sets, is to use simple 'exploratory data analysis' techniques (Tukey, 1977) to make a qualitative assessment of the distribution shape and the range of values in order to better define 'background', 'average' and 'anomalous' data.

Samples

Samples comprise a variety of fine grained lithologies and all were collected from drill core. The sampled cores are housed in the Geological Survey of Queensland (GSQ) core repository and are available for public inspection. Three (A83-1, A83-2, and A83-4) were drilled by Amoco as stratigraphic holes in the second year of a proposed four year petroleum exploration project that was terminated after two years (Dorrins et al., 1983). The other hole (GSQ LH 4) was drilled in late 1979 (Hutton, 1983). The locations of the four holes are shown on Figure 1. They provide a broad stratigraphic coverage of the McNamara Group (Fig. 2), with each of the holes largely confined to a single (different) formation. Hole A83-2 was collared near the top of the Lawn Hill Formation about 7 km west of Century and penetrated 361 m of this unit and 190 m of the underlying Termite Range Formation. Hole A83-1, 17 km southeast of Century

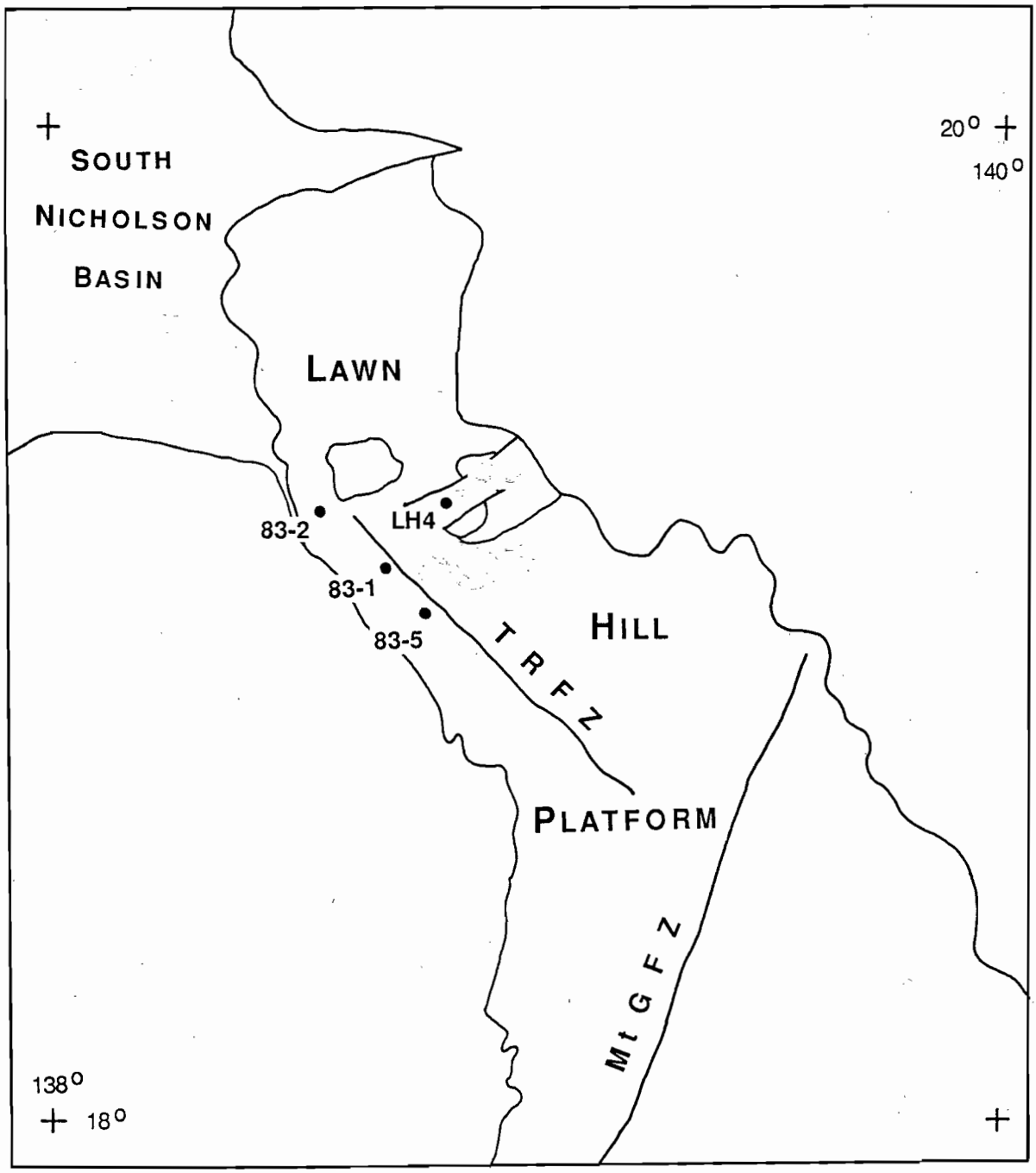

Figure 1—Map of the north west corner of the Mount Isa Basin showing the location of the drill holes referred to in the text (TRFZ = Termite Range Fault Zone, MtGFZ = Mount Gordon Fault Zone).

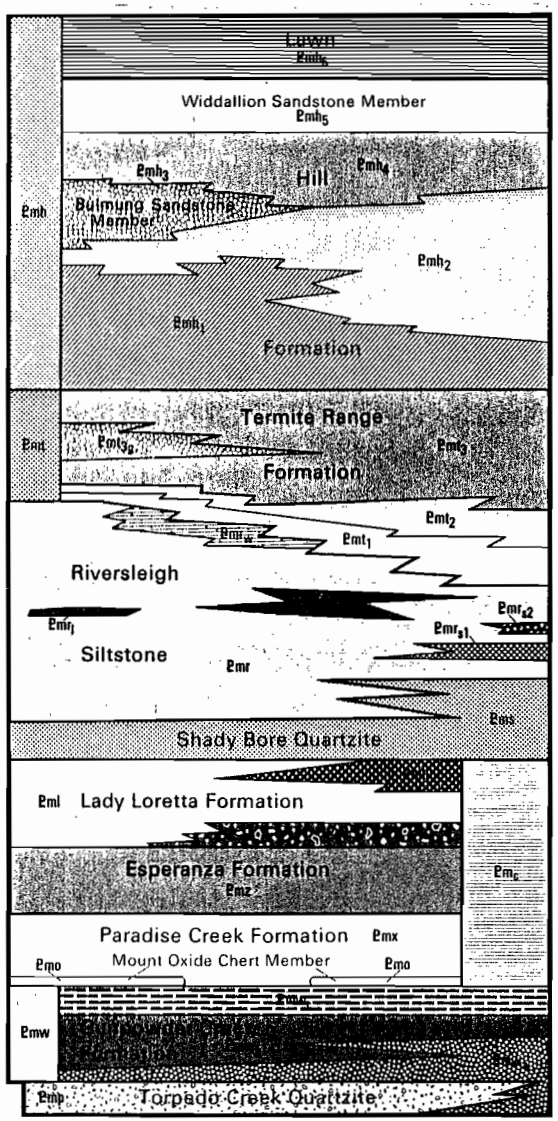

Emh	*Siltstone, shale, tuff, minor sandstone and dolomite*
Emh_6	*Brown and green shale and flaggy, thin-bedded siltstone and fine sandstone*
Emh_5	*Reddish-brown, flaggy to blocky, fine to medium ferruginous micaceous, feldspathic sandstone; brown to purple siltstone interbeds*
Emh_4	*Grey, fissile to flaggy siltstone and shale; tuffaceous siltstone and sandstone; flaggy tuff beds; minor dolomite*
Emh_3	*Flaggy to blocky, micaceous, lithic sandstone and conglomeratic sandstone, shale clasts common near base*
Emh_2	*Greenish-grey, fissile to flaggy tuff and tuffaceous siltstone, thinly interbedded siltstone, sandstone and shale*
Emh_1	*Grey to black, carbonaceous shale, flaggy siltstone interbeds and grey silty concretions; minor tuff*
Emt	*Interbedded sandstone, quartzwacke, greywacke, siltstone and shale*
Emt_3	*White to light brown and grey, thick bedded, fine to coarse, poorly sorted sandstone and lithic greywacke interbedded with laminated siltstone*
Emt_{3g}	*Dark grey, medium to thick-bedded, silicified quartzwacke interbedded with laminated siltstone and shale*
Emt_2	*Thin to medium-bedded, light brown clayey siltstone and ferruginous, fine to medium sandstone*
Emt_1	*Thick-bedded, poorly-sorted sandstone and quartzwacke interbedded with siltstone*
Emr	*Laminated and thin-bedded, fine to coarse quartz siltstone and shale; dolomitic and carbonaceous in places; thin sandstone interbeds*
Emr_w	*White, leached, clayey siltstone and shale*
Emr_{s3}	*Light grey, thin to thick-bedded, medium to coarse quartz sandstone with clayey matrix; strongly cross-bedded*
Emr_1	*Laminated quartz siltstone*
Emr_{s2}	*Thick-bedded, silicified, fine to medium dolomitic sandstone with siltstone interbeds*
Emr_{s1}	*Flaggy to blocky fine clayey sandstone with siltstone interbeds*
Ems	*White, flaggy to massive, medium orthoquartzite and fine sandstone; siltstone and dolomite interbeds*
Eml	*Thinly bedded to laminated intraclastic and stromatolitic dolomite; interbeds of dolomitic siltstone and fine sandstone*
Eml_1	*Basal blocky orthoquartzite overlain by flaggy, fine sandstone, siltstone and dolomite*
Eml_b	*Breccia of chert and altered siltstone cemented by limonite*
Em_c	*Deeply weathered rocks — some leached, porous beds, some silicified, some ferruginised*
Emz	*Stromatolitic chert, siltstone, sandstone, dolomite*
Emx	*Laminated and stromatolitic dolomite, dolomitic siltstone and sandstone; minor chert*
Emo	*Grey laminated chert*
Emw	*Sandstone, siltstone*
Emw_c	*Dolomite, dolomitic siltstone, oolitic dolomite, dolomitic sandstone, carbonaceous siltstone and fine sandstone*
Emw_b	*Ferruginous arkosic sandstone, minor conglomerate, siltstone, stromatolitic dolomite*
Emw_a	*Micaceous siltstone, pyritic carbonaceous shale, siltstone and sandstone; graded bedding common*
Emp	*Massive to blocky, medium sandstone; conglomeratic, particularly near base; malachite staining common*

Figure 2—Lithostratigraphic subdivision of the McNamara Group from the Lawn Hill Region 1:100,000 geological map.

drilled 77 metres in the base of the Termite Range Formation and a further 578 m into the Riversleigh Siltstone. Hole A83-5 was located 35 km southeast of Century and drilled 582 m all within Lady Loretta Formation. Both A83-1 and A83-5 were collared within a couple of kilometres of the Termite Range Fault. GSQ-LH4 was drilled on the western flank of the Kamarga Dome and cored 377 metres mainly in the Paradise Creek Formation.

A selection of samples were chosen for geochemical analysis with a view to covering some of the more typical grey-black, green and buff-red finer grained rock types. Because of the fine grain size no attempt was made to use thin section petrography to describe the samples, and for the purpose of this report a lithostratigraphic grouping of samples will be used.

Results

Preliminary XRF analyses for major and trace elements in 43 sedimentary rocks from the McNamara Group are presented in Table 1. Final data will include carbonate and organic carbon and will be made available to sponsors in digital format with the final report for project P384.

Vectors to mineralisation

Figure 3 displays the CaO and MgO relationship for all 43 McNamara Group Samples. The data indicate that the samples from the Lady Loretta Formation, Paradise Creek Formation are carbonate-rich lithologies. Samples from the Lawn

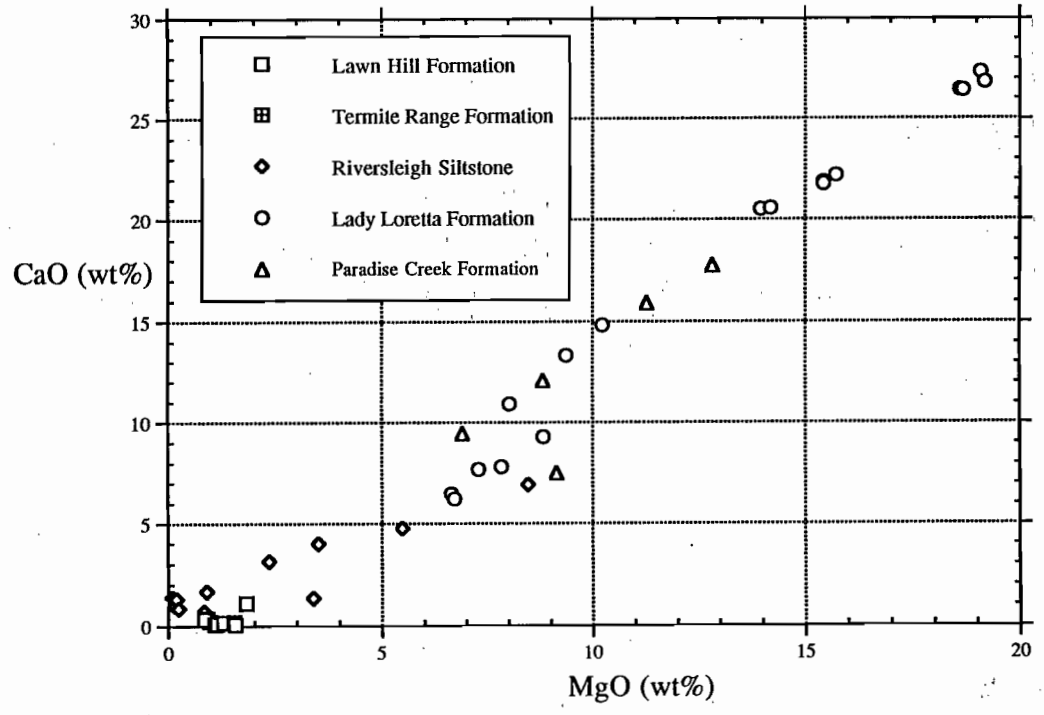

Figure 3 —CaO v MgO for 43 samples from the McNamara Group.

Hill Formation and the Termite Range Formation are siliciclastics, and, although some Riversleigh Siltstone samples are siliciclastic, a number contain significant amounts of carbonate. The CaO:MgO ratio for all the carbonate-bearing samples indicates that dolomite is the major carbonate phase.

Large and McGoldrick (1994) recommend samples with less than about one percent CaO should not been used for calculating the 'Sedex Alteration Index' (AI), 'Alteration Index Mark 3' (AI3), or MnOD. For this reason the Termite Range Formation samples and all but one of the Lawn Hill Formation samples have been excluded from the data set for calculating these indices.

Figure 4 displays the relationship between Zn and AI and between Zn and AI3. The Zn values are between about ten and a hundred parts per million, and all the Lady Loretta Formation and PCF samples have AI and AI3 values less than 40 and 30, respectively (the 'background' levels defined empirically by Large and McGoldrick (1993,1994) and Large (this volume)). In contrast, several of the Riversleigh Formation and the Lawn Hill Formation sample have quite high AI values, but their AI3 values are much less anomalous looking.

Figure 5 displays the relationship between MnO_D and AI and between MnO_D and AI3. As for Zn, when MnO_D is plotted against AI the Riversleigh Formation and TRF samples are quite anomalous and plot in the prospective fields of Large and McGoldrick (1994). In contrast, using the AI3 pushes all but one of these samples into the 'unprospective' part of the plot.

Discussion: The contrasting behaviour AI and AI3 for the Riversleigh Formation samples is explained by the fact that they contain less than 25% carbonate. Large (this volume) cautions that using the old AI for shales will generate spurious high values because the aluminosilicate component of the rock is not accounted for.

Because the sampled drill holes are remote from known mineralisation it can be argued intuitively that these samples have compositions which represent background. This is confirmed by the low AI3 and MnO_D for these samples and indicates that upper limits of 30 for AI3 and 0.5% for MnO_D are geologically reasonable for background values for these indices.

Conclusions

- Thirty samples of McNamara Group sediments from stratigraphic drill holes remote from known mineralisation provide a geochemical data set representing the 'background' compositions for late Palaeoproterozoic carbonate-bearing fine grained sedimentary rocks.
- AI and AI3 behave quite differently in dolomitic shales from the Riversleigh Siltstone, confirming conclusions of Large (this volume) that AI3 is a more suitable mineralisation vector in 'dirty' carbonates.
- Recommended background values of AI3 and MnOD are less than about 30 and 0.5%, respectively.

References

Dorrins, P. K., Humphreville, R. G., & Womer, M. B. (1983). Results of 1983 field program, Lawn Hill area, ATP 327P, Queensland. Department of Minerals and Energy, Qld. Open File, CR1248C.

Hutton, L. (1983). Stratigraphic drilling report — GSQ Lawn Hill 1-4. Queensland Government Mining Journal, 84, 228-240.

Large, R. R., & McGoldrick, P. J. (1994). Refinement of the Sedex Alteration Index and MnOD vectors. CODES AMIRA/ARC Project P384 — Proterozoic sediment-hosted base metal deposits Report No. 5, 1-17.

McConachie, B. A., Barlow, M. G., Dunster, J. N., Meaney, R. A., & Schaap, A. D. (1993). The Mount Isa Basin — definition, structure and petroleum geology. APEA Journal, 33, 237-257.

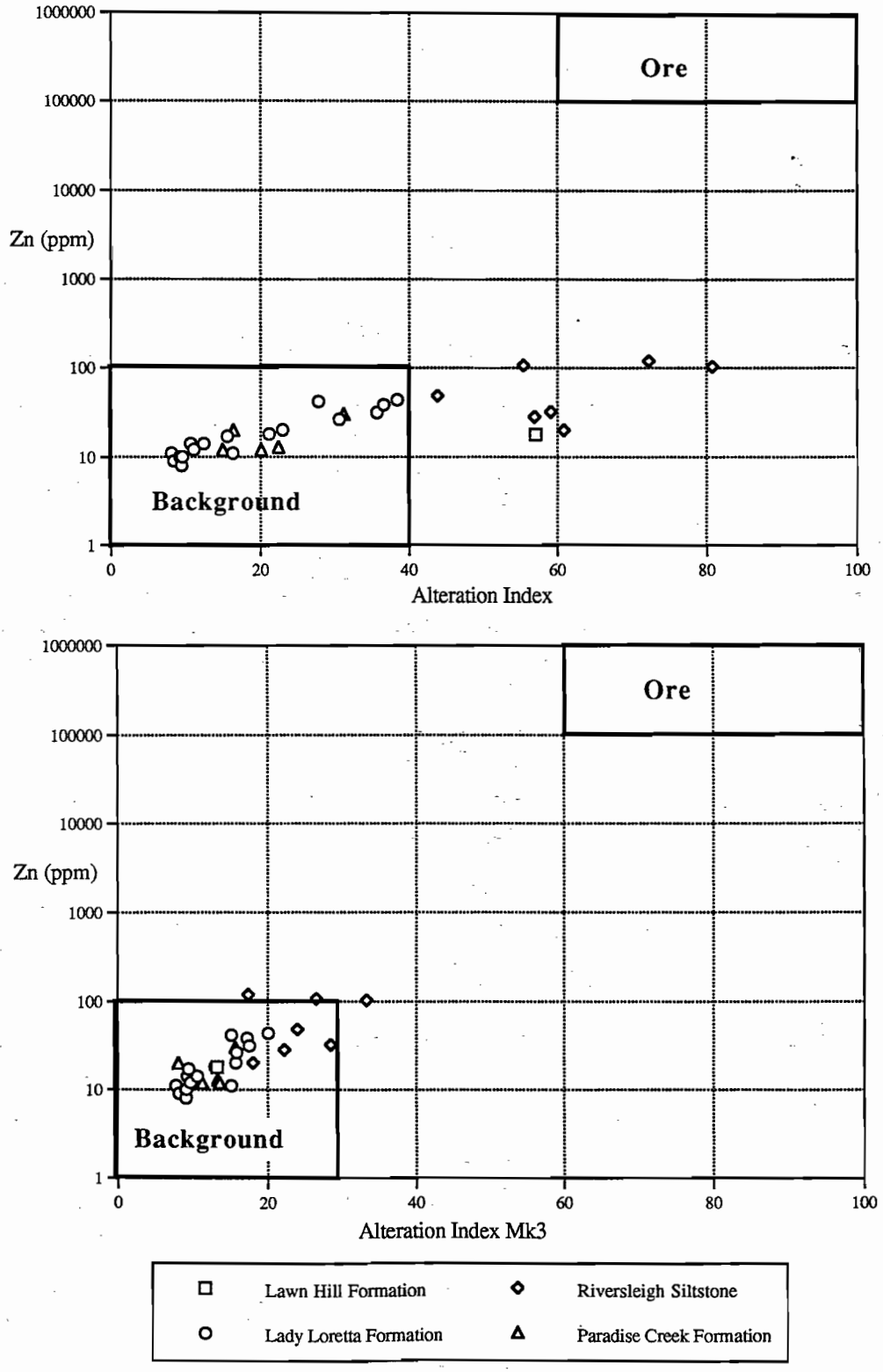

Figure 4—Zn v AI and Zn v AI3 for 30 samples from the McNamara Group.

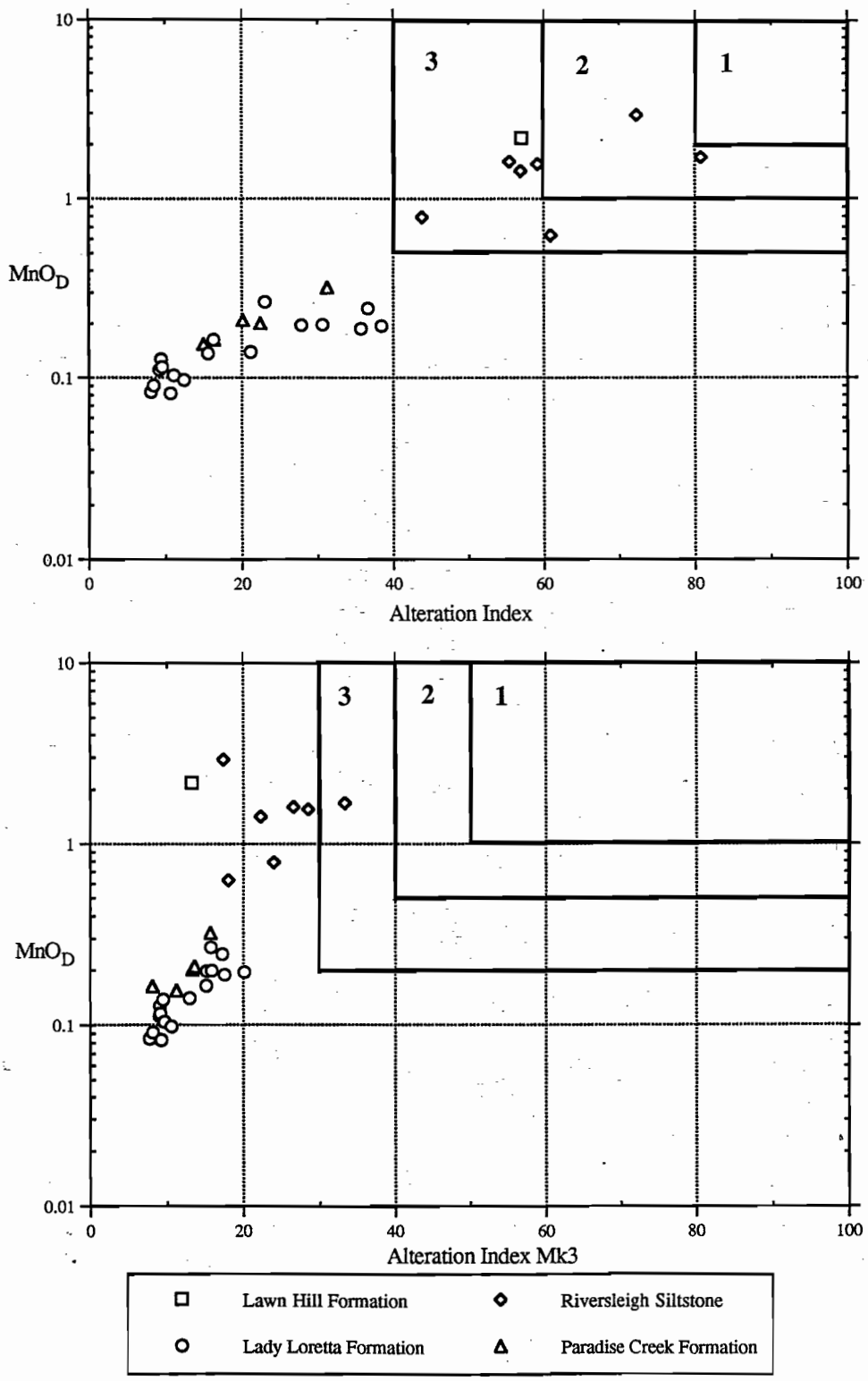

Figure 5—MnOD v AI and MnOD v AI3 for 30 samples from the McNamara Group.

Table 1. Major and trace element analyses of 43 McNamara Group sedimentary rocks.

Drill Hole	Depth		SiO2	TiO2	Al2O3	Fe2O3	MnO	MgO	CaO	Na2O	K2O	P2O5	Loss	Total	S
	metres		wt%	wt%	wt%	wt%	wt%	wt%	wt%	wt%	wt%	wt%	wt%	wt%	wt%
A83-1/9	484.5	Riversleigh Siltstone	58.48	0.32	11.60	3.35	0.29	4.75	5.49	1.28	3.69	0.12	11.58	101.55	0.22
A83-1/7	540.0	Riversleigh Siltstone	51.86	0.35	10.14	3.55	0.22	6.92	8.47	0.66	3.65	0.13	14.59	101.15	0.22
A83-1/6	561.6	Riversleigh Siltstone	64.88	0.26	10.52	4.43	0.18	4.00	3.51	1.45	3.40	0.12	6.93	99.68	
A83-1/1	634.8	Riversleigh Siltstone	76.20	0.17	8.08	1.52	0.07	1.33	3.39	1.89	2.93	0.09	4.34	100.01	0.21
A83-1/10	454.1	Riversleigh Siltstone	71.83	0.37	12.06	3.02	0.01	1.29	0.19	0.71	4.64	0.14	5.23	99.49	1.15
A83-1/14	406.7	Riversleigh Siltstone	60.80	0.44	12.36	7.24	0.05	1.67	0.90	1.04	3.70	0.43	10.56	99.19	4.58
A83-1/16	327.1	Riversleigh Siltstone	72.17	0.28	11.66	4.08	0.03	1.39	0.09	1.43	3.14	0.07	5.29	99.62	1.18
A83-1/17	295.9	Riversleigh Siltstone	74.11	0.29	11.16	2.86	0.03	0.84	0.24	1.88	3.44	0.10	4.48	99.43	1.36
A83-1/23	204.9	Riversleigh Siltstone	71.83	0.39	12.31	4.11	0.02	0.98	0.14	1.75	4.43	0.10	3.58	99.64	1.34
A83-1/26	110.7	Riversleigh Siltstone	82.06	0.18	7.74	1.08	0.08	0.68	0.83	2.55	2.22	0.06	2.21	99.69	0.39
A83-1/3	608.1	Riversleigh Siltstone	68.50	0.37	11.28	3.36	0.11	3.12	2.35	1.06	4.17	0.13	5.89	100.33	0.24
A83-1/34	61.4	Termite Range Formation	73.13	0.37	11.16	3.76	0.02	0.96	0.21	1.03	4.19	0.11	4.47	99.40	1.77
A83-1/37	17.1	Termite Range Formation	72.05	0.32	13.75	2.57	0.01	1.39	0.15	0.06	4.88	0.10	4.60	99.88	0.41
A83-2/10	416.1	Termite Range Formation	77.11	0.32	11.25	1.29	0.02	0.90	0.35	0.29	4.23	0.09	4.09	99.94	0.21
A83-2/27	319.0	Lawn Hill Formation	65.28	0.56	14.43	4.52	0.02	1.52	0.19	0.09	4.18	0.13	9.28	100.20	1.17
A83-2/39	153.6	Lawn Hill Formation	78.62	0.18	10.00	1.21	0.02	0.84	0.32	0.31	4.90	0.06	3.31	99.77	
A83-2/40	133.2	Lawn Hill Formation	70.86	0.29	14.11	1.80	0.08	1.82	1.11	0.04	4.65	0.05	5.17	99.98	
A83-2/41	85.6	Lawn Hill Formation	73.03	0.24	13.67	1.79	0.16	1.08	0.09	0.02	4.36	0.06	5.57	100.07	
A83-2/44	30.3	Lawn Hill Formation	77.16	0.29	12.61	1.20	0.01	1.09	0.07	0.05	4.12	0.05	3.34	99.99	0.03
A83-2/50	26.3	Lawn Hill Formation	84.29	0.29	7.38	2.86	0.02	1.13	0.08	0.05	2.93	0.04	2.44	101.53	
A83-2/42	84.8	Lawn Hill Formation	78.05	0.15	9.10	4.47	0.14	1.55	0.07	0.06	2.49	0.04	3.87	99.99	
A83-2/33	199.0	Lawn Hill Formation	79.43	0.38	9.72	2.72	0.02	1.28	0.16	0.07	3.49	0.07	3.32	101.31	0.23
A83-5/1	494.2	Lady Loretta Formation	21.97	0.12	2.99	1.65	0.07	15.44	21.84	0.10	1.94	0.04	34.11	100.27	0.02
A83-5/15	26.8	Lady Loretta Formation	40.11	0.21	6.14	1.95	0.13	10.23	14.81	0.10	3.28	0.20	23.57	100.72	0.22
A83-5/17	72.2	Lady Loretta Formation	53.51	0.34	9.74	3.01	0.05	7.29	7.68	0.05	4.24	0.10	14.13	100.13	0.21
A83-5/22	256.9	Lady Loretta Formation	30.28	0.06	1.22	1.79	0.11	13.97	20.51	0.07	0.81	0.01	31.69	100.52	
A83-5/25	395.0	Lady Loretta Formation	10.15	0.04	0.93	1.07	0.10	18.60	26.42	<0.03	0.57	0.01	41.21	99.10	0.06
A83-5/33	395.2	Lady Loretta Formation	8.51	0.01	0.32	1.03	0.10	19.09	27.32	<0.03	0.23	0.00	42.35	98.96	0.09
A83-5/38	420.0	Lady Loretta Formation	48.19	0.39	11.54	4.87	0.05	7.84	7.80	0.13	4.92	0.10	14.52	100.34	0.03
A83-5/40	428.4	Lady Loretta Formation	47.38	0.37	10.20	3.11	0.06	8.83	9.27	0.08	4.41	0.10	16.45	100.25	0.01
A83-5/41	439.2	Lady Loretta Formation	53.98	0.42	11.92	3.76	0.05	6.73	6.21	0.10	5.02	0.10	12.10	100.38	0.01
A83-5/48	496.0	Lady Loretta Formation	22.46	0.11	2.54	1.41	0.06	15.72	22.17	0.12	1.86	0.03	34.38	100.86	0.03
A83-5/49	529.1	Lady Loretta Formation	43.12	0.31	7.08	1.25	0.06	9.38	13.32	0.08	4.74	0.10	21.11	100.55	0.01
A83-5/16	59.5	Lady Loretta Formation	27.60	0.08	2.25	1.18	0.07	14.20	20.56	0.26	1.38	0.15	31.96	99.69	
A83-5/24A	398.5	Lady Loretta Formation	50.91	0.24	6.47	1.84	0.05	8.03	10.90	0.19	3.46	0.09	17.76	99.93	
A83-5/24B	398.5	Lady Loretta Formation	56.56	0.39	10.65	3.65	0.04	6.65	6.47	0.17	4.12	0.10	12.28	101.08	
A83-5/36	407.7	Lady Loretta Formation	9.35	0.04	0.67	0.93	0.11	18.67	26.39	0.34	0.49	0.05	41.28	98.32	
A83-5/54	538.4	Lady Loretta Formation	25.69	0.03	0.68	0.84	0.06	15.44	21.74	0.26	0.52	0.04	34.17	99.48	
A83-5/56	548.0	Lady Loretta Formation	8.45	0.02	0.60	1.07	0.08	19.18	26.80	0.33	0.41	0.05	42.06	99.06	
LH4-16	217.6	Paradise Creek Formation	34.95	0.24	6.76	1.93	0.11	11.28	15.90	0.09	3.52	0.07	25.35	100.19	0.18
LH4-24	300.4	Paradise Creek Formation	31.58	0.19	4.93	1.50	0.09	12.83	17.73	0.09	2.83	0.05	28.02	99.84	0.17
LH4-30	368.8	Paradise Creek Formation	49.29	0.40	11.16	1.54	0.04	9.14	7.49	0.05	7.09	0.11	13.17	99.48	0.37
LH4-34	437.9	Paradise Creek Formation	49.31	0.36	9.96	2.37	0.10	6.91	9.46	0.11	6.86	0.17	15.01	100.61	0.00
LH4-36	432.5	Paradise Creek Formation	44.22	0.29	7.76	1.94	0.08	8.82	12.06	0.10	4.94	0.09	19.63	99.93	0.49

Drill Hole	Depth		S	Sb	Ba	Sr	Cr	V	Zr	Y	U	Rb	Th	Pb	Tl	Br	As	Zn	Cu	Ni	Mo
	metres		wt%	ppm	ppm	ppm	ppm	ppm	ppm	ppm	ppm	ppm	ppm	ppm	ppm	ppm	ppm	ppm	ppm	ppm	ppm
A83-1/9	484.5	Riversleigh Siltstone	0.22	3	421	38	17	25	252	38	4	161	18	17	1	1	15	106	7	11	
A83-1/7	540	Riversleigh Siltstone	0.22	1	429	67	29	46	138	24	3	181	13	13	1	2	6	48	10	11	
A83-1/6	561.6	Riversleigh Siltstone		1	664	35	14	26	193	25	4	138	14	11	1	1	3	32	3	10	
A83-1/1	634.8	Riversleigh Siltstone	0.21	<2	518	48	8	10	196		2.4	102	10.4	65	<1		7	20	8	7	3.1
A83-1/10	454.1	Riversleigh Siltstone	1.15	<2	558	28	41	47	275		4.8	217	15.7	17	2.2		11	27	9	12	2.7
A83-1/14	406.7	Riversleigh Siltstone	4.58	<2	444	33	43	56	219		6	198	14.7	44	3.7		49	103	18	23	4.2
A83-1/16	327.1	Riversleigh Siltstone	1.18	<2	480	36	18	22	272		4.2	143	13.5	17	2.1		16	25	8	12	1.6
A83-1/17	295.9	Riversleigh Siltstone	1.36	<2	602	43	23	31	257		4.4	154	14.3	20	1.8		14	26	10	13	3.4
A83-1/23	204.9	Riversleigh Siltstone	1.34	<2	700	50	34	37	249		3.4	175	12.6	25	1.6		10	21	13	13	2.6
A83-1/26	110.7	Riversleigh Siltstone	0.39	<2	602	46	14	9	340		2.3	66	7.7	19	<1		<4	119	25	4	1.8
A83-1/3	608.1	Riversleigh Siltstone	0.24	<2	535	23	26	36	198		3.8	177	15.3	10	1		5	28	4	10	1.5
A83-1/34	61.4	Termite Range Formation	1.77	<2	620	41	36	38	276		3.8	169	12.2	29	1.5		16	30	12	18	2.4
A83-1/37	17.1	Termite Range Formation	0.41	<2	538	31	23	26	266		4.7	197	19	18	1.3		5	28	9	11	1.1
A83-2/10	416.1	Termite Range Formation	0.21	<2	501	41	33	34	209		4.3	185	14.9	13	<1		5	14	7	11	1.1
A83-2/27	319	Lawn Hill Formation	1.17	2.3	365	45	62	88	235		7.5	204	18	18	1.5		9	26	22	31	9.1
A83-2/39	153.6	Lawn Hill Formation		<2	1096	25	2	5	160		4.4	163	15.4	3	1.7		<4	19	2	4	<1
A83-2/40	133.2	Lawn Hill Formation		<2	267	27	5	11	262		5.7	208	24.1	3	<1		<4	18	7	5	<1
A83-2/41	85.6	Lawn Hill Formation		<2	303	21	2	6	232		5.7	183	22.8	5	1.1		<4	26	1	6	1.5
A83-2/44	30.3	Lawn Hill Formation	0.03	<2	242	15	7	11	266		4.5	179	21.6	5	<1		<4	14	1	4	<1
A83-2/50	26.3	Lawn Hill Formation		2	358	22	9	13	418	32	5	112	13	6	<1	1	3	18	1	5	
A83-2/42	84.8	Lawn Hill Formation		1	195	13	2	5	147	33	4	94	14	2	<1	<1	4	233	5	5	
A83-2/33	199	Lawn Hill Formation	0.23	2	450	37	41	65	137	43	4	163	9	8	1	1	6	152	7	16	
A83-5/1	494.2	Lady Loretta Formation	0.02	<2	879	48	17	19	62		1.7	42	4.4	<1.5	1.2		<4	14	1	6	<1
A83-5/15	26.8	Lady Loretta Formation	0.22	<2	205	25	28	36	70		2.4	94	6.2	9	<1		4	20	10	9	1.1
A83-5/17	72.2	Lady Loretta Formation	0.21	<2	241	35	43	53	176		3.1	182	10.6	4	<1		<4	26	4	14	<1
A83-5/22	256.9	Lady Loretta Formation		<2	41	39	6	12	13		0.7	16	1.6	<1.5	<1		<4	11	3	3	<1
A83-5/25	395	Lady Loretta Formation	0.06	<2	1811	72	7	8	15		1.2	14	1.1	<1.5	<1		<4	10	7	2	<1
A83-5/33	395.2	Lady Loretta Formation	0.09	<2	3380	129	2	3	5		1.2	4	<1	<1.5	<1		<4	10	5	1	<1
A83-5/38	420	Lady Loretta Formation	0.03	<2	1212	68	54	60	116		3.4	214	11.6	4	<1		<4	43	3	17	<1
A83-5/40	428.4	Lady Loretta Formation	0.01	<2	445	43	49	57	107		3.1	174	11.5	4	<1		<4	41	3	16	<1
A83-5/41	439.2	Lady Loretta Formation	0.01	<2	334	33	55	60	164		3.7	216	12.9	5	<1		<4	38	2	16	<1
A83-5/48	496	Lady Loretta Formation	0.03	<2	57	40	14	16	43		1.4	35	3.8	3	<1		<4	14	1	4	1.1
A83-5/49	529.1	Lady Loretta Formation	0.01	<2	193	38	37	33	171		3.3	101	10.7	3	<1		<4	17	3	8	<1
A83-5/16	59.5	Lady Loretta Formation		<2	110	43	14	17	35	7	2	34	3	1	1	2	<4	12	0	4	
A83-5/24A	398.5	Lady Loretta Formation		<2	219	38	28	27	145	18	3	112	9	6	1	2	1	18	3	10	
A83-5/24B	398.5	Lady Loretta Formation		2	215	29	45	52	157	22	4	178	13	6	1	2	3	31	4	20	
A83-5/36	407.7	Lady Loretta Formation		<2	29	55	6	9	37	10	2	10	0	0	<1	2	2	8	1	2	
A83-5/54	538.4	Lady Loretta Formation		<2	15	41	7	7	13	2	2	8	1	6	1	2	4	11	2	4	
A83-5/56	548	Lady Loretta Formation		<2	18	47	5	8	12	4	1	7	0	5	<1	3	4	9	1	2	
LH4-16	217.6	Paradise Creek Formation	0.18	<2	737	53	31	38	104		2.9	77	7.3	6	<1		<4	12	6	6	<1
LH4-24	300.4	Paradise Creek Formation	0.17	<2	797	57	24	28	66		1.7	60	5.4	5	<1		<4	12	5	6	<1
LH4-30	368.8	Paradise Creek Formation	0.37	<2	1410	34	55	57	126		5.6	194	11.2	10	<1		<4	20	8	14	<1
LH4-34	437.9	Paradise Creek Formation	0.00	<2	425	39	44	51	124		3.5	169	11.5	28	<1		15	30	12	18	<1
LH4-36	432.5	Paradise Creek Formation	0.49	<2	404	45	36	38	113		4.7	107	8.9	13	<1		4	13	10	9	1.5

Conditions of formation for siderite and barite from sedimentary brines — implications for the formation of sediment-hosted base metal deposits

David R. Cooke
Centre for Ore Deposit and Exploration Studies

Introduction

This report presents results of the continuing study into controls on siderite deposition from low-moderate temperature hydrothermal fluids. Some brief comments on siderite deposition from low temperature (50°C) brines are provided prior to a discussion of the relationships between barite, siderite and metalliferous brines. The report concludes with a discussion of preliminary chemical models for sediment-hosted base metal deposits.

Summary of Previous Work

The initial report in this series (Cooke et al., 1994) discussed siderite and ferroan carbonate deposition from 150° and 250°C brines. The major conclusions from that study were:

- Siderite and ferroan carbonate are stabilised by high ΣC and low ΣS concentrations in hydrothermal solutions. Lower temperatures will stabilise siderite at constant $a_{(CO2\ aq)}$. CO_2 concentrations are probably the dominant control on carbonate formation.
- Aqueous carbon and sulfur species are involved in reactions between siderite and other Fe-sulfide and oxide minerals. This allows the formation of two distinct domains (oxidised and reduced) for ferroan carbonates in $f_{(O2)}$-pH space
- Ferroan carbonates that form under relatively oxidised to oxidised conditions in association with pyrite or hematite are favoured by lower temperatures and/or high ΣS concentrations, and have the potential to be associated with base metal-rich solutions
- Ferroan carbonates precipitated from reduced solutions are more likely to form at higher temperatures and/or low ΣS concentrations, and will be associated with base metal-deficient but possibly precious metal-rich solutions
- Detailed petrographic and electron microprobe studies are required to establish the paragenetic relationships between pyrite, base metal sulfides, dolomite and siderite at Lady Loretta, Century and other siderite-bearing SHMS deposits. If siderite and base metal mineralisation are synchronous, then depths of formation (either in a replacement or sedimentary-exhalative setting) must have been at least several hundred metres below the surface/palaeowater table.

Siderite deposition from 50°C brines

Figure 1 is a log $f_{(O2)}$-pH diagram that portrays the stability fields of pure siderite, the common Fe-O-S minerals (hematite, magnetite, pyrite, pyrrhotite), the predominance boundaries between oxidised and reduced sulfur species, and oxidised and reduced carbon species, and Ba^{+2} solubility contours at 100 and 1000 ppm. This diagram and the following diagrams have been constructed for 10 eq. wt. % NaCl solutions that contain 0.001 molal ΣS, 0.256 molal ΣC (≈ 1 wt. % $CO_{2\,(aq)}$), 1 wt. % $CaCl_2$ and 36 ppm Mg; the same conditions assumed for the hypothetical fluids used by Cooke (1993A and B) for numerical simulations of mineral deposition from sedimentary brines. The dolomite field is overlain on Figure 1 for reference purposes.

Low temperature surface or near-surface waters are not capable of dissolving large amounts of $CO_{2\,aq)}$, because confining pressures are too low. Modern ocean water contains ≈ 0.01 wt. % $CO_{2\,(aq)}$, which (in conjunction with low Fe/Ca and Fe/Mg ratios) prevents siderite from forming as a sedimentary carbonate in most marine environments (eg. Blatt et al., 1980). In siderite-bearing marine shales and ironstones, siderite is stabilised because the primary Fe-bearing minerals precipitated were FeS or $Fe(OH)_3$, rather than pyrite or hematite (Fig. 2; Maynard, 1983). In lacustrine settings (eg. freshwater lakes or swamps) and freshwater deltas, low ΣS contents and high Fe/Ca and Fe/Mg ratios stabilise siderite over pyrite, calcite and dolomite (Maynard, 1983). In contrast, siderite can form in hydrothermal environments when CO_2 concentrations and Fe/Ca ratios are high (eg. the periphery of the Broadlands geothermal system; Simmons and Christenson, 1994).

Figure 1 illustrates that at 50°C and $CO_{2\,(aq)}$ concentrations of 1 wt. %, siderite is significantly more stable than at higher temperatures (compare with Cooke et al., 1994), occupying a position in log $f_{(O2)}$-pH space between the pyrite and hematite stability fields. However, significant $CO_{2\,(aq)}$ cannot be dissolved in seawater at low pressures, because CO_2 effervescence will occur.

High CO_2-low temperature fluids could be generated during late diagenesis. Late diagenetic carbonate cements in sandstones are commonly Fe- and Mg-rich (Bjørlykke, 1981). As suggested in Cooke et al. (1994), it may be that in the Proterozoic sediment-hosted base metal deposits, siderite represents a low temperature, late diagenetic overprint on sulfide mineralisation, with the abundant pre-existing iron sulfides providing a local source of Fe that helped to stabilise siderite over dolomite. A late diagenetic origin would help to explain the distribution of siderite at Lady Loretta (in the footwall and hangingwall of the orebody).

Barite solubilities in sedimentary brines

Equation 1.1 illustrates how barite solubilities are controlled by pH, oxygen fugacity and ΣS concentrations:

$$Ba^{+2}{}_{(aq)} + H_2S{}_{(aq)} + 2\,O_{2\,(g)} \;<=>\; BaSO_{4\,(s)} + 2\,H^{+}{}_{(aq)} \qquad (1.1)$$

Oxygen fugacity provides the strongest control on barite solubilities, as shown by the near-horizontal Ba solubility contours at 50°, 150° and 250°C (Figures 1, 3 and 4). Large quantities of Ba^{+2} can be transported under reduced (pyrite-, magnetite- or pyrrhotite-stable) conditions, and barite deposition occurs when the reduced fluids are oxidised (eg. exhalation of VHMS-style fluids into sulfate-bearing seawater). In contrast, Ba^{+2} is insoluble under oxidised (hematite-stable) conditions — no significant Ba^{+2} transport or barite deposition can occur from oxidised fluids.

Figure 5 illustrates the range of temperatures and salinities determined from fluid inclusions in the Selwyn Basin and MVT style Pb-Zn deposits. The Selwyn basin deposits form at temperatures around 250°C from fluids that contain ≈ 10 eq. wt. % NaCl. Because the Selwyn basin deposits contain abundant barite, the mineralising fluids must be

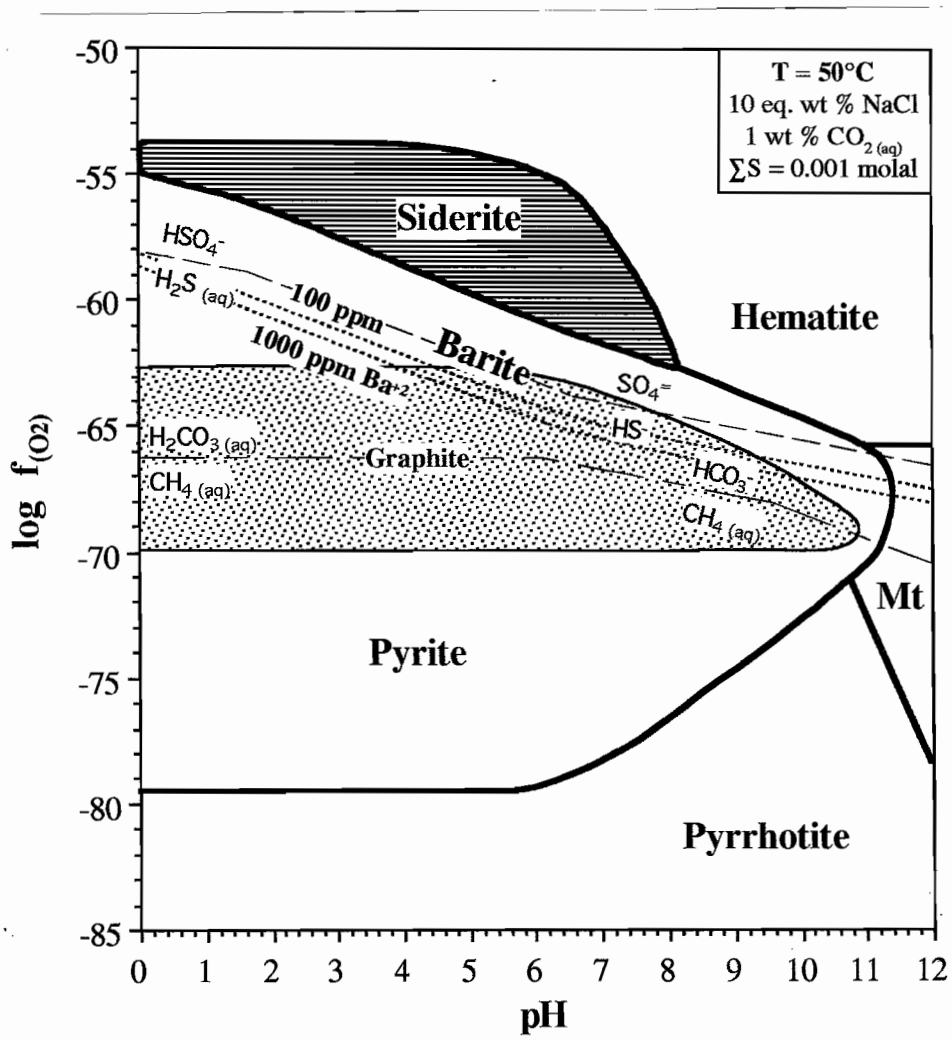

Figure 1 - Log f_{O2}-pH diagram showing the stability fields of siderite, graphite, the common Fe-O-S minerals (hematite, magnetite, pyrite, pyrrhotite), solubility contours for barite at 100 and 1000 ppm Ba^{+2}, and the predominance boundaries between oxidised and reduced sulfur species, and oxidised and reduced carbon species at 50°C. This diagram and Figures 3, 4 and 6 have been constructed for 10 eq. wt. % NaCl solutions that contain 0.001 molal ΣS, 0.256 molal ΣC (≈ 1 wt. % $CO_{2\,(aq)}$), 1 wt % $CaCl_2$ and 36 ppm Mg^{+2}, (the same conditions assumed for the hypothetical fluids used by Cooke (1993A, B) for numerical simulations of mineral deposition from sedimentary brines.

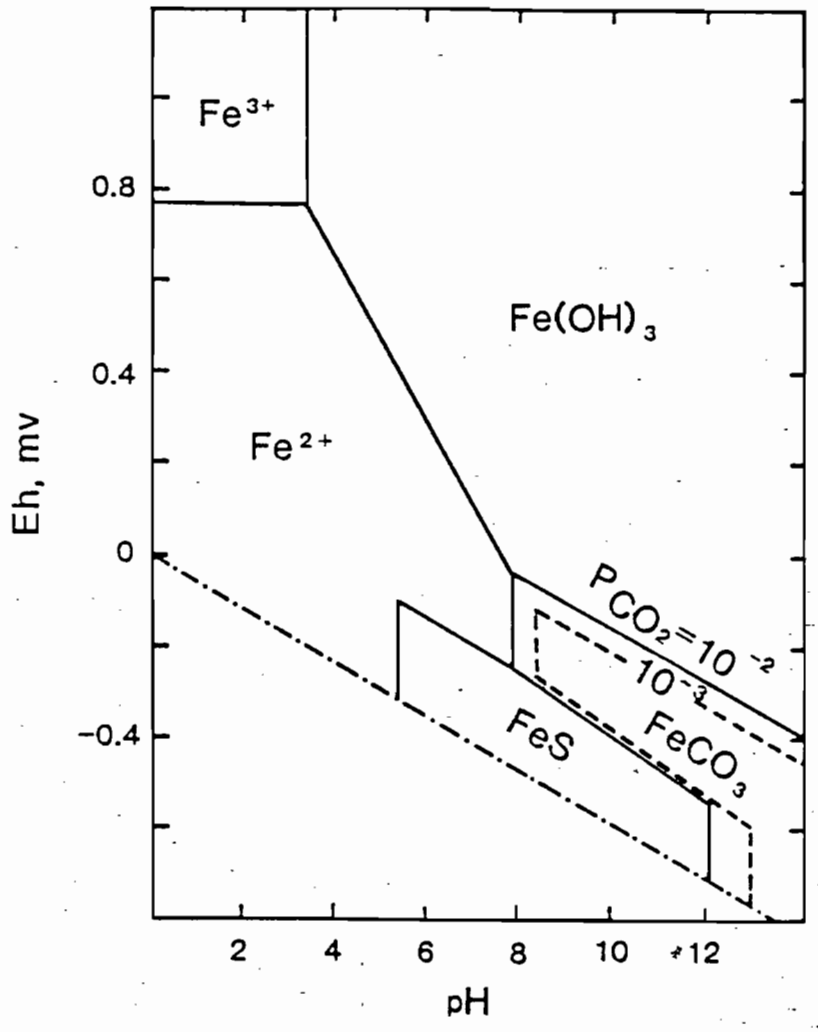

Figure 2 - Eh-pH diagram for some common phases in ironstone deposits. Siderite is a stable phase under normal seawater conditions ($\Sigma S = 10^{-2.2}$) if $Fe(OH)_3$ and FeS are used instead of hematite and pyrite (from Maynard, 1983).

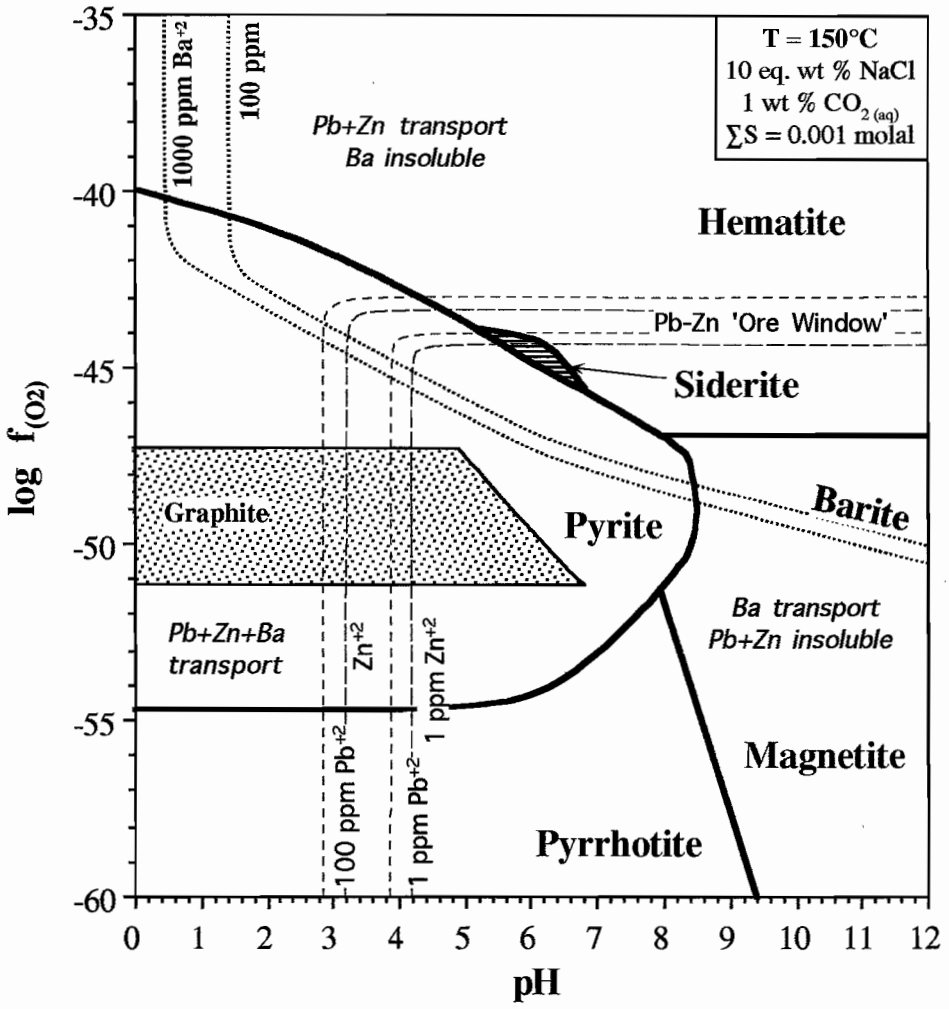

Figure 3 - Log f_{O2}-pH diagram at 150°C showing the stability fields of siderite, graphite, the common Fe-O-S minerals (hematite, magnetite, pyrite, pyrrhotite), solubility contours for barite at 100 and 1000 ppm Ba^{+2}, and solubility contours for galena and sphalerite at 100 and 1 ppm Pb^{+2} and Zn^{+2} respectively. See Figure 1 for the parameters used to construct this diagram.

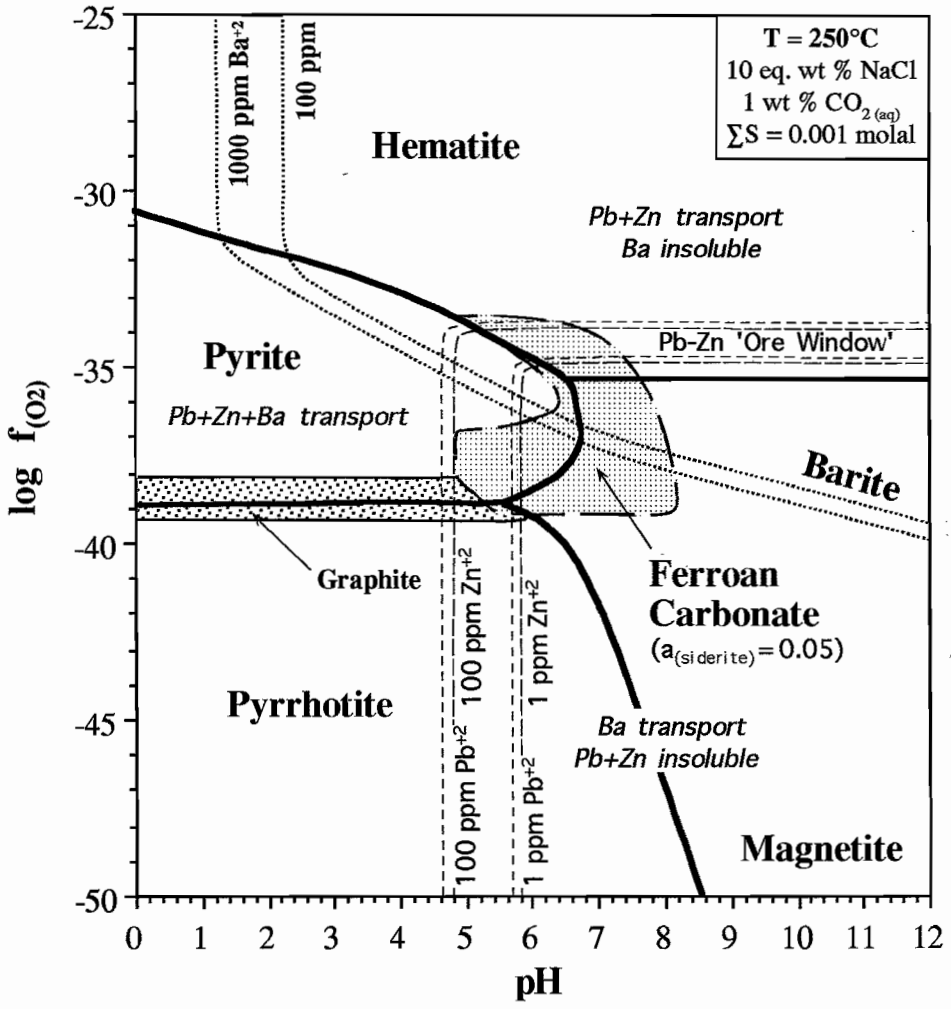

Figure 4 - Log fO2-pH diagram at 250°C showing the stability fields of ferroan carbonate (a_{sid} = 0.05), graphite, the common Fe-O-S minerals (hematite, magnetite, pyrite, pyrrhotite), solubility contours for barite at 100 and 1000 ppm Ba^{+2}, and solubility contours for galena and sphalerite at 100 and 1 ppm Pb^{+2} and Zn^{+2} respectively. See Figure 1 for the parameters used to construct this diagram. Siderite is not stable under the conditions portrayed; higher CO_2 concentrations are required at 250°C to stabilise siderite..

reduced and acidic to accommodate Pb, Zn and Ba transport (Fig. 4). The Selwyn basin is dominated by siliciclastics, and the presence of sericite, clays, pyrite and graphite in the sediments would help to buffer the fluids to reduced, moderately acidic conditions during metal transport.

With the exception of Lady Loretta, the Proterozoic sediment-hosted Pb-Zn-Ag deposits of Northern Australia are devoid of barite. The sedimentary environments are dominated by carbonates, evaporites, hematitic sandstones and red shales. Reduced lithologies are minor, with the most significant examples (eg. HYC pyritic shale member) occurring at the trap site for Pb-Zn mineralisation. The lack of barite suggests that the Northern Australian deposits formed from fluids that were too oxidised to carry significant Ba^{+2}.

Pb and Zn solubilities at 150°C and 250°C

At high salinities, Pb and Zn will be transported by chloride species, and the total Pb and Zn in solution will be determined by the concentrations of the individual Pb and Zn chloride species:

$$\Sigma Pb\ (molal) = m(PbCl^+) + m(PbCl_2^0) + m(PbCl_3^-) + m(PbCl_4^{=}) \quad (1.2)$$

$$\Sigma Zn\ (molal) = m(ZnCl^+) + m(ZnCl_2^0) + m(ZnCl_3^-) + m(ZnCl_4^{=}) \quad (1.3)$$

In reduced fluids (dominated by $H_2S \pm HS^-$), pH, temperature and salinity are the dominant controls on galena and sphalerite solubilities:

$$PbCl_4^{=}{}_{(aq)} + H_2S_{(aq)} \Leftrightarrow PbS_{(s)} + 2\,H^+_{(aq)} + 4\,Cl^-_{(aq)} \quad (1.4)$$

$$ZnCl_2^0{}_{(aq)} + H_2S_{(aq)} \Leftrightarrow ZnS_{(s)} + 2\,H^+_{(aq)} + 2\,Cl^-_{(aq)} \quad (1.5)$$

The strong pH controls are illustrated by the vertical contours for Pb and Zn on Figures 3 and 4. Note that galena and sphalerite solubilities are independent of oxygen fugacity in reduced fluids. Pb-Zn deposition from reduced fluids will be driven by pH increase, temperature decrease, increased ΣS concentrations and/or dilution. Reduction will not be important.

In oxidised fluids (dominated by $SO_4^{=} \pm HSO_4^-$), galena and sphalerite solubilities are independent of pH. Instead, oxygen fugacity, temperature and salinity are the dominant controls on galena and sphalerite solubilities:

$$PbCl_3^-{}_{(aq)} + SO_4^{=}{}_{(aq)} \Leftrightarrow PbS_{(s)} + 2\,O_{2\,(g)} + 3\,Cl^-_{(aq)} \quad (1.6)$$

$$ZnCl^+_{(aq)} + SO_4^{=}{}_{(aq)} \Leftrightarrow ZnS_{(s)} + 2\,O_{2\,(g)} + Cl^-_{(aq)} \quad (1.7)$$

The strong controls of oxygen fugacity on Pb-Zn solubilities in oxidised brines are illustrated by the horizontal solubility contours on Figures 3 and 4. Pb-Zn deposition from oxidised brines will be driven by reduction, temperature decrease, increased ΣS concentrations and/or dilution.

Figure 4 shows that at 250°C, 10 wt % reduced fluids are capable of carrying significant base metals (1 - 100 ppm) at weakly acidic (muscovite-stable) pH values (pH ≈ 4.6 - 5.8). However, when the temperature decreases to 150°C, reduced 10 wt. % fluids must be highly acidic (pH ≈ 2.8 - 4.2) to carry significant Pb and Zn. Higher salinities (> 15 eq. wt % NaCl) are required to carry Pb and Zn at lower temperatures in reduced fluids (eg. the fields for Silvermines and MVT deposits on Fig. 5).

Discussion: Preliminary chemical models for sediment-hosted base metal deposits

Figure 6 illustrates possible fluid evolution pathways for the northern Australian and Selwyn Basin-style sediment-hosted base metal deposits. The diagram is drawn at 150°C, which is too low for the Selwyn Basin deposits, but the general

trajectory for Selwyn-Basin fluid evolution (A-B) will be the same.

Three important regions can be defined on Figure 6 with respect to Pb, Zn and Ba transport. Fluids in region 1 are reduced, acidic and can carry large quantities of Pb, Zn and Ba. Fluids in region 2 are oxidised, and can carry significant Pb and Zn, but essentially no barite. Fluids in region 3 are reduced and alkaline; they can carry significant Ba but no Pb and Zn.

The fluids responsible for the Pb-Zn-Ba deposits of the Selwyn Basin must be derived from region 1 of Figure 6. In an exhalative model, galena and sphalerite deposition would occur in response to temperature decrease, dilution, pH increase and/or increasing m(H_2S) during mixing with anoxic seawater. Barite deposition would occur in response to progressive oxidation during mixing with seawater. Note that these acidic fluids would dissolve any carbonate they came in contact with. ***Fluids in region 1 cannot be transported significant distances through carbonate-dominated sedimentary basins.***

The absence of barite, and the abundance of carbonates, evaporites and hematitic sandstones suggest that most Proterozoic Pb-Zn deposits of northern Australia are formed from fluids with compositions in region 2 of Figure 6. Pb-Zn deposition occurs primarily in response to reduction, temperature decrease and possibly dilution or increasing m(H2S) at the trap site. The fluids are in equilibrium with carbonates, and can be in equilibrium with K-feldspar (i.e weakly acidic to alkaline), which is consistent with the presence of adularia at HYC. In this model, siderite could form during Pb-Zn deposition at temperatures around 150°C, provided CO_2 concentrations were high enough and water depths were sufficient to prevent boiling (depths > 250-500 m at 150°C and 1 wt % CO_2; Cooke et al., 1994).

Region 3 (Fig. 6) will not be important for the formation of sediment-hosted Pb-Zn deposits. These reduced, alkaline fluids could generate sediment-hosted barite deposits that contain no significant Pb or Zn (eg. the shale-hosted barite deposits of Arkansas; Maynard, 1991), and may be responsible for anomalous barite occurrences in the McArthur Basin and elsewhere.

It appears that the type of sedimentary basin strongly controls the chemistry of the mineralising fluids, and therefore the character of the Pb-Zn deposit. Sediment-hosted Pb-Zn deposits that form in basins dominated by siliciclastics (Selwyn-type) will be generated by fluids from region 1 of Figure 6 (reduced, acidic) and will show a strong association with barite. In contrast, those deposits that form in carbonate ± evaporite-dominated basins (McArthur-type) are likely to form from fluids in region 2 of Figure 6. The fluids would be oxidised, in equilibrium with carbonate, Ba-deficient and could potentially generate siderite at the trap site.

In addition to fluid chemistry and basinal setting, depositional processes can be fundamentally different for McArthur-type and Selwyn-type sediment hosted Pb-Zn deposits. While temperature decrease will be an important depositional process in both deposit types, reduction will only be significant in McArthur-type deposits, and pH increase will only be important in Selwyn-type deposits.

Further work is planned for this study. In particular, Fe, Mn, and possibly Cu, Ag and/or Au solubility contours will be added to the diagrams presented in the current report to address the problems of Fe transport, Mn anomalies, and to fully explain the metallogenic associations of sediment-hosted Pb-Zn deposits.

References

Blatt, H., Middleton, G., and Murray, R., 1980. Origin of sedimentary rocks. Prentice Hall, New Jersey. 780 p.

Bjørlykke, K., 1981. Diagenetic reactions in sandstones. in A. Parker and B.W. Sellwood (editors) - Sediment diagenesis. D. Reidel Pub. Co., NATO ASI Series C: v. 115, p. 169-213.

Cooke, D.R., 1993A. Transport and deposition of base metals from high temperature (250°C) sedimentary brines. AMIRA/ARC Project P384, report No. 4 (unpub.), 111-130.

Cooke, D.R., 1993B. Transport and deposition of base metals from low temperature (150°C) sedimentary brines. AMIRA/ARC Project P384, report No. 4 (unpub.), 131-139.

Cooke, D.R., Large, R.R., and McGoldrick, P.J., 1994. Progress report: Conditions of formation for siderite and ferroan

carbonate - implications for the formation of sediment-hosted base metal deposits. AMIRA/ARC Project P384, report No. 5 (unpub.), 55-64.

Maynard, J.B., 1983. Geochemistry of sedimentary ore deposits. Springer-Verlag, New York. 305 p.

Maynard, J.B., 1991. Shale-hosted deposits of Pb, Zn and Ba: syngenetic deposition from exhaled brines in deep marine basins. in E.R. Force, J. Eidel and J.B. Maynard (Editors) - Sedimentary and diagenetic mineral deposits: a basin analysis approach to exploration. Rev. Econ. Geol. 5; 177-185.

Sangster, D.F., 1993. Evidence for, and implications of, a genetic relationship between MVT and SEDEX Zinc-Lead deposits. World Zinc '93 symposium, Hobart. p. 85-94.

Simmons, S.F., and Christenson, B.W., 1994. Origins of calcite in a boiling geothermal system. Am. J. Sci., 294, p. 361-400.

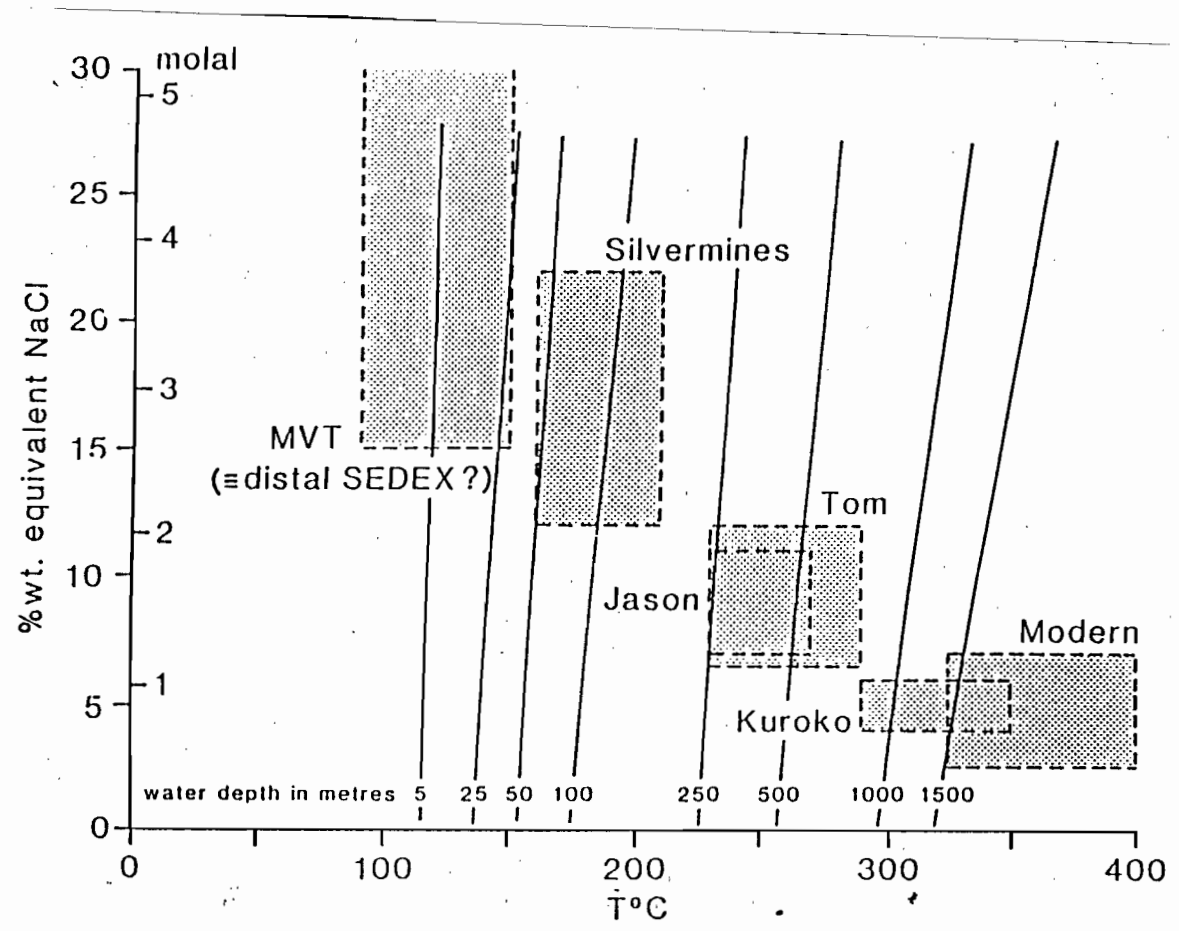

Figure 5 - Relationships between hydrothermal fluids of various temperature-salinity values and minimum water depth required to prevent boiling. Silvermines, Tom and Jason are proximal SEDEX deposits; 'modern' refers to black smoker vents on spreading seafloor ridges (from Sangster, 1993).

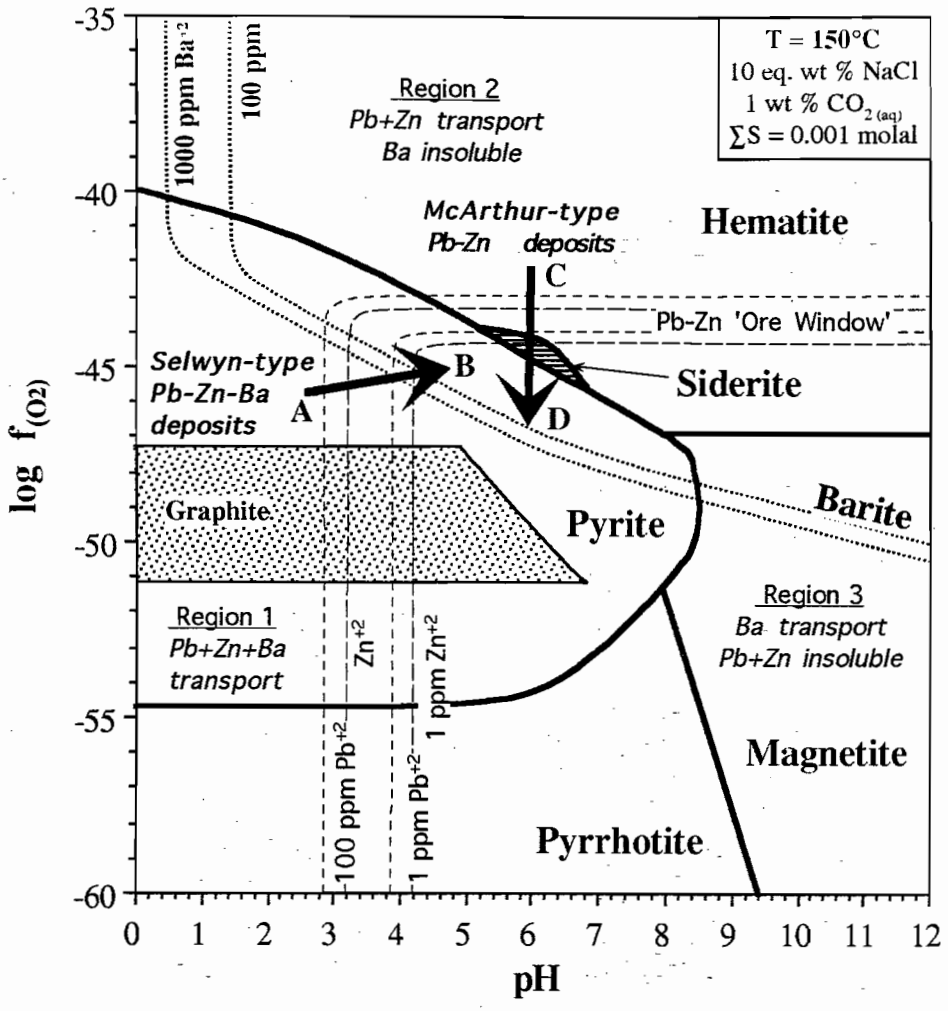

Figure 6 - Log f_{O2}-pH diagram at 150°C. See Figure 1 for the parameters used to .construct this diagram. Selwyn-type sediment hosted Pb-Zn-Ba deposits form from reduced, acidic fluids (region 1) that can carry significant Pb, Zn and Ba. Pb and Zn deposition occurs in response to T decrease, pH increase (A-B), dilution and/or increasing m(H_2S). Barite deposition occurs in response to oxidation during mixing with seawater (A-B). McArthur-type sediment hosted Pb-Zn deposits form from oxidised, carbonate-stable fluids (region 2) that can carry significant Pb and Zn but are Ba-deficient. Pb and Zn deposition occurs in response to T decrease, reduction (C-D), dilution and/or increasing m(H_2S). Barite-only deposition occurs in region 3, when reduced, alkaline Ba-rich, Pb-Zn-deficient fluids are oxidised by mixing with seawater or reaction with evaporites.

Appendix

APPLICATION OF MAGNETICS TO BASIN STRUCTURES

D.E. Leaman
Leaman Geophysics, GPO Box 320, Hobart, Tasmania, Australia 7001

The following paper has been submitted to the EAEG for publication in Geophysical Prospecting. It is included in this AMIRA report for the general information of participants since it does quantify and illustrate many of the issues exposed and analysed during the McArthur Basin interpretations.

It, with two previous documents of this type ("Do volcanic piles exist?" and "Criteria for interpretation of potential fields") explains why and how the interpretations can be made, and accepted, with some assurance even though many details should be refined.

The application of magnetic data to basin problems has been restricted by the general assumption that most responses are related to local included volcanics or basement sources. This paper shows that these assumptions need to be reviewed, or accepted with care. It may well be that much can be learnt about the architecture of the basin and its contents.

ABSTRACT

Although magnetic surveys and basic interpretation methods have been used in basin studies for several decades the data have generally been underutilised. The formations of a relatively undeformed basin appear similar to sub horizontal tabular sources which are known to generate negligible anomalies. It can be shown, however, that very small angular deviations from tabularity, or horizontality, will generate very large responses at basin scale. The response is largely independent of source contrast, thickness, dip, or the orientation of either the source or the field. The result is definitive in terms of source shape and is very sensitive to small changes in dip differentials between upper and lower surfaces of the source. Basin anomalies must be reviewed with basin scale perspective and not as isolated elements.

Classical rift sequence forms may account for many of the anomalies observed and no presumption of basement sources is justified generally.

INTRODUCTION

Magnetic surveys of basins or proposed exploration areas is virtually standard practice. The resultant maps and profiles are normally used as mapping aids or for clues to regional structure, and then gradients or discrete anomalies are appraised. The surveys may be used to guide or orient seismic surveys although many surveys are undertaken out of sequence and cannot fulfill this role. More detailed surveys may suggest structural texture within the basin, or its basement, and perhaps

define areas with shallow volcanics which may be seismically misleading.

Most interpretation presently undertaken is simple, or semi-automatic, and based on various gradient-based rules or methods to estimate magnetic source depths which are usually assigned to basement. The methods used are variations or developments of those described by Grant & West (1965) or Vacquier *et al* (1951).

This approach assumes that the content of the basin is non magnetic, that the basement rocks possess substantial contrasts and depth ranges, and are essentially prismatic sources, and that there is negligible interference between sources or responses. It also assumes that all gradients are generated as a simple function of source depth or edges.

This paper examines the form of units within a basin, their likely magnetic response and then offers some salutory cautions about the assumptions which have been almost universally adopted in commercial practice.

BASIN FORMS

Formations within a typical basin may display various wedge or sheet forms. This paper considers forms typical of large basins which may be defined as those in which the horizontal extent is at least an order of magnitude greater than its maximum depth. The North Sea Basin (Europe), the Bass, Sydney and McArthur Basins (Australia) and the Great South Basin (New Zealand) represent examples of relatively undeformed large scale basins of various ages. Each of these basins contains several phases of deposition, narrow onset rifting, rapid spreading rifting, and several sag stages. Volcanic rocks may be present at the rift style conversions stage or late in the sag stages. Massive volcanism, where present, is usually preserved in the deep rift foci.

The rift conversions phase, often several tens of millions of years into the evolution of the basin, is the most significant in terms of rate of deposition and erosion, depositional variation, concurrent block rotation, local loss of sequence and differential subsidence and uplift.

All units below the sag onset tend to be wedge shaped and the wedges may be pinched to onlaps or be fault bounded. Typical fault blocks may range from one to 40 km across and several units may approach continuity at the later stages of rotation as the depressions are filled and sedimentation overlaps crestal hinges due to subsidence.

Units within the sag cover sequences are essentially tabular. All are widespread and relatively thin in proportion to lateral extent. Such formations may thicken slightly toward the basin axis and may taper to fine onlaps marginally.

Dips, as observed today, in the rotated rift blocks may locally exceed 35 degrees but 15 degrees is common in many basins. A differential of more than 1 degree may exist between upper and lower surfaces of thick units due to differential erosion or rotation during or after deposition. This angular variation may also apply to volcanic members of the sequence, whether present in the form of extrusive piles, associated pyroclastics, formations of volcanic provenance derived from primary members, or large intrusives. These rocks simply become part of the sequence. However, most such units will present magnetic contrasts with the normal sedimentary formations of the basin and some will be intensely magnetised.

Within the sag or cover sequences dips will be much less and any differential between upper and lower surfaces of the much thinner units will be very subtle. Such units approach tabularity and surfaces are almost parallel. Volcanic units within the cover sequences, the only magnetic rocks likely, often mark a tectonic event, possible uplift, erosion and exposure. The volcanics preserved at such an horizon, once perhaps part of a large flood event, tend to be patchy, thin, variable in properties due to alteration or weathering, but generally tabular in basin terms.

Basin studies must consider several possible source forms if magnetic analysis is to be applied.

1. Patchy, perhaps weathered, irregular and

generally thin piles may occur at one or two shallow horizons.

2. Relatively thin, essentially tabular bodies may occur at any depth within the basin depending on the part of the basin reviewed.
3. Isolated thick and narrow (perhaps <5 to 10 km wide) wedge and slab forms which reflect regional erosion and a lower surface rift controls.
4. Isolated wedges which may be very thick and extend for tens of kilometres.
5. Semi-continuous wedge and slab forms where upper surfaces may overlap rift hinges.

These styles are suggested in Figure 1 either as a general style or as examples from various basins.

THE TABULAR RESPONSE

The well known tabular, or horizontal slab, response is shown in Figure 2. This consists of two end anomalies and a negligible variation over the body itself. This null magnetic effect is quite unlike the gravitational effect of such a source shape and the combination of the two methods can resolve any ultimate ambiguity.

The figure shows that the near null effect extends for up to 80% of the length of the source and may actually be zero if the body length exceeds ten times the top depth or thickness. Where the body is shorter the proportions begin to approach prism, rather than slab, shape.

Figure 2 also shows that any variation in thickness modifies only the amplitude of the end effects.

All calculations and diagrams presented in this paper are based on a field vector specified by an amplitude of 50000 nT, an inclination of –45 degrees and a declination of 5 degrees. Unless otherwise stated all profiles have been oriented south to north and assume a sensor elevation of 150 m. None of the conclusions is affected by any change in the vector or source orientation although some detailed variation will occur. Use of northern hemisphere vectors will invert the calculated profiles. No other change is involved. This is illustrated by the E-W calculation shown for body C. The end anomalies are modified but the overall effect remains zero. The calculations have also assumed a consistent source magnetisation of 0.005 cgs (0.065 SI) for purposes of comparison but variation in the actual contrast is not relevant to this discussion.

Figure 3 illustrates the effect of dip on the tabular response. Each diagram has a very large vertical exaggeration and the dips are very small. Regardless of dip the effect remains near zero but may vary slightly depending on orientation of the source and the sense of dip (see body C). Spikes or marked changes are confined to the ends of the body but dip introduces asymmetry; the amplitude of the spike, its peak gradients, and exact form being a function of orientation (field or source). The effect of change in thickness is as shown in Figure 2.

Faulting of the slab (Figure 4), so common in basins at all levels. does not lead to any basic change in form; the end peaks reflect only the depth or dip of the source and the general effect remains near zero — except in the region of the fault. Changes in depth affects the magnitude of the end spikes only.

Various response patterns may be induced by faulting and the figure illustrates only the effect of depth on the response where the displacement is less than slab thickness. All responses are, however, comparable since the disrupted site is marked by a modified end effect and no other variation can be observed unless the slab is of limited length in proportion to the displacement (see Figure 2).

The tabular response patterns suggest that we should expect to see many limited, but subtle, long wavelength anomalies across a basin where relatively thin magnetic sources are present. There could be many semi-continuous spike or end-style anomalies where units are disrupted by faulting or terminated by erosion.

At no stage would it be possible to predict the

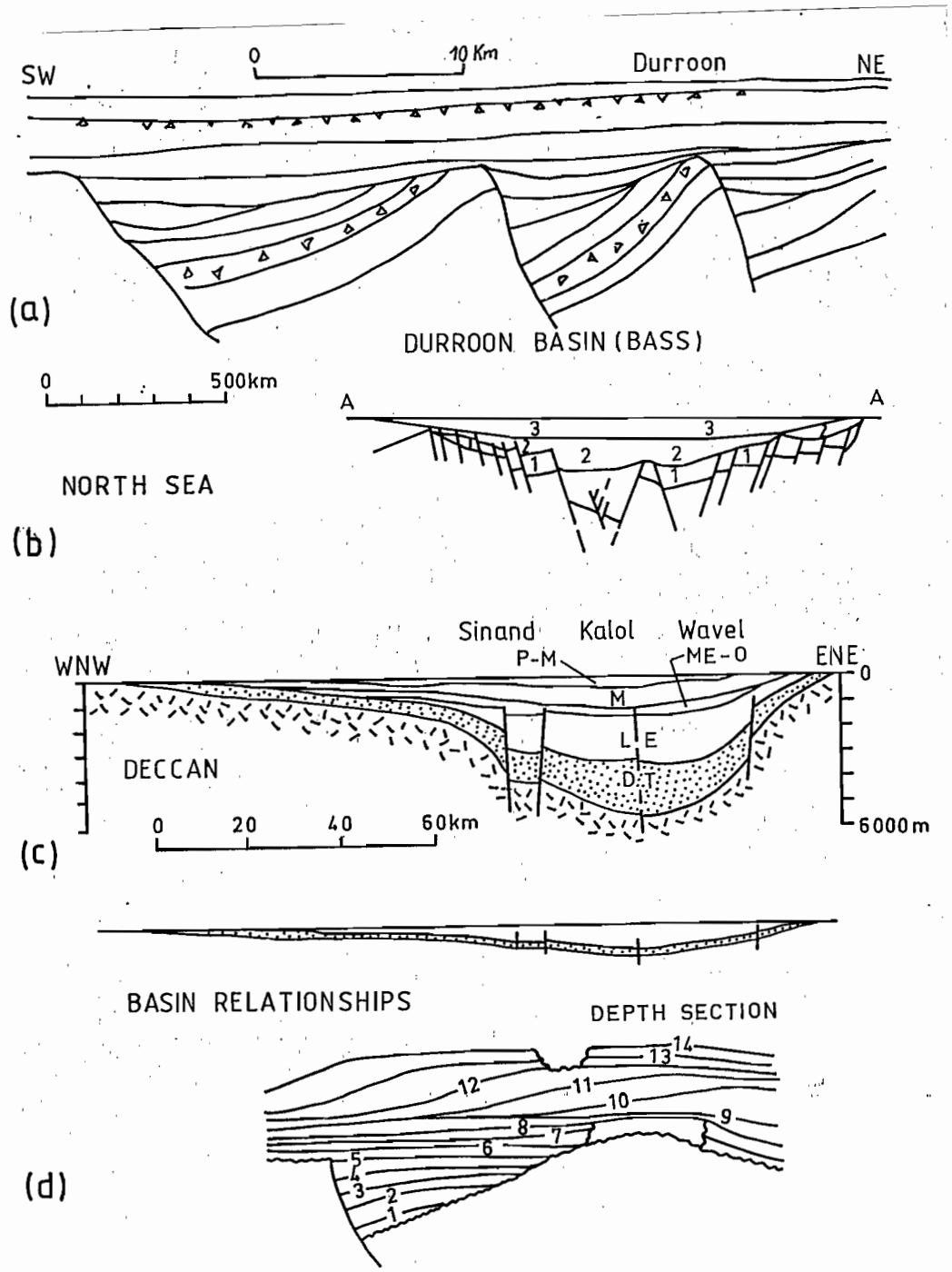

FIGURE 1. Examples of typical basin forms. (a) based on seismic section from Boobyalla sub basin of Bass Basin, Australia with volcanics present in two sequences, (b) across Viking Graben, North Sea Basin with some deep volcanics, (c) Deccan Trap structure, India, (d) illustration of general relationships between units within basins. Volcanics may be present at various stages, usually 1, 2 and 13; 3, 4, 13; 1–2, or 13/14. Each basin, or part of a basin, may display different patterns.

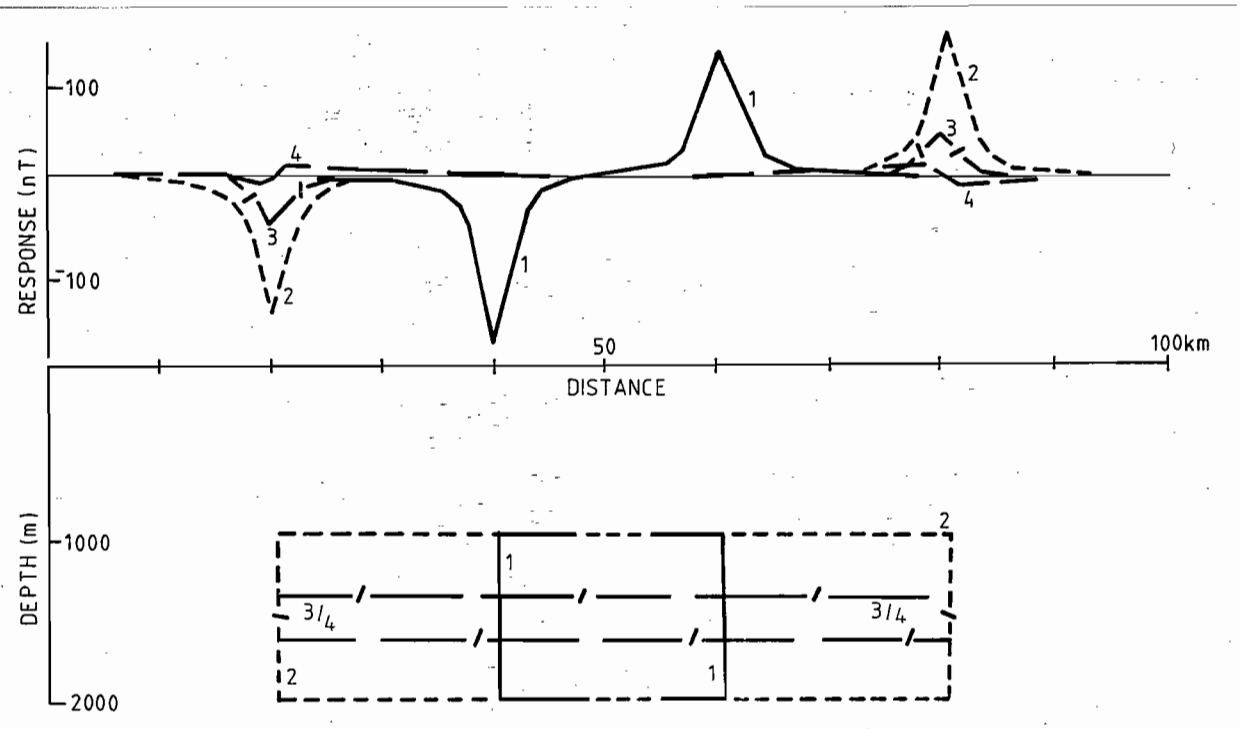

FIGURE 2. Typical responses from horizontal slabs where surfaces are parallel and thickness is a small fraction of length. Profiles 1–3 are oriented N–S, 4, E–W. All sources have a magnetisation of 0.005 cgs (0.065 SI).

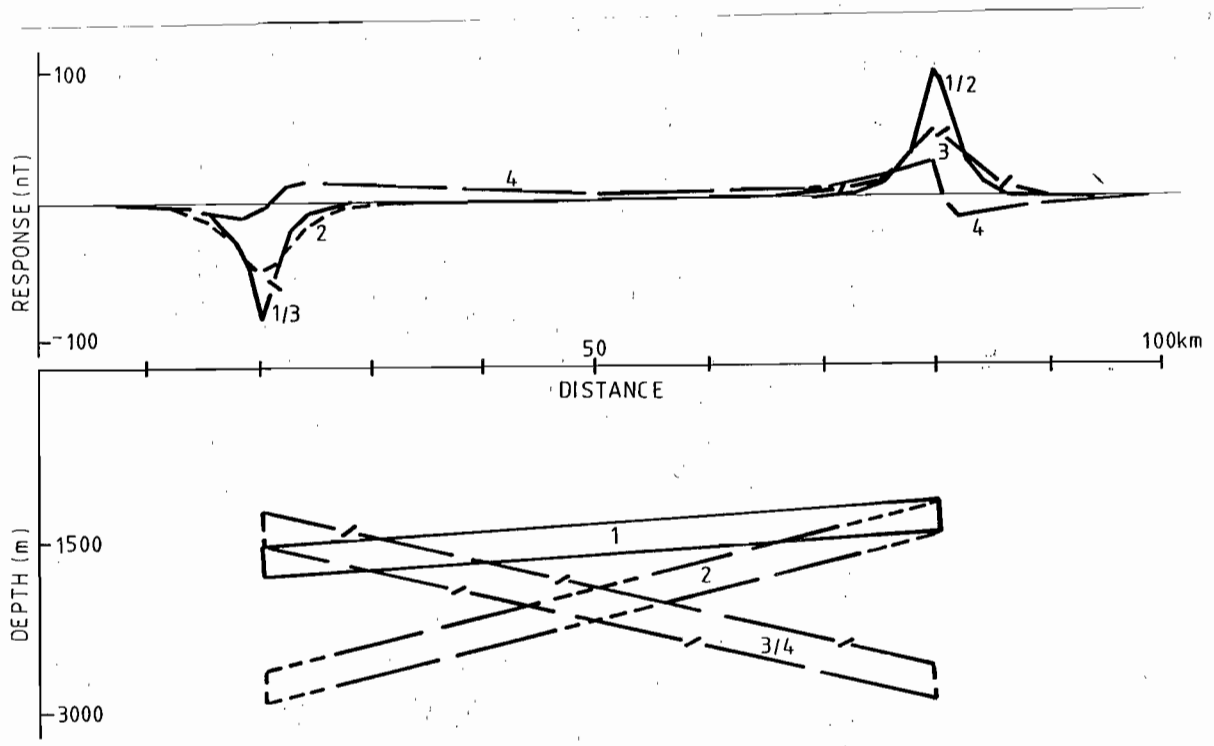

FIGURE 3. Response of dipping slabs with parallel sides. Profiles 1–3 are oriented N–S, 4, E–W.

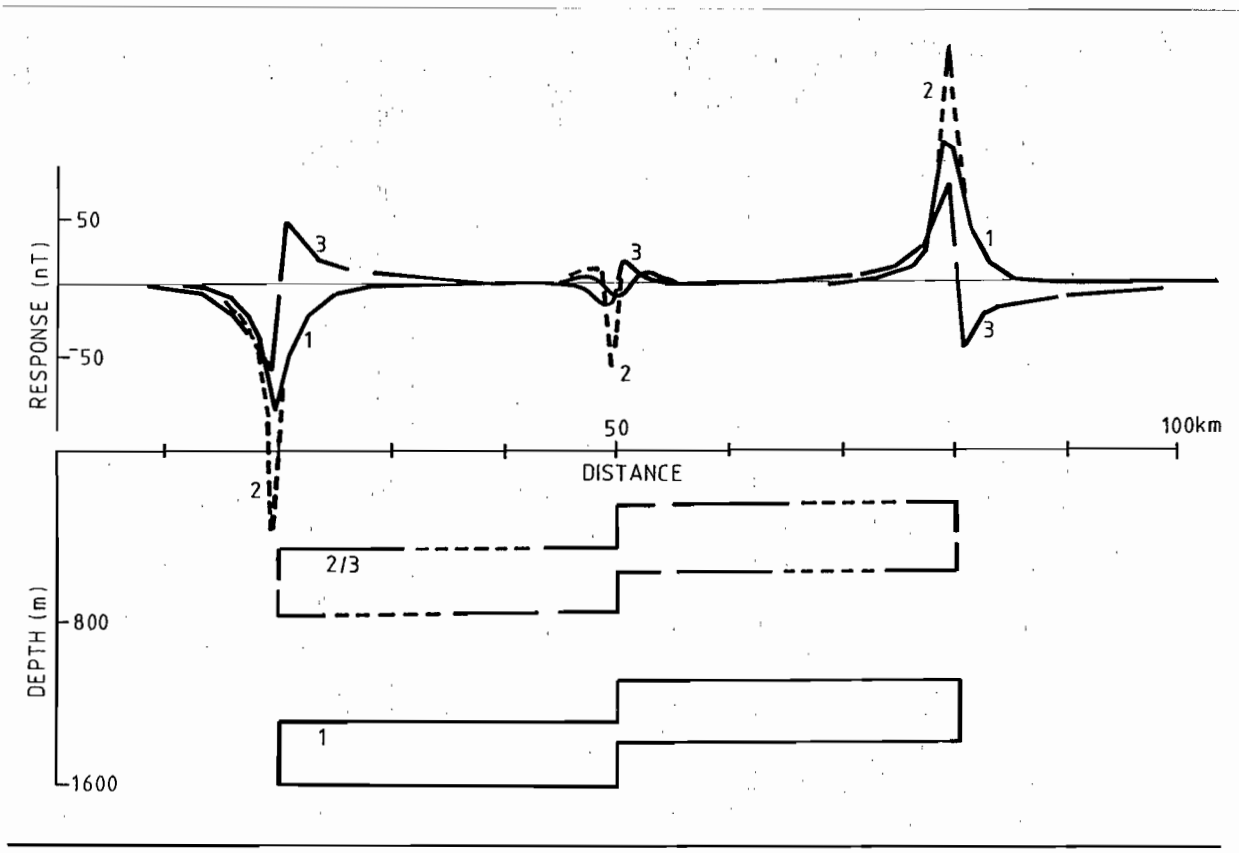

FIGURE 4. Effect of faulting and depth on slab response. Profiles 1–2 are oriented N–S, 3, E–W.

true source extent from an inspection of the mapped magnetic field whether in map or image form and it might not be deduced unless quantitative calculation could be controlled by well or outcrop information or another method (such as gravity or seismic).

These conclusions apply regardless of the position of the unit within the basin sequence but is most relevant to sources within the sag-cover sequences.

Many of the effects from tabular sources may also be confused by the presence of larger anomalies of no particular pattern. The possible origin of these is considered below.

THE WEDGE RESPONSE

The wedge response may be considered to arise in the cover sequence of more restricted basins at their margins or, more generally, in the rift stages of the basin.

Figure 5 suggests several types of wedge and their magnetic responses. All wedges have horizontal upper surfaces but varying lower surface dips determined by their thickness, and orientations. The end effects remain marked and their amplitude is related to the thick end of the wedge regardless of orientation. The response magnitude is, however, a function of both magnetisation and maximum thickness and both relationships are essentially linear.

The wedge introduces an important variation to the slab response.

As thickness is increased the background level of the field above the body is shifted. This is quite different from the normal tabular response. The sense of shift depends on both dip and orientation but may exceed 100 nT for thick sources (e.g., D). This means that interpretation within a basin may be undertaken against a false base level if the edge effect has not been observed or recognised. While this may not be a problem for simple estimation methods (arguable since the gradients vary

considerably and according to orientation) it may lead to interpretation failure when modelling methods are used (see Leaman, 1994).

The crucial observation, however, is that the anomalous field remains nearly uniform *above* the source. In this respect the wedge response is similar to the tabular response.

It is this knowledge, and recognition that a consistent or near zero response occurs over an extended magnetic source, which has led most workers and texts to ignore the potential of the response and to imply that most anomalies observed in basinal areas must be generated either within the basement or from shallow, localised sources. This may be a valid judgment in many cases, or many parts of a basin, but it is not universally valid and should not be presumed to be.

It is clear, where tabular sources are present, that the end effect anomalies, or fault step anomalies, could be misread as basement prism effects and so interpreted. Interpretations of this type will be suspect although the fact may not be obvious, and important information about the basin sequence and history will have been missed.

All wedges in Figure 5 possess a horizontal upper surface and the anomalies generated depend on the dip of the lower face.

Figure 6 indicates the nature of responses when the angular differential is generated by the difference in dip of both surfaces.

In this situation the thickness of the body is also varied and the amplitude of the end effects reflects this factor. The anomaly form is varied and more asymmetric. Source length is less critical but a tabular style offset of more than 150 nT can be generated over more than half of the source length and the apparent base offset may, again, not be recognised. The anomaly generated can be warped slightly by giving the wedge real half graben forms.

The addition of faulting to such a structure simply adds small internal spikes as in Figure 4.

Figure 6 shows that wedge thickness and length may also be factors which determine both the amplitude of the end effects and the consistency of the effect over the wedge.

BASIN FORMS

Figure 7 suggests some simple source forms which may be seismically and stratigraphically recognised depending upon erosion or depositional history. Each shape may be considered a simplified envelope form which may be composed of several internal serrations or rift wedges.

The responses are similar to simple wedge responses but these persist for the width of the basin. Changes in thickness affect the end or step response amplitudes but not the over-unit signal. The general offset and long wavelength effects about the source are ± 80 nT depending on sense of dip. All dips are very subtle. Variations in response are related to the differing angular relationships between upper and lower surfaces. The more extended forms (contrast Figure 6) generate a generally flat response across the source.

Some more complex forms are shown in Figure 8 which include two sources and may be considered representative of sequences with bimodal volcanics or basal volcanics and overlying volcano-sedimentary or derived materials. The figure indicates that dip and thickness are not critical factors. Near zero responses result whenever the package becomes quasi-tabular even though a contrast difference may exist within the overall form. The figure shows that units with thicknesses consistent with those observed in the Jurassic-Cretaceous portions of the Bass-Otway-Boobyalla Basins of SE Australia, or the mid Proterozoic McArthur and Isa Basins of N Australia may generate responses up to 500 nT with wavelengths and amplitudes typical of the fields observed.

There is a temptation in normal practice, however, to interpret the step and end anomalies in terms of source depth. This is clearly invalid since the responses are derived from basal form changes and the gradients are affected by dip or geometry, and not simply depth, and cannot be treated accurately as a prism response.

The diagram shows, further, that the responses ae diagnostic in terms of such basin elements and contents. It may also be observed that the materials

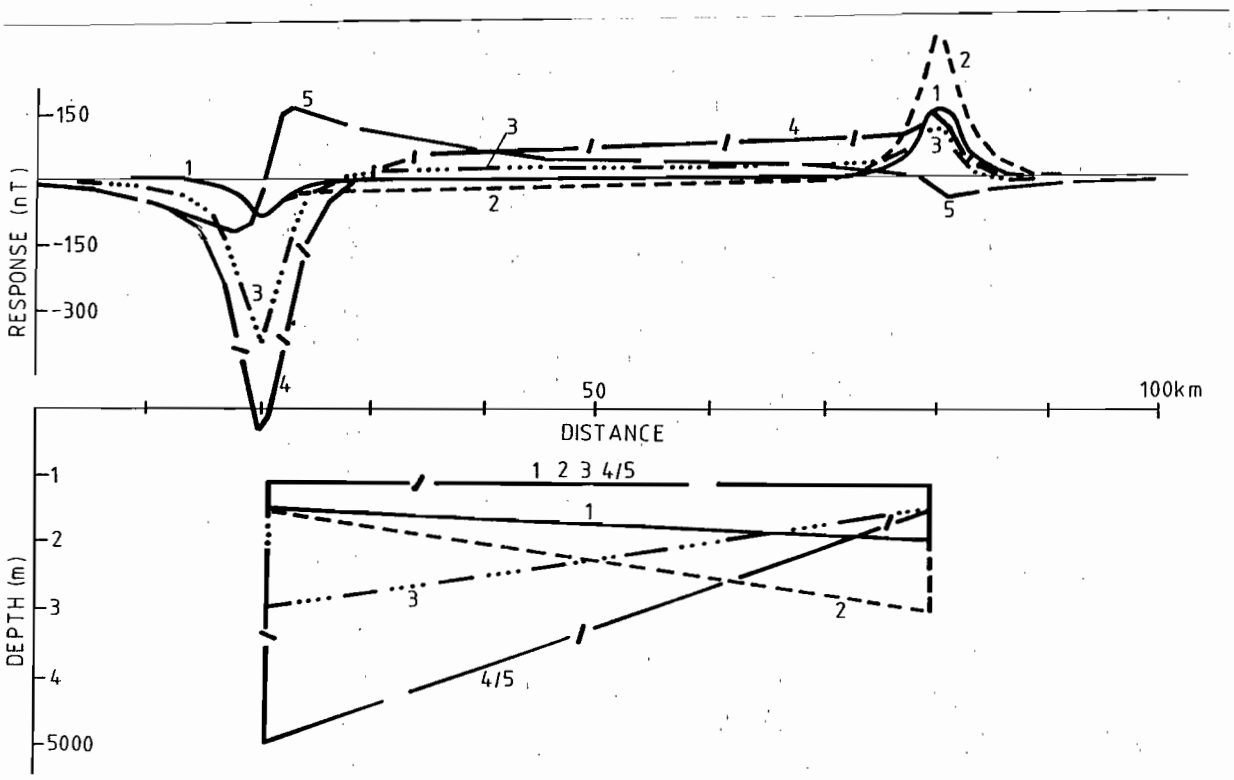

FIGURE 5. Response of wedge-shaped sources with horizontal upper surface where depth and thickness is a small fraction of length. Profiles 1–3 are oriented N–S, 4, E–W. Note the non zero response above the wedge; this increases with thickness.

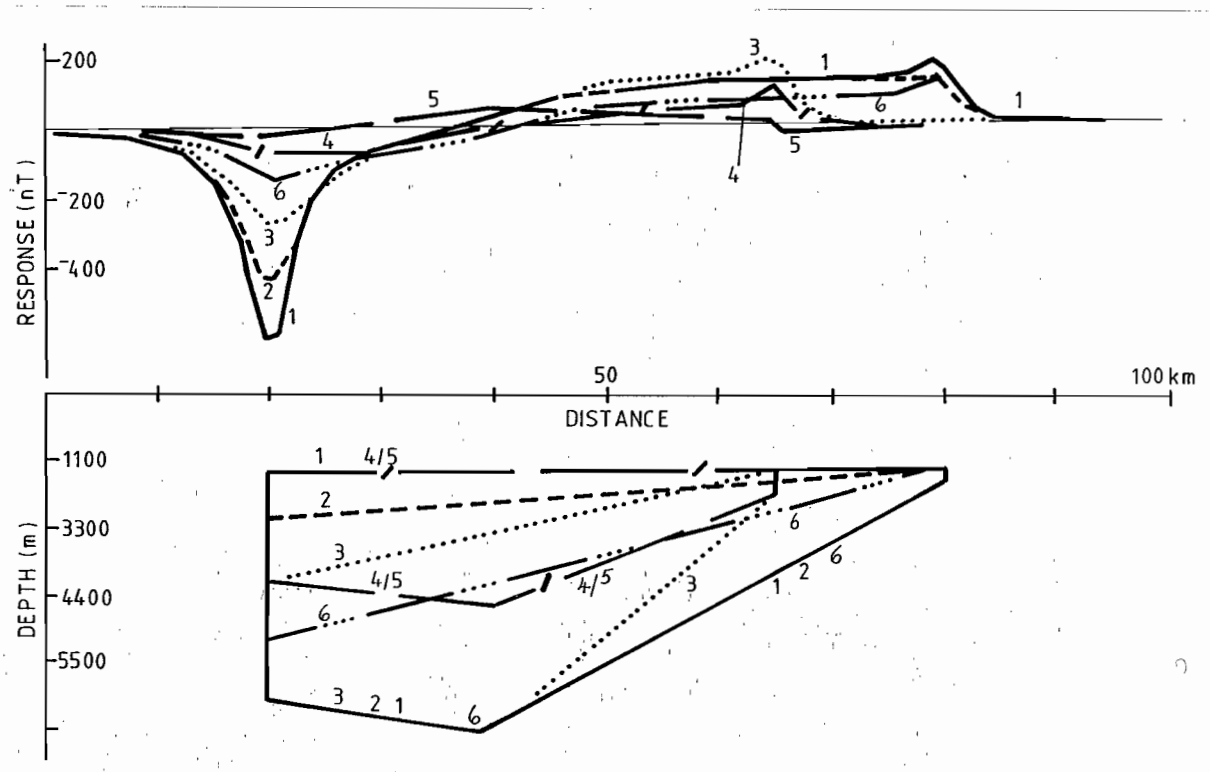

FIGURE 6. Response of complex wedge typical of single half grabens where the upper surface is horizontal (sources 1, 4, 5) Sources 2, 3 and 6 have a base shape as in wedge 1 but with upper surfaces of varied dip and reduced thickness. Profiles 1–4, 6 are oriented N–S, 5, E–W.

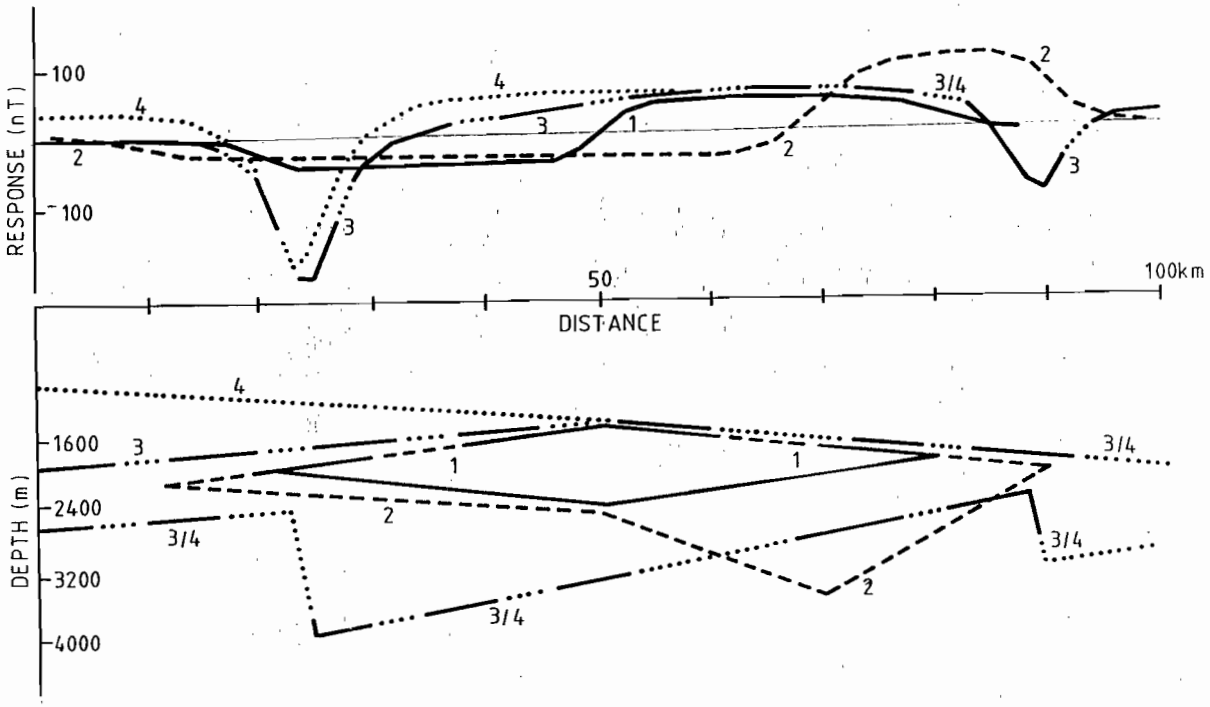

FIGURE 7. Response of typical large scale basin forms where substantial horizontal extent is involved. Note the general change in base levels above the source irrespective of orientation. All profiles are oriented N–S. No surface is horizontal. The forms are typical of repeated graben structures.

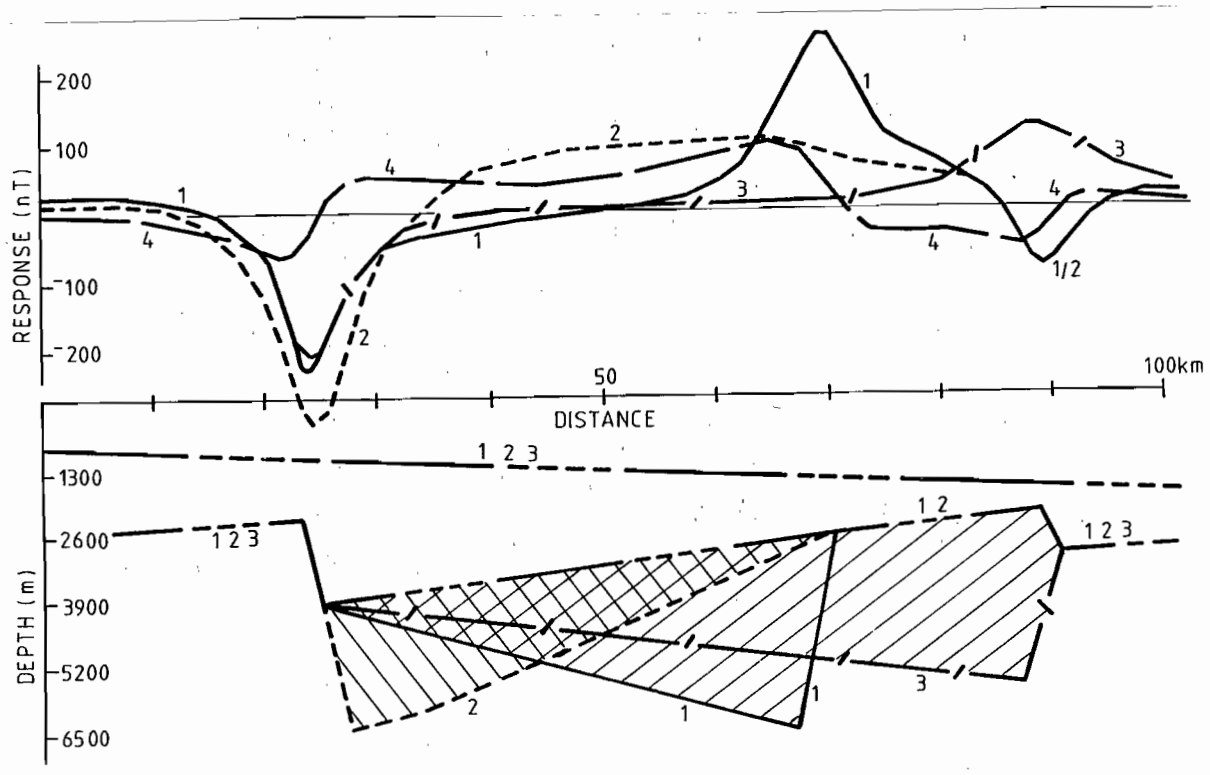

FIGURE 8. Nature of responses where two source wedges are present. This pattern may occur deep in some large basins. The upper and lower sources have magnetisations of 0.005 cgs (0.065 SI), 0.003 (0.039 SI) respectively. Profiles 1–3 are oriented N–S, 4, E–W. Shape 4 is the same as 1. Note the large offset from base level above the deep wedge elements.

involved rarely generate clear seismic reflections. Magnetic methods may thus support and clarify seismic records from the deeper and more complex parts of the basin and can certainly define or confirm the location of major faults.

Regional effects may appear similar to primary prism effects in terms of many relationships to base level but the shifts in base level noted in Figures 5, 6 and 7 are never produced by prismatic sources. And the difference can only be recognised where profiles are of sufficient length. This means that the survey, or a sub set of profiles, must extend clear to the basin onto undoubted basement exposure. Unless this is done it may not be possible to discriminate between prism, tabular and wedge sources and any interpretation is therefore at risk.

SHALLOW VOLCANIC SOURCES

The style of responses which might be associated with shallow volcanics is suggested in Figure 9. A tabular sheet would respond as in Figure 2 but disrupted fragments may act as shown — or in various combinations — depending on fragment length. Where such a sheet has been eroded or weathered then patchy or irregular responses not dissimilar to small fault effects might be expected. No long wavelength effects of any substance can be generated and the features can be easily separated from deeper basin or basement sources.

BASIN EXAMPLES

The first example, Figure 10, shows typical rift forms from eastern Bass Basin in Southern Australia. The magnetic profile corresponds to seismic line 306 acquired by the Australian Geological Survey Organisation. The seismic section unambiguously reproduces the sequence above the Upper Cretaceous unconformity and below that depth (below deepest well) the content of the section and sequence is most uncertain. The style of the sequence is suggested in Figure 1a.

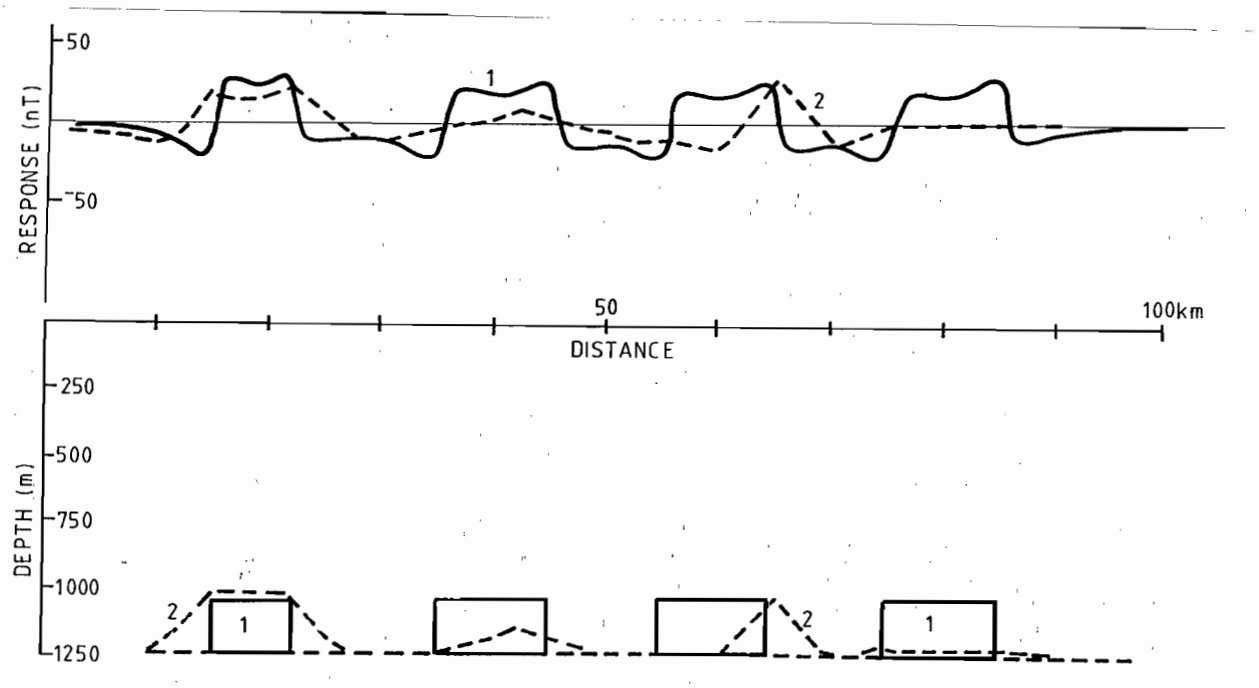

FIGURE 9. Nature of responses associated with patchy shallow volcanics of irregular form. Responses for regular and irregular forms are shown. All magnetisations are 0.005 cgs (0.065 SI). Profiles are oriented N–S.

The magnetic data show that large parts of the Cretaceous sequence contain volcanic rocks — other parts of the basin suggest a mix of lavas and derived sediments — captured in half grabens. The shape interpreted, and the location of the deposits, helps define and locate the important faults of the deep basin. None of these are clearly displayed seismically.

The second example, Figure 11, is from the Sydney Basin of eastern Australia. The diagram presents both gravity and magnetic data from the continental shelf. The gravity interpretation has included the effects of the continental margin and is needed to place the volcanic pile in both stratigraphic and structural context.

Seismic data define the upper domed surface of the volcanic unit which has been drilled, but not penetrated, by one well. Magnetic data confirm the presence of much basalt. The unit lies within the Lower Permian sequence and it has been presumed to be basal by previous explorers. Drilling of the basalt caused the structure to be discounted.

The magnetic and gravity data show, however, that the volcanics are relatively localised and not especially thick. More importantly, they conceal a deeper extension of the late Carboniferous(?) basins exposed on the coast nearly 250 km further north. If the underlying rocks have been structured in the same manner as the volcanics by a late Permian or late Triassic event then there is considerable potential to this offshore basin. The magnetic interpretation has also been able to trace the volcanics to their much-thinned correlates on the coast and this indicates that the pile is not basal to either the basin rocks or the Permian sequence. The solution shown has been extracted from 3D models.

A third example from the central part of Bass Basin in southern Australia illustrates the effect of irregular volcanic remnants within the sag sequence

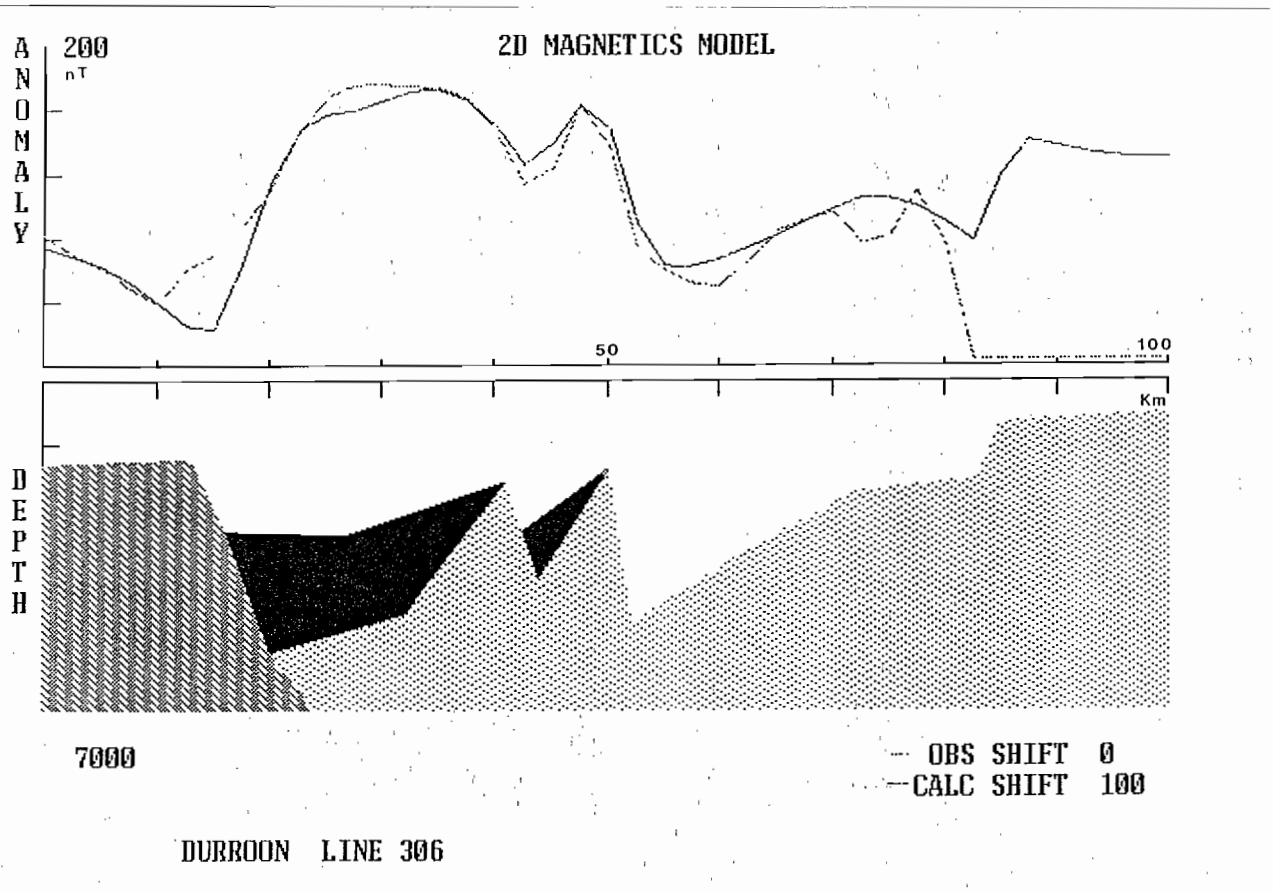

FIGURE 10. Basin model, Durroon Sub Basin, Bass Basin, Australia. Based on seismic line 306. See also Figure 1a. Volcanics are shown in black and have been drilled at 39 km along the section.

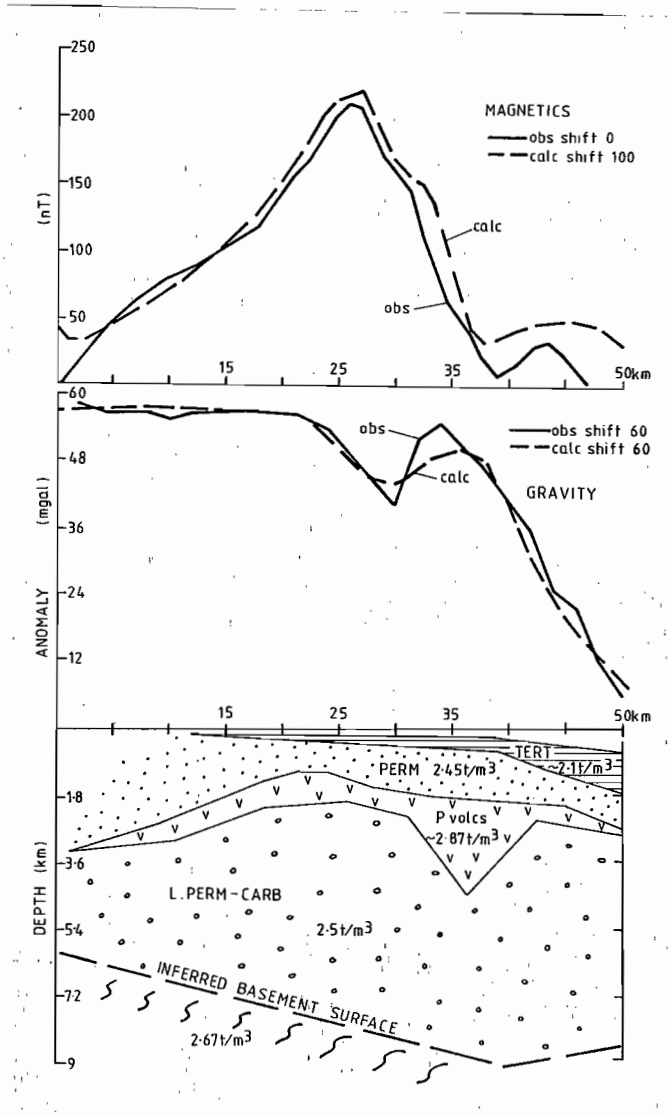

FIGURE 11. Magnetic and gravity models along seismic line 24, offshore Sydney Basin, eastern Australia. The gravity model allows for continental and crustal effects and young slope sedimentation. Both data sets show that the volcanics are domed and thin and that a substantial sequence exists beneath them. Seismic data display only the upper surface of the volcanics.

(Figure 12). The seismic data in this region indicate a possible unconformity and some local deformation. The magnetic data, regardless of any assumptions about variations in the ultimate basement, indicate that high contrast magnetic rocks are present near the unconformity. This prediction was confirmed by drilling (well: Tilana, at 15 km on the section). Major changes in porosity and reservoir potential were established near this level and no significant yield was possible from the indicated structures. The magnetic interpretation tested implied that a significant time break, possible uplift, and erosion were all involved at this level.

In the context of this Amira project a final example illustrates concealed conditions in an old undeformed part of the McArthur basin in N Australia (Figures 9, 10, 11 of the main Lawn Hill interpretation report).

The basin sequence includes various clastic and evaporitic units and several thin and sometimes patchy volcanic units. In the vicinity of the section many units display normal erosional and onlap conditions but felsic volcanics appear to underlie the known sequence. Very little material other than the youngest cover sequences is exposed. Magnetic anomalies display both high and low frequency forms and it can be shown that the thin, upper, virtually tabular cover volcanics cannot account for the anomalies. Disruptions of the cover by small faults with displacements less than 100 m can, however, generate the systematic high frequency patterns of low relief anomalies. The major anomalies can be explained by a thickening pile of volcanics deep in the basin. No basement form, or sources, can produce an equivalent explanation in basin perspective and an additional test is provided by regional gravity data which confirms that the basement is granitic and that there is no correlation between basement sources and the magnetic field. Seismic data nearby indicate onlapped lower units and show that the required volume of volcanics could be fitted into the basin section. The seismic data give no indication of the volcanic content and appear normally stratified.

CONCLUSIONS

Analysis of the magnetic response of tabular forms, whether horizontal or dipping suggests that the substantial anomalies generated at the limits of the source might be mistaken for isolated prism sources and wrongly interpreted. Disruption of such sources

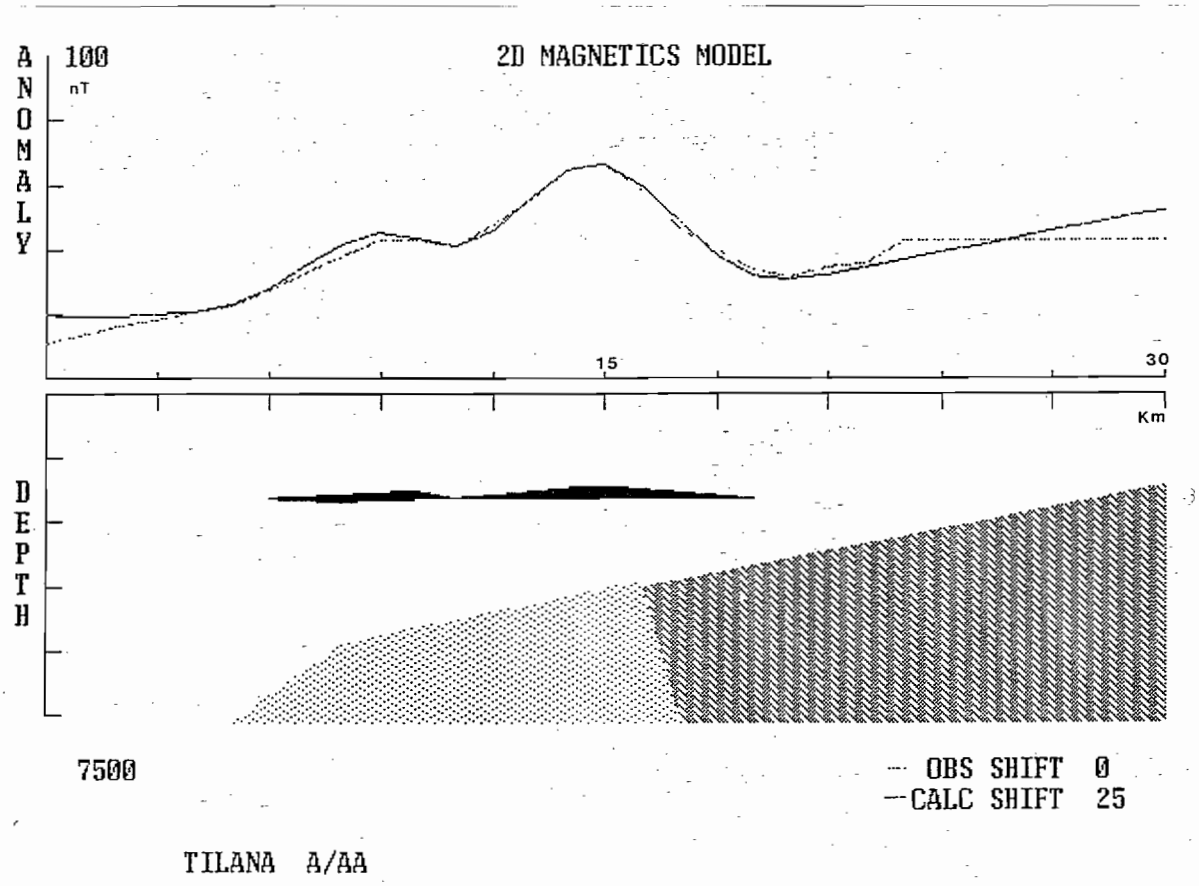

FIGURE 12. Example of effect of shallow volcanic units within Bass Basin, Southern Australia. Seismic data indicate a possible unconformity at the level of the magnetic source. These units were drilled in well Tilana at 15 km subsequent to the interpretation and confirmed a substantial change in the properties of the rocks at this level. The thickness of volcanics implied was confirmed.

by faulting can produce significant effects which might also be mis-read.

Where the source has simple or compound wedge-shaped forms the results may appear comparable unless very long profiles are inspected. Significant base level shifts may occur above such sources and the effect is largely independent of source or field orientation, or body thickness, dip or depth. The shift response is diagnostic if the profile is long enough to define it.

Tabular or wedge-shaped source forms may be observed in many basins. Where these contain volcanics it is possible to clarify much of the deep basin form which may assist appraisal, exploration or reconstruction of basin history.

Shallow, sub tabular volcanic suites in the sag sequences may be readily evaluated and defined even if locally eroded and variable in properties.

The results suggest that many basic interpretations across large basins which have presumed that either all magnetic sources are in the form of shallow and thin volcanics or in the basement may contain significant error. Many such interpretations may be valid serendipitously but this should not be assumed since both parts of wedge and prism responses can appear similar. Simple assumption that all large sources can be treated as basement prisms is not warranted generally but the style of source, and consequent improvement in interpretation. is possible since the source-response style can be discriminated if the profiles cover much of the basin and its surrounds.

REFERENCES

Grant, F.S., & West, G.F., 1965. *Interpretation theory in applied geophysics.* McGraw-Hill, New York. 584pp.

Vacquier, V., Steenland, N.C., Henderson, R.G., & Zeitz, I., 1951. *Interpretation of Aeromagnetic Maps.* Geological Society of America, Memoir, 47.

Leaman, D.E., 1994. Criteria for evaluation of potential field interpretations. *First Break,* 12, 181-191.